



Monolithically integrated polymeric Lab-on-(Bio)Chips with photonic/electrochemical detection

Bergoi Ibarlucea Cantón

PhD Thesis

PhD in Chemistry

**Directors:
Dr. Andreu Llobera
Dr. César Fernández Sánchez**

**Chemistry Department
Science Faculty**

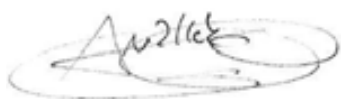
2013

Memòria presentada per aspirar al Grau de Doctor per Bergoi Ibarlucea Cantón

A handwritten signature in black ink, consisting of a stylized 'B' followed by 'Ibarlucea Cantón'.

Bergoi Ibarlucea Cantón

Vist i plau

A handwritten signature in black ink, appearing to read 'Andreu Llobera'.

Dr. Andreu Llobera (Director)

A handwritten signature in black ink, appearing to read 'César Fernández Sánchez'.

Dr. César Fernández Sánchez (Director)

A handwritten signature in black ink, appearing to read 'María del Mar Puyol'.

Dr. María del Mar Puyol (Tutora)

Bellaterra, 25 de Julio de 2013

Table of Contents

Acknowledgments	8
Related publications:	11
List of abbreviations	13
List of Figures	15
List of Tables	18
List of Schemes	19
Summary	21
Resumen	22
1. GENERAL CONCEPTS	23
1.1. Introduction	24
1.2. Performance of LOCs	25
1.3. Fabrication, materials and procedures.....	26
1.4. Surface modification of Microsystems.....	31
1.4.1. Plasma activation	31
1.4.2. Chemical vapor deposition (CVD).....	32
1.4.3. UV irradiation.....	33
1.4.4. Wet chemical modifications.....	34
1.5. Detection techniques	36
1.5.1. UV/Vis absorbance measurement	36
1.5.2. Fluorescence detection	36
1.5.3. Chemiluminescence detection	37
1.5.4. Interferometric detection	38
1.5.5. Surface-enhanced Raman spectroscopy (SERS).....	39
1.5.6. Surface plasmon resonance (SPR)	40
1.5.7. Mass spectrometry.....	40
1.5.8. Electrochemical detection	41
1.5.9. Surface-acoustic wave (SAW) detection.....	42
1.5.10. Mechanical detection.....	42
1.6. Fields of application	43
1.7. References	44
2. OBJECTIVES	51
3. CELL SCREENING USING DISPOSABLE MICROFLUIDIC CHIP SYSTEMS WITH OPTICAL READOUT	53
3.1. Summary	54
3.2. Introduction	54
3.3. Experimental details	56
3.3.1. Materials and reagents	56
3.3.2. Optofluidic system design and fabrication	56
3.3.3. Cell culture and labeling	57

3.3.4.	Measurement setup	58
3.4.	Results and discussion	58
3.4.1.	Measurement protocols	58
3.4.2.	Live cells: LS regime	59
3.4.3.	Dead cells: LS + ABS and ABS regimes	61
3.4.4.	Dead/Live ratio measurement	63
3.5.	Conclusions	67
3.6.	References	67
4.	PDMS-BASED PHOTONIC LAB-ON-A-CHIP FOR THE SELECTIVE OPTICAL DETECTION OF HEAVY METAL IONS	69
4.1.	Summary	70
4.2.	Introduction	70
4.3.	Experimental details	71
4.3.1.	Materials and reagents	71
4.3.2.	Ligands	71
4.3.3.	Design and fabrication of the PhLOCs	73
4.3.4.	Experimental setup and measurement protocol	74
4.4.	Results and discussion	74
4.5.	Conclusions	78
4.6.	References	78
5.	SELECTIVE FUNCTIONALIZATION OF PDMS-BASED PHOTONIC-LAB-ON-A-CHIP FOR BIOSENSING	81
5.1.	Summary	82
5.2.	Introduction	82
5.3.	Experimental details	83
5.3.1.	Materials and reagents	83
5.3.2.	Fabrication of the microsystem	84
5.3.3.	Modification and characterization of the PDMS surfaces	84
5.3.4.	Fabrication of the biosensor approach	85
5.3.5.	Stability of the microsystems	86
5.4.	Results and discussion	86
5.4.1.	Structural characterization of the modified PDMS surfaces	87
5.4.2.	Analytical performance of the different biosensor approaches	95
5.5.	Conclusions	97
5.6.	References	98
6.	DUAL OPTICAL/ELECTROCHEMICAL READOUT BIOFUNCTIONALIZED LAB-ON-A-CHIP SYSTEMS	99
6.1.	Summary	100
6.2.	Introduction	100
6.3.	Experimental details	101
6.3.1.	Materials and reagents	101
6.3.2.	Design and fabrication of the DLOCs	102
6.3.4.	Characterization of the mixer	104

6.3.6.	Enzyme immobilization	104
6.3.7.	Optimization of the GOx:HRP ratio	105
6.4.	Results and discussion	106
6.4.1.	Characterization of the mixer	106
6.4.2.	Characterization of the electrodes	108
6.4.3.	Optimization of the GOx:HRP ratio	109
6.4.4.	Glucose detection and crosstalk test	110
6.5.	Conclusions	115
6.6.	References	115
7.	OTHER FUNCTIONALIZATION APPROACHES EXPLORED	117
7.1.	Summary	118
7.2.	Introduction	118
7.3.	Experimental details	119
7.3.1.	Materials and reagents	119
7.3.2.	Polymer biofunctionalization.....	120
7.3.3.	Immobilization of bacteria	121
7.3	Results.....	122
7.3.4.	Characterization of the polymer modification steps	122
7.3.5.	Characterization of the analytical performance of the PC surfaces	124
7.3.6.	Characterization of the analytical performance of the biofunctionalized PMMA	127
7.3.7.	Immobilization of bacteria	128
7.4	Conclusions	129
7.5	References	130
8.	CONCLUDING REMARKS	133
9.	ANNEX: RELATED PUBLICATIONS	135

Acknowledgments

The research leading to this thesis has received funding from:

- The European Research Council under the European Community's Seventh Framework Programme (FP7/2007-2013) / ERC grant agreement no. 209243.
- The IST Programme (P. CEZANNE, Grant IST-2-IP-031867).
- The DGI grants (EMOCIONa (CTQ2006-06333), POMAs (CTQ2010-19501)).
- The Networking Research Center on Bioengineering, Biomaterials and Nanomedicine (CIBER-BBN).
- The Generalitat de Catalunya (grants 2009SGR00516 and 2009SGR00277).

During these years I have had the possibility to develop myself, both as a person and as a researcher, and deepen my knowledge in the field of the Lab-on-Chip (LOC) systems. This would have not been possible without the opportunity offered by my supervisors, Dr. Andreu Llobera and Dr. César Fernández Sánchez, at the Institut de Microelectrònica de Barcelona (IMB-CNM, CSIC). I want to thank them for their continuous help, useful suggestions and invaluable knowledge and experience transfer. This gratitude is extendable to my tutor M^a del Mar Puyol.

I would also like to thank other people who have made possible all this research work: the research group FOR 856, mikroPART "Mikrosysteme für partikuläre Life-Science-Produkte" (Technische Universität Braunschweig, Germany) and Institut für Mikrosystemtechnik – IMTEK (Albert-Ludwigs-Universität Freiburg, Germany) for their support, Dr. Manuel Gutierrez for his kind help with the Atomic Force Microscopy studies, Nidia Santamaría for her kind help with the soldering of the electrical contact pads of the dual Lab-on-a-Chip systems.

Although most of the research has been carried out at the facilities of the Chemical Transducers Group (GTQ) and the the IMB-CNM clean room, contact angle studies were done at Dr. Laura Lechuga's Nanobiosensors and Bioanalytical Applications laboratory at the Catalan Institute of Nanoscience and Nanotechnology (ICN2). On the other hand, staining of bacteria and their microscopic analysis was carried out at the facilities of the Grup de Recerca de Microbiologia Ambiental (Universitat Autònoma de Barcelona) with the help of Nuria Vigués. I am grateful to both groups.

I cannot forget to mention the GTQ members and the rest of the current and former IMB-CNM staff for their personal and professional discussions.

And travelling back in time, of course I have to thank Professor Isabel Barcina and her Microbiology laboratory at the Universidad del País Vasco – Euskal Herriko Unibertsitatea (UPV-EHU). There it is where everything began, where I first learnt to work in a laboratory, together with a generation of students who gave me a bunch of invaluable moments. I could include Ana Perea here, who while not being from the lab, is somehow connected to this time. Probably without the experience lived at Prof. Barcina's lab it would have been much more difficult to start my next cycle at Inasmet – Tecnalia Foundation, to which I am also deeply grateful. Here I started to learn about biofunctionalization from Dr. Jesús Valero and Nerea Briz. It was a really important step in my life, during two years that were made even happier with the help of the great student generation and the lab mates that I met.

There are many people that have been present in my life. They come and they go. But there are some that I believe they are here to stay. Those are the ones that I feel I need to thank most. Aitor eta Koldo, urte hauetan egindako bazkariak, bidalitako mezuak, emailak eta bisitak eskertzen dizkizuet, karrerako momentu onenak gogoratuz [Koldotesis 2010]: Koipu Leptospirosiko, Pierre Poirot, Canis Vomit, arraultz frejituak hormaren kontran, zazpiretatik aurrerako desbideratze estandar mentala... Aita, ama y Olatz, porque la familia es la familia y siempre está ahí para apoyar. Y, por supuesto, mi Mari, acompañándome en el mismo camino y mostrando un incomparable apoyo y amor.

Related publications:

Papers included in this Thesis:

- B. Ibarlucea, C. Díez-Gil, I. Ratera, J. Veciana, A. Caballero, F. Zapata, A. Tárraga, P. Molina, S. Demming, S. Büttgenbach, C. Fernández-Sánchez, A. Llobera. PDMS based photonic lab-on-a-chip for the selective optical detection of heavy metal ions. *Analyst* 138(3), **2013**, 839-844.
- J. Vila-Planas, E. Fernández-Rosas, B. Ibarlucea, S. Demming, C. Nogués, J.A. Plaza, C. Domínguez, S. Büttgenbach, A. Llobera. Cell analysis using a multiple internal reflection photonic lab-on-a-chip. *Nature Protocols* 6 (10), **2011**, 1642-1655.
- B. Ibarlucea, C. Fernández-Sánchez, S. Demming, S. Büttgenbach, A. Llobera. Selective functionalisation of PDMS-based photonic lab on a chip for biosensing. *Analyst* 136, **2011**, 3496-3502.
- B. Ibarlucea, C. Fernández-Sánchez, S. Demming, S. Büttgenbach, A. Llobera. Biofunctionalization of PDMS-based microfluidic systems. *Nature Protocol Exchange*, 2011, DOI: 10.1038/protex.2011.271
- B. Ibarlucea, E. Fernández-Rosas J. Vila-Planas, S. Demming, C. Nogués, J.A. Plaza, S. Büttgenbach, A. Llobera. Cell screening using disposable photonic Lab on A Chip systems. *Analytical Chemistry* 82, **2010**, 4246-4251
- B. Ibarlucea, X. Muñoz-Berbel, P. Ortiz, S. Büttgenbach, C. Fernández-Sánchez, A. Llobera. Dual optical electrochemical readout biofunctionalized Lab-on-a-Chip systems (in preparation).

List of abbreviations

(μ)TAS: (Micro) Total Analysis System
ABS: absorption
ABTS: 2,2'-azino-bis (3-ethylbenzthiazoline-6-sulfonic acid)
AFM: Atomic Force Microscopy
APTES: 3-aminopropyltriethoxysilane
BIS: Bureau of Indian Standards
BSA: Bovine Serum Albumin
COC: cycloolefin copolymer
CV-AAS: Cold Vapour Atomic Absorption Spectrometry
CVD: Chemical Vapor Deposition
DI H₂O: Deionized water
(D)LOC: (Dual) Lab-on-a-Chip
DNT : 2,4-dinitrotoluene
EDC: 1-ethyl-3-(dimethylaminopropyl)carbodiimide
EPA: Environmental Protection Agency
ESI: Electrospray Ionization
GOx: Glucose Oxidase
HPLC: High Performance Liquid Chromatography
HRP: Horseradish Peroxidase
HTS: High-Throughput System
ICP-MS: Inductively Coupled Plasma Mass Spectrometry
IMTEK: Institut für Mikrosystemtechnik
LOD: Limit of Detection
LS: light scattering
LUCAS: Lensless, ultrawide field cell monitoring array platform based on shadow imaging
NHS: N-hydroxysuccinimide
OLED: organic light emitting diode
OPL: Optical Path Length
PBS(T): Phosphate Saline Buffer (Tween 20)
PBT: poly(butylenes terephthalate)
PC: polycarbonate
PCL: polycaprolactone
PCR: polymerase chain reaction
PDMS: poly(dimethyl siloxane)
PEG: polyethylene glycol
PGMEA: Propylene Glycol Methyl Ether Acetate
PhLOC : Photonic Lab-on-a-Chip
(P)MIR: (Propagating) Multiple Internal Reflection
PMMA: poly(methyl methacrylate)
POC: Point of Care
PPFDA: poly(1H,1H,2H,2H-perfluorodecyl acrylate)
PS: polystyrene
PVA: polyvinyl alcohol
RMIR: Ring Multiple Internal Reflection

RT: room temperatura
SAW: Surface-Acoustic Wave
SERS: Surface-enhanced Raman spectroscopy
SPR: Surface Plasmon resonance
TIR: Total Internal Reflection
UV/Vis: Ultraviolet/visible
SNR: Signal-to-Noise Ratio
TEA: Triethylamine
TESU: 11-triethoxysilyl undecanal
TIR: Total Internal Reflection
XRF: X-Ray Fluorescence spectroscopy
XPS: X-ray Photoelectron Spectroscopy

List of Figures

Figure 1.1. Representation of the evolution from standard analytical procedures to the miniaturization of these processes.	24
Figure 1.2. Representation of a typical (a) thermoplastic polymer and (b) a thermosetting polymer.	27
Figure 1.3. Soft lithography process for microfabrication with PDMS.	28
Figure 1.4. Photolithography process using a negative photoresist over a silicon wafer.	29
Figure 1.5. Selective removal process on bulk material by etching.....	29
Figure 1.6. Fabrication process by (a) hot embossing and (b) injection molding.	30
Figure 1.7. Representation of a surface treatment with plasma oxygen.	32
Figure 1.8. Representation of a CVD process.....	32
Figure 1.9. Representation of a surface modification process by UV irradiation.....	33
Figure 1.10. Representation of the silanization process of a hydroxylated surface with APTES in an acetone solution.....	34
Figure 1.11. Representation of a surface modification process by sol – gel chemistry.	35
Figure 1.12. Representation of absorbance process of a sample.....	36
Figure 1.13. Representation of fluorescence emission process of a sample.....	37
Figure 1.14. Representation of chemiluminescence emission of an analyte after its recognition process.	38
Figure 1.15. Representation of an interferometric detection system.....	39
Figure 1.16. Representation of a surface-enhanced Raman spectroscopy detection process. .	39
Figure 1.17. Representation of the detection by surface plasmon resonance using the Kretschmann configuration.....	40
Figure 1.18. Representation of the mass spectrometry detection technique.....	41
Figure 1.19. Representation of the electrochemical detection method.	42
Figure 1.20. Representation of a SAW detection system.	42
Figure 1.21. Representation of the mechanical detection technique.	43
Figure 3.1. Picture of the PDMS-based MIR system..	57
Figure 3.2. Results obtained for the scattering measurements using unlabeled cells and sensitivity and LOD as a function of the wavelength for the LS regime.	60
Figure 3.3. (a) Absorbance as a function of the wavelength for the three regimes studied. (b) Absorbance vs concentration and sensitivity and LOD as a function of the wavelength for LS + ABS and ABS regimes.	62
Figure 3.4. (a) Measurement of the dead/live ratio. A constant cell concentration of 2000 kcell/mL has been selected, varying the live/ dead ratio. (b) Image of a concrete region of the MIR filled with cells. (c) Close view of the labeled monocytes.	64
Figure 3.5. (a) Absorbance vs % of dead cells for different wavelengths. (b) Sensitivity and LOD values.	65
Figure 4.1. (a) PMIR and (b) RMIR systems used for the detection of heavy metals. The analyzed region was filled with a red-color solution for better contrast.	73
Figure 4.2. Absorbance spectra recorded in solutions acetonitrile containing 0.1 mM ligand 1 and increasing concentrations of Hg^{2+} in a range from 1 μM to 90 μM , with the RMIR system. Inset shows a picture of acetonitrile solutions containing 0.1 mM ligand 1 and the change in color of this solution upon addition of 1 equivalent of Hg^{2+}	75

Figure 4.3. (a) Sensitivity and (b) LOD values for the detection of Hg^{2+} in a solution of ligand 1 using a cuvette, PMIR and RMIR system in a spectral range that varies from 300 to 800 nm...	76
Figure 4.4. (a) Picture showing acetonitrile solutions containing 0.1 mM ligand 2 and the change in color of this solution upon addition of 1 equivalent of Pb^{2+} . (b) Sensitivity and Limit of detection (LOD) values for the detection of Pb^{2+} in a solution of ligand 2 using the RMIR system through a spectral range ranging from 300 to 800 nm.	77
Figure 5.1. Photography of the photonic Lab-on-a-Chip microfluidic system.....	83
Figure 5.2. Contact angle values measured following every step of each modification procedure. Error bars correspond to the standard deviation of three replicates.	87
Figure 5.3. High resolution XPS spectra of the C (1s) region corresponding to (a) intact PDMS, (b) after the adsorption of PVA and (c) after the silanization process with TESU (c).	89
Figure 5.4. High resolution XPS spectra of the C (1s) region corresponding to PEG-modified PDMS (a) before and (b) after the silanization process with TESU.....	90
Figure 5.5. High resolution XPS spectra of the C(1s) region corresponding to PDMS (a) after the chemical oxidation and (b) after the silanization process.	91
Figure 5.6. Topographic and phase AFM pictures of the PDMS surface before and after the modification with PVA and silane.	93
Figure 5.7. Topographic and phase AFM pictures of the PDMS surface after the modification with PEG and further silanization with TESU.	94
Figure 5.8. Topographic and phase AFM images of the PDMS surface after the chemical oxidation and further silanization with TESU.....	95
Figure 5.9. Calibration plots recorded with the different biosensor approaches.	96
Figure 5.10. Sensitivity measurements of the microsystems through time after keeping them in PBS pH 7 at 4°C.	97
Figure 6.1: photography of DLOC1.....	102
Figure 6.2: (a) Photography of DLOC2. Close view of the (b) mixer structure, (c) passive valves and (d) biconvex lens.	103
Figure 6.3: Representation of the surface modification protocol.	105
Figure 6.4. (a) Optical spectra of samples containing different ink concentrations and (b) corresponding calibration plot.....	107
Figure 6.5 (a) Cyclic voltammograms recorded in solutions containing different ferri/ferrocyanide concentrations at 100 $\mu\text{L}/\text{min}$ flow rate. (b) Calibration curve obtained by plotting the current values corresponding to the ferrocyanide oxidation at +0.3 V vs. Au pseudo-reference.....	108
Figure 6.6. Stability test of the electrodes. First and last three out of 100 cyclic voltammograms are shown.....	109
Figure 6.8. (a) Limit of detection and (b) sensitivity for glucose of the Abbe prism microsystems functionalized with different glucose oxidase and horseradish peroxidase ratios.	110
Figure 6.9. Cyclic voltammetry of ABTS and PBS buffer. As ABTS concentration decreases, current at 0.3 V also decreases.	110
Figure 6.10. Electrochemical and optical measurements of glucose at 30 $\mu\text{L}/\text{min}$ using DLOC1.	111
Figure 6.11. Electrochemical and optical measurements of glucose at 100 $\mu\text{L}/\text{min}$ using DLOC2.	111

Figure 6.12. Simultaneous measurement of (a) absorbance at 420 nm and current at 0.3 V through time showing signal response after injections of buffer and different glucose concentrations in a range from 10 μ M to 90 μ M.....	112
Figure 6.13. Optical and electrochemical measurements of glucose at 10 μ L/min using DLOC2.	113
Figure 6.14. Optical detection of glucose samples through time at 10 μ L/min using DLOC2. Peak 1, 2 and 3 represent injections of 600, 1200 and 1800 μ M glucose respectively.....	113
Figure 7.1. Contact angle values measured following every step of each modification procedure. Error bars correspond to the standard deviation of three replicates.	123
Figure 7.2. Topographic and phase AFM pictures of the PC surface before and after the modification with PVA and silane.	124
Figure 7.3. Calibration plots for the hydrogen peroxide sensing surfaces on (a) modified PC and (b) directly adsorbed PC.	125
Figure 7.4. Stability study for the hydrogen peroxide sensing surfaces on modified and unmodified PC.	126
Figure 7.5. (a) PC wells (1) with and (2) without immobilized enzymes. (b) Color comparison between glucose samples after incubation on (3) biofunctionalized and (4) non-biofunctionalized PC wells.	126
Figure 7.6. (a) PC wells (1) with and (2) without immobilized enzymes. (b) Color comparison between glucose samples after incubation on (3) biofunctionalized and (4) non-biofunctionalized PC wells.	127
Figure 7.7. Calibration plots for the glucose biosensor approach in the PMMA PhLOC.	127
Figure 7.8. Comparative quantification of dead and live immobilized bacteria on unmodified and modified PDMS.....	128
Figure 7.9. Fluorescence microscopy picture of (a) unmodified and (b) modified PDMS after bacteria immobilization protocol.....	128
Figure 7.10. Comparative quantification of dead and live immobilized bacteria on unmodified and modified PC.	129
Figure 7.11. Fluorescence microscopy picture of (a) unmodified and (b) modified PC after bacteria immobilization protocol.....	129

List of Tables

Table 3.1. Linear fits and LODs of LS measurements for different wavelengths.....	60
Table 3.2. Linear fits and LODs of the LS + ABS measurements for different wavelengths.	62
Table 3.3. Linear fits and LODs of the ABS measurements for the wavelengths of interest.....	63
Table 3.4. Linear fits and LODs of the live/dead cell measurements using LS+ABS for different wavelengths with a constant population of 2000 kcell/mL.	66
Table 3.5. Linear fits and LODs of the live/dead cell measurements using ABS for the wavelengths of interest with a constant population of 2000 kcell/mL.	66
Table 5.1. Atomic percentages of the different surfaces analyzed by XPS.....	88
Table 5.2. C percentages corresponding to the different chemical groups introduced on the PDMS surface after each modification step.....	92
Table 5.3. Analytical parameters of the four different biosensor approaches.	96
Table 6.1. Calculation of the absorbance increase rate depending on the ink increase rate. .	107
Table 6.2. Linear fittings, R^2 values, LODs and sensitivity values for the glucose measurements in continuous flow.....	114

List of Schemes

Scheme 4.1. Chemical structure of ligand 1 (1,4-disubstituted 2,3-diaza-1,3-butadiene bearing two ferrocene groups) for the detection of Hg^{2+}	72
Scheme 4.2. Chemical structure of ligand 2 (2-ferrocenyylimidazo[4,5-b]phenazine) for the detection of Pb^{2+}	72
Scheme 5.1. Representation of the different methods employed for the modification of PDMS surface.....	84
Scheme 5.2. HRP-catalyzed reduction of hydrogen peroxide mediated by colorless ABTS, which generates water and green-color ABTS radical cation counterpart.	85
Scheme 6.1. Enzymatic cascade reactions for glucose detection.....	101
Scheme 7.1. Surface modification protocol on PC prior to protein immobilization.....	120

Summary

In this PhD Thesis low-cost functionalized Lab-on-(bio)Chip systems (LOC) for their use as analytical tools for environmental and biomedical applications have been developed.

Based on photonic LOC approaches (PhLOC) previously defined in our group, the potential of these devices in analysis was explored first. Multiple Internal Reflection (MIR) optofluidic systems made of cost-effective polymers, such as polydimethylsiloxane (PDMS), using rapid fabrication processes were applied for the detection of different analytes (cells and heavy metal ions) and their performance compared with other more conventional analytical techniques.

In order to confer selectivity to the PhLOCs, different surface modification protocols for protein immobilization on the polymeric materials used in this work were developed and compared. These methods keep the optical and structural properties of the material unaltered. Horseradish peroxidase (HRP) was chosen as a model protein in these studies, and the resulting biofunctionalized surfaces tested by measuring the enzymatic activity to hydrogen peroxide in the presence of 2,2'-azino-bis (3-ethylbenzthiazoline-6-sulfonic acid) (ABTS) redox mediator, whose green colored enzymatic product could be detected by absorbance measurements. The stability of the immobilized HRP was also tested for periods longer than one month.

Finally, other fluidic components and functionalities were added to the previously applied PhLOCs in order to enhance their performance. Microfluidic structures such as biofunctionalized mixers (therefore also playing the role of reactors) were monolithically integrated with a MIR, resulting in a PhLOC with enhanced analytical performance. These new elements decreased the analysis time and sample / reagent volumes. With the integration of a gold electrochemical cell in the substrate, a dual readout LOC (DLOC) was developed, which enabled simultaneous optical and electrochemical transduction and made the developed system self-verifying, thereby improving its reliability. The potential of this DLOC was shown by developing an analytical tool for measuring glucose. Glucose oxidase (GOx) and HRP were immobilized following the protocol developed in this Thesis and applied as the specific receptors for the detection of glucose based on an enzymatic cascade reaction also using ABTS redox mediator.

As an additional study, the applicability of the developed functionalization protocol was tested on different polymers and the immobilization of biological components other than enzymes was also carried out.

Resumen

En esta Tesis de Doctorado se han desarrollado sistemas lab-on-a-chip (LOC) funcionalizados de bajo coste para su uso como herramientas analíticas en aplicaciones medio ambientales y biomédicas.

Inicialmente se exploró el potencial de LOCs fotónicos (PhLOC) previamente definidos en nuestro grupo, como sistemas en análisis. Se aplicaron sistemas microfluídicos de Reflexión Interna Múltiple (MIR) fabricados en polímeros de bajo coste, como polydimetilsiloxano (PDMS), siguiendo un procedimiento rápido de fabricación, en la detección de diferentes analitos (células e iones de metales pesados) y su funcionamiento se comparó con el de otras técnicas analíticas más convencionales.

Para dotar de selectividad a los PhLOCs se desarrollaron y compararon diferentes protocolos de modificación de superficies para la inmovilización de proteínas en los materiales poliméricos utilizados para la fabricación de estos sistemas. Estos métodos mantienen inalteradas las propiedades ópticas y estructurales del material. Se utilizó la peroxidasa de rábano (HRP) como proteína modelo para estos estudios, y las superficies biofuncionalizadas resultantes se testaron mediante la medición de la actividad enzimática en la reacción de reducción de peróxido de hidrógeno en presencia del mediador redox 2,2'-azino-bis (3-ethylbenzthiazoline-6-sulfonic acid) (ABTS), cuyo producto enzimático de color verde pudo ser detectado mediante medidas de absorbancia. Se midió la robustez del proceso de inmovilización mediante la medida de la actividad del HRP durante un periodo superior a un mes.

Finalmente, se añadieron nuevos componentes fluídicos y funcionalidades a los PhLOCs previamente aplicados para mejorar su desempeño. Estructuras microfluídicas tales como mezcladores biofuncionalizados (actuando en consecuencia como reactores) se integraron monolíticamente con el MIR, dando lugar a un PhLOC con mejores prestaciones analíticas. Estos nuevos elementos disminuyeron el tiempo de análisis y el volumen de muestra y reactivo. Con la integración de una celda electroquímica de oro en el substrato, se desarrolló un LOC con lectura de medida dual (DLOC), que permitió la transducción simultánea óptica y electroquímica e hizo el sistema desarrollado autoverificable, mejorando así su fiabilidad. Se mostró el potencial de este DLOC mediante el desarrollo de una herramienta analítica para la medida de glucosa. Se inmovilizaron glucosa oxidasa (GOx) y HRP siguiendo el protocolo desarrollado en esta Tesis y se aplicaron como receptores específicos para la detección de glucosa basada en una reacción enzimática en cascada utilizando el mediador redox ABTS.

Como estudio adicional, se testó la aplicabilidad del protocolo de funcionalización en diferentes polímeros y también se llevó a cabo la inmovilización de componentes biológicos diferentes a enzimas.

1. GENERAL CONCEPTS

1.1.	Introduction	24
1.2.	Performance of LOCs	25
1.3.	Fabrication, materials and procedures.....	26
1.4.	Surface modification of Microsystems.....	31
1.4.1.	Plasma activation	31
1.4.2.	Chemical vapor deposition (CVD).....	32
1.4.3.	UV irradiation.....	33
1.4.4.	Wet chemical modifications.....	34
1.5.	Detection techniques	36
1.5.1.	UV/Vis absorbance measurement	36
1.5.2.	Fluorescence detection	36
1.5.3.	Chemiluminescence detection	37
1.5.4.	Interferometric detection.....	38
1.5.5.	Surface-enhanced Raman spectroscopy (SERS).....	39
1.5.6.	Surface plasmon resonance (SPR)	40
1.5.7.	Mass spectrometry.....	40
1.5.8.	Electrochemical detection	41
1.5.9.	Surface-acoustic wave (SAW) detection.....	42
1.5.10.	Mechanical detection.....	42
1.6.	Fields of application	43
1.7.	References	44

1.1.Introduction

The term Total Analysis Systems (TAS) refers to analytical platforms that integrate all (or most of) the components required for performing a complete analytical protocol¹. Sampling, sample pre-treatment, chemical reactions, separations, analyte detection, product isolation and data analysis can be directly carried out without minimum manipulation by the user. The starting idea in the development of TAS was to offer a solution to the limited performance of existing sensor devices by offering the possibility to directly manipulate complex samples and incorporate several steps during the analysis^{2,3}. Such systems have greatly evolved by the application of microfabrication processes that gave rise to the miniaturization of the different integrated components and the addition of more and more complex analytical procedures (Figure 1.1).

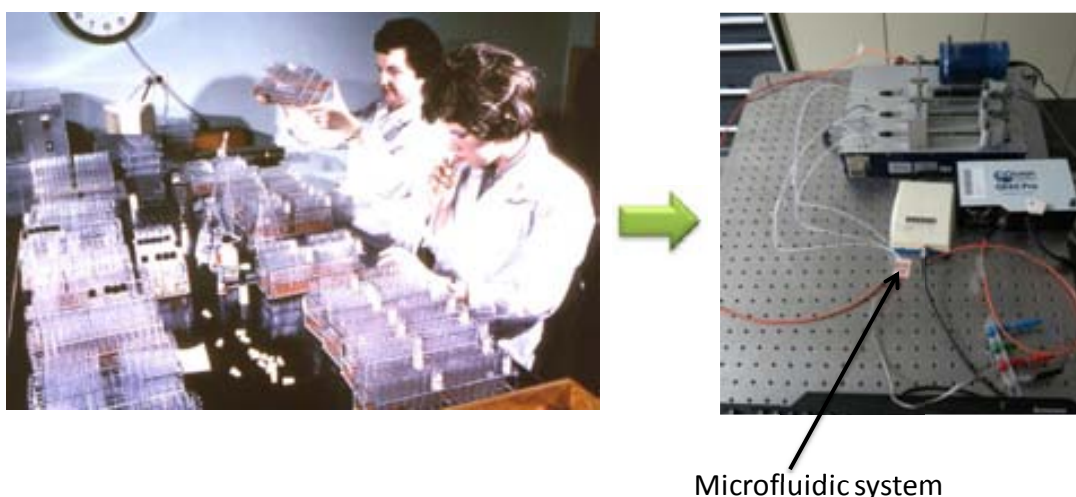


Figure 1.1. Representation of the evolution from standard analytical procedures to the miniaturization of these processes.

Thus, Manz *et al.* in the year 1990⁴ introduced the term Micro TAS (μ TAS), also known as Lab-on-a-Chip (LOC). Usually, LOCs make use of microfluidics. This term refers to the science and technology of systems that process or manipulate small amounts of fluids, in a range from 10^{-9} to 10^{-18} liters. Here, channels between tens and hundreds of micrometers are commonly used⁵, although the technology is nowadays able to provide with structures with much smaller dimensions. Rigorously speaking, the first microfluidic analytical system was presented more than a decade before the introduction of the μ TAS concept by S.C. Terry⁶. From that seminal work, microfluidic systems have dramatically evolved, primarily due to the advances in micro/nanofabrication techniques⁷. Today, a large variety of different structures are ready to be included in LOCs in order to carry out all the required steps in analytical processes, such as channels, reactors, pumps, chromatographic columns or detectors. LOC research field is inherently multi-disciplinary, combining the knowledge of different areas for their design, fabrication and application. Physics provides with the understanding of microfluidics, behavior

of the different materials employed, as well as some detection methods⁸. Microtechnology assures high quality LOC elements, as could be electrodes or other electronic components⁹. Chemistry provides with the chemical reactions that are used in analytical and synthetic processes¹⁰, and also in the chemical modifications of the microsystems¹¹. Biology is also important since many of the applications are biomedical and the incorporation of biosensors into LOC requires the manipulation of biological agents as recognition element¹². All these recent advances have brought important advantages that are not offered by other analytical tools and that will be described below.

1.2. Performance of LOCs

LOCs offer many advantages that come not only from the miniaturization, but also from the emergence of a variety of structures with different purposes for sample handling and manipulation. The advantages include the need of small volume of sample and reagents, separations with a high resolution, low cost set-ups³ and minimization of power consumption and analysis time¹³. Monolithic fabrication processes can be used, reducing dead volumes and eliminating the coupling of different fluidic components that can be cumbersome and may give rise to poor system performance. Miniaturization also enables taking advantage of different physicochemical phenomena that are not dominant at larger scales, such as laminar flow¹⁴, different diffusion regimes¹⁵, electrokinetic pumping¹⁶, surface tension-driven flows¹⁷ or acoustic streaming¹⁸. These phenomena can be used to improve the performance of the systems. While the fluids in the macroscale present a chaotic movement, in microfluidic systems they present a laminar flow behavior, since the fluid viscosity dominates instead of its inertial behavior and thus Reynolds number values below one¹⁴ are common. A fluid with a laminar flow is very predictable and can be used together with other fluids to create gradients of physicochemical properties¹⁹. Péclet number defines the type of mixing that can be found in fluids, by relating diffusive and advective mass transport. In the microscale, diffusion is dominant, since the Péclet number becomes very small ($P \ll 1$)²⁰. Diffusion can be used to mix liquids, or special structures that increase the turbulence can be designed and fabricated in order to reduce the mixing time¹⁵. Separations by on-chip chromatography can also be improved since the elapsed time for the diffusion of analytes from one flow to another is decreased compared to the diffusion at the macroscale². Another property of the miniaturized systems is that the ratio between the liquid volume and the wall surface of the LOC are decreased and the interactions between the walls and the analytes that are found in the liquids get more efficient. This is important for processes like immune-affinity assays, chromatographic interactions and electrochemical detection. However, this last advantage can become a drawback if nonspecific adsorption occurs. Surface modifications are very important to avoid this problem²¹ and several studies have been made in order to solve this problem by depositing protein-repellent molecules on the LOC walls such as polyethylene glycol (PEG)²² or polyvinyl alcohol (PVA)²³.

Hence, it becomes clear why LOCs have evolved from simple microchannels to a myriad of different systems ranging from drop generators to single-cell cultivation systems²⁴⁻²⁹. In this

way, more complex and high throughput experiments can be performed, with multiplexed measurements for the detection of different analytes at the same time.

For the existence of such a high diversity of LOCs the development of microfabrication techniques and new materials has been essential. Here, some of the most usual procedures will be described.

1.3. Fabrication, materials and procedures

The first LOCs were based on silicon micro-machining³⁰. **Silicon** has the advantage of being extensively used by the semiconductor industry. It is a widely studied material that can be patterned by well-established fabrication techniques. Nevertheless, it also has limitations: when applying electrical detection modes, it requires the growth of a relatively thick SiO₂ insulating layer³¹. In addition, it is non-compatible with the strong potentials used in capillary electrophoresis and with electrokinetic pumping, which are widely used in LOCs³². **Glass** has also been used, which is chemically stable and transparent, being suitable for optical detection methods like fluorescence or surface Plasmon resonance (SPR). However, it can present impurities that interfere with the fabrication processes and the final device operation³¹. In the last years, **polymers** have become more popular due to their high chemical resistance and good optical properties. In addition, they can be modified for their functionalization, they are cheap³⁰, biocompatible³¹ and some of them biodegradable (e.g., polycaprolactone, PCL)³³, and their microfabrication process is more cost effective than when working with silicon or glass³².

Many different polymers have been used for the fabrication of LOCs. **Thermoplastics** (Figure 1.2a) such as polystyrene (PS), poly(methyl methacrylate) (PMMA), cycloolefin copolymer (COC) or polycarbonate (PC), are composed of chains that are weakly bonded together, or even not bonded, making it possible to soften with the increase of the temperature. Some of them, such as PC or PMMA, are transparent in the visible part of the electromagnetic spectrum (reaching deep-UV light in the case of COC), making them suitable for fabricating optical detection systems. All these materials are soluble in most organic solvents, but they are resistant to acetonitrile, which is used in liquid chromatography³⁴. They are electrical insulators but they can be functionalized with the adequate substances that make them conducting or to change their magnetic properties³². By contrast, poly(phenylene vinylene) and polyaniline are thermoplastic materials with an inherent conductivity and have been used for the fabrication of electronic components. The **thermosetting** polymers (Figure 1.2b), like poly(dimethyl siloxane) (PDMS), are elastomers that can be patterned on a mold via a cross-linking process. They are not soluble in organic solvents³² and they present a higher thermal and structural stability than thermoplastics³⁵. Overall, in spite of the above mentioned advantages of polymeric materials for LOCs, they also show drawbacks, mostly related to their elastic behavior. They have a low Young's modulus and then microstructures of these materials are prone to collapse and deform. In addition, they show non-specific adsorption to biomolecules, thus limiting their use for bioanalytical applications³¹.

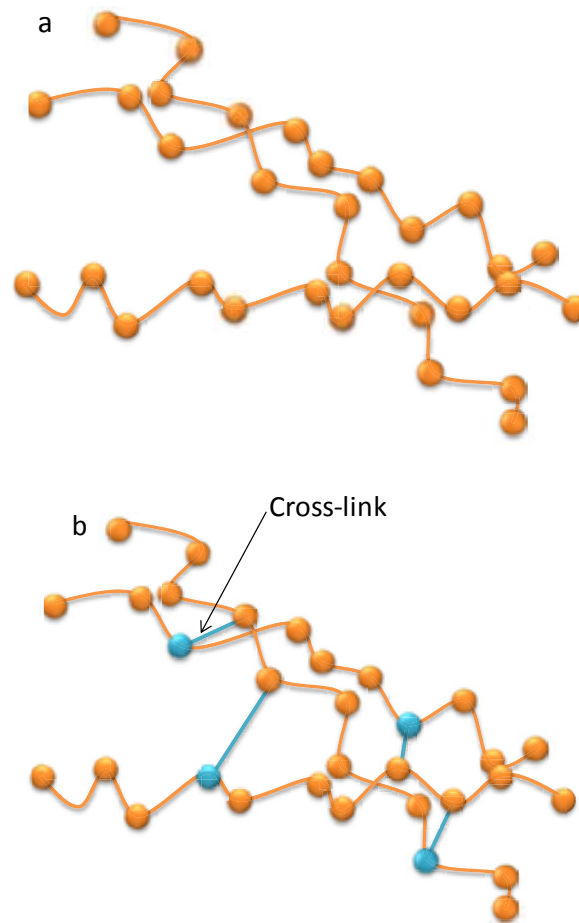


Figure 1.2. Representation of a typical (a) thermoplastic polymer and (b) a thermosetting polymer.

The development of micro-/nanostructures with the mentioned polymeric materials can be carried out using different micro- and nanofabrication techniques. Among them, **soft lithography** (also known as cast molding)³⁶ is a parallel technique widely applied for rapid prototyping and also mass-production, mainly due to its cost-effectiveness and simplicity comparing with the well-known photolithographic processes. It consists of the preparation of a soft mold by casting a liquid polymer precursor against a rigid master. The advantage of soft lithography over other lithographic techniques is that, once the master is obtained, the resolution of the mold is determined by van der Waals interactions, wetting and kinetic factors, but not by optical diffraction. Different polymers can be used for molding, but the most common one is PDMS. Its liquid precursor is mixed with a curing agent and poured over the master, as it is shown in Figure 1.3. Then, it is cured to induce cross-linking and then it is peeled off. The resulting mold can be sealed to define a fluidic structure, or it can be used as another master for printing the desirable material on a surface by microcontact printing³⁷, microtransfer molding³⁸ or micromolding in capillaries³⁹.

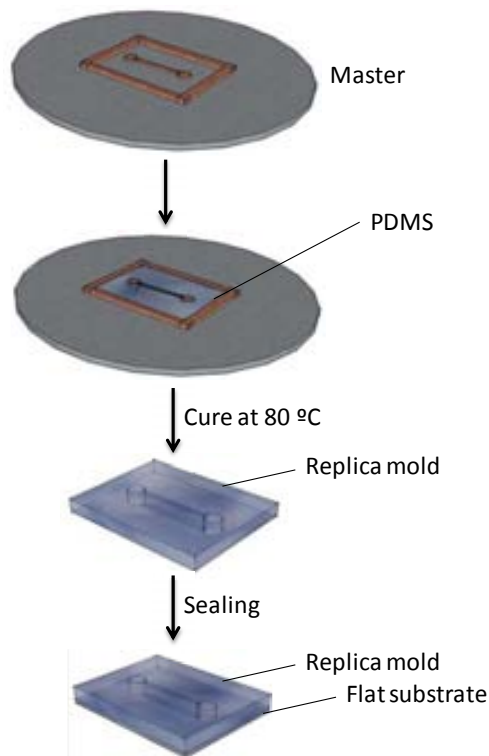


Figure 1.3. Soft lithography process for microfabrication with PDMS.

There are several ways and materials to obtain the master. Some of the most usual materials are photoresists. They are light-sensitive polymers that are coated onto a substrate and patterned through a mask containing the desired geometries, as shown in Figure 1.4. A photochemical reaction is induced on the photoresist with the irradiation using the adequate light power density⁴⁰ (at a specific wavelength, normally being G-, H- or I-line, corresponding to 435.8 nm, 404.7 nm and 365.4 nm, respectively). In positive photoresists, the solubility of the irradiated area increases, while the opposite effect happens in the negative-tone photoresists. Then, the soluble areas are removed by the adequate developer. The master fabrication process is the most expensive and time consuming step in soft lithography, but it only needs to be done once. Replica molding can be carried out many times from one single master to obtain a relatively high number of replicas⁴¹, until the degradation of the master occurs. The most usual photoresist is SU-8, which is an epoxy-based negative resist, invented together by IBM and EPFL and patented in 1989⁴². Using this resist, generally the master withstand up to 50 replicas without compromising its quality.

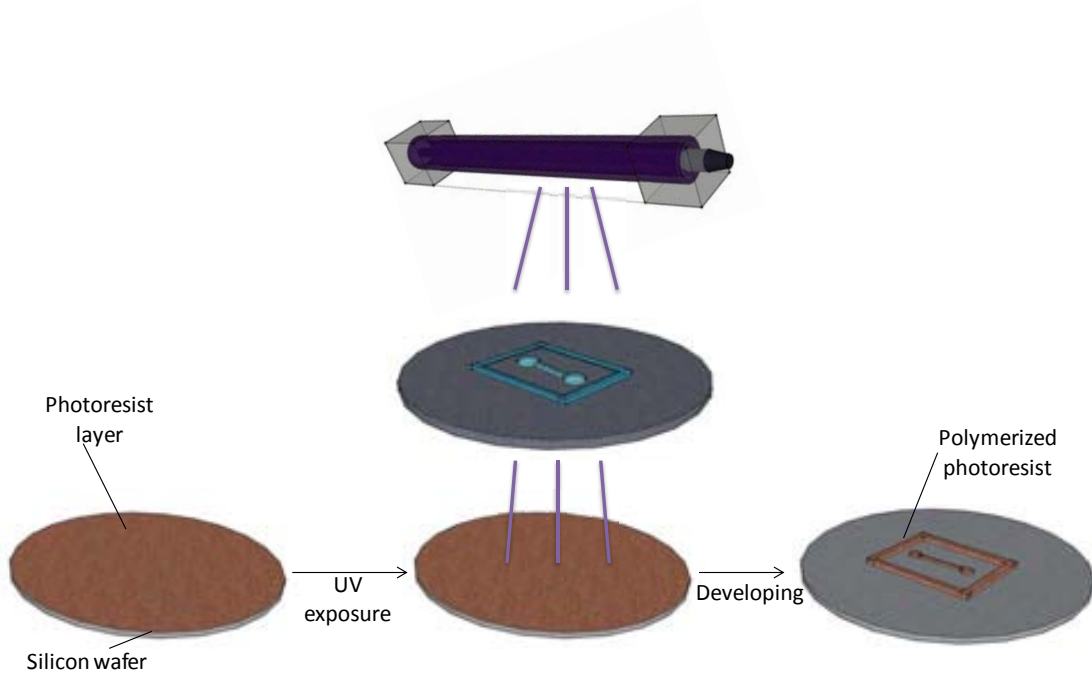


Figure 1.4. Photolithography process using a negative photoresist over a silicon wafer.

Masters, and microsystems in general, can also be fabricated by micromachining. Here, two main techniques are used: Bulk micromachining consists in the selective etching of the substrate material (usually silicon, using the BOSCH process⁴³) in order to define the required structures. A sequence of masking layer formation and etching processes are used (Figure 1.5). An advantage of this technique is that the structure presents high quality, low-stress and excellent mechanical properties. On surface micromachining, a similar process is followed but sequentially deposited layers are patterned and etched. An important advantage of this technique is that the structures obtained can be much smaller than the ones produced by bulk micromachining⁴⁴.

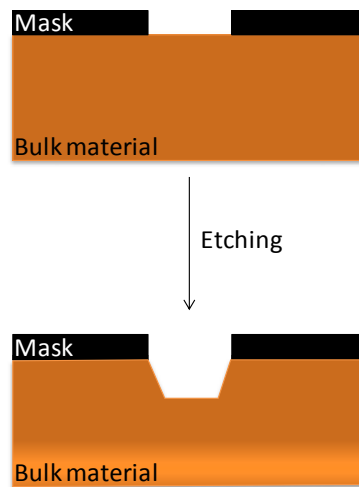


Figure 1.5. Selective removal process on bulk material by etching.

Micromilling can also be used as a low cost alternative towards obtaining masters, enabling the machining of metallic materials, which have a longer duration. However, the diameter of the drill limits the resolution of the structures. This problem can be solved by using the laser machining technique (laser ablation). In this method, a high power density is applied on a very small spot area (up to $>1 \times 10^{14} \text{ W/cm}^2$)⁴⁵. It is suitable for producing high quality structures on hard materials like ceramics, silicon carbide and hardened steel⁴⁶. Another important advantage is that a mask is not required and the pattern can be directly written on the final material, even in 2 ½ dimensions. The main disadvantage is that it is time consuming. In addition, if it is applied on polymers, effective ablation depends on the polymers absorption at the laser wavelength⁴¹.

Once the master is fabricated, the replica mold can be obtained not only by soft lithography as previously described, but also by hot embossing (Figure 1.6a). In this technique, a thermoplastic flat material is heated above its glass transition temperature, with the aim of softening it as it is pressed against the master. Then the material is cooled and the thermoplastic is separated from the master, with the patterns already defined³². It is a rapid, inexpensive, simple and straightforward process. Its resolution is limited by the process used for the fabrication of the master. If three-dimensional structures are desired, injection molding process can be used by melting a polymer inside a closed master under high pressure (Figure 1.6b)⁴¹.

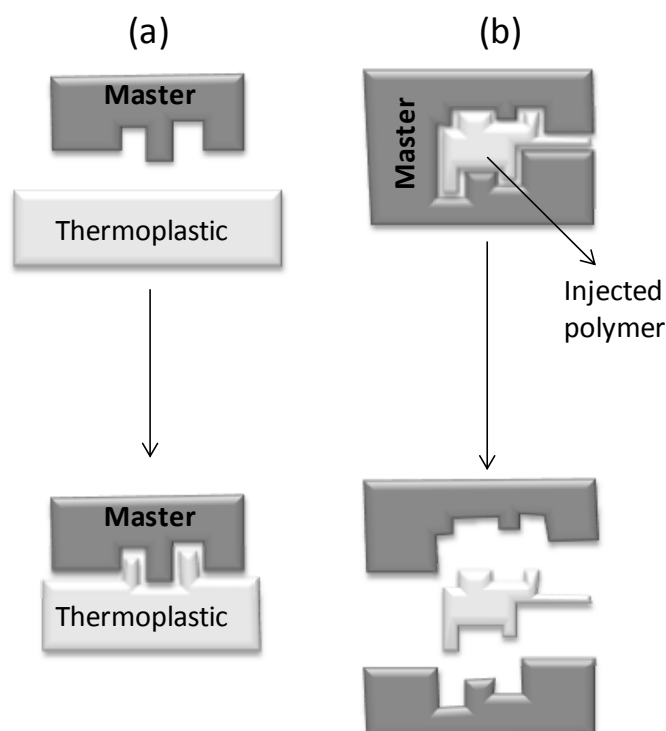


Figure 1.6. Fabrication process by (a) hot embossing and (b) injection molding.

Polymeric materials commonly used for LOC fabrication are hydrophobic and suffer from serious fouling processes when working with hydrophobic molecules and macromolecular structures such as proteins. Here, surface modification processes that avoid or minimize these effects are required²¹. In addition, LOCs sometimes incorporate areas or components that are functionalized with biomolecules in order to provide them with the capacity to selectively interact with target analytes and be applied for separation or sensing purposes⁴⁷. Surface modification procedures for achieving these objectives will be described next.

1.4. Surface modification of Microsystems

There are two categories in which surface modification methods can be divided depending on their effect on the surface: physical and chemical: (i) Physical methods induce the change of roughness, grain sizes and grain boundaries of the material without affecting the chemical composition of the surface. Examples of this group include surface polishing or grinding and thermal treatments⁴⁸. (ii) Chemical methods introduce changes in the chemical composition on the surface of a material by breaking chemical bonds of the polymer structure and creating functional groups.

The main approaches reported so far regarding the chemical methods are described below.

1.4.1. Plasma activation

The energetic species that are present in a plasma (ions, electrons, radicals, metastable species, UV photons) (Figure 1.7) can modify a surface in a variety of ways such as surface activation by introduction of new chemical functionalities, cleaning by removal of contaminants or etching by material volatilization and removal. These processes are limited to the most outer layer of the substrate⁴⁹. The composition of the surface material and the gases used, together with the process parameters (pressure, power and exposure time) have to be controlled in order to optimize the activation process⁵⁰. For example, plasma treatments using oxygen, ammonia or air could generate carboxyl or amine groups on polymer surfaces. The appropriate selection of the plasma source and gas plays a role in the introduction of different surface functional groups. They modulate a variety of surface properties such as wettability, adhesion and biocompatibility. These functional groups could also be useful for the covalent immobilization of other molecules⁵¹. As an example, Peng-Ubol *et al.* applied oxygen plasma to create carboxylic groups on polyethylene surfaces prior to further carry out wet chemical modifications for immobilizing antibodies against *Salmonella Typhimurium*⁵².

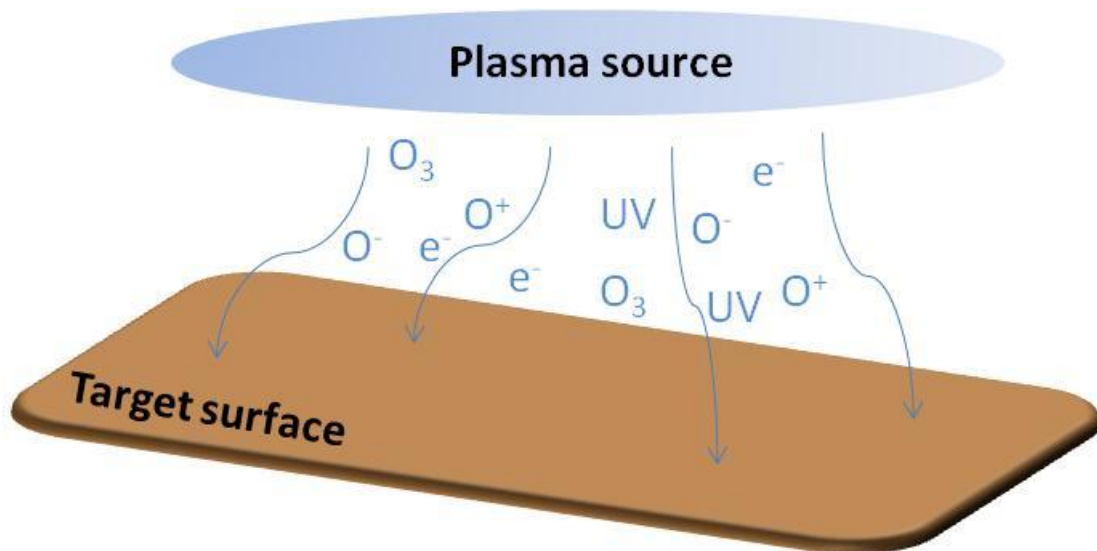


Figure 1.7. Representation of a surface treatment with plasma oxygen.

1.4.2. Chemical vapor deposition (CVD)

This technique consists in the deposition of thin films by reaction of gas phase precursors with the surface of the material, as shown in Figure 1.8. CVD systems deliver a mixture of reactive and carrier gases (typically hydrogen, nitrogen or argon) and volatile reactive compounds (i.e. metal halides, carbonyls or alkoxides). These gases and compounds are flowed over the surface at a controlled temperature. The deposition is achieved by different methods such as thermal decomposition, oxidation and hydrolysis, leading to a reaction between the surface and the constituents of the vapor phase⁵³. As an example, Gupta *et al.* used this method to coat the surface of high aspect ratio capillary pore membranes and silicon trenches with poly(1H,1H,2H,2H-perfluorodecyl acrylate) (PPFDA) with the aim of demonstrating that it is possible to use this method to coat high aspect ratio microstructures with organic polymers⁵⁴.

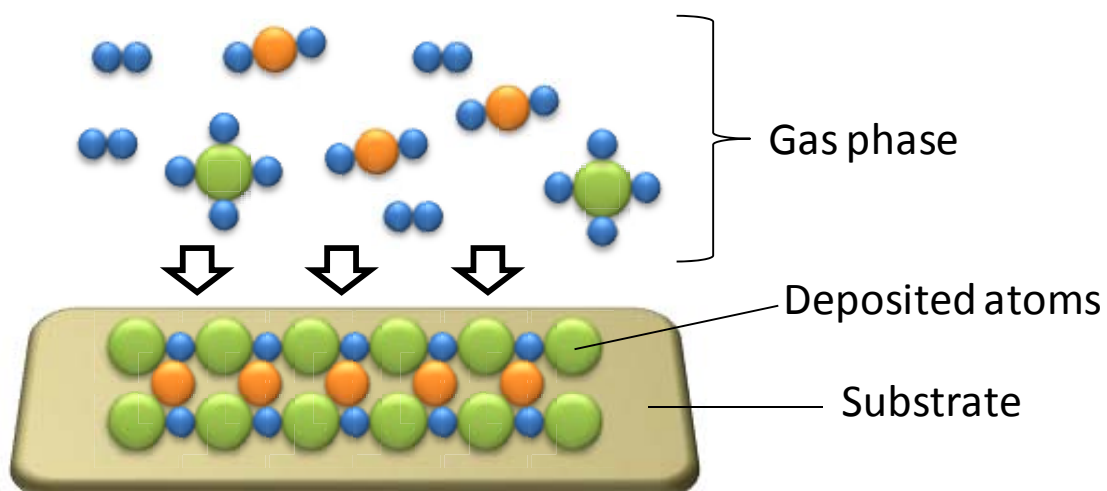


Figure 1.8. Representation of a CVD process.

1.4.3. UV irradiation

This technique is based on the fact that the energy of the photons is high enough to dissociate various chemical bonds, forming free radicals on a surface, which can react with photo-excited species present in the surrounding medium (reactive gases or other specific compounds) (see Figure 1.9)⁵⁰. Okajima *et al.* demonstrated that UV irradiation of poly(butylene terephthalate) (PBT) removes alkyl chains and ester bonds and forms anhydride groups⁵⁵. This process does not require costly equipment and patterned surface modifications can be carried out by using lithographic techniques⁵⁶. However, if lasers are used to perform the irradiation in specific small areas instead of UV lamps, the cost can be increased considerably⁵⁰.

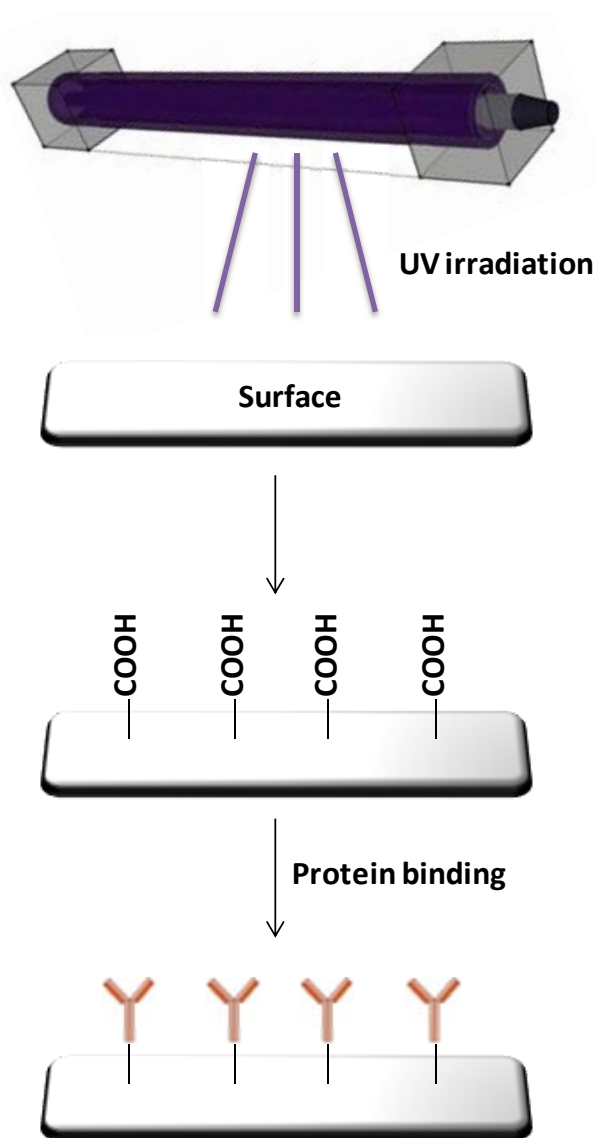


Figure 1.9. Representation of a surface modification process by UV irradiation.

1.4.4. Wet chemical modifications

Functional groups can be introduced on surfaces by directly incubating liquid phase reagents. These treatments are sometimes preferred due to their low cost compared to plasma processes¹¹. Once these groups are introduced, other molecules can be easily attached through covalent bonds. As an example, the hydrophilic nature of silicon oxide can be improved by immersion in an acidic solution of hydrogen peroxide. The reactivity of silanes with the silanol groups of silicon oxide can be used to introduce new functional groups through incubation in a silane containing solution⁵⁷. 3-aminopropyltriethoxysilane (APTES) is a very common silane and it introduces amine groups on the modified surface (Figure 1.10). These groups can further react with a crosslinker (i.e. glutaraldehyde) in order to obtain new additional groups that enabled the covalent attachment of proteins or other biomolecules. Molecules containing amine and ester residues can also be attached to surfaces that present carboxylic groups with the help of thionyl chloride or 1-ethyl-3-(dimethylaminopropyl)carbodiimide (EDC)⁵⁸. Following this approach, Brault *et al.*⁵⁹ activated carboxylic acid groups on a chip surface by submerging them in an aqueous solution of EDC and N-hydroxysuccinimide (NHS) prior to the immobilization of antibodies. The attached antibodies could then detect different analytes directly from undiluted human plasma.

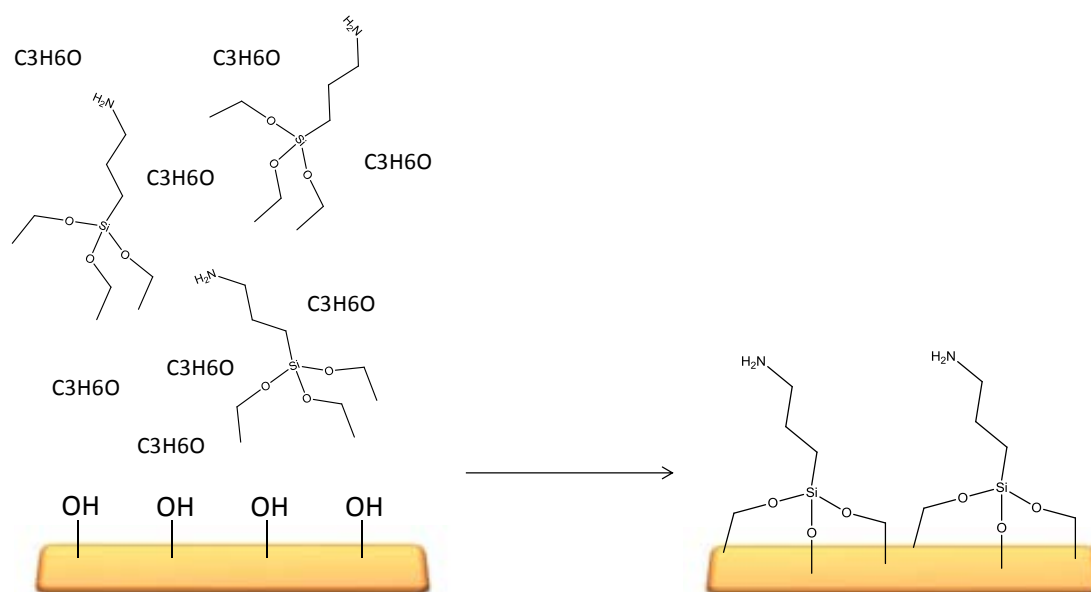


Figure 1.10. Representation of the silanization process of a hydroxylated surface with APTES in an acetone solution.

One very specific kind of wet chemistry is the modification by sol – gel chemistry. The term sol – gel refers to a process that includes hydrolysis and condensation reactions of precursors to synthesize inorganic or hybrid organic-inorganic polymer matrices. It includes two main steps (represented in Figure 1.11): the formation of a colloidal suspension, the sol, which upon further assembly and drying gives rise to a gel. Further curing and ageing steps produces stable polymeric materials. Dopants can be included inside the gel in order to provide it with the desired functional properties⁶⁰. Carregal-Romero *et al.*⁶¹ used this technique for the fabrication

of polymers doped with fluorescent molecules and demonstrated their performance by fabricating waveguides with absorption and emission bands that corresponded to the doping dyes. Orhan *et al.*⁶² used the sol – gel technique to modify a PDMS microchannel with a coating using tetraethyl orthosilicate and trimethoxyboroxine as precursors. This coating served as a protector with no cracks for PDMS, avoiding the diffusion of harsh chemicals chemicals as toluene that could swell PDMS. The diffusion was visualized using the fluorescent dye rhodamine B dissolved in toluene.

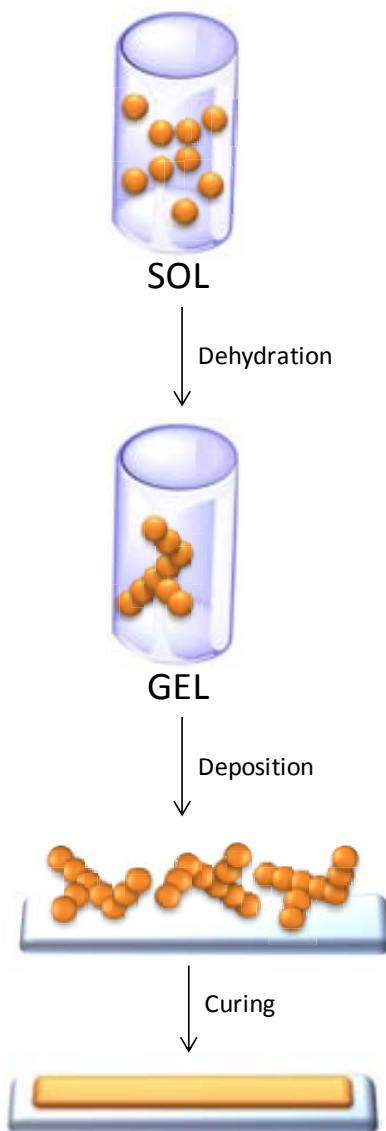


Figure 1.11. Representation of a surface modification process by sol – gel chemistry.

The previously described fabrication and modification methods also depend on the detection technique that will be used. Due to the growing popularity of LOCs and their great diversification, many detection methods have been reported, being most of them optical,

electrochemical or mass detection methods. These can be integrated in the LOCs following different strategies, as is described below.

1.5. Detection techniques

1.5.1. UV/Vis absorbance measurement

In this technique (represented in Figure 1.12), a spectrophotometer is used to measure the attenuation of the light as it crosses the sample. A spectrum of the light is obtained and the peaks located therein are used to identify the compounds and their concentration that are present in the sample⁶³. This method is very common in biochemical analysis⁶⁴. Optical signals present immunity to electromagnetic interferences and multiplexed detection can be carried out in a single system⁶⁵. In addition, the cost of the fabrication is low since micro-optic structures can be defined in a single photolithographic step and fabricated in one single polymer piece⁶⁶. However, the miniaturization of the LOCs leads to a shortening of the optical path length, decreasing the absorbance signal which is proportional to it⁶⁷. This problem was solved by Llobera *et al.* by including air mirrors that lengthen the optical path⁶⁸. As an example of a LOC with optical readout, Balslev *et al.*³⁰ presented a system with a liquid dye laser, waveguides and fluidic channels with mixers. The laser emitted the light into five waveguides that brought the light to a fluidic channel that plays the role of a spectrophotometry cuvette and that transmitted the light to a photodiode array for the absorbance measurements. A microfluidic mixer directs the samples to the cuvette in order to obtain the absorbance results of different fluid mixes. They tested the LOC with a Rhodamine 6G solution as laser dye for the absorbance measurement of different xylenol orange dye concentrations.

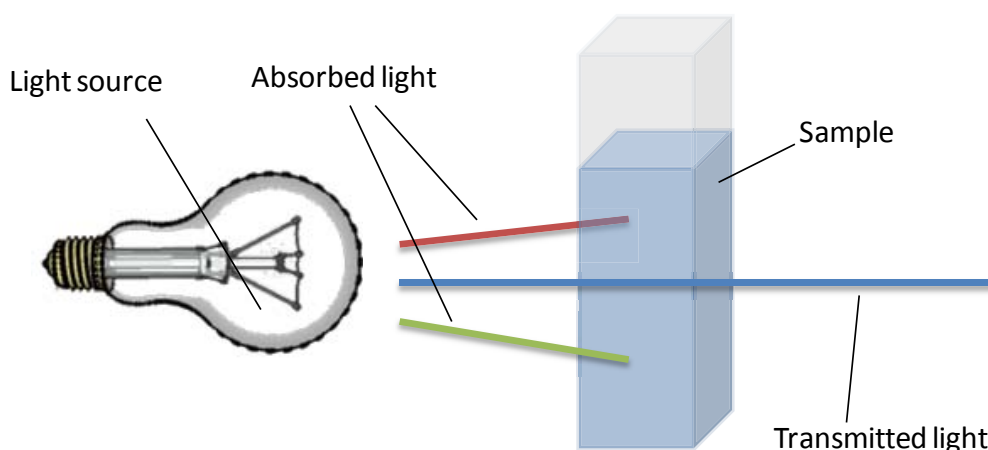


Figure 1.12. Representation of absorbance process of a sample.

1.5.2. Fluorescence detection

In this method, which is shown in Figure 1.13, a light source (typically a laser) is used to excite a fluorescent sample. Its emission is detected by either a photodetector or a spectrometer⁶⁹. It

is widely used for molecular sensing as it is very well-established, very sensitive⁶³ and suitable when working with small sample volumes. However, it is limited to the detection of analytes showing inherent fluorescent properties or labeled with fluorescent molecules⁷⁰. A problem when using this method is that the Stokes shift (difference between excitation and emission wavelengths) is generally very short, thus requiring expensive, orientation dependent interferometric filters. In addition, many polymers and even some molecules present auto-fluorescence, which may interfere in the detection of the target analyte⁶³. Finally, mercury lamps and lasers are used as light sources⁶⁹ as well as detectors attached to microscopes, which makes the setup bulky and expensive. For this reason, miniaturization of the different elements of the setup is being pursued. Carregal-Romero *et al.* for example, developed xerogel polymeric absorbance micro-filters that could be integrated into microfluidic devices in order to eliminate the signal of the excitation light⁷¹. Lefevre *et al.* published a microfluidic chip for water pollutant detection that presented a blue organic light emitting diode (OLED) for illumination, an organic photodetector (OPD) to detect the emission of the excited sample (algal fluorescence in the near infrared region), a filter between the OLED and the detection chamber to eliminate the undesired part of the OLED emission, and a second filter between the detection chamber and the OPD to remove the excitation light that was not adsorbed by the algae⁷².

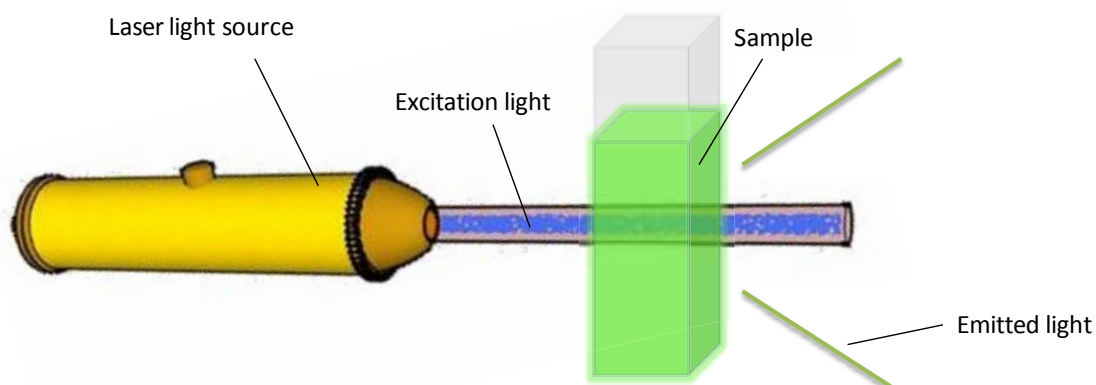


Figure 1.13. Representation of fluorescence emission process of a sample.

1.5.3. Chemiluminescence detection

This technique is similar to the fluorescence detection, but the emission of light is photochemically caused by a specific reaction with the target analyte (Figure 1.14). In this way, the excitation light source is avoided. Very sensitive detectors are required due to the weak intensity that the signal commonly shows⁶³. Nevertheless, the technique is highly sensitive, it provides with wide linear measurable ranges, simple instrumentation is required and there is no interference from background light⁷³. Kamruzzaman *et al.* presented a microfluidic chip for the detection of L-phenylalanine by detecting the enhancement effect that this compound has

on the chemiluminescent signal of the luminol-Cu²⁺-hydrogen peroxide (H₂O₂) system in an alkaline medium⁷⁴.

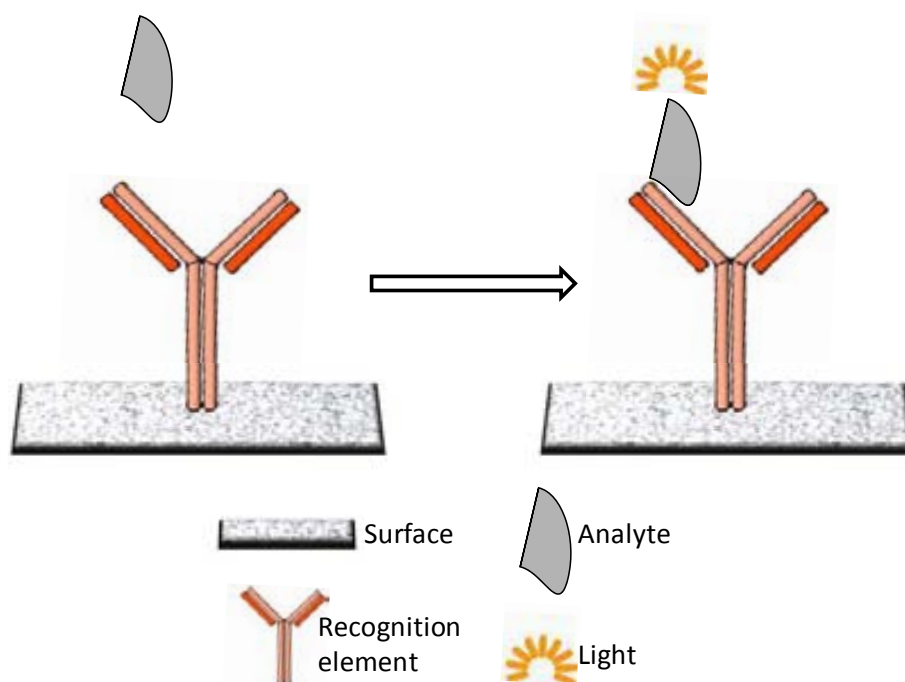


Figure 1.14. Representation of chemiluminescence emission of an analyte after its recognition process.

1.5.4. Interferometric detection

For carrying out this method (Figure 1.15), a single light source is split into two beams. Only one of them is sensitive to the analyte present in the sample, which causes a change in the effective refractive index. This, in turn results in a phase shift that, when recombining the optical beams, produces an interferometric pattern. It is highly sensitive and can be readily used for label-free detection approaches⁶³. Their main disadvantages are the complexity of the design, fabrication and required positioning accuracy⁷⁵.

Crespi *et al.*⁶⁵ for example designed a three-dimensional Mach-Zehnder interferometer, which was integrated in two different microfluidic chips: a self-made one and a commercial LOC for capillary electrophoresis, providing label-free detection with a spatial resolution of about 10 μm . They tested the interferometer integrated in the self-made chip by monitoring the change in the refractive index due to the transition between pure water and glucose solutions of different concentrations, while the interferometer integrated in the commercial LOC was tested by measuring the change between ethanol and peptides after a calibration with glucose solutions. They obtained a limit of detection (LOD) of 5 mM glucose with the first approach, while the second one presented a larger responsivity and a LOD of 5 mM for the glucose and 9 mM for the peptides.

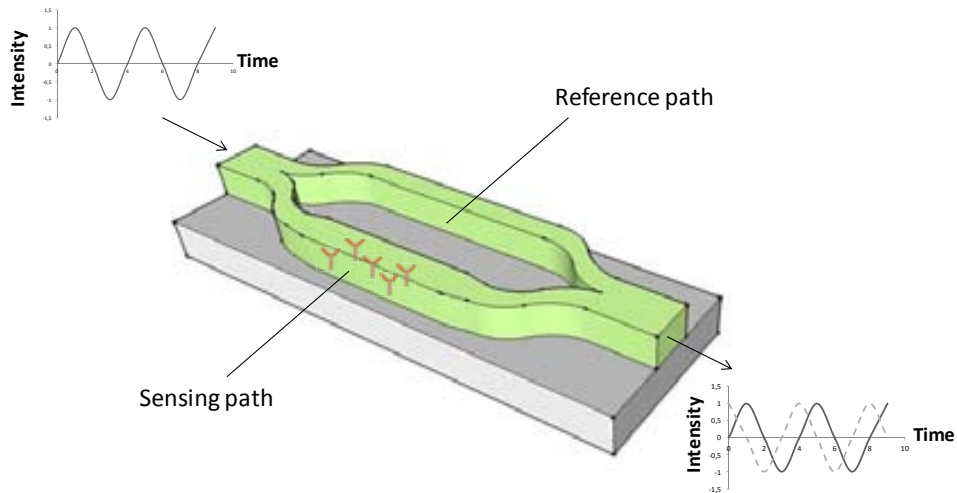


Figure 1.15. Representation of an interferometric detection system.

1.5.5. Surface-enhanced Raman spectroscopy (SERS)

SERS is a very sensitive technique (Figure 1.16) that makes use of a nanostructured surface whose Raman scattering response is enhanced by the adsorption of molecules⁷⁶. However, it is limited by the inconsistency in the reproducibility and preparation of the substrates, requiring an optimization of the nanofabrication strategies⁷⁷.

Taylor *et al.* fabricated a microfluidic separation device that integrated a diffusive mixing region for SERS detection of analytes during continuous monitoring, and they tested it by detecting rhodamine 6G⁷⁸.

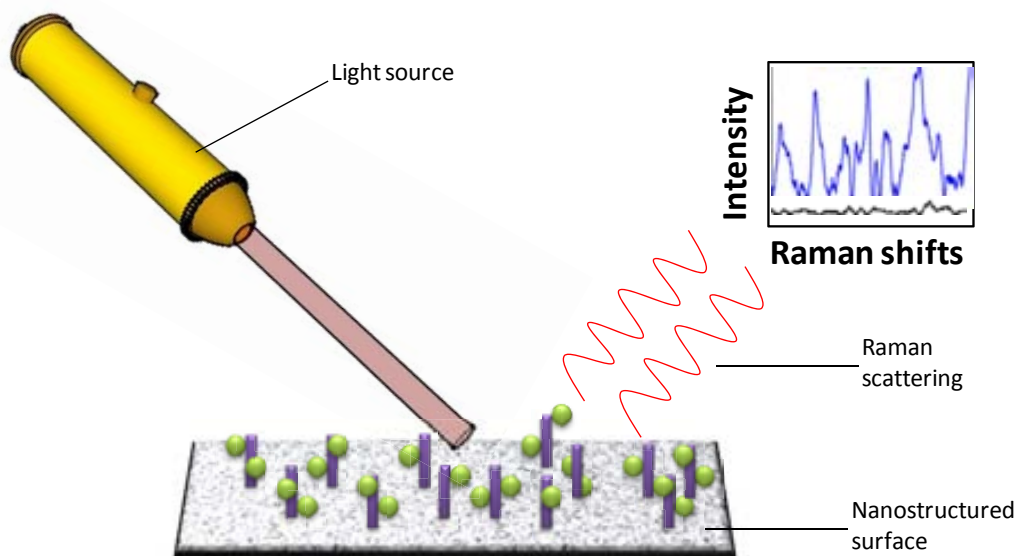


Figure 1.16. Representation of a surface-enhanced Raman spectroscopy detection process.

1.5.6. Surface plasmon resonance (SPR)

In this technique, a polarized light beam is focused onto a noble metal layer and it is reflected to a detector. At a specific incidence angle, the oscillating electric charges (called surface plasmon) generated in the metal layer resonate with the light, resulting in light absorption. A shift in this resonance can be measured as a consequence of the change on the thickness or the refractive index of the sensing layer, for example after a recognition process during the analytical experiment⁷⁹. It is a label free technique that is carried out in real time, it is specific, rapid and cost-effective⁸⁰. The plasmon field has a small penetration depth into the aqueous media, being the bulk effects from the analyte solution negligible. This makes the signal readable before carrying out the washing steps. However, an immobilization of a recognition element is needed and the tethering of molecules to the surface can affect the measurement⁸¹. A representation of the technique in Kretschmann configuration can be seen in Figure 1.17. Ouellet *et al.* developed a microfluidic device with a serial dilution network for the simultaneous detection of up to six different analyte concentrations by SPR. The device was tested by monitoring the immobilization, binding and regeneration processes for human factor IX, human α -thrombin and their respective antibodies⁸².

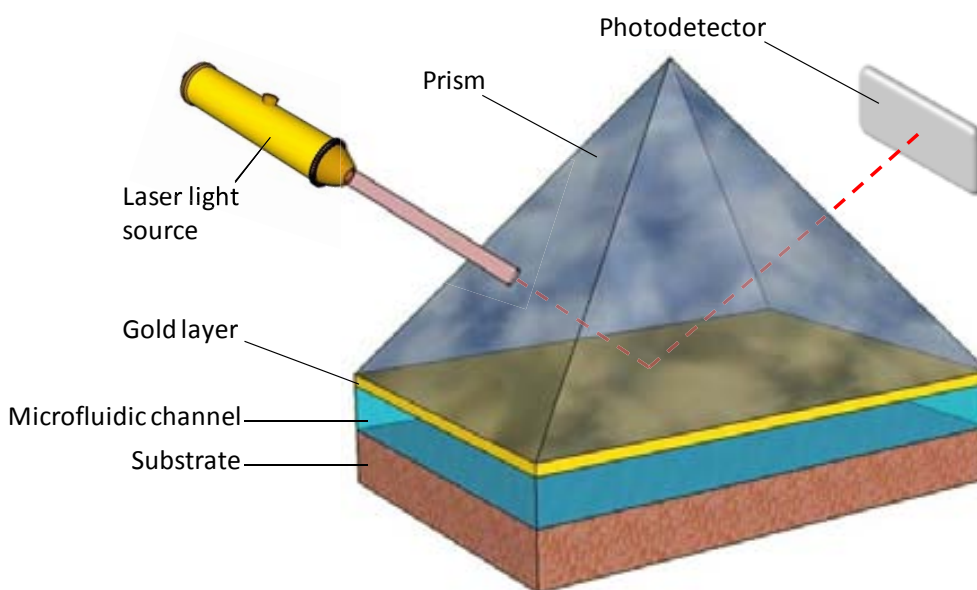


Figure 1.17. Representation of the detection by surface plasmon resonance using the Kretschmann configuration.

1.5.7. Mass spectrometry

This technique (shown in Figure 1.18) is based on the measurement of mass-to-charge ratio of ions generated by fragmentation of molecules by electrospray ionization (ESI). The miniaturization of the electrospray device improves the results when compared to the ones obtained with their bulky counterparts⁷⁰. Rob *et al.* published a microfluidic device for time resolved ESI-mass spectrometry that incorporated a capillary mixer and they characterized it by monitoring acid induced cytochrome *c* unfolding kinetics⁸³.

Mass spectrometry by ESI can be problematic with samples that contain high concentration of salts or other non-desired compounds because the formation of ions can be suppressed making the analysis cumbersome. In addition, the interpretation of the spectra is challenging since many peaks can appear due to the generation of many different charged species⁸⁴.

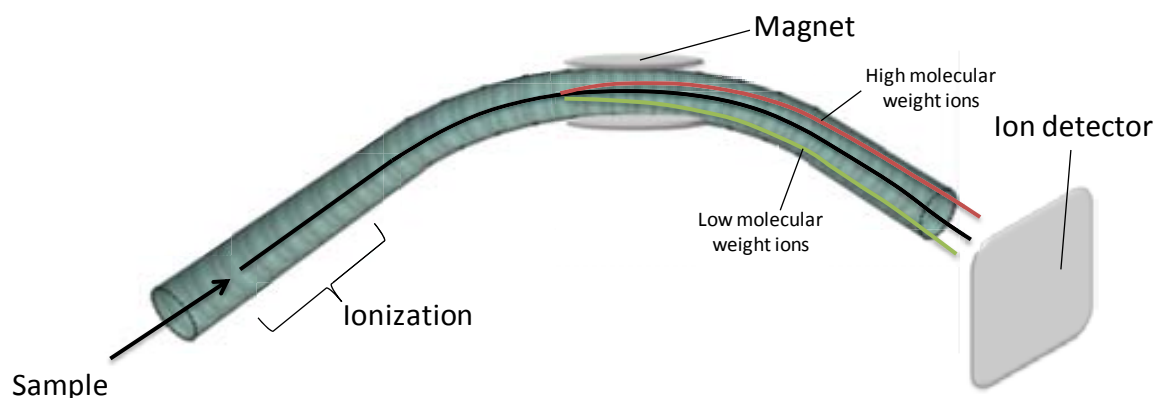


Figure 1.18. Representation of the mass spectrometry detection technique.

1.5.8. Electrochemical detection

This method is based on the charge transfer processes taking place at the interface between a solution and a transducer device (electrode) (Figure 1.19). Most of them rely on the polarization of the electrode at potentials at which redox reactions of electroactive species take place. These reactions give rise to the measurement of faradaic currents, which are related to the concentration of the electroactive species in solution. The potentials at which the redox reactions of the target analytes occur are quite selective for each compound. This characteristic can be used for analyte identification⁷⁰. Unlike the UV/Vis absorbance technique, electrochemical devices can be miniaturized without any loss of sensitivity and materials do not need to be transparent. Another notable difference is that with electrochemistry, only analytes present at the electrode solution interface are detected while with UV/Vis absorbance measurements all the volume through which the light passes can be considered the interrogation region. Microelectrodes can be easily fabricated by conventional microfabrication methods. However, this technique cannot be applicable to any target analyte, as is restricted to those showing electroactivity or that can be labeled with electroactive species. Another drawback of these techniques is that the surface-to-volume ratio is high and adsorption of analytes on electrodes is difficult to avoid⁸⁵. This usually gives rise to fouling of the electrodes by sample components or chemical species produced during the analysis that limit the sensitivity of the analysis or can even inhibit the electrode response. Webster *et al.* carried out the electrochemical detection of pyocyanin using a nanofluidic chip that integrated a palladium hydride reference electrode and a gold working electrode⁸⁶.

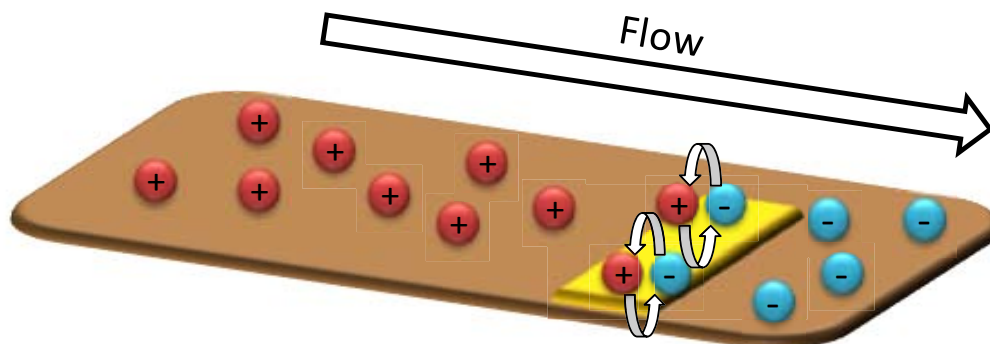


Figure 1.19. Representation of the electrochemical detection method.

1.5.9. Surface-acoustic wave (SAW) detection

This technique (Figure 1.20) uses the changes in the propagation of acoustic waves through a surface due to changes in the mass or viscosity produced on the surface layer. SAW systems operate at high frequencies, which leads to high sensitivities because the penetration depth of the acoustic wave into the adjacent media is reduced, being in this way more sensitive toward the changes occurred on the substrate surface⁸⁷. They can also be low-cost and simple, and they have a good mechanical property. However, they present low chemical resistance and poor stability due to the piezoelectric substrate⁸⁸. Länge *et al.* integrated a SAW biosensor in a microfluidic chip for the monitorization of the adsorption of bovine serum albumin (BSA)⁸⁹.

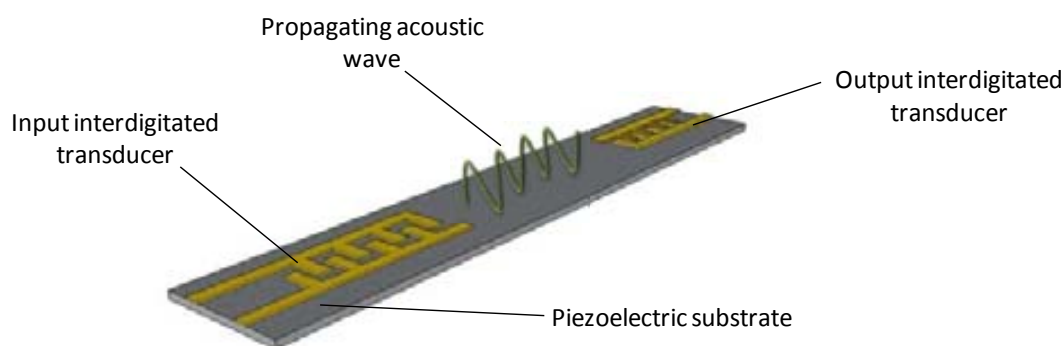


Figure 1.20. Representation of a SAW detection system.

1.5.10. Mechanical detection

Micromechanical structures are integrated into LOCs and functionalized with probe molecules to selectively recognize the analytes of a sample. The most common geometry is with cantilever-like structures. The mass changes taking place on the surface upon the selective binding process induce the deflection of the cantilever. Figure 1.21 illustrates an example of an antigen binding event to an antibody-functionalized cantilever. The deflection of the cantilever or the shift in the resonant frequency can be optically (with a laser beam)⁹⁰ or electrically (with piezoresistors)⁹¹ measured, respectively. The main advantage of this detection system is that it is label free, but its low signal-to-noise ratio (SNR) together with the long response times are

important obstacles⁹². Bosco *et al.* applied a DVD-based read-out system with cantilever arrays for vapor and liquid phase detection of 2,4-dinitrotoluene (DNT)⁹⁰.

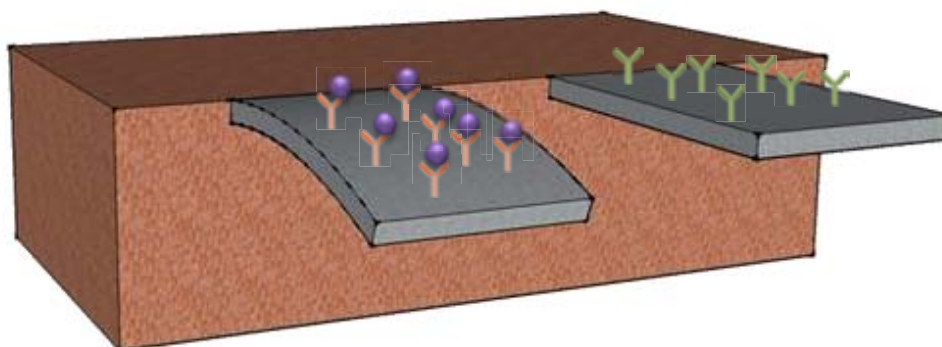


Figure 1.21. Representation of the deflection of a cantilever after the mass increase due to the antigen reaction with the antibody recognition element. The cantilever where no recognition process takes place does not deflect.

1.6. Fields of application

Clearly, cheap, portable and disposable LOCs may represent a breakthrough in healthcare medicine and high-throughput drug discovery⁹³. Here, it is the biological and biomedical fields, including drug screening, single cell or single molecule analyses, biosensing and point-of-care diagnostics (POC), the main fields of application of LOCs. Genetic analyses can be done by integrating fluidic and thermal components such as heaters and temperature sensors carrying out on-chip polymerase chain reactions (PCR)⁹⁴. Proteins can also be analyzed and their reactions can be monitored in real time⁹⁵. Even complete cells and cell cultures can be manipulated and analyzed by using biocompatible materials and controlling temperature⁹⁶. Biomolecules and pathogens can be identified and quantified by incorporating chip-based biosensors in LOCs³¹. The use of high-throughput systems could accelerate the required bioassays for the discovery of new drugs⁹⁷. Finally, POC diagnostics cannot be understood without the application of LOCs, leading to cheap, portable and easy-to-use tests that can be used for early detection of a disease and in decentralized disease screening programmes without the need of a specialized training and can be also applied in the developing countries or in disaster situations⁹³.

Less numerous applications have been carried out in the environmental, food and toxicological fields³. As examples, water contaminants like nitrates and nitrites have been analyzed in a system by performing colorimetric measurements⁹⁸; bacterial contamination (*Listeria monocytogenes*) in food has been genetically detected by capillary electrophoresis⁹⁹; and cocaine has been optically detected by a mid-infrared waveguide integrated with a microfluidic chip¹⁰⁰.

As example of highly developed LOCs that have already been applied to analyte detection in real samples, Kim *et al.*¹⁰¹ published a fully integrated centrifugal microfluidic system capable

of carrying out detection of analytes directly from biological samples (blood, urine, saliva). It performs an enzyme-linked immune-sorbent assay (ELISA) and then a flow-enhanced electrochemical detection. This was validated for the quantification of C-reactive protein. Fragoso *et al.*¹⁰² presented a microsystem with several parts. First, a fluid storage section is found, which consists of five reservoirs to store the reagents and the sample. Second, an electrochemical detection zone is defined, which incorporates electrode arrays divided in separate chambers for performing the measurements from the samples and for the calibration. The system integrates various microfluidic operations such as reagent storage and transport, metering, incubation and detection. It was validated for antibody-based detection of protein markers of breast cancer, also in real serum samples.

1.7. References

1. J. Hübner, K.B. Mogensen, A.M. Jorgensen, P. Friis, P. Telleman, J.P. Kutter. Integrated optical measurement system for fluorescence spectroscopy in microfluidic channels. *Review of Scientific Instruments* 72(1), **2001**, 229-233.
2. M.U. Kopp, H.J. Crabtree, A. Manz. Developments in technology and applications of microsystems. *Current Opinion in Chemical Biology* 1, **1997**, 410-419.
3. A. Ríos, M. Zougagh, M. Avila. Miniaturization through lab-on-a-chip: Utopia or reality for routine laboratories? *Analytica Chimica Acta* 740, **2012**, 1-11.
4. A. Manz, N. Graber, H.M. Widmer. Miniaturized total chemical analysis systems: a novel concept for chemical sensing. *Sensors and Actuators B1*, **1990**, 244-248.
5. G. Whitesides. The origins and the future of microfluidics. *Nature* 442, **2006**, 368-373.
6. S. Terry. A gas chromatography system fabricated on a silicon wafer using integrated circuit technology. Ph.D. dissertation, department of Electrical, Stanford University, Stanford, California, USA, 1975.
7. M.J. Madou. Manufacturing Techniques for Microfabrication and Nanotechnology. *CRC Press*, **2009**.
8. D.J. Beebe, G.A. Mensing, G.M. Walker. Physics and applications of microfluidics in biology. *Annual Review of Biomedical Engineering* 4, **2002**, 261-286.
9. S. Cheng, Z. Wu. Microfluidic electronics. *Lab on a Chip* 12, **2012**, 2782-2791.
10. C.J. Kastrupp, M.K. Runyon, E.M. Lucchetta, J.M. Price, R.F. Ismagilov. Using chemistry and microfluidics to understand the spatial dynamics of complex biological networks. *Accounts of Chemical Research* 41(4), **2008**, 549-558.
11. S. Siau, A. Vervaet, E. Schacht, U. Demeter, A.V. Calster. Epoxy polymer surface modification through wet-chemical organic surface synthesis for adhesion improvement in microelectronics. *Thin Solid Films* 495, **2006**, 348-356.
12. L. De Stefano, E. Orabona, A. Lamberti, I. Rea, I. Rendina. Microfluidics assisted biosensors for label-free optical monitoring of molecular interactions. *Sensors and Actuators B* 179, **2013**, 157-162.
13. J.D. Salgado, K. Horiuchi, P. Dutta. A conductivity-based interface tracking method for microfluidic application. *Journal of Micromechanics and Microengineering* 16, **2006**, 920-928.

14. A.E. Kamholz, P. Yager. Theoretical analysis of molecular diffusion in pressure-driven laminar flow in microfluidic channels. *Biophysical Journal* 80, **2001**, 155-160.
15. C.C. Hong, J.W. Choi, C.H. Ahn. A novel in-plane passive microfluidic mixer with modified Tesla structures. *Lab on a Chip* 4, **2004**, 109-113.
16. J. Yang, D. Kwok. Analytical treatment of electrokinetic microfluidics in hydrophobic microchannels. *Analytica Chimica Acta* 507(1), **2004**, 39-53.
17. C. Galusinski, P. Vigneaux. On stability condition for bifluid flows with surface tension: application to microfluidics. *Journal of Computational Physics* 227(12), **2008**, 6140-6164.
18. M. Wiklund, R. Green, M. Ohlin. Acoustofluidics 14: applications of acoustic streaming in microfluidic devices. *Lab on a Chip* 12, **2012**, 2438-2451.
19. M.A. Holden, S. Kumar, E.T. Castellana, A. Beskok, P.S. Cremer. Generating fixed concentration arrays in a microfluidic device. *Sensors and Actuators B* 92, **2003**, 199-207.
20. T. Kulrattanak. R.G.M. van der Sman, C.G.P.H. Schroën, R.M. Boom. Classification and evaluation of microfluidic devices for continuous suspension fractionation. *Advances in Colloid and Interface Science* 142, **2008**, 53-66.
21. J. Zhou, A.V. ellis, N.H. Voelcker. Recent developments in PDMS surface modification for microfluidic devices. *Electrophoresis* 31, **2010**, 2-16.
22. H. Bi, S. Meng, Y. Li, K. Guo, Y. Chen, J. Kong, P. Yang, W. Zhong, B. Liu. Deposition of PEG onto PMMA microchannel surface to minimize nonspecific adsorption. *Lab on a Chip* 6, **2006**, 769-775.
23. D.A. Barret, M.S. Hartshorne, M.A. Hussain, P.N. Shaw, M.C. Davies. Resistance to nonspecific protein adsorption by poly(vinyl alcohol) thin films adsorbed to a poly(styrene) support matrix studied using surface plasmon resonance. *Analytical Chemistry* 73, **2001**, 5232-5239.
24. R.W. Applegate, J. Squier, T. Vestad, J. Oakey, D.W.M. Marr, P. Bado, M.A. Dugan, A.A. Said. Microfluidic sorting system based on optical waveguide integration and diode laser bar trapping. *Lab on a Chip* 6, **2006**, 422-426.
25. J. West, A. Michels, S. Kittel, P. Jacob, J. Franzke. Microplasma writing for surface-directed millifluidics. *Lab on a Chip*, 2007, **7**, 981-983.
26. A.M. Skelley, O. Kirak, H. Suh, R. Jaenisch, J. Voldman. Microfluidic control of cell pairing and fusion. *Nature Methods* 6, **2009**, 147-152.
27. H.N. Joensson, M.L. Samuels, E.R. Brouzes, M. Medkova, M. Uhlén, D.R. Link, H. Andersson-Svahn. Detection and analysis of low-abundance cell-surface biomarkers using enzymatic amplification in microfluidic droplets. *H. Angewandte Chemie International Edition* 48(14), **2009**, 2518-2521.
28. J. Godin, C.H. Chen, S.H. Cho, W. Qiao, F. Tsai, Y.H.J. Lo. Microfluidics and photonics for bio-system-on-a-chip: a review of advancements in technology towards a microfluidic flow cytometry chip. *Journal of Biophotonics* 1(5), **2008**, 355-376.
29. S. Lindström, R. Larsson, H. Andersson-Svahn. Towards high-throughput single cell/clone cultivation and analysis. *Electrophoresis* 29(6), **2008**, 1219-1227.
30. S. Balslev, A.M. Jorgensen, B. Bilenberg, K.B. Mogensen, D. Snakenborg, O. Geschke, J.P. Kutter, A. Kristensen. Lab-on-a-chip with integrated optical transducers. *Lab on a Chip* 6, **2006**, 213-217.

31. S. Prakash, M. Pinti, B. Bhushan. Theory, fabrication and applications o microfluidic and nanofluidic biosensors. *Philosophical Transactions of the Royal Society A* 370, **2012**, 2236-2303.
32. P. Abgrall, A.M. Gué. Lab-on-chip technologies: maiking a microfluidic network and coupling it into a complete microsystem – a review. *Journal of Micromechanics and Microengineering* 17, **2007**, R15-R49.
33. D.K. Armani, C. Liu. Microfabrication technology for polycaprolactone, a biodegradable polymer. *Journal of Micromechanics and Microengineering* 10, **2000**, 80-84.
34. C.W. Tsao, D.L. DeVoe. Bonding of thermoplastic polymer microfluidics. *Microfluidics and Nanofluidics* 6, **2009**, 1-16.
35. N.B. Shenogina, M. Tsige, S.S. Patnaik, S.M. Mukhopadhyay. Molecular modeling of elastic properties of thermosetting polymers using a dynamic deformation approach. *Polymers* 54, **2013**, 3370-3376.
36. Nanotechnologies: Principles, applications, implications and hands-on-activities. *European Commission*, **2012**, Chapter 7: Fabrication methods, 139-141.
37. A. Kumar, G.M. Whitesides. Features of gold having micrometer to centimeter dimensions can be formed through a combination of stamping with an elastomeric stamp and an alkanethiol “ink” followed by chemical etching. *Applied Physics Letters* 63(14), **1993**, 2002-2004.
38. Y. Xia, E. Kim, X. Zhao, J. Rogers, M. Prentiss, G.M. Whitesides. Complex optical surfaces by replica molding against elastomeric masters. *Science* 273, **1996**, 347-349.
39. E. Kim, Y. Xia, G.M. Whitesides. Polymer microstructures formed by molding in capillaries. *Nature* 376, **1975**, 581-584.
40. N.T. Nguyen. Micromixers; Fundamentals, Design and Fabrication, 2nd Ed. Chapter 4 – Fabrication technologies. William Andrew – Elsevier, Waltham, USA, **2012**, 113-161.
41. M.T. Koedsjojo. Fabrication and application of polymer based microfluidic devices. *Oregon State University*, **2009**, Chapter 1.4: Soft lithography, 9-10.
42. U.S. Patent No. 4882245
43. C. Chang, Y.F. Wang, Y. Kanamori, J.J. Shih, Y. Kawai, C.K. Lee, K.C. Wu, M. Esashi. Etching submicrometer trenches by using the Bosch process and its application to the fabrication of antireflection structures. *Journal of Micromechanics and Microengineering* 15, **2005**, 580-585.
44. P.B. Grabiec, T. Gotszalk, F. Shi, P. Hudek, P. Dumania, I.W. Rangelow. The integration of CMOS with plasma-enhanced micromachining. *Surface and Coatings Technology* 97, **1997**, 475-480.
45. X. Zhao, Y.C. Shin. Femtosecond laser ablation of aluminum in vacuum and air at high laser intensity. *Applied Surface Science*, **2013**, <http://dx.doi.org/10.1016/j.apsusc.2013.06.037>
46. A. Schubert, S. Groß, B. Schulz, U. Eckert. Sequential combination of micro-milling and laser structuring for manufacturing of complex micro-fluidic structures. *Physics Procedia* 12, **2011**, 221-229.
47. C.W. Beh, W. Zhou, T.H. Wang. PDMS-glass bonding using grated polymeric adhesive – alternative process flow for compatibility with patterned biological molecules. *Lab on a Chip* 12, **2012**, 4120-4127.
48. S. Prakash, M.B. Karacor, S. Banerjee. Surface modification in microsystems and nanosystems. *Surface Science Reports* 64, **2009**, 233-254.

49. R.A. Jelil, X. Zeng, L. Koehl, A. Perwelz. Modeling plasma surface modification of textile fabrics using artificial neural networks. *Engineering Applications of Artificial Intelligence*, **2013**, <http://dx.doi.org/10.1016/j.engappai.2013.03.015>
50. M. Kitsara, J. Ducreé. Integration of functional materials and surface modifications for polymeric microfluidic systems. *Journal of Micromechanics and Microengineering* **23**, **2013**, 033001-033019.
51. S. Yoshida, K. Hagiwara, T. Hasebe, A. Hotta. Surface modification of polymers by plasma treatments for the enhancement of biocompatibility and controlled drug release. *Surface & Coatings Technology*, **2013**, <http://dx.doi.org/10.1016/j.surfcoat.2013.02.042>
52. T. Peng-Ubol, P. Phinyocheep, P. Daniel, W. Panbangred, J.F. Pilard, G. Thouand, M.J. Durand-Thouand. Plasma-treated polyethylene film: A smart material applied for *Salmonella Typhimurium* detection. *Materials Science and Engineering C32*, **2012**, 2641-2648.
53. S.J. Khatib, S.T. Oyama. Silica membranes for hydrogen separation prepared by chemical vapor deposition (CVD). *Separation and purification technology* **111**, **2013**, 20-42.
54. M. Gupta, K.K. Gleason. Surface modification of high aspect ratio structures with fluoropolymer coatings using chemical vapor deposition. *Thin solid films* **517**, **2009**, 3547-3550.
55. T. Okajima, K. Hara, M. Yamamoto, K. Seki. NEar edge X-ray absorption fine structure spectroscopic and infrared reflection absorption spectroscopic studies of surface modification of poly(butylene terephthalate) induced by UV irradiation. *Polymer* **53**, **2012**, 2956-2963.
56. J. Spanring, C. Buchgraber, M.F. Ebel, R. Svagera, W. Kern. Trialkylsilanes as reagents for the UV-induced surface modification of polybutadiene. *Polymer* **47**, **2006**, 156-165.
57. Z. Wang, G. Jin. Feasibility of protein A for the oriented immobilization of immunoglobulin on silicon surface for a biosensor with imaging ellipsometry. *Journal of Biochemical and Biophysical methods* **57**, **2003**, 203-211.
58. Y. Bai. Surface modifications for enhanced immobilization of biomolecules: applications in biocatalysis and immuno-biosensor. *The Ohio State Univesrity*, **2006**, Chapter 2.1: Modification of Biosensor Surface, 8-10.
59. N.D. Brault, A.D. White, A.D. Taylor, Q. Yu, S. Jiang. Directly functionalizable surface platform for protein arrays in undiluted human blood plasma. *Analytical Chemistry* **85**, **2013**, 1447-1453.
60. S.V. Aurobind, K.P. Amirthalingam, H. Gomathi. Sol-gel based surface modification of electrodes for electro analysis. *Advances in Colloid and Interface Science* **121**, **2006**, 1-7.
61. E. Carregal-Romero, A. Llobera, V.J. Cadarso, M. Darder, P. Aranda, C. Domínguez, E. Ruiz-Hitzky, C. Fernández-Sánchez. One-step patterning of hybrid xerogel materials for the fabrication of disposable solid-state light emitters. *Applied Materials & Interfaces* **4**(9), **2012**, 5029-5037.
62. J.B. Orhan, V.K. Parashar, J. Flueckiger, M.A.M. Gijs. Internal modification of poly(dimethylsiloxane) microchannels with a borosilicate glass coating. *Langmuir* **24**, **2008**, 9154-9161.
63. F.B. Myers, L.P. Lee. Innovations in optical microfluidic technologies for point-of-care diagnostics. *Lab on a Chip* **8**, **2008**, 2015-2031.

64. A. Llobera, R. Wilke, S. Büttgenbach. Enhancement of the response of poly(dimethylsiloxane) hollow prisms through air mirrors for absorbance-based sensing. *Talanta* 75, **2008**, 473-479.
65. A. Crespi, Y. Gu, B. Ngamsom, H.J.W.M. Hoekstra, C. Dongre, M. Pollnau, R. Ramponi, H.H. van den Vlekkert, P. Watts, G. Cerullo, R. Osellame. Three-dimensional Mach-Zehnder interferometer in a microfluidic chip for spatially-resolved label-free detection. *Lab on a Chip* 10, **2010**, 1167-1173.
66. A. Llobera, R. Wilke, S. Büttgenbach. Poly(dimethylsiloxane) hollow Abbe prism with microlenses for detection based on absorption and refractive index shift. *Lab on a Chip* 4, **2004**, 24-27.
67. L. Ceriotti, K. Weible, N.F. de Rooij, E. Veerporte. Rectangular channels for lab-on-a-chip applications. *Microelectronic Engineering* 67-68, **2003**, 865-871.
68. A. Llobera, S. Demming, R. Wilke, S. Büttgenbach. Multiple internal reflection poly(dimethylsiloxane) systems for optical sensing. *Lab On a Chip* 7, **2007**, 1560-1566.
69. L. Novak, P. Neuzil, J. Pipper, Y. Zhang, S. Lee. An integrated fluorescence detection system for lab-on-a-chip applications. *Lab on a Chip* 7, **2007**, 27-29.
70. S.J. Trietsch, T. Hankemeier, H.J. van der Linden. Lab-on-a-chip technologies for massive parallel data generation in the life sciences: A review. *Chemometrics and Intelligent Laboratory Systems* 108, **2011**, 64-75.
71. E. Carregal-Romero, C. Fernández-Sánchez, A. Eguizabal, S. Demming, S. Büttgenbach, A. Llobera. Development and integration of xerogel polymeric absorbance micro-filters into lab-on-chip systems. *Optics Express* 20(21), **2012**, 23700-23719.
72. F. Lefevre, Annie Chalifour, L. Yu, V. Chodavarapu, P. Juneau, R. Izquierdo. Algal fluorescence sensor integrated into a microfluidic chip for water pollutant detection. *Lab on a Chip* 12, **2012**, 787-793.
73. L. Liu, Q. Ma, Y. Li, Z. Liu, X. Su. Detection of biothiols in human serum by QDs based flow injection "turn off-on" chemiluminescence analysis system. *Talanta* 114, **2013**, 243-247.
74. M. Kamruzzaman, A.-Mahmmur Alam, K. Min Kim, S.H. Lee, Y.H. Kim, G.M. Kim, T.D. Dang. Microfluidic chip based chemiluminescence detection of L-phenylalanine in pharmaceutical and soft drinks. *Food Chemistry* 135, **2012**, 57-62.
75. A.B. González-Guerrero, S. Dante, D. Duval, J. Osmond, L.M. Lechuga. Advanced photonic biosensors for point-of-care diagnostics. *Procedia Engineering* 25, **2011**, 71-75.
76. M. Medina-Sanchez, S. Miserere, A. Merkoçi. Nanomaterials and lab-on-a-chip technologies. *Lab on a Chip* 12, **2012**, 1932-1943.
77. S.L. Hennigan, J.D. Driskell, R.A. Dluhy, Y. Zhao, R.A. Tripp, K.B. Waites, D.C. Krause. Detection of *Mycoplasma pneumonia* in simulated and true clinical throat swab specimens by nanorod array-surface-enhanced raman spectroscopy. *PLoS ONE* 5(10), **2010**, e13633 1-8.
78. L.C. Taylor, T.B. Kirchner, N.V. Lavrik, M.J. Sepaniak. Surface enhanced Raman spectroscopy for microfluidic pillar arrayed separation chips. *Analyst* 137, **2012**, 1005-1012.
79. J. Treviño, A. Calle, J.M.R. Frade, M. Mellado, L.M. Lechuga. Surface plasmon resonance immunoassay analysis of pituitary hormones in urine and serum samples. *Clinica Chimica Acta* 403, **2009**, 56-62.

80. N. Gosh, N. Gupta, G. Gupta, M. Boopathi, V. Pal, A.K. Goel. Detection of protective antigen, an anthrax specific toxin in human serum by using surface Plasmon resonance. *Diagnostic Microbiology and Infectious Disease*, **2013**, <http://dx.doi.org/10.1016/j.diagmicrobio.2013.05.006>
81. T. Neumann, H.D. Junker, K. Schmidt, R. Sekul. SPR-based fragment screening: advantages and applications. *Current Topics in Medicinal Chemistry* **7**, **2007**, 1630-1642.
82. E. Ouellet, C. Lausted, T. Lin, C.W.T. Yang, L. Hood, E.T. Lagally. Parallel microfluidic surface Plasmon resonance imaging arrays. *Lab on a Chip* **10**, **2010**, 581-588.
83. T. Rob, D.J. Wilson. A versatile microfluidic chip for millisecond time-scale kinetic studies by electrospray mass spectrometry. *Journal of the American Society for Mass Spectrometry* **20**, **2009**, 124-130.
84. S.L.S. Freire, A.R. Wheeler. Encyclopedia of Micro- and Nanofluidics 2: Interfaces between microfluidics and mass spectrometry. *Springer*, Heidelberg (Germany), **2008**, 849-854.
85. L. Nyholm. Electrochemical techniques for lab-on-a-chip applications. *Analyst* **130**, **2005**, 599-605.
86. T.A. Webster, E.D. Goluch. Electrochemical detection of pyocyanin in nanochannels with integrated palladium hydride reference electrodes. *Lab on a Chip* **12**, **2012**, 5195-5201.
87. M.I. Rocha-Gaso, C. March-Iborra, A. Montoya-Baides, A. Arnau-Vives. Surface generated acoustic wave biosensors for the detection of pathogens: a review. *Sensors* **9**, **2009**, 5740-5769.
88. H. Oh, K.J. Lee, J. Baek, S.S. Yang, K. Lee. Development of a high sensitive pH sensor based on shear horizontal surface acoustic wave with ZnO nanoparticles. *Microelectronic Engineering* **111**, **2013**, 154-159.
89. K. Länge, G. Blaess, A. Voigt, R. Götzen, M. Rapp. Integration of a surface acoustic wave biosensor in a microfluidic polymer chip. *Biosensors and Bioelectronics* **22**, **2006**, 227-232.
90. F.G. Bosco, M. Bache, E.T. Hwu, C.H. Chen, S.S. Andersen, K.A. Nielsen, S.S. Keller, J.O. Jeppesen, L.S. Hwang, A. Boisen. Statistical analysis of DNT detection using chemically functionalized microcantilever arrays. *Sensors and Actuators B: Chemical* **8**, **2012**, 1054-1059.
91. A. Johansson, G. Blagoi, A. Boisen. Polymeric cantilever-based biosensors with integrated readout. *Applied Physics Letters* **89**, **2006**, 173505 1-3.
92. H.F. Ji, B.D. Armon. Approaches to increasing surface stress for improving signal-to-noise ratio of microcantilever sensors. *Analytical Chemistry* **82**, **2010**, 1634-1642.
93. L.Y. Yeo, H.C. Chang, P.P.Y. Chan, J.R. Friend. Microfluidic devices for bioapplications. *Small* **7**(1), **2011**, 12-48.
94. R. Pal, M. Yang, R. Lin, B.N. Johnson, N. Srivastava, S.Z. Razzacki, K.J. Chomistek, D.C. Heldsinger, R.M. Haque, V.M. Ugaz, P.K. Thwar, Z. Chen, K. Alfano, M.B. Yim, M. Krishnan, A.O. Fuller, R.G. Larson, D.T. Burke, M.A. Burns. An integrated microfluidic device for influenza and other genetic analyses. *Lab on a Chip* **5**, **2005**, 1024-1032.
95. C. Benz, H. Retzbach, S. Nagl, D. Belder. Protein-protein interaction analysis in single microfluidic droplets using FRET and fluorescence lifetime detection. *Lab on a Chip*, **2013**, DOI: 10.1039/c3lc00057e
96. H. Lee, Y. Liu, D. Ham, R.M. Westervelt. Integrated cell manipulation system-CMOS/microfluidic hybrid. *Lab on a Chip* **7**, **2007**, 331-337.

97. P.S. Ditrich, A. Manz. Lab-on-a-chip: microfluidics in drug discovery. *Nature Reviews* 5, **2006**, 210-218.
98. A.D. Beaton, C.L. Cardwell, R.S. Thomas, V.J. Sieben, F.E. Legiret, E.M. Waugh, P.J. Statham, M.C. Mowlem, H. Morgan. Lab-on-a-chip measurement of nitrate and nitrite for in situ analysis of natural waters. *Environmental Science & Technology* 46, **2012**, 9548-9556.
99. E. Delibato, A. Gattuso, A. Minucci, B. Auricchio, D.D. Medici, L. Toti, M. Castagnola, E. Capoluongo, M.V. Gianfranceschi. PCR experion automated electrophoresis system to detect *Listeria monocytogenes* in food. *The Journal of Separation Science* 32, **2009**, 3817-3821
100. Y.C. Chang, P. Wägli, V. Paeder, A. Homsy, L. Hvozdar, P. van der Wal, J. Di Francesco, N.F. de Rooij, H.P. Herzig. Cocaine detection by a mid-infrared waveguide integrated with a microfluidic chip. *Lab on a Chip* 12, **2012**, 3020-3023.
101. T.H. Kim, K. Abi-Samra, V. Sunkara, D.K. Park, M. Amasia, N. Kim, J. Kim, H. Kim, M. Madou, Y.K. Cho. Flow-enhanced electrochemical immunosensors on centrifugal microfluidic platforms. *Lab on a Chip*, **2013**, DOI: 10.1039/c0xx00000x
102. A. Fragoso, D. Latta, N. Laboria, F. von Germar, T.E. Hansen-Hagge, W. Kemmner, C. Gärtner, R. Klemm, K.S. Drese, C.K. O'Sullivan. *Lab on a Chip* 11, **2011**, 625-631.

2. OBJECTIVES

The main objective of this PhD Thesis was the development of low-cost functionalized lab-on-a-chip devices (LOC) with the potential to be applied as analytical tools for environmental and biomedical applications. Starting from a few photonic LOC approaches (PhLOC) that had already been defined in our group, the aim of this work was to explore the potential of these devices in analysis and, by increasing their degree of complexity, integrate additional functionalities to them that resulted in new PhLOC devices with a clear application in the above mentioned fields.

Several steps were followed to achieve this objective:

- Development of analytical procedures for the detection of target analytes of different nature, such as cells and heavy metal ions, which could be implemented with low-cost polymer-based PhLOCs and demonstrate the versatility and real potential of these devices for analytical purposes.
- Development of immobilization protocols for proteins on the polymeric materials used for the fabrication of PhLOCs. In order to integrate sensing components to these devices, different surface modification methods were compared so that the stable immobilization of proteins was attained while keeping their activity.
- Monolithic integration of specific microfluidic components which provided the resulting PhLOC with enhanced analytical performance, such as reactors and mixing components. Different transduction methods could also be integrated in order to get devices that were more robust and could also be self-verifying thus greatly improving their reliability and/or allow multiplexing. Here, the simultaneous integration of optical and electrochemical detection approaches was carried out.

3. CELL SCREENING USING DISPOSABLE MICROFLUIDIC CHIP SYSTEMS WITH OPTICAL READOUT

3.1.	Summary	54
3.2.	Introduction	54
3.3.	Experimental details	56
3.3.1.	Materials and reagents	56
3.3.2.	Optofluidic system design and fabrication	56
3.3.3.	Cell culture and labeling	57
3.3.4.	Measurement setup	58
3.4.	Results and discussion	58
3.4.1.	Measurement protocols	58
3.4.2.	Live cells: LS regime	59
3.4.3.	Dead cells: LS + ABS and ABS regimes	61
3.4.4.	Dead/Live ratio measurement	63
3.5.	Conclusions	67
3.6.	References	67

The work included in this chapter has been reported in a paper entitled “*Cell screening using disposable photonic Lab-On-a-Chip systems*”, by Bergoi Ibarlucea, Elisabet Fernandez-Rosas, Jordi Vila-Planas, Stefanie Demming, Carme Nogués, José A. Plaza, Stephanus Büttgenbach and Andreu Llobera, *Analytical Chemistry* 82, **2010**, 4246-4251.

The protocol followed for the experimental sections was described in detail in a paper entitled “*Cell analysis using a multiple internal reflection photonic lab-on-a-chip*”, by Jordi Vila-Planas, Elisabet Fernández-Rosas, Bergoi Ibarlucea, Stephanie Demming, Carme Nogués, José A. Plaza, Carlos Domínguez, Stephanus Büttgenbach and Andreu Llobera, *Nature Protocols* 6, **2011**, 1642-1655.

3.1. Summary

A low-cost photonic lab-on-a-chip (PhLOC) with three different working regimes for cell screening is presented. The proposed system is able to perform scattering, scattering + absorption, and absorption measurements without any modification. Opposite to the standard flow cytometers, in this proposed configuration, a single 30 ms scan allows to obtain information regarding the cell optical properties. An additional novelty is that the whole spectrum is obtained and analyzed, being then possible to determine for each regime which is the optimal working wavelength that would provide the best performance in terms of sensitivity and Limit of Detection (LOD). Experimental results have provided with a LOD of 54.9 ± 0.7 cells (in the scattering regime using unlabeled cells), 53 ± 1 cells (in the scattering + absorption regime using labeled cells), and 105 ± 4 cells (in the absorption regime using labeled cells). Finally, the system has also been used for measuring the dead/live cell ratio, obtaining LODs between $7.6 \pm 0.4\%$ and $6.7 \pm 0.3\%$, depending on the working regime used.

3.2. Introduction

In the area of cell culture analysis, the main issues that Lab-on-a-Chip (LOC) systems have to address are the isolation of the cells of interest and their fast screening. Cell isolation is generally evaluated with immunofluorescent labeling, which provides high specificity at the expenses of increasing the time and the required steps of sample processing. Additionally, for population measurements, the counting repetition at random points is required in order to avoid errors due to irregular or random patterns of uneven cell distribution^{1,2}. Some interesting approaches have recently been presented trying to tackle this issue³. Nevertheless, a microscope is still required, being then necessary for manual counting of the entrapped cells on a single device (with the possibility of having computer-assisted systems). A step forward is the lensless, ultrawide field cell monitoring array platform based on shadow imaging (LUCAS) that records the shadow of each individual cell^{4,5}. Although these results are a significant step towards white light microscopy on a chip, they cannot perform multiwavelength measurements (as could be the case of fluorescent labeling). Hence, the use of the LUCAS configuration is restricted to cell counting.

Generally speaking, manual counting chambers, automated cell counters, and flow cytometry are the standard methods used to determine cell concentration in cultures. Several dyes are also used to evaluate live and dead cells in culture, based on the assumption that only dead cells are stained⁶. In this approach, human errors caused by operator subjectivity in manual counters and statistical errors due to dilutions or sample concentration in manual and automated counters are common. Flow cytometry solves this issue but at the expense of a high price. Hence, a fast, multiparametric, disposable system for Point of Care (POC) applications able to count cells in a constant volume is yet to be presented.

This open issue is currently addressed with the LOCs. Regarding the detection methods, the optical readout that is made with photonic LOCs (PhLOCs) makes possible to perform

measurements that do not require direct contact with the cell culture or the use of potentials which could either interfere or modify the cell properties⁷. Two different approaches toward LOC can be found in the literature: performance enhancement, which means the development of High-Throughput Systems (HTS) for multiparametric detection⁸, or accuracy enhancement, with the most significant example as the use of optical tweezers for single cell analysis and manipulation⁹. In both cases, the low-cost assumption is not fulfilled. The tackling of this issue is generally associated with the use of polymers, especially poly(dimethylsiloxane) (PDMS), using soft lithographic methods¹⁰. Considering its excellent optical and structural properties, microfluidic and photonic elements can be monolithically defined. Not surprisingly, it has already been used in laser-induced fluorescence systems¹¹ and optical cytometers¹². Moreover, multiplexing/filtering can also be included^{13,14}. The integration of photonic elements also allows removing the bulky inverted microscope and the external filters from the experimental setup, hence having an in-plane configuration with much higher accessibility. Besides, a final result is given directly, avoiding the possibility of interpretation errors. Finally, its biocompatibility and its low cost make this material the most suitable for meeting the previously mentioned requirements. Hence, polymeric PhLOC is a promising configuration, especially in the field of cellular biology, where time dependent multiparametric measurements have to be done without compromising the environmental conditions of either the cells or the media. The low cost also assures having disposable systems, being then possible to use sterile systems for each measurement.

Currently, fluorescence is the most common analytical method¹⁵. Nevertheless, as it was previously mentioned, the labeling adds another step to the cell preparation. Additionally, fluorescence is emitted in $4\pi sr$, which makes it challenging to have a reasonable amount of fluorescence reaching the detector. Conversely, absorbance measurements can be done much faster without requiring labeling or with a simpler labeling method. Since the absorbance is directly proportional to the path length, larger interrogation regions reduce the Limit of Detection (LOD). It has to be noted, however, that the increase of the optical path requires having reflections inside the interrogation volume. Because of the low refractive index contrast between the PDMS and the liquid that fills the interrogation region (as could be phosphate saline buffer, PBS), the reflection coefficients at the PDMS-PBS are 0.029 for TE-polarization and 0.062 for its TM counterpart, requiring hence long integration times for achieving a reasonable signal-to-noise ratio (SNR) and thus inherently preventing the possibility of implementing them in high-throughput screening (HTS).

In an attempt to go beyond this state of the art, the low cost, disposable, polymeric PhLOC system in multiple internal reflection (MIR) configuration is used. Such MIR systems have already been used for fluorophore detection¹⁶, but to the best of our knowledge, up to now there has been no contribution regarding using such systems for cell screening. In addition, we show in this manuscript that MIRs can work in the three working regimes: LS (scattering), LS + ABS (scattering + absorption), and ABS (absorption). Opposite to cell cytometers, where the cells are successively counted, in our approach a single measurement of 30 ms is done in the entire interrogation region. If the cells are unlabeled or do not have absorption bands in the wavelength range under study, a scattering band (flat absorption band) is obtained. Conversely, when they are labeled, a superimposed absorbance band is observed. In both working regimes, the population can be determined. Finally, by subtraction of the two

previous results, we obtain the spectra related only to the absorption (ABS). To show the viability of the proposed system, it has been used not only for determining the population of labeled and unlabeled cells but also for determining the dead/live ratio. This is the first time, to the best of our knowledge, that a PhLOC that simultaneously tackles both the human errors of the Neubauer chamber and the cost issue of the cell counters is presented to the scientific community.

3.3.Experimental details

3.3.1. Materials and reagents

PDMS Sylgard 184 elastomer kit was from Dow Corning (Midland, MI, US). EPON SU-8 photoresist (SU8-25) and propylene glycol methyl ether acetate (PGMEA) were from Micro-Chem Corporation (Newton, MA, USA). RPMI 1640 medium, fetal bovine serum and trypan blue (Gibco®) were from Life Technologies Corporation (Carlsbad, CA 92008, USA).

3.3.2. Optofluidic system design and fabrication

Optically, these PhLOCs¹⁶ form a complex system with a high degree of monolithic integration, since they comprise self-alignment systems for adequate positioning of fiber optics, lenses, and focusing mirrors. Light propagates in the system following a zigzag path with the help of integrated air mirrors¹⁷. In such conditions, the air mirrors meaningfully lengthen the optical path without dramatically increasing the overall size of the reactor. The MIR system can be seen in Figure 3.1.

The inherent diffraction of the light coming from the input fiber optic is corrected with a cylindrical biconvex microlens, getting parallel light beams into the interrogation region. In a phosphate buffered saline (PBS)-PDMS interface without air mirrors, light propagates from a low refractive index (RI) media ($n_{PBS} = 1.334$) to a high RI media ($n_{PDMS} = 1.41$). In this way, the light would escape from the microchannel without reaching to the output fiber optic. Instead, when the air mirrors are added, the light that propagates through PDMS reaches to a region with a lower RI ($n_{air} = 1$). If the incidence angle is appropriate, the light will be reflected by Total Internal Reflection (TIR) again into the PDMS. Based on Snell's law ($n_1 \sin \theta_1 = n_2 \sin \theta_2$, where θ_1 is the incidence angle and θ_2 is the reflection angle), it is possible to determine the critical angle in which the reflection occurs. For the air-PDMS interface it is 45.17°. Higher angles will produce TIR. However, for the PBS-PDMS interface, the critical angle is 70.6°. The mirrors are designed with the aim of fulfilling TIR conditions for the air-PDMS interface but not in the PBS-PDMS interface. Thus, will not get confined in PDMS, and it will be reintroduced in the interrogation region until it reaches the biconvex lens that collects the light into the output fiber optic.

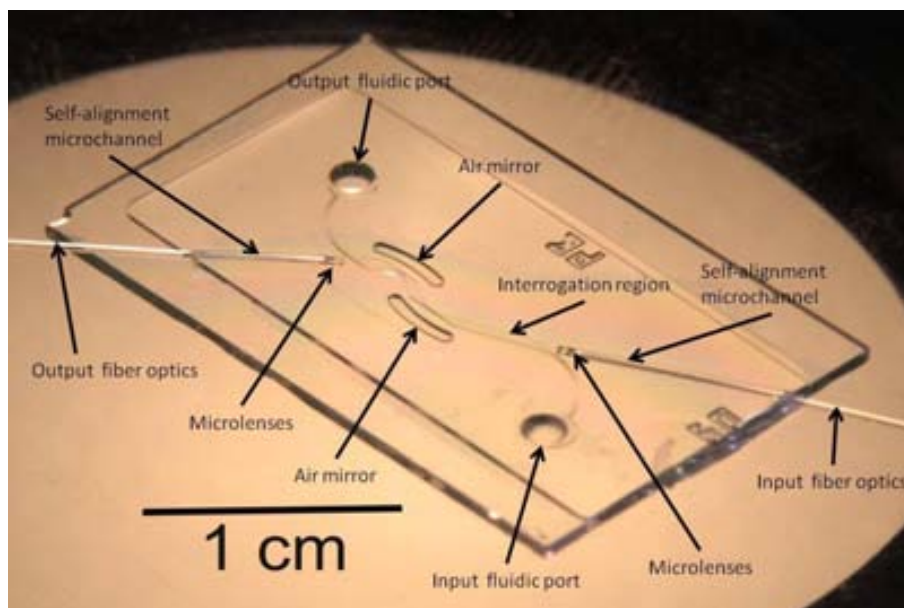


Figure 3.1. Picture of the PDMS-based MIR system. It comprises self-alignment microchannels for accurate fiber optics positioning, microlenses, and air mirrors. All these microoptic elements ensure an adequate zigzag path of the light along the interrogation region, which can be filled through the input fluidic port.

For the fabrication, first a master was fabricated with EPON SU-8 25 negative tone resist. The resist was twice spin coated in order to reach a height of 250 nm. It was dried at 95 °C for 3 hours and then a standard UV-photolithographic process was carried out, followed by a baking step for 20 min at 95 °C, and a consecutive developing step in PGMEA. The master was ended by a final hard bake at 120 °C for 2 hours in an inert atmosphere to harden it. Then PDMS was used for the replication of the master. Pre-polymer was prepared by mixing the curing agent and the base elastomer in a 1:10 (v/v) ratio and degasifying it in a vacuum chamber. The pre-polymer was poured on the master and cured on a hot plate at 80 °C for 20 min. Then it was peeled off from the master and sealed over a flat soda-lime glass substrate using a plasma treatment. For this, the PDMS and the glass were placed in a TePla plasma processor (PVA TePla AG, Munich, Germany) and exposed to oxygen plasma (500 W, 18 s). Immediately after the treatment they were put in contact and kept at 80 °C for 30 min, irreversibly sealing the fluidic systems. The final volume of the PhLOC is 1.6 μ L.

3.3.3. Cell culture and labeling

Human monocytic cell line THP-1 (ECACC No.88081201) was maintained in RPMI 1640 medium with 20% fetal bovine serum at 37 °C in 5% CO₂. Before each experiment, cells were rinsed twice in PBS tempered at 37 °C and kept alive in an incubator under controlled temperature and atmosphere. To obtain the dead cell population, monocytes were fixed with 4% paraformaldehyde in PBS for 10 min. Afterwards, cells were stained with trypan blue in PBS (1:1) for 5 min and rinsed twice in PBS to maintain the label only inside the cells and not in the buffer. Trypan blue is one of the most commonly used methods for assessment of viability in a given cell population¹⁸ and gives the possibility to differentiate the dead/live cells with an easy staining procedure. The trypan chromophore is negatively charged. Hence, this stain does not enter inside the cells unless the membrane is damaged. When it penetrates into the cytoplasm

of dead cells through the membrane, it can be seen as a blue color on the whole area of the cells, while live cells are still transparent¹⁹. Finally, for the dead/live ratio measurement, both populations were diluted to obtain the desired cell proportions. All the measurements have been performed in PBS buffer to ensure that results are due only to the cell signals

3.3.4. Measurement setup

A broadband light source (Ocean Optics HL-2000, Dunedin, USA) is coupled into the input multimode fiber optics with a diameter of 230 μm , which in turn is located in the self-alignment microchannels. At the end of this microchannel, a microlens corrects the numerical aperture of the fiber optics, having then parallel beams. Light enters into the interrogation region and interacts with the media that fills this region. As previously discussed, because of the reflection coefficients, most of the light is transferred to the PDMS. When it reaches the air mirror, the conditions of total internal reflection (TIR) hold. Hence, light is reflected towards the interrogation region, reaching the second air mirror, which reflects again the light while focusing it on the vicinity of the collecting fiber optics. Hence, light propagates in the system following a zigzag path. The readout comprises an identical fiber optics, which carries the signal to a spectrometer (Ocean Optics HR4000, Dunedin, USA) with a spectral resolution of 2 nm. The integration time has been fixed to 30 ms. All the measurements have been done at room temperature in a temperature-controlled lab. This setup remains unchanged throughout the experiment, that is, for the three regimes and for labeled/unlabeled cells.

3.4. Results and discussion

3.4.1. Measurement protocols

Three different experiments have been carried out with the proposed systems and using the previously mentioned working regimes: counting of living cells by LS, counting of trypan blue stained cells (both by LS + ABS and ABS) and finally the determination of the dead/live ratio at a constant population (again by LS + ABS and ABS). The main objective is to determine the LOD of the system for each experiment and for each regime. The following experimental procedure has been carried out: first, the system has been filled with buffer solution (PBS) and the readout obtained was considered as the reference for all subsequent experiments. Then, for the LS and the LS + ABS experiments, dilutions with progressively higher concentrations of live or dead cells from 50 to 2000 kcells/mL have been injected in the MIR. In the case of determining the LOD of dead cells, trypan blue is used since it is a direct, nearly instantaneous vital stain able to be used at room temperature with an optimal detection peak located at a wavelength of 580 nm. For each cell concentration, the average of 10 consecutive scans was taken. After measurement of the highest available cell concentration, the buffer solution is injected again to check possible drifts of the reference signal. In all the measured sets, the reference signal had a constant value within the experimental error. Then, the absorbance as a function of the cell concentration has been plotted, obtaining a linear fit for different wavelengths. In accordance to the 3σ IUPAC definition²⁰, from the values of this linear fit, the LOD are obtained for live and dead cells. It is noteworthy mentioning IUPAC states that the LOD is not the lowest detectable cell concentration but also depends both on the sensitivity

and the accuracy of the linear fit. From these data, it is possible to determine at which wavelength the LOD has a minimum and the sensitivity is maximal, being then able to obtain the optimal working parameters according to the cells under study. Once this optimization has been done, a third experiment (live/dead) is pursued. A total of 11 serial tubes were arranged with a 10% of variation in the live/dead cell ratio between them and a constant cell concentration of 2000 kcells/mL. In this case, LS + ABS and ABS working regimes were used to measure the dead cells percentage. The value obtained therein was afterwards compared and confirmed using a Neubauer-counting chamber; images of this experiment were recorded with a digital camera under an IX71 inverted microscope (Olympus) with a differential interference contrast and a 20x objective.

To avoid non-desired cell death and minimize non-controlled variations in the optical measurements, all the experimental work was carried out with the minimum required time and keeping the monocytic cell line under culture conditions (37 °C in 5% CO₂) until the measurements were done.

3.4.2. Live cells: LS regime

The absorbance spectra as a function of the live cell concentration are shown in Figure 3.2a. As expected, because of the size of such cells (between 7 and 15 μm in diameter), a nearly flat absorption band can be observed for all cell concentrations. There are two main differences of the proposed PhLOC with those previously presented: (i) the cell detection is done in parallel. That is, it does not work cell by cell (serial counting) as most of the cytometers but is able to provide information regarding the cell population in the volume by a single 30 ms measurement. (ii) Instead of measuring the absorption at a concrete wavelength, with the proposed MIR systems, the whole cell spectral response is obtained. This approach allows simultaneous in situ multiparametric detection by choosing the appropriate working wavelengths. Once the LS spectral response is obtained for the different cell concentrations, the absorbance as a function of the cell concentration can also be determined for several wavelengths (see Table 3.1), obtaining the expected linear behavior in all cases, which is in accordance to the Beer-Lambert law. Interestingly, and as an improvement of the state of the art, the linear fits allow one to determine the sensitivity and the LOD for each wavelength. From them, it is possible to determine which wavelength has the highest sensitivity and/or lower LOD, optimizing the response of the PhLOC.

The results of this optimization for live cells can be seen in Figure 3.2b, where the sensitivity and the LOD are plotted as a function of the wavelength. It can be seen that a plateau of maximal sensitivity is obtained at wavelengths between 580 and 700 nm, which simultaneously corresponds to a LOD minima, with values between 60 ± 1 and 38.4 ± 0.5 kcell/mL. Considering that the system has a volume of 1.43 μL , these LODs correspond to 86 ± 1 and 54.9 ± 0.7 cells, respectively.

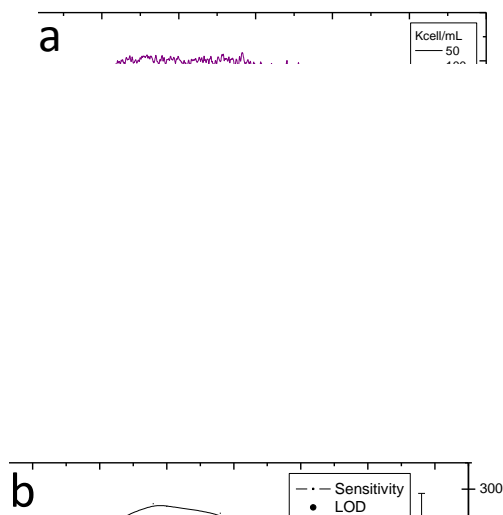


Figure 3.2. Results obtained for the scattering measurements using unlabeled cells: (a) absorbance as a function of the wavelength for concentrations ranging from 50 to 2000 kcell/mL. The flat absorption band is due to the cell scattering, which have a size between 7 and 15 μm . From these results, the absorbance as a function of the concentration is obtained, which can afterward be linearly fitted (Beer-Lambert regime). From this fit, sensitivity and LOD as a function of the wavelength for the LS regime is obtained, which is shown in part b, which determines the optimal working wavelength.

Table 3.1. Linear fits and LODs of LS measurements for different wavelengths.

LS							
Wavelength (nm)	Intercept		Slope		R^2	LOD (Kcell/mL)	
	Value	Error	Value	Error		Value	Error
400	-0.0015	2×10^{-4}	8.2×10^{-6}	3×10^{-7}	0.988	105	4
480	-0.013	1×10^{-3}	4.6×10^{-5}	1×10^{-6}	0.991	90	3
500	-0.012	1×10^{-3}	5.3×10^{-5}	1×10^{-6}	0.994	75	2
580	-0.013	1×10^{-3}	5.7×10^{-5}	1×10^{-6}	0.996	60	1
600	-0.0121	9×10^{-4}	5.6×10^{-5}	1×10^{-6}	0.997	48.7	0.9
680	-0.0105	7×10^{-4}	5.55×10^{-5}	8×10^{-7}	0.998	38.4	0.5
700	-0.012	1×10^{-3}	5.3×10^{-5}	1×10^{-6}	0.996	60	1
780	-0.004	1×10^{-3}	4.8×10^{-5}	1×10^{-6}	0.993	79	2
800	-0.007	1×10^{-3}	4.7×10^{-5}	1×10^{-6}	0.993	81	2
880	0.002	1×10^{-3}	2.7×10^{-5}	1×10^{-6}	0.986	112	5
900	0.0012	3×10^{-4}	2.23×10^{-5}	4×10^{-7}	0.997	50.2	0.9
980	0.0018	6×10^{-4}	6.5×10^{-6}	6×10^{-7}	0.926	269	26

3.4.3. Dead cells: LS + ABS and ABS regimes

When a vital stain or a dye is used for cell labeling, two effects simultaneously occur: absorption and scattering. Generally, it is challenging to uncouple them, especially if measurements at a single wavelength are done. This issue is also addressed and solved with the proposed system: as it is shown in Figure 3.3a, the absorbance as a function of the wavelength for 2000 kcell/mL shows the trypan blue peak at 580 nm and the scattering band in the wavelength range studied. In the previous subsection, the absorption band for such a cell concentration was determined (also shown in Figure 3.3a for clarification). Hence, simply by subtraction of both spectra, the trypan blue absorption band can be isolated.

Interestingly with labeled cells, the MIR-based PhLOC system allows working in two distinct regimes: scattering + absorption (LS + ABS) or absorption (ABS). In the first case, the procedure is identical to that presented in the previous section: The results of these fits are presented in figure 3b and at also in Table 3.2. As expected, because of the strong trypan absorption band, the maximum sensitivity is obtained at 580-600 nm. At such a range, a minimum LOD between 53 ± 1 and 61 ± 1 cells is obtained. It is also noticeable that the scattering band still can be seen at longer wavelengths, which allows one to have LODs of some hundreds of cells in the NIR range (>700 nm). Such configuration is of interest for measuring samples without preprocessing (such as labeling). Nevertheless, in the most general situation, cell labeling is used. Then, overall spectra is formed both by contributions of biomarkers and scattering. In this situation the scattering can be considered as a background noise, which modifies the overall shape of the spectra. Hence, having the possibility to subtract the scattering effects, and only obtaining the absorption/fluorescence contribution, is highly advantageous. The results obtained in the previous section have been taken as reference and subtracted from the spectra, as previously discussed. Again, several key wavelengths have been taken, and their linear fit is shown in Table 3.3. Since only the trypan blue band is obtained, the mentioned table just shows the linear fits of interest, with a minimum LOD of 105 ± 4 cells. The comparison between both regimes can also be seen in Figure 3.3b. Although the absorbance has a slightly smaller sensitivity, it provides a much higher specificity, since outside the trypan blue region, LODs higher than 350 cells are obtained.

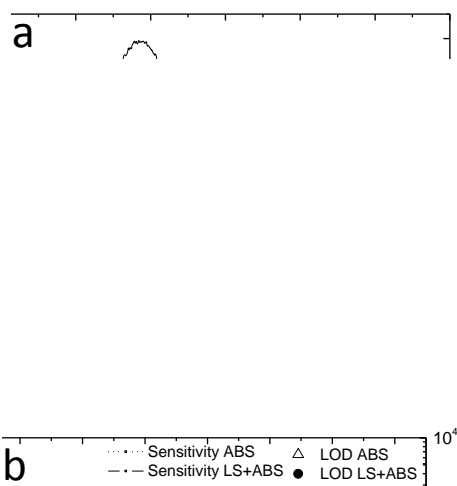


Figure 3.3. (a) Absorbance as a function of the wavelength for the three regimes studied: LS (flat absorption band), LS + ABS (flat scattering band and a strong trypan peak superimposed), and ABS (only showing the trypan peak) for a cell concentration of 2000 kcell/mL. This latter regime is obtained by subtraction of the first two regimes. Identical to the previous figure, labeled cell concentrations ranging from 50 to 2000 kcell/mL have been used. Absorbance vs concentration is plotted, and from these graphs, the sensitivity and LOD as a function of the wavelength for LS + ABS and ABS regimes are obtained, which are shown in part b.

Table 3.2. Linear fits and LODs of the LS + ABS measurements for different wavelengths.

LS+ABS							
Wavelength (nm)	Intercept		Slope		R^2	LOD (Kcell/mL)	
	Value	Error	Value	Error		Value	Error
400	8×10^{-4}	3×10^{-4}	1.04×10^{-5}	4×10^{-7}	0.984	95	4
480	-0.009	2×10^{-3}	9.30×10^{-5}	2×10^{-6}	0.994	57	1
500	-0.016	2×10^{-3}	1.85×10^{-4}	3×10^{-6}	0.997	37.4	0.7
580	-0.016	2×10^{-3}	1.80×10^{-4}	4×10^{-6}	0.997	42.7	0.9
600	-0.011	3×10^{-3}	9.0×10^{-5}	4×10^{-6}	0.982	100	5
680	-0.011	3×10^{-3}	7.0×10^{-5}	4×10^{-6}	0.978	110	6
700	-0.005	2×10^{-3}	5.6×10^{-5}	3×10^{-6}	0.972	125	7
780	-0.006	2×10^{-3}	5.2×10^{-5}	2×10^{-6}	0.983	96	4
800	-0.001	2×10^{-3}	3.2×10^{-5}	3×10^{-6}	0.947	174	14
880	-0.004	1×10^{-3}	2.6×10^{-5}	2×10^{-6}	0.965	141	9
900	3×10^{-4}	2×10^{-4}	8.8×10^{-6}	3×10^{-7}	0.986	86	3
980	8×10^{-4}	3×10^{-4}	1.04×10^{-5}	5×10^{-7}	0.984	95	4

Table 3.3. Linear fits and LODs of the ABS measurements for the wavelengths of interest.

Wavelength (nm)	ABS						
	Intercept		Slope		R ²	LOD (Kcell/mL)	
	Value	Error	Value	Error		Value	Error
480	0.008	2×10^{-3}	1.9×10^{-5}	3×10^{-6}	0.761	405	79
500	0.004	3×10^{-3}	3.800×10^{-3}	4×10^{-6}	0.907	234	26
580	0.003	3×10^{-3}	1.24×10^{-4}	4×10^{-6}	0.99	74	3
600	0.003	3×10^{-3}	1.21×10^{-4}	5×10^{-6}	0.988	82	3
680	0.001	4×10^{-3}	3.2×10^{-5}	5×10^{-6}	0.823	338	54

Up until now, we have shown that the proposed PhLOC is able to work in three different regimes: scattering (LS), scattering + absorption (LS + ABS), and absorption (ABS), obtaining comparable sensitivities and LODs, although each of them with distinct features. To confirm this last point, we have selected a key application, namely, the detection of dead/live cell ratios. To this effect, different proportions of labeled (dead) and non-labeled (live) cells (10% variation between conditions) are mixed at a constant concentration (2000 kcells/mL) and afterward injected in the MIR. The results of the conducted experiments are presented in the next subsection.

3.4.4. Dead/Live ratio measurement

The absorbance as a function of the wavelength for different dead/live cell ratio is presented in Figure 3.4a. Since the samples injected range from 0% to 100% labeled cells, the spectra also vary from only the flat absorption band (0% of dead cells) to the conditions where the trypan absorption peak is superimposed (100% of dead cells). An image of labeled and non-labeled cells inside the MIR can be seen in Figure 3.4b. A closer view of the labeled cells is shown in Figure 3.4c. Similar to the previous section, these spectra have been analyzed with two of the previously presented regimes: LS + ABS and ABS. In the first case, the absorbance as a function of the percentage of dead cells is presented in Figure 3.5a. The highest sensitivity corresponds to the trypan blue region (580-600 nm), decreasing sharply both for longer and shorter wavelengths. The values above the 70% of dead cells do not match the tendency. This effect is understood when the same dead/live cell ratio was placed in a Neubauer counting chamber. While the percentage of dead cells counted corresponds to the dead/live cell ratio analyzed, the total number of cells did not; dilutions above 70% have a significant cell deficit, which explains why these points do not follow the expected linear tendency. This point is also noteworthy, since this behavior can be understood as a self-test system: if the experimental value falls outside the calibration curve, a cell deficit is likely to have happened.

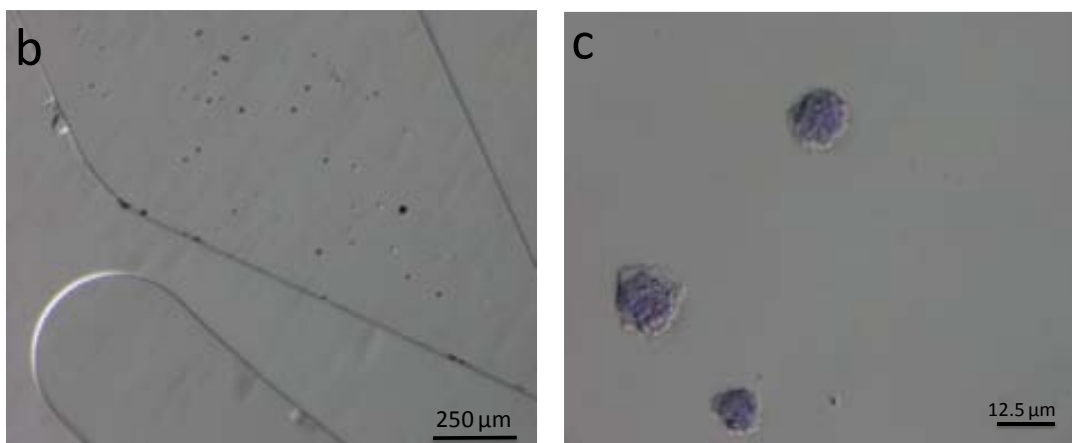
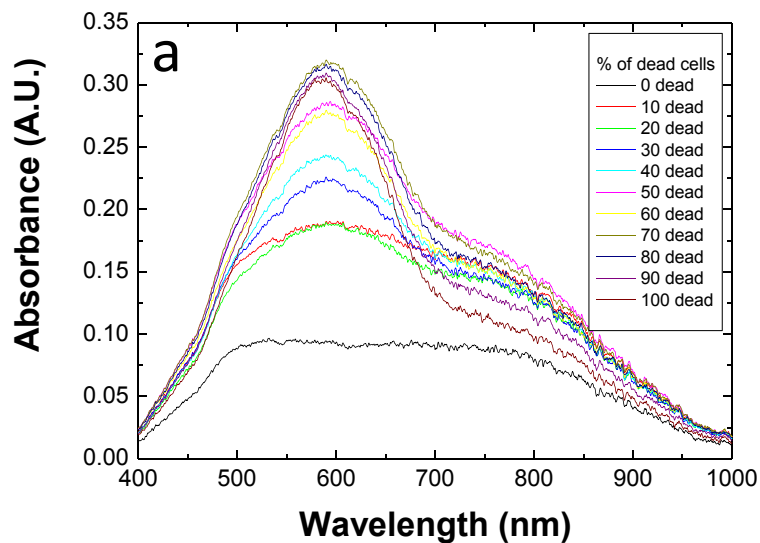


Figure 3.4. Measurement of the dead/live ratio. A constant cell concentration of 2000 kcell/mL has been selected, varying the live/ dead ratio in the 11 samples taken. In the absorbance as a function of the wavelength, the spectra shift from the LS regime (scattering) when all cells are alive to the LS + ABS regime (scattering + trypan peak), when only measuring dead cells. (b) Image of a concrete region of the MIR filled with dead and alive cells in a 50/50 ratio. (c) Close view of the labeled monocytes.

Once the values above 70% had been understood, they have not been used for the determination and the sensitivity and the LOD, which are presented in Figure 3.5b and Table 3.4. In this case, no scattering effects are observed even though we are using the whole spectra, namely, LS + ABS. Only the wavelengths where the trypan blue absorbs show a high sensitivity peak and an LOD of the percentage of dead cells of $7.6 \pm 0.4\%$. This effect can be understood if we take into account that we are using a constant population of 2000 kcell/mL. Hence, the scattering band is similar in all the samples used, and no difference in both parameters (sensitivity, LOD) should be observed. As it was presented in the previous section, if a variation of any of these parameters were seen, it could only be due to the variation of the population.

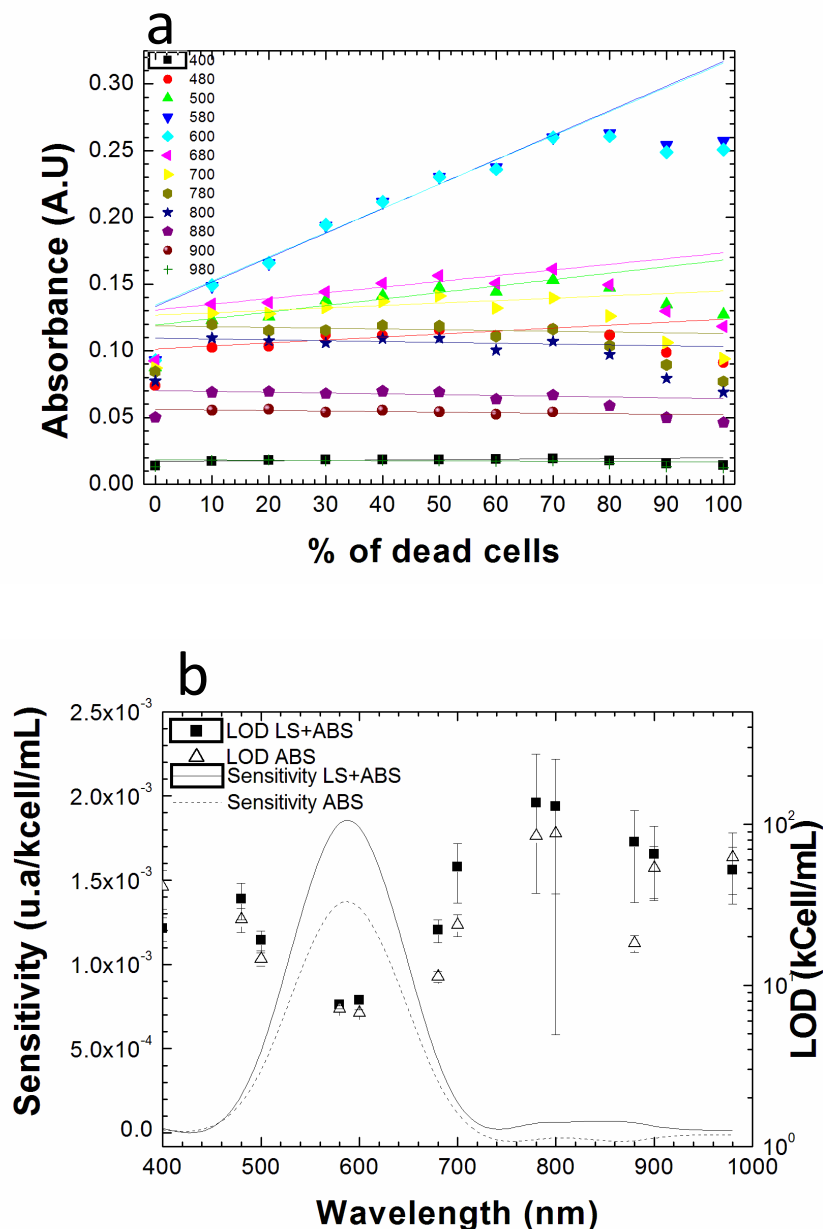


Figure 3.5. From the results obtained in the previous figure, the absorbance vs % of dead cells for different wavelengths are obtained, which are plotted in part a, together with their respective linear fit (using a constant concentration of 2000 kcell/mL). The wavelengths absorbed by the trypan blue have the highest sensitivity and the lowest LOD (both in the LS + ABS and ABS regimes) as shown in part b.

Because of the constant population level, the absorption measurements are suitable to provide lower LODs. The procedure has been similar to that previously presented, and the results are shown in Figure 3.5b and Table 3.5. In this case, the experimental and statistical errors of the LS + ABS make it difficult to compare their specificity, although the thinner full-width half-maximum (FWHM) of the sensitivity for the ABS may suggest that this latter regime has a slightly higher specificity. Again, a decrease of the sensitivity is obtained, although the LOD for the percentage of dead cells using ABS has been experimentally measured to be $6.7 \pm 0.3\%$.

Table 3.4. Linear fits and LODs of the live/dead cell measurements using LS+ABS for different wavelengths with a constant population of 2000 kcell/mL.

LS+ABS							
Wavelength (nm)	Intercept		Slope		R ²	LOD (% of dead cells)	
	Value	Error	Value	Error		Value	Error
400	0.0170	2 x 10 ⁻⁴	2.7 x 10 ⁻⁵	4 x 10 ⁻⁶	0.851	22	4
480	0.101	3 x 10 ⁻³	2.2 x 10 ⁻⁴	6 x 10 ⁻⁵	0.704	34	9
500	0.119	3 x 10 ⁻³	4.9 x 10 ⁻⁴	7 x 10 ⁻⁵	0.889	19	3
580	0.133	5 x 10 ⁻³	0.0018	1 x 10 ⁻⁴	0.981	7.6	0.4
600	0.134	5 x 10 ⁻³	0.0018	1 x 10 ⁻⁴	0.978	8.1	0.5
680	0.131	3 x 10 ⁻³	4.3 x 10 ⁻⁴	7 x 10 ⁻⁵	0.857	22	3
700	0.127	3 x 10 ⁻³	1.8 x 10 ⁻⁴	7 x 10 ⁻⁵	0.46	54	22
780	0.119	3 x 10 ⁻³	6 x 10 ⁻⁵	6 x 10 ⁻⁵	0	135	137
800	0.109	3 x 10 ⁻³	6 x 10 ⁻⁵	6 x 10 ⁻⁵	0.013	129	124
880	0.070	2 x 10 ⁻³	6 x 10 ⁻⁵	3 x 10 ⁻⁵	0.251	77	44
900	0.0561	8 x 10 ⁻⁴	4 x 10 ⁻⁵	2 x 10 ⁻⁵	0.348	65	32
980	0.0183	3 x 10 ⁻⁴	1.4 x 10 ⁻⁵	6 x 10 ⁻⁶	0.483	52	20

Table 3.5. Linear fits and LODs of the live/dead cell measurements using ABS for the wavelengths of interest with a constant population of 2000 kcell/mL.

ABS							
Wavelength (nm)	Intercept		Slope		R ²	LOD (% of dead cells)	
	Value	Error	Value	Error		Value	Error
480	-0.003	2 x 10 ⁻³	1.8 x 10 ⁻⁴	3 x 10 ⁻⁵	0.828	26	4
500	-0.004	2 x 10 ⁻³	3.7 x 10 ⁻⁴	4 x 10 ⁻⁵	0.939	14	1
580	7.0 x 10 ⁻⁴	3 x 10 ⁻³	1.36 x 10 ⁻³	6 x 10 ⁻⁵	0.985	7.1	0.3
600	2.0 x 10 ⁻⁴	3 x 10 ⁻³	1.34 x 10 ⁻³	6 x 10 ⁻⁵	0.986	6.7	0.3
680	5.0 x 10 ⁻⁴	1 x 10 ⁻³	3.0 x 10 ⁻⁴	2 x 10 ⁻⁵	0.962	11.3	0.8
700	0.0028	9 x 10 ⁻⁴	1.1 x 10 ⁻⁴	2 x 10 ⁻⁵	0.85	23.7	3

Regarding the direct applications and as an example, a CD4⁺T cells count below 200 cells/ μ L is given as a key diagnosis for AIDS²¹. Such cells have not been used in our experiments but, due to its size and its common hematopoietic origin, are comparable to these used in our measurements. Therefore, it could be estimated that the performance of the presented PhLOC would be similar when using CD4⁺T cells, and the presented LODs of the three detection methods are far below the requested CD4⁺T cells limit. When comparing the performance of the presented system with the LUCAS configuration^{4,5}, it can be seen that the integration time has been reduced more than 80 times while having a much lower LOD, reducing the technological complexity and keeping the same error count (less than 10%).

3.5. Conclusions

A low-cost polymeric PhLOC is presented with the attempt to tackle the inherent drawbacks of the Neubauer cell counters: counting error due to uneven distribution, measuring speed, and cost of the system. The proposed system takes advantage of the definition of air mirrors in the vicinity of the interrogation region which meaningfully lengthen the optical path while keeping the overall dimensions of the system at a reasonable size. Optically, the system has a high degree of integration, since it comprises self-alignment systems, microlenses, and air mirrors. Nonetheless, the whole PhLOC is defined with a single photolithographic mask using low-cost materials (PDMS and soda-lime glass as substrates). Cell measurement has allowed determining three distinct working regimes: scattering, where no significant absorption band has been observed in the studied UV-NIR spectra, scattering + absorption, where over the scattering band a clear absorption band is superimposed, and absorption, in which the two previously mentioned spectra have been subtracted in order to have a clear view of the bands of interest. For such characterization, and opposite to the standard procedure, a broadband spectrum has been analyzed, being then possible to determine the optimal working wavelengths in terms of sensitivity and LOD. Such regimes have been demonstrated with labeled and non-labeled cells, obtaining LODs between 53 and 105 cells depending on the working regime. Finally, as a concrete demonstration of the applications of the presented configuration, it has also been used for measuring the dead/live cell ratio of a constant cell concentration. The two studied regimes show LODs between $7.6 \pm 0.4\%$ and $6.7 \pm 0.3\%$, that is, with a performance comparable to the Neubauer cell counters but only requiring 30 ms for its measurements and with the possibility of multiparametric (by detecting different wavelengths) and continuous cell monitoring.

3.6. References

1. G. Chakravarti, K.A. Bhattacharya. Handbook of Clinical Pathology, 3rd ed.; *Academic Publishers*: Kolkata, India, **1984**, 1-8.
2. J.P. Greer. Wintrobe's Clinical Hematology 1, 12th ed., *LWW Medical Book Collection*, Lippincott Williams & Wilkins, Philadelphia, USA, **2009**, 1-19.
3. X. Cheng, D. Irimia, M. Dixon, K. Sekine, U. Demirci, L. Zamir, R.G. Tompkins, W. Rodriguez, M. Toner. A microfluidic device for practical label-free CD4(+) T cell counting of HIV-infected subjects. *Lab on a Chip* **7**, **2007**, 170-178.
4. X. Cui, L.M. Lee, X. Heng, W. Zhong, P.W. Stemberg, D. Psaltis, C. Yang. Imaging microorganisms with a high resolution on-chip optofluidic microscope. *Proceedings of the National Academy of Sciences* **105**(31), **2008**, 10670-10675.
5. A. Ozcan, U. Demirci. Ultra wide-field lens-free monitoring of cells on-chip. *Lab on a Chip* **8**, **2008**, 98-106.
6. S. Tolnai. A method for viable cell counting: Tissue Culture Association Manual 1. *Tissue Culture Association*: Rockville, USA, **1975**, 37-38.

7. X. Cheng, Y.S. Liu, D. Irimia, U. Demirci, L. Yang, L. Zamir, W.R. Rodríguez, M. Toner, R. Bashir. Cell detection and counting through cell lysate impedance spectroscopy in microfluidic devices. *Lab on a Chip* 7, **2007**, 746-755.
8. D.C. Duffy, H.L., Gillis, J. Lin, N.F. Sheppard, Jr., G.J. Kellogg. Microfabricated centrifugal microfluidic systems: characterization and multiple enzymatic assays. *Analytical Chemistry* 71, **1999**, 4669-4678.
9. T.D. Perroud, J.N. Kaiser, J.C. Sy, T.W. Lane, C.S. Branda, A.K. Singh, K.D. Patel. Microfluidic-based cell sorting of *Francisella tularensis* infected macrophages using optical forces. *Analytical Chemistry* 80, **2008**, 6365-6372.
10. Y. Xia, G.M. Whitesides. Soft Lithography. *Angewandte Chemie International Edition* 37, **1998**, 550-575.
11. S. Camou, H. Fujita, T. Fujii. PDMS 2D optical lens integrated with microfluidic channels: principle and characterization. *Lab on a Chip* 3, **2003**, 40-45.
12. C.H. Lin, G.B. Lee. Micromachined flow cytometers with embedded etched optic fibers for optical detection. *Journal of Micromechanics and Microengineering* 13, **2003**, 447-453.
13. A. Llobera, R. Wilke, S. Büttgenbach. Poly(dimethylsiloxane) hollow Abbe prism with microlenses for detection based on absorption and refractive index shift. *Lab on a Chip* 4, **2004**, 24-27.
14. O. Hofmann, X. Wang, A. Cornwell, S. Beecher, A. Raja, D.C. Bradley, A.J. deMello, J.C. deMello. Monolithically integrated dye-doped PDMS long-pass filters for disposable on-chip fluorescence detection. *Lab on a Chip* 6, **2006**, 981-987.
15. B.P. Cormack, R.H. Valdivia, S. Falkow. FACS-optimized mutants of the green fluorescent protein (GFP). *Gene* 173(1), **1996**, 33-38.
16. A. Llobera, S. Demming, R. Wilke, S. Büttgenbach. Multiple internal reflection poly(dimethylsiloxane) systems for optical sensing. *Lab on a Chip* 7, **2007**, 1560-1566.
17. A. Llobera, R. Wilke, S. Büttgenbach. Enhancement of the response of poly (dimethylsiloxane) hollow prisms through air mirrors for absorbance-based sensing. *Talanta* 75, **2008**, 473-479.
18. T.F. Uliasz, S.J. Hewett. A microtiter trypan blue absorbance assay for the quantitative determination of excitotoxic neuronal injury in cell culture. *Journal of Neuroscience Methods* 100, **2000**, 157-163.
19. L.L. Cheng, Y.Y. Luk, C.J. Murphy, B.A. Israel, N.L. Abbott. Compatibility of lyotropic liquid crystals with viruses and mammalian cells that support the replication of viruses. *Biomaterials* 26, **2005**, 7173-7182.
20. G.L. Long, J.D. Wineforder. Limit of detection - a closer look at the IUPAC definition. *Analytical Chemistry* 55(7), **1983**, A712-A724.
21. Centers for Disease Control and Prevention. Revised classification of HIV infection and expanded surveillance case definition for AIDS among adolescents and adults. *Morbidity and Mortality Weekly Report*, **1992**, 1-19.

4. PDMS-BASED PHOTONIC LAB-ON-A-CHIP FOR THE SELECTIVE OPTICAL DETECTION OF HEAVY METAL IONS

4.1.	Summary	70
4.2.	Introduction	70
4.3.	Experimental details	71
4.3.1.	Materials and reagents	71
4.3.2.	Ligands	71
4.3.3.	Design and fabrication of the PhLOCs	73
4.3.4.	Experimental setup and measurement protocol	74
4.4.	Results and discussion	74
4.5.	Conclusions	78
4.6.	References	78

The work included in this chapter has been reported in a paper entitled “PDMS based photonic lab-on-a-chip for the selective optical detection of heavy metal ions”, by Bergoi Ibarlucea, César Díez-Gil, Inma Ratera, Jaume Veciana, Antonio Caballero, Fabiola Zapata, Alberto Tárraga, Pedro Molina, Stephanie Demming, Stephanus Büttgenbach, César Fernández-Sánchez and Andreu Llobera, *Analyst* 138, **2013**, 839-844.

4.1. Summary

The selective absorbance detection of mercury(II) (Hg^{2+}) and lead(II) (Pb^{2+}) ions using ferrocene-based colorimetric ligands and miniaturized Multiple Internal Reflection (MIR) systems implemented in a low-cost photonic Lab-on-a-Chip (PhLOC) is reported. The detection principle is based on the formation of selective stable complexes between the heavy metal ion and the corresponding ligand. This interaction modulates the ligand spectrum by giving rise to new absorbance bands or wavelength shifting of the existing ones. A comparative study for the detection of Hg^{2+} was carried out with two MIR-based PhLOC systems showing optical path lengths (OPLs) of 0.64 cm and 1.42 cm as well as a standard cuvette (1 cm OPL). Acetonitrile solutions containing the corresponding ligand and increasing concentrations of the heavy metal ion were pumped inside the systems and the absorbance in the visible region of the spectra was recorded. The optical behavior of all the tested systems followed the expected Beer–Lambert law. Thus, the best results were achieved with the one with the longest OPL, which showed a linear behavior in a concentration range of 1 mM–90 mM Hg^{2+} , a sensitivity of 5.6×10^{-3} A.U. mM^{-1} and a LOD of 2.59 mM (0.49 ppm), this being 1.7 times lower than that recorded with a standard cuvette, and using a sample/reagent volume around 190 times smaller. This microsystem was also applied for the detection of Pb^{2+} and a linear behaviour in a concentration range of 3–100 mM was obtained, and a sensitivity of 9.59×10^{-4} A.U. mM^{-1} and a LOD of 4.19 mM (0.868 ppm) were achieved. Such a simple analytical tool could be implemented in portable instruments for automatic in-field measurements and, considering the minute sample and reagent volume required, would enable the deployment of high throughput environmental analysis of these pollutants and other related hazardous species.

4.2. Introduction

Heavy metal ions can injure human health and pollute the environment. It is well known that these metals are able to enter organisms and interfere with metabolic processes¹, producing physiological problems including neurological, neuromuscular, or nephritic disorders. Among the different metals, mercury and lead are considered to be the most toxic non-radioactive chemical elements. They are highly water-soluble, being bioavailable for animals by ingestion of water². The divalent cation of mercury (Hg^{2+}) is non-biodegradable, accumulative and toxic even at very low concentrations. It can damage heart, kidney, stomach and intestines, also causing sensory and neurological damage³. In the case of the divalent cation of lead (Pb^{2+}), exposure to very low levels can cause neurological, reproductive, cardiovascular and developmental disorders⁴.

There are several analytical techniques that enable the sensitive detection of heavy metal ions, such as inductively coupled plasma mass spectrometry (ICP-MS)⁵, cold vapour atomic absorption spectrometry (CV-AAS)⁶, X-ray fluorescence (XRF) spectroscopy⁷ and high performance liquid chromatography (HPLC)⁸. However, the corresponding analyses have to be carried out in centralized laboratories, making them expensive and not suitable for the rapid

detection of these target analytes^{2,3}. In this context, the high toxicity of heavy metal ions has given rise to a necessity of new systems for their detection and quantification that were simple, portable and inexpensive. Miniaturization of analytical systems is nowadays a real alternative to perform in situ and continuous monitoring of pollutants, which could be used as alarm systems to target potential contamination outbreaks and thus give rise to a faster response to tackle the problem. Lab-on-a-Chip (LOC) systems have already been applied for the detection and quantification of heavy metal ions. Most of them rely on electrochemical or optical detection approaches. Among the former, Zhu *et al.*⁹ developed a chip including a mercury droplet based microelectrode to detect lead and cadmium ions. Zou *et al.*¹⁰ further incorporated the possibility to carry out in situ and online measurements to their electrochemical detection based chip. However, these approaches are based on the cumbersome implementation of different materials and the application of highly toxic electrodes. Optical detection approaches (photonic LOCs, PhLOCs) are gaining a preeminent position mainly because they are highly sensitive non-contact techniques that show immunity to electromagnetic interferences and provide with the capability of multiplexed detection in a single analytical system¹¹. In environmental applications, optical approaches have also been reported for the measurement of heavy metal ions. There is a wealth of molecular metal ion receptors that provide with the possibility of performing optical detection, many of them included in a recent review by Kim *et al.*¹² such as 1-pyrenecarboxaldehyde thiosemicarbazone (a fluorescent ligand that binds Hg^{2+})¹³, or an hybridized DNAzyme with an intercalated Picogreen (PG) fluorescent molecule (which is cleaved in the presence of Pb^{2+} resulting in a release of PG and a decrease of the fluorescent signal)¹⁴.

In this context, this work aims to show the benefits of simply combining two colorimetric ferrocene-based ligands^{15,16}, which selectively interacted in solution with Hg^{2+} and Pb^{2+} ions, with low-cost miniaturized PhLOCs for the rapid detection of these pollutants. Two different PhLOCs based on MIR approaches¹⁷, showing different OPLs, are applied for the detection and quantification of highly toxic metal ions (Hg^{2+} and Pb^{2+}) by using colorimetric ligands that form selective stable complexes with the corresponding ion and, upon complex formation, new absorbance bands or wavelength shift of the existing ones appear. The successful performance of these PhLOCs makes them potential candidates to carry out rapid decentralized studies directed towards monitoring these pollutants in the environment.

4.3. Experimental details

4.3.1. Materials and reagents

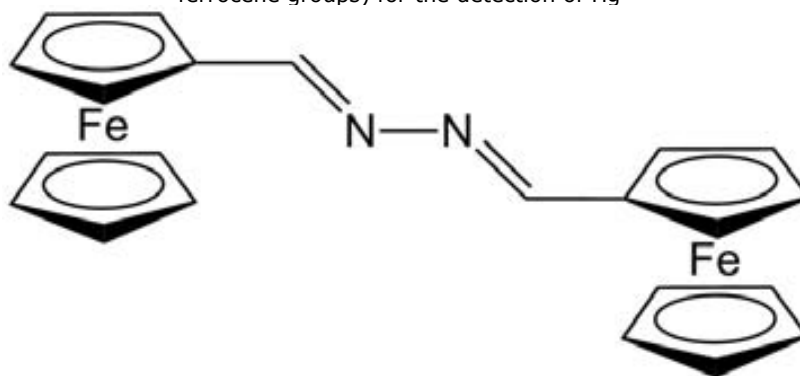
$\text{Hg}(\text{ClO}_4)_2$ and $\text{Pb}(\text{ClO}_4)_2$ were purchased from Sigma Aldrich (St. Louis, MO, US). PDMS Sylgard 184 elastomer kit was from Dow Corning (Midland, MI, US). EPON SU-8 photoresist (SU8-25) and propylene glycol methyl ether acetate (PGMEA) were from Micro-Chem Corporation (Newton, MA, US).

4.3.2. Ligands

Analytical measurements in the PhLOCs were carried out by previously mixing the heavy metal ions with the corresponding selective ligands. Previously published works have already

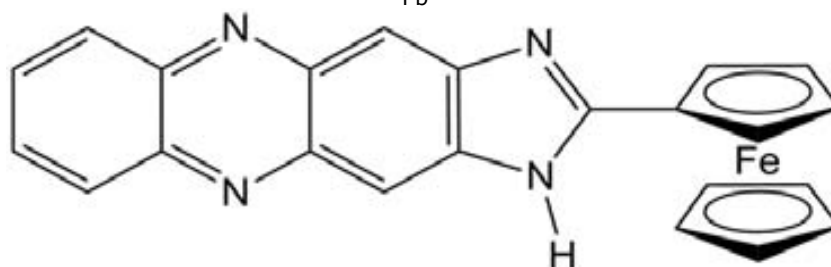
demonstrated that certain derivatives of 2,3-diaza-1,3-butadiene can act as sensitive and very selective molecular probes for the detection and preconcentration of Hg^{2+} in standard solutions^{15,18,19} and real water samples²⁰. Here, an azine derivative bearing two ferrocene groups was used (Scheme 4.1, ligand **1**). This molecule was prepared using previously reported procedures²¹. A solution of ligand **1** in acetonitrile shows an absorbance band at 476 nm. The addition of increasing amounts of an aqueous solution of $\text{Hg}(\text{ClO}_4)_2$ to this solution causes the appearance of a new band at 551 nm, a secondary peak at 405 nm and the disappearance of the initial band at 476 nm. The three well-defined isosbestic points indicate that a neat interconversion between the uncomplexed and complexed species occurs. The new band is red-shifted by 45 nm and is responsible for the change in color from yellow (neutral ligand **1**) to deep purple (complexed ligand **1**). The absorption spectral data indicate a 1:1 binding model and an association constant of $4.35 \times 10^5 \text{ M}^{-1}$ in acetonitrile¹⁵.

Scheme 4.1. Chemical structure of ligand **1** (1,4-disubstituted 2,3-diaza-1,3-butadiene bearing two ferrocene groups) for the detection of Hg^{2+}



The detection of Pb^{2+} was carried out using an imidazophenazine-ferrocene ligand (Scheme 4.2, ligand **2**) whose absorbance spectra also change upon complexation with Pb^{2+} cations. This ligand was prepared using a previously published method²¹. A solution of ligand **2** in acetonitrile shows an absorbance band at 503 nm. The addition of increasing amounts of $\text{Pb}(\text{ClO}_4)_2$ to this solution gives rise to a new absorbance band at 404 nm and the shift of the initial band from 503 nm to 515 nm. Binding assays previously performed¹⁶ using the method of continuous variations (Job's plot) suggest a 1:1 binding model with an association constant of $1.4 \times 10^5 \text{ M}^{-1}$.

Scheme 4.2. Chemical structure of ligand **2** (2-ferrocenylimidazo[4,5-b]phenazine) for the detection of Pb^{2+}



4.3.3. Design and fabrication of the PhLOCs

The PhLOCs¹⁷ consist of a microfluidic system with a defined geometry embedded in a PDMS chip and sealed on a soda-lime glass. The analyzed volume/region is constructed so as to reduce the mean flow cell volume. Thus, in the vicinity of the micro channels, micro-optical elements are defined in the PDMS in the same fabrication step. These micro-optical elements include alignment channels for positioning the input/output optical fibers as well as bioconvex microlenses for the correction of the fibers numerical aperture. In addition, air mirrors have been included to meaningfully lengthen the optical path without dramatically increasing the overall size of the analytical system. Taking into account the low cost issue, all these elements have been defined considering the refractive indices of air ($n_{\text{air}} = 1.00$), PDMS ($n_{\text{PDMS}} = 1.41$) and acetonitrile ($n_{\text{ace}} = 1.34$)²², the latter being used as the solvent for the preparation of the heavy metal ion samples. It has been reported that this solvent does not swell the PDMS or induce other negative effects that could affect the performance of the analytical system²³.

Images of the two PhLOC systems presented in this work can be seen in Figure 1. Both are based on a MIR detection approach. The first one is the Propagating Multiple Internal Reflection (PMIR) system (Figure 4.1a), in which two air mirrors are included, causing the light to follow a zigzag path along the detection region with a total OPL of 6357 μm . The second system is the Ring Multiple Internal Reflection (RMIR) approach (Figure 4.1b), in which three air mirrors have been included in order to increase the light path without significantly increasing the chip size. The total OPL in the RMIR is 14264 μm .

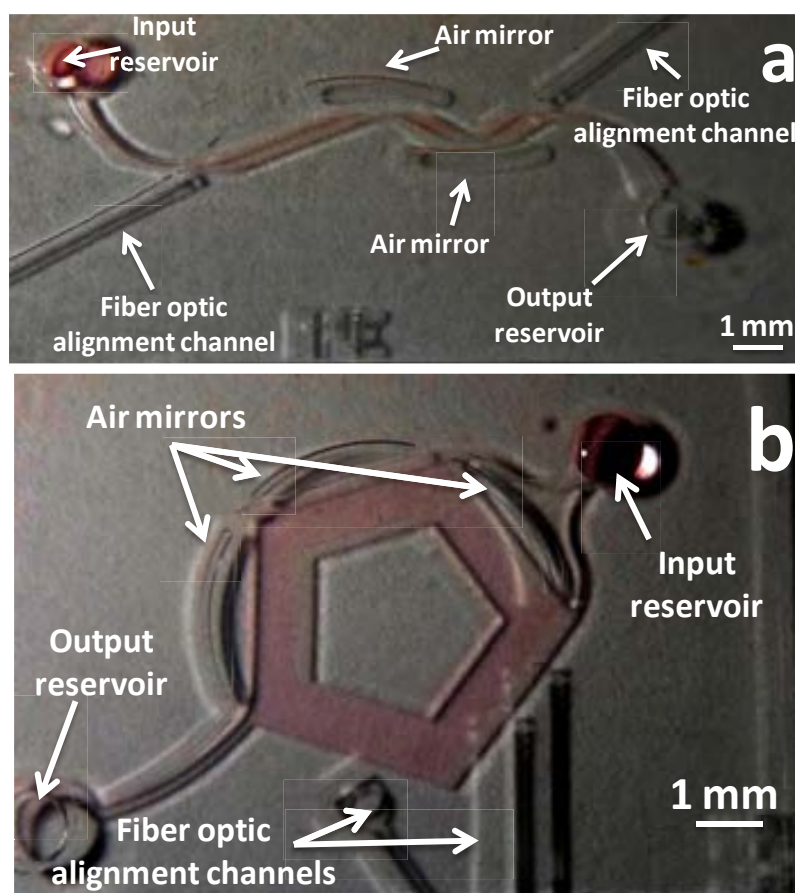


Figure 4.1. (a) PMIR and (b) RMIR systems used for the detection of heavy metals. The analyzed region was filled with a red-color solution for better contrast.

The systems were fabricated by casting of PDMS against a master made of the EPON SU-8 2025 negative tone polymer, which in turn was fabricated by standard photolithographic processes. The methodology is described in Chapter 3 and it was previously reported by Llobera and co-workers¹⁷.

4.3.4. Experimental setup and measurement protocol

A comparative analytical study of the performance of the two fabricated systems as well as a standard cuvette, which is commonly used in spectrophotometric methods (10 mm OPL, 1 mL minimum working volume; CVD-UV15 plastic cuvettes, Ocean Optics, Dunedin, USA), was carried out. To this effect, multimode optical fibers with a diameter of 230 μm were inserted in the alignment channels. The input fiber optic was connected to the light source (Ocean Optics HL-2000, Dunedin, USA), whereas the output fiber optic was connected to a microspectrophotometer (Ocean Optics HR4000, Dunedin, USA). The spectral response was recorded using the SpectraSuite software (Ocean Optics, Dunedin, USA).

Samples containing increasing Hg^{2+} concentrations from 1 μM to 1 mM and a 0.1 mM constant concentration of ligand **1** in acetonitrile were pumped into the PhLOC systems by using a vacuum pump and the resulting absorbance spectra were recorded in the visible wavelength range (from 300 nm to 800 nm) under quiescent conditions. For each concentration, the average of 10 spectra recorded consecutively was taken. Measurements were carried out starting with the lowest Hg^{2+} concentration. Acetonitrile was pumped in between measurements to clean the microsystem. The results obtained with the two PhLOC systems were compared to the ones obtained with the standard cuvette.

Once the PhLOC systems for Hg^{2+} detection were characterized, the system that presented the best performance was selected to carry out the analysis of Pb^{2+} using ligand **2** under the same conditions in terms of concentration and experimental setup as for Hg^{2+} .

4.4. Results and discussion

Figure 4.2 shows the change of the absorbance spectra with increasing concentrations of Hg^{2+} , measured with the RMIR system. A similar behavior was observed with the PMIR. The signal recorded in an acetonitrile solution just containing ligand **1** was taken as a reference. Two new peaks were observed at 405 nm and 551 nm when solutions with increasing amounts of Hg^{2+} were flowed through the system. Due to the fact that the ligand shows several wavelengths at which a significant change in absorbance takes place upon increasing amounts of Hg^{2+} in the sample, the sensitivity and LOD estimated from the calibration curves recorded for each wavelength of the spectra were plotted against the wavelength, as in Vila-Planas *et al.*²⁴ (Figure 3a and b, respectively). The LOD was calculated as the lowest analyte concentration for which the signal exceeds the relative standard deviation of the background signal divided by the slope of the calibration curve by a factor of 3. The calibration curves showed in all cases the expected linear behavior (Beer–Lambert law) in a Hg^{2+} concentration range between 20 μM and 100 μM for the PMIR and between 1 μM and 90 μM for the RMIR system.

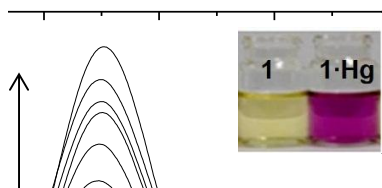


Figure 4.2. Absorbance spectra recorded in solutions acetonitrile containing 0.1 mM ligand **1** and increasing concentrations of Hg²⁺ in a range from 1 μ M to 90 μ M, with the RMIR system. Spectrum of the ligand **1** solution was taken as reference value and two new peaks were observed at 405 nm and 551 nm when Hg²⁺ was present in solution. Inset shows a picture of acetonitrile solutions containing 0.1 mM ligand **1** and the change in color of this solution upon addition of 1 equivalent of Hg²⁺.

Figure 4.3 clearly provides with the working wavelength that shows the highest sensitivity (Figure 4.3a) and lowest LOD (Figure 4.3b) for Hg²⁺ ions. These values were $5.6 \times 10^{-3} \pm 1 \times 10^{-4}$ A.U. μ M⁻¹ and $2.59 \times 0.04 \mu$ M (0.49 ppm), respectively, at a wavelength of 551 nm for the RMIR system. The LOD and sensitivity parameters attained with the cuvette were $4.38 \pm 0.14 \mu$ M and $4.2 \times 10^{-3} \pm 1 \times 10^{-4}$ A.U. μ M⁻¹, whereas for the PMIR these values were $7.0 \pm 0.2 \mu$ M and $1.67 \times 10^{-3} \pm 6 \times 10^{-5}$ A.U. μ M⁻¹, respectively. These variations are consistent with the different optical paths of the RMIR, the cuvette and the PMIR system. Similar analytical values were previously reported using this ligand either in solution or deposited on a nitrocellulose membrane by measuring the absorbance or fluorescence behavior of this molecular probe^{15,18}. It is worth mentioning that the sample/reagent volume was 190 times lower when applying the RMIR system (5.34 μ L) compared with the volume required when the standard cuvette (1 mL minimum working volume) was used.

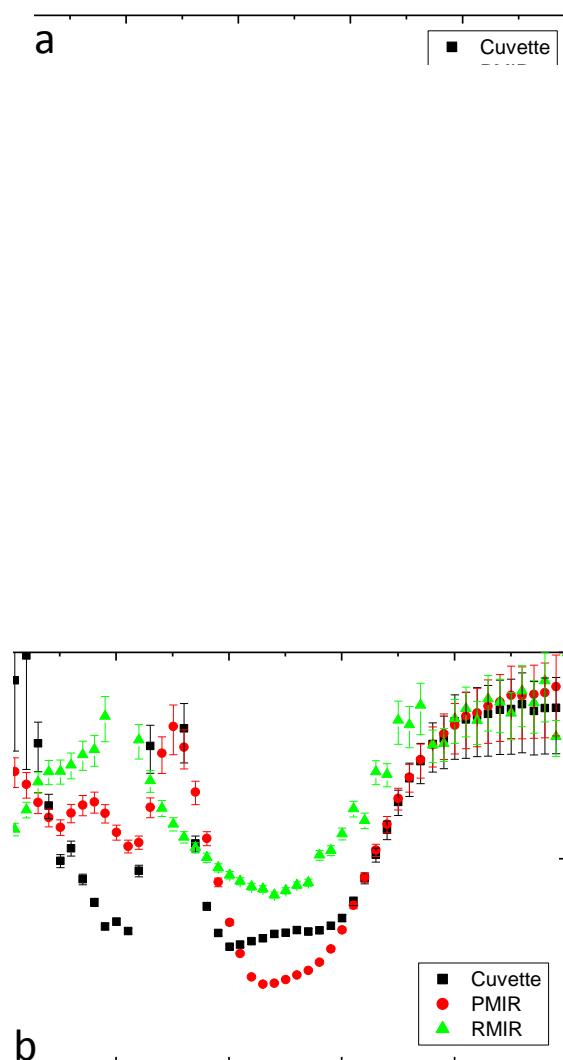


Figure 4.3. (a) Sensitivity and (b) LOD values for the detection of Hg^{2+} in a solution of ligand **1** using a cuvette, PMIR and RMIR system in a spectral range that varies from 300 to 800 nm.

The versatility of the presented analytical approach, which combines the use of molecular ligands that selectively interact with heavy metal ions with easy-to-use low-cost PhLOC systems, is demonstrated by carrying out the detection of Pb^{2+} . The RMIR system was chosen because of its best performance in the detection of Hg^{2+} . Thus, an identical RMIR system to the one used for the detection of Hg^{2+} was used. The analytical measurement was based on the use of ligand **2** described in the experimental section. Here, the sensitivity and LOD were also calculated as a function of the detection wavelength and results are shown in Figure 4.4. A linear behavior in a concentration range of $3\ \mu\text{M}$ – $100\ \mu\text{M}$ Pb^{2+} was obtained, with $9.6 \pm 0.2 \times 10^{-4}\ \text{A.U.}\ \mu\text{M}^{-1}$ and $4.2 \pm 0.1\ \mu\text{M}$ (0.868 ppm) being the highest sensitivity and lowest LOD values respectively. These results were recorded at 515 nm, at which the spectra of ligand **2** show a peak when interacts with Pb^{2+} , as described above. These results are similar to the

ones previously reported using the same ligand and fluorescence detection¹⁶ but with the added advantage of requiring minute sample volumes.

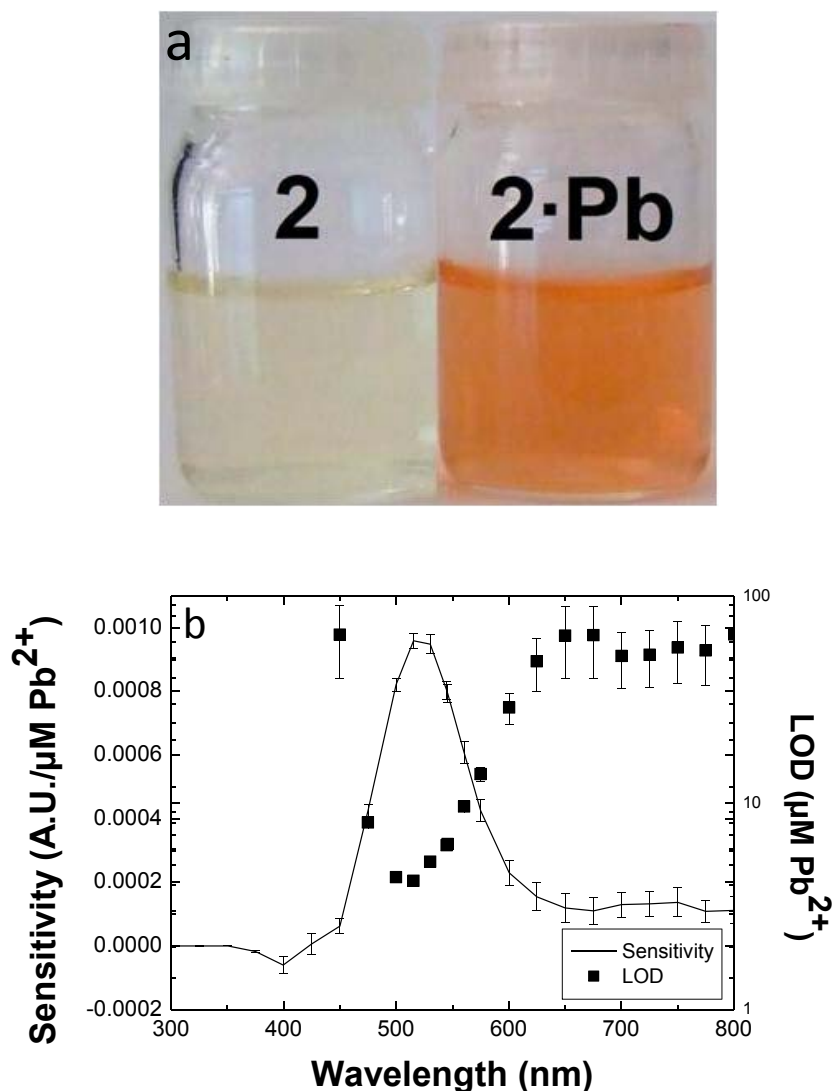


Figure 4.4. (a) Picture showing acetonitrile solutions containing 0.1 mM ligand **2** and the change in color of this solution upon addition of 1 equivalent of Pb^{2+} . (b) Sensitivity and Limit of detection (LOD) values for the detection of Pb^{2+} in a solution of ligand **2** using the RMIR system through a spectral range ranging from 300 to 800 nm.

Although the results do not allow detection of mercury²⁵ or lead²⁶ ion levels below the threshold for drinking water defined by the US Environmental Protection Agency (EPA), the LOD could be decreased by simply lengthening the optical path even more without significantly affecting the overall size of the chip. Nevertheless, it should be highlighted that the LOD is also limited in this work by the ligands themselves, which have been previously shown to provide similar sensitivities and LOD to those achieved in this work, even when applying a fluorescence detection approach in the case of Hg^{2+} analysis^{15,16,18,19}. The increase in the length of the optical

path is relatively simple to carry out compared with the application of other more complicated approaches such as surface plasmon resonance²⁷, or electrochemistry²⁸. Nevertheless, it is worth mentioning that in some countries the tolerance limits are higher. For example, in India, the allowed levels prescribed by the Bureau of Indian Standards (BIS) for Hg²⁺ are 10 ppm for inland surface water and 1 ppm for drinking water²⁹, which make the system presented here with the potential to be directly applied in these scenarios.

4.5. Conclusions

Two low-cost polymeric PhLOC systems were presented and their potential showed when combined with highly selective ligands for the quick in situ testing of heavy metal ions using very small sample volumes. The described systems included air mirrors to lengthen the optical path without increasing their inherent dimensions and presented high absorbance signals, making them useful in miniaturized optical detection approaches.

Overall, the here presented PhLOCs could be implemented as miniaturized analytical systems for detecting Hg²⁺ and Pb²⁺ in an easy and cheap way. They outperform other previously reported systems just by considering the ease and cost of their fabrication process as well as the simplicity of the applied absorbance-based detection approach, which avoids the implementation of electrodes^{10,30}, heaters or the incorporation of toxic substances such as mercury droplets that make the system non-disposable⁹. Finally, these PhLOCs offer the possibility of carrying out rapid analysis of such kind of pollutants if a continuous flow operation mode is used. In addition, they can be included in more complex PhLOCs, incorporating mixers for mixing the sample with the ligand or filters to eliminate particles in suspension that would induce light scattering, as it is usually done with real samples following the guidelines from the United States (US)³¹ and from the European Union³².

4.6. References

1. O. Krystofova, L. Trnkova, V. Adam, J. Zehnalek, J. Hubalek, P. Babula, R. Kizek. Electrochemical microsensors for the detection of cadmium(II) and lead(II) ions in plants *Sensors* 10, **2010**, 5308-5328.
2. F. Loe-Mie, G. Marchand, J. Berthier, N. Sarrut, M. Pucheault, M. Blanchard-Desce, F. Vinet, M. Vaultier. Towards an efficient microsystem for the real-time detection and quantification of mercury in water based on a specifically designed fluorogenic binary task-specific ionic liquid. *Angewandte Chemie International Edition*. 49, **2010**, 424-427.
3. D. Arunbabu, A. Sannigrahi, T. Jana. Photonic crystal hydrogel material for the sensing of toxic mercury ions (HG²⁺) in water. *Soft Matter* 7, **2011**, 2592-2599.
4. Y.L. Hung, T.M. Hsiung, Y.Y. Chen, C.C. Huang. A label-free colorimetric detection of lead ions by controlling the ligand shells of gold nanoparticles. *Talanta* 82, **2010**, 516-522.
5. E.M. Krupp, B.F. Milne, A. Mestrot, A.A. Meharg, J. Feldmann. Investigation into mercury bound to biothiols: structural identification using ESI-ion-trap MS and introduction of a

- method for their HPLC separation with simultaneous detection by ICP-MS and ESI-MS. *Analytical and Bioanalytical Chemistry* 390, **2008**, 1753.
6. F.A. Duarte, C.A. Bizzi, F. Goldschmidt-Antes, V.L. Dressler and E.M. de Moraes-Flores. Organic, inorganic and total mercury determination in fish by chemical vapor generation with collection on a gold gauze and electrothermal atomic absorption spectrometry. *Spectrochimica Acta Part B* 64, **2009**, 513-519.
 7. S. Arzhantsev, X. Li, J.F. Kauffman. Rapid limit tests for metal impurities in pharmaceutical materials by X-ray fluorescence spectroscopy using wavelet transform filtering. *Analytical Chemistry* 83, **2011**, 1061-1068.
 8. Q. Hu, G. Yang, Y. Zhao, J. Ying. Determination of copper, nickel, cobalt, silver, lead, cadmium, and mercury ions in water by solid-phase extraction and the RP-HPLC with UV-Vis detection. *Analytical and Bioanalytical Chemistry* 375, **2003**, 831-835.
 9. X.S. Zhu, C. Gao, J.W. Choi, P.L. Bishop, C.H. Ahn. On-chip generated mercury microelectrode for heavy metal ion detection. *Lab on a Chip* 5, **2005**, 212-217.
 10. Z. Zou, A. Jang, E. MacKnight, P.M. Wu, J. Do, P.L. Bishop, C.H. Ahn. Environmentally friendly disposable sensors with microfabricated on-chip planar bismuth electrode for *in situ* heavy metal ions measurement. *Sensors and Actuators B* 134, **2008**, 18-24.
 11. B. A. Flusberg, E.D. Cocker, W. Piyawattanametha, J.C. Jung, E.L.M. Cheung, M.J. Schnitzer. Fiber-optic fluorescence imaging. *Nature Methods* 2(12), **2005**, 941-950.
 12. H.N. Kim, W.X. Ren, J.S. Kim, J. Yoon. Fluorescent and colorimetric sensors for detection of lead, cadmium, and mercury ions. *Chemical Society Reviews* 41, **2012**, 3210-3244.
 13. X.M. Wang, H. Yan, X.L. Feng, Y. Chen. 1-pyrenecarboxaldehyde thiosemicarbazone: a novel fluorescent molecular sensor towards mercury (II) ion. *Chinese Chemical Letters* 21, **2010**, 1124-1128.
 14. L. Zhang, B. Han, T. Li, E. Wang. Label-free DNAzyme-based fluorescing molecular switch for sensitive and selective detection of lead ions. *Chemical Communications* 47, **2011**, 3099-3101.
 15. A. Caballero, R. Martínez, V. Lloveras, I. Ratera, J. Vidal-Gancedo, K. Wurst, A. Tárraga, P. Molina, J. Veciana. Highly selective chromogenic and redox or fluorescent sensors of Hg²⁺ in aqueous environment based on 1,4-disubstituted azines. *Journal of the American Chemical Society* 127, **2005**, 15666-15667.
 16. F. Zapata, A. Caballero, A. Espinosa, A. Tárraga, P. Molina. *The Journal of Organic Chemistry* 74, **2009**, 4787-4796.
 17. A. Llobera, S. Demming, R. Wilke, S. Büttgenbach. Multiple internal reflection poly(dimethylsiloxane) systems for optical sensing. *Lab on a Chip* 7, **2007**, 1560-1566.
 18. C. Díez-Gil, A. Caballero, I. Ratera, A. Tárraga, P. Molina, J. Veciana. Naked-eye and selective detection of mercury (II) ions in mixed aqueous media using a cellulose-based support. *Sensors* 7, **2007**, 3481-3488.
 19. C. Díez-Gil, R. Martínez, I. Ratera, A. Tárraga, P. Molina, J. Veciana. Nanocomposite membranes as highly selective and sensitive mercury(II) detectors. *Journal of Materials Chemistry* 18, **2008**, 1997-2002.
 20. M. Soleimani, M.S. Mahmodi, A. Morsali, A. Khani, M.G. Afshar. Using a new ligand for solid phase extraction of mercury. *Journal of Hazardous Materials* 189, **2011**, 371-376.
 21. R.M.T. Casey, P. Guinan, A. Canavan, M. McCann, C. Cardin, N.B. Kelly. Reaction of 1,1'-diacetylferrocene with hydrazine hydrate: Synthesis and X-ray crystal structures of bis(hydrazine)bis(hydrazinecarboxylato-N',O)iron(II), [Fe(N₂H₄)₂(O₂CNHNH₂)₂], and the cyclic biferrocene diazine, [--N(Me)CC,H,FeC,H,C(Me)N-]₂. *Polyhedron* 10, **1991**, 483-489.
 22. G. Openhaim, E. Grushka. Temperature-dependent refractive index issues using a UV-visible detector in high-performance liquid chromatography. *Journal of Chromatography A* 942, **2002**, 63.
 23. J.N. Lee, C. Park, G.M. Whitesides. Solvent compatibility of poly(dimethylsiloxane)-based microfluidic devices. *Analytical Chemistry* 75, **2003**, 6544-6554.

24. J. Vila-Planas, E. Fernández-Rosas, B. Ibarlucea, S. Demming, C. Nogués, J.A. Plaza, C. Domínguez, S. Büttgenbach, A. Llobera. Cell analysis using a multiple internal reflection photonic lab-on-a-chip. *Nature Protocols* 6(10), **2011**, 1642-1655.
25. S. Ando, K. Koide. Development and applications of fluorogenic probes for mercury(II) based on vinyl ether oxymercuration. *Journal of the American Chemical Society* 133, **2011**, 2556-2566.
26. W. Wang, Y. Jin, Y. Zhao, X. Yue, C. Zhang. Single-labeled hairpin probe for highly specific and sensitive detection of lead(II) based on the fluorescence quenching of deoxyguanosine and G-quartet. *Biosensors and Bioelectronics* 41, **2013**, 137-142.
27. C. Díez-Gil, R. Martínez, I. Ratera, T. Hirs, A. Espinosa, A. Tárraga, P. Molina, O.S. Wolfbeis, J. Veciana. Selective picomolar detection of mercury(II) using optical sensors. *Chemical Communications* 47, **2011**, 1842-1844.
28. W. Jung, A. Jang, P.L. Bishop, C.H. Ahn. A polymer lab chip sensor with microfabricated planar silver electrode for continuous and on-site heavy metal measurement. *Sensors and Actuators B* 155, **2011**, 145-153.
29. N. Kannan, S.J.S. Malar. Removal of mercury(II) ions by adsorption onto dates nut and commercial activated carbons: A comparative study. *Indian Journal of Chemical Technology* 12, **2005**, 522-527.
30. J. Tanyanyiwa, E.M. Abad-Villar, M.T. Fernández-Abedul, A. Costa-García, W. Hoffman, A.E. Guber, D. Hermann, A. Gerlach, N. Gottschlich, P.C. Hauser. High-voltage contactless conductivity-detection for lab-on-chip devices using external electrodes on the holder. *Analyst* 128, **2003**, 1019-1022.
31. R. Wagner, R.W. Boulger, Jr., C.J. Oblinger, B.A. Smith. U.S. Geological Survey: Guidelines and standard procedures for continuous water-quality monitors: station operation, record computation, and data reporting, **2006**.
32. Official Journal of the European Union, Directive 2008/105/EC of the European parliament and of the Council, **2008**.

5. SELECTIVE FUNCTIONALIZATION OF PDMS-BASED PHOTONIC-LAB-ON-A-CHIP FOR BIOSENSING

5.1.	Summary	82
5.2.	Introduction	82
5.3.	Experimental details	83
5.3.1.	Materials and reagents	83
5.3.2.	Fabrication of the microsystem	84
5.3.3.	Modification and characterization of the PDMS surfaces	84
5.3.4.	Fabrication of the biosensor approach	85
5.3.5.	Stability of the microsystems	86
5.4.	Results and discussion	86
5.4.1.	Structural characterization of the modified PDMS surfaces	87
5.4.2.	Analytical performance of the different biosensor approaches	95
5.5.	Conclusions	97
5.6.	References	98

The work included in this chapter has been reported in a paper entitled “Selective functionalisation of PDMS-based photonic lab on a chip for biosensing”, by Bergoi Ibarlucea, César Fernández-Sánchez Stephanie Demming, Stephanus Büttgenbach, and Andreu Llobera, *Analyst* 136, **2011**,3496-3502.

The methodology followed in the experimental section has been described in detail in a protocol entitled “Biofunctionalization of PDMS-based microfluidic systems” by Bergoi Ibarlucea, César Fernández-Sánchez, Stephanie Demming, Stephanus Büttgenbach and Andreu Llobera. *Nature Protocol Exchange*, 2011, DOI: 10.1038/protex.2011.271

5.1. Summary

A comparative study of different approaches for the selective immobilization of biomolecules on the surface of poly(dimethylsiloxane) (PDMS) is reported. The motivation of this work is to set a robust and reliable protocol for the easy implementation of a biosensor device in a PDMS-based photonic Lab-on-a-Chip (PhLOC). A hollow prism configuration, previously reported for the colorimetric detection of analytes was chosen for this study. Here, the inner walls of the hollow prism were initially modified by direct adsorption of either polyethylene glycol (PEG) or polyvinyl alcohol (PVA) linear polymers as well as by carrying out a light chemical oxidation step. All these processes introduced hydroxyl groups on the PDMS surface to a different extent. The hydroxyl groups were further silanized using a silane containing an aldehyde end-group. The interaction between this group and a primary amine moiety enabled the selective covalent attachment of a biomolecule on the PDMS surface. A thorough structural characterization of the resulting modified-PDMS substrates was carried out by contact angle measurements, X-ray photoelectron spectroscopic (XPS) analysis and atomic force microscopy (AFM) imaging. Using horseradish peroxidase as a model recognition element, different biosensor approaches based on each modification process were developed for the detection of hydrogen peroxide target analyte in a concentration range from 0.1 μM to 100 μM . The analytical performance was similar in all cases, a linear concentration range between 0.1 μM and 24.2 μM , a sensitivity of 0.02 A.U. mM^{-1} and a limit of detection around 0.1 μM were achieved. However, important differences were observed in the reproducibility of the devices as well as in their operational stability, which was studied over a period of up to two months. Considering all these studies, the PVA-modified approach appeared to be the most suitable one for the simple fabrication of a biosensor device integrated in a PDMS PhLOC.

5.2. Introduction

The huge impact of the Lab-on-a-Chip (LOC) concept cannot be understood without the development of polymeric materials, being polydimethylsiloxane (PDMS) one of the most usual ones. However, one important drawback of PDMS lies in its ability to nonspecifically adsorb biomolecules and other macromolecules, which hampers its application for chemical sensing. In this context, its surface can be easily tailored in order to avoid such undesirable process, or by contrast, to selectively immobilize different molecules¹. PDMS surfaces have already been treated with oxygen plasma² or UV/ozone³, in order to make the surface hydrophilic by replacing the surface methyl groups, bound to the Si on the PDMS structure, by silanol groups (Si–OH). These new groups are prone to chemically interact with different functional groups, thus enabling the selective modification of the PDMS surface. However, it should be taken into account that the properties of these silanol groups are dynamic in the sense that the surface progressively recovers its hydrophobicity. Keeping in mind this drawback, the fact that these processes required special instrumentation and cannot be applied in microfluidic channels that were embedded in PDMS matrices⁴, alternative processes for the selective modification of PDMS surfaces, which were easy to implement, are required.

In this work, a study of different liquid-based surface chemical biofunctionalization methods was carried out using a PDMS photonic LOC (PhLOC) consisting of a hollow Abbe prism transducer configuration (Figure 5.1)⁵. On one hand, physical adsorption of two different polymers containing hydroxyl groups, such as polyethylene glycol (PEG) or polyvinyl alcohol (PVA) enabled the further silanization of the surface for the introduction of chemical functional groups and the eventual covalent immobilization of the protein receptor. Both polymers were previously applied to the modification of PDMS in order to avoid the non-specific binding of proteins^{6,7}. On the other hand, a covalent modification approach was tested based on the chemical oxidation of the PDMS surface, thus generating silanol groups onto which a silanization process and further immobilization of the protein receptor were carried out, as above. A thorough structural and analytical characterization of the resulting modified PDMS surfaces was carried out. These methods could be performed in chemical and biological laboratories and applied to PDMS microfluidic systems without the need for special instrumentation.

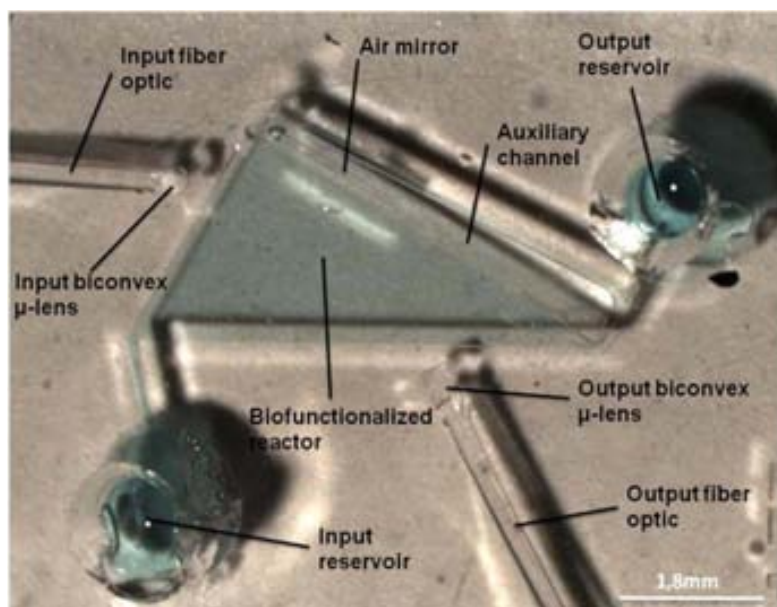


Figure 5.1. Photography of the photonic Lab-on-a-Chip microfluidic system.

5.3. Experimental details

5.3.1. Materials and reagents

The EPON SU-8 2025 negative tone polymer and the propylene glycol methyl ether acetate (PGMEA) were purchased from MicroChem Corporation (Newton, MA, USA). The PDMS Sylgard 184 elastomer kit was bought from Dow Corning (Midland, MI, USA) and used according to the datasheet.

99% PVA, PEG (molecular weight: 12 000 g), 30% (v/v) H₂O₂, 99% triethylamine (TEA), HRP type VI, 99% 2,2'-azino-bis (3-ethylbenzthiazoline-6-sulfonic acid) (ABTS), sodium cyanoborohydride

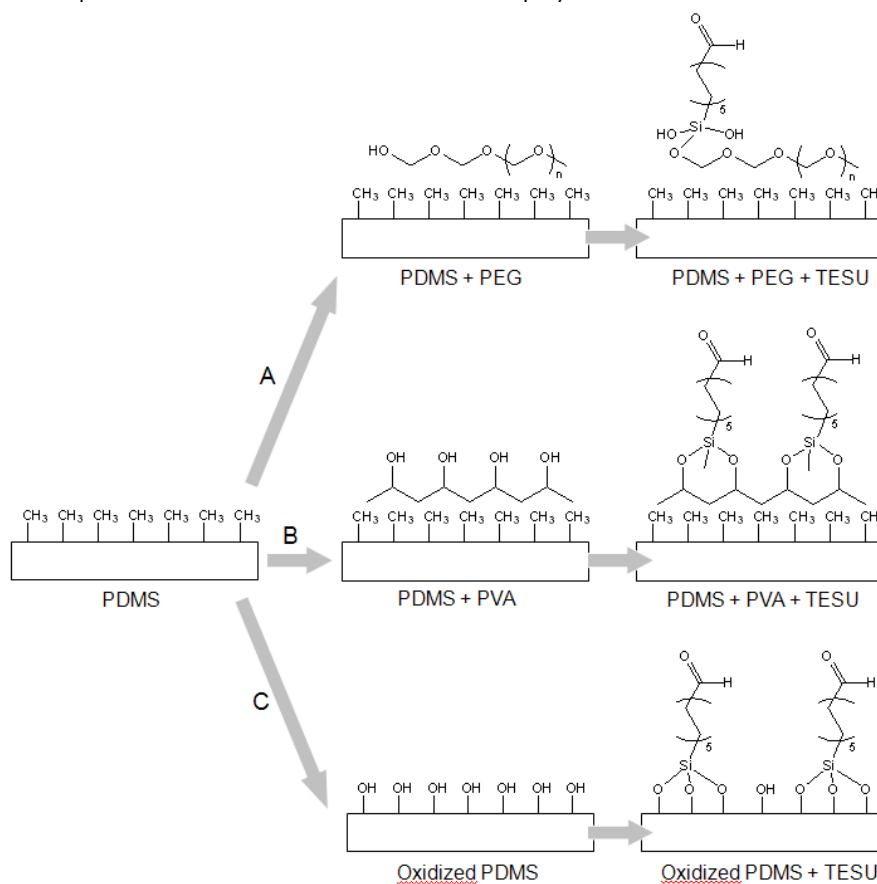
(NaBH_3CN) and Tween 20 were from Sigma-Aldrich Co. (St Louis, MO 63103, USA). 90% 11-triethoxysilyl undecanal (TESU) was from ABCR GmbH & Co. KG (76187 Karlsruhe, Germany). All other chemicals were of analytical grade.

5.3.2. Fabrication of the microsystem

The PhLOC was fabricated by cast molding, following the protocol described in Chapter 3 and previously reported by Llobera and co-workers⁸. The final volume of the PhLOC is 1.6 μL .

5.3.3. Modification and characterization of the PDMS surfaces

Scheme 5.1. Representation of the different methods employed for the modification of PDMS surface.



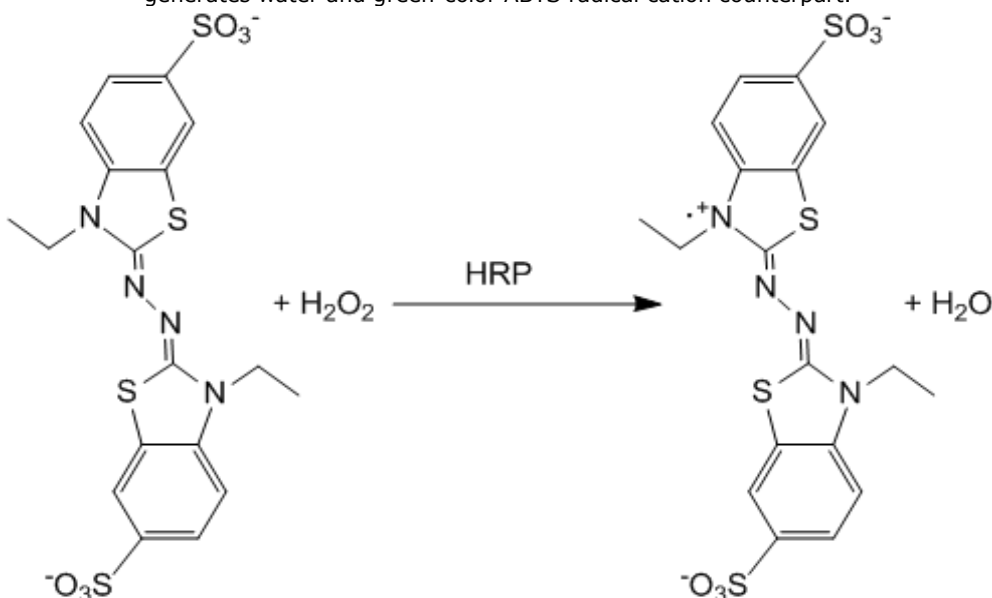
The three selected approaches for the PDMS surface modification are based on the introduction of hydroxyl ($-\text{OH}$) groups. Scheme 5.1 shows a representation of the different steps required for each functionalization process. First, the PDMS surfaces were cleaned with ethanol and deionized water (DI H_2O). For the modification shown in scheme 5.1A, a 1 mg ml^{-1} PEG solution in DI H_2O was pumped inside the system and left to react for 1 hour at room temperature (RT). For the modification in scheme 5.1B, the system was filled with a 1 mg ml^{-1} PVA solution in DI H_2O and left to react for 1 hour at room temperature (RT). Scheme 5.1C shows the direct introduction of $-\text{OH}$ groups on the PDMS surface, using an acidic solution containing DI H_2O , 37% HCl and 30% H_2O_2 in a 5:1:1 (v/v/v) ratio⁴. After each of these steps, the surfaces were rinsed with DI H_2O and dried under a N_2 stream. Next, a silanization process

was carried out by incubating the modified PDMS systems in a 99.5% ethanol solution containing 2% TESU and 2% TEA for 1 hour at RT. Then the surfaces were thoroughly rinsed with 99.5% ethanol and dried at 80 °C for 2 hours. The TEA induces a highly nucleophilic oxygen in the –OH group that readily interacts with a silane⁹ having its ethoxy groups previously hydrolyzed. In this way, the silane covalently bound to the surface. All these modifications were also applied to flat PDMS surfaces having an area of 1 cm² to facilitate the structural characterization of the resulting modified material by the different techniques described below.

Contact angle measurements were carried out with the sessile drop method, using a Krüss Easydrop contact angle meter and DS1 analysis software (Krüss GmbH, Hamburg, Germany). A drop of water was deposited on the modified PDMS surface and the angle formed between the liquid and the solid surface was measured. XPS analysis was carried out at the facilities of the Instituto de Nanociencia de Aragon (Spain) on an Axis Ultra-DLD spectrometer (Kratos Analytical Ltd, Manchester, England), using a monochromatized Al Ka source (1486.6 eV). Signals were deconvoluted with the software provided by the manufacturer, using a weighted sum of Lorentzian and Gaussian component curves after background subtraction. The binding energies were referenced to the internal standard C1s (284.9 eV). Atomic force microscopy topographic and phase images of the modified surfaces were taken with a Veeco Nanoscope Dimension 3100 (Veeco, Plainview, NY, USA), working in tapping mode.

5.3.4. Fabrication of the biosensor approach

Scheme 5.2. HRP-catalyzed reduction of hydrogen peroxide mediated by colorless ABTS, which generates water and green-color ABTS radical cation counterpart.



The analytical performance of the different modification protocols was tested by developing a biosensor for the detection of H₂O₂ based on the use of HRP as a model recognition element. The resulting aldehyde-modified PDMS surfaces bound HRP through the amine groups of lysine residues, by forming a Schiff base that is further reduced to a stable secondary amine

with sodium cyanoborohydride¹⁰. HRP catalyzes the reduction of H₂O₂ in the presence of colorless 2,2'-azino-bis (3-ethylbenzthiazoline-6-sulfonic acid) (ABTS) charge transfer mediator, which is concomitantly oxidized to the green-colored ABTS^{•+} radical cation¹¹ (Scheme 5.2). This redox species shows an absorption peak at 420 nm and two secondary peaks at 650 nm and 720 nm, the first one being chosen for the absorbance detection of this enzymatic reaction.

The overall procedure is described in detail below. PhLOC was filled with a solution containing 1 mg ml⁻¹ HRP type VI and 5 mM sodium cyanoborohydride in 0.05M carbonate buffer pH 8, and incubated for 1 hour at RT. Then, a 0.1 M phosphate buffer saline solution pH 7.0 containing 0.02% (v/v) Tween 20 (PBST) was pumped inside the system in order to remove the nonspecifically adsorbed HRP molecules. The resulting biosensor systems were filled with PBS and stored at 4 °C until use.

A fourth biosensor approach was developed by direct adsorption of the HRP enzyme on the intact PDMS surface of the microsystem. It has been previously reported that proteins easily physisorbed on the surface of PDMS due to its high hydrophobicity¹². In this work, the PDMS system was incubated in a 1 mg ml⁻¹ HRP solution in 0.05 M carbonate buffer pH 8 for 1 hour at RT. Then, the system was rinsed in PBST and stored at 4 °C, in the same fashion as above.

Finally, solutions of 0.1 M acetate buffer pH 5.5 containing 0.5 mM ABTS and increasing concentrations of H₂O₂, from 0.1 μM to 100 μM were sequentially pumped inside each PhLOC. The resulting response was detected by using a LED working at a wavelength of 430 nm (spectrally very close to the previously mentioned first absorption band of ABTS^{•+}), and measuring the spectral response using a microspectrometer (OceanOptics HR4000).

5.3.5. Stability of the microsystems

The microsystems were stored in PBS at 4 °C for over two months. The stability of the immobilized enzyme was studied by repeating the calibration curve in a H₂O₂ concentration range from 0.1 μM to 1.53 μM. The slope (sensitivity) of the calibration curve was plotted over time for comparative purposes.

5.4. Results and discussion

Each one of the three different approaches for the modification of PDMS was chosen with the aim of providing the surface with a different density of hydroxyl groups. The PVA adsorption process could give rise to a higher proportion of these groups comparing with the PEG adsorption one, taking into account the chemical structures of both polymers. As for the chemical oxidation process of the PDMS surface, the conditions were set following an optimization study, which showed that higher concentrations of H₂O₂ and HCl in the solution or longer incubation times gave rise to the PDMS surface degradation. As for the selection of the TESU aldehyde-terminated silane, this molecule enabled the straightforward covalent immobilization of the biomolecule receptor without the need of using cross-linking molecules.

5.4.1. Structural characterization of the modified PDMS surfaces

A rough but rapid estimation of the degree of modification of the PDMS surface following every step of each modification protocol was firstly provided by contact angle measurements. Given the hydrophobic nature of the intact PDMS surface, it was apparent that the introduction of chemical functional groups would give rise to a decrease of the contact angle value. The PVA-based approach was the one that appeared to induce the most significant changes on the PDMS surface. The contact angle of a native PDMS surface was found to be 114.57° , which is a similar value to that reported in previous studies³⁴. Following the PVA modification step, it decreased to 102.47° . However, the contact angle did not change when PEG was adsorbed. This may be related to the higher density of hydroxyl groups that PVA contains in its linear structure compared with PEG, which only presents two hydroxyl groups at both ends of its chain. This facilitates the incorporation of a higher number of silane molecules during the silanization step, which indeed gave rise to a further decrease of the contact angle on the PVA-modified surface to 96.9° , whereas no difference in this value was measured with the PEG-modified samples. The chemical oxidation approach induced a change in the contact angle value to 110.75° , which appeared to be not significant since such a value was not altered following the silanization process. The light chemical oxidation of the PDMS surface that took place using the HCl/H₂O₂/H₂O solution may account for such small differences in the measured contact angles. All these values were plotted in a bar graph, which can be found in Figure 5.2.

Figure 5.2. Contact angle values measured following every step of each modification procedure. Error bars correspond to the standard deviation of three replicates.

XPS analysis was carried out to make a fine estimation of the density of hydroxyl and aldehyde groups introduced on the PDMS surface during the different modification steps. Table 5.1 shows the atom content in percentage values extracted from the XPS survey scan. An increase in the carbon content occurred following the PVA modification step, from 43.38% to 51.74%, while the Si percentage decreased from 36.90% to 27.05%. This is a clear indication of the adsorption of PVA molecules on to the PDMS surface. These changes were smaller in the samples prepared by the other treatments. High resolution spectra of the C1s region were also

recorded. After the deconvolution of the C1 signal (Figures 5.3-5.5), new peaks could be detected that were related to each step of the PDMS modification processes. The native PDMS presents a unique peak that corresponds to the carbon atom of the methyl group, with a binding energy of 284.90 eV. After the first modification steps carried out to introduce –OH groups on the PDMS surface, a new peak was observed in all cases with energy of 286.50 eV, which is ascribed to C–O bonds (Table 5.2). Both PVA and PEG molecules contain this bond, but PEG has it in lower quantities, thus giving a smaller signal in the XPS spectra. In the case of the modification by chemical oxidation, Si–OH groups must have been introduced on the PDMS surface, instead of C–O bonds. However, it is reported that the oxidation of PDMS could give rise to –OH groups bound to the carbon atom of its methyl groups (–CH₃)¹⁴. This may be responsible for the appearance of such a peak in the XPS analysis of the chemically oxidized samples. Nevertheless, its signal is significantly lower than that of the PVA-modified surface. Additionally, a new peak was observed in all samples further silanized with TESU. This peak is ascribed to the C=O bonds being part of the aldehyde end group of the silane molecules. Again, the highest density of this group appeared in the PVA-modified PDMS. From these results, it can be assumed that the PVA-based modification process seems to be more effective for the introduction of chemical functional groups on the surface of PDMS, which enabled the attachment of biomolecule receptors and thus the fabrication of biosensors.

Table 5.1. Atomic percentages of the different surfaces analyzed by XPS.

SAMPLE	ATOMIC CONCENTRATION (%)	
PDMS	O1s	19.71
	C1s	43.38
	Si 2p	36.9
PVA	O1s	21.21
	C1s	51.74
	Si 2p	27.05
PEG	O1s	19.05
	C1s	43.85
	Si 2p	37.11
OXIDATION	O1s	20.09
	C1s	44.92
	Si 2p	34.99
PVA + TESU	O1s	21.29
	C1s	50.69
	Si 2p	28.02
PEG + TESU	O1s	19.13
	C1s	45.36
	Si 2p	35.51
OXIDATION + TESU	O1s	20.26
	C1s	44.25
	Si 2p	35.48

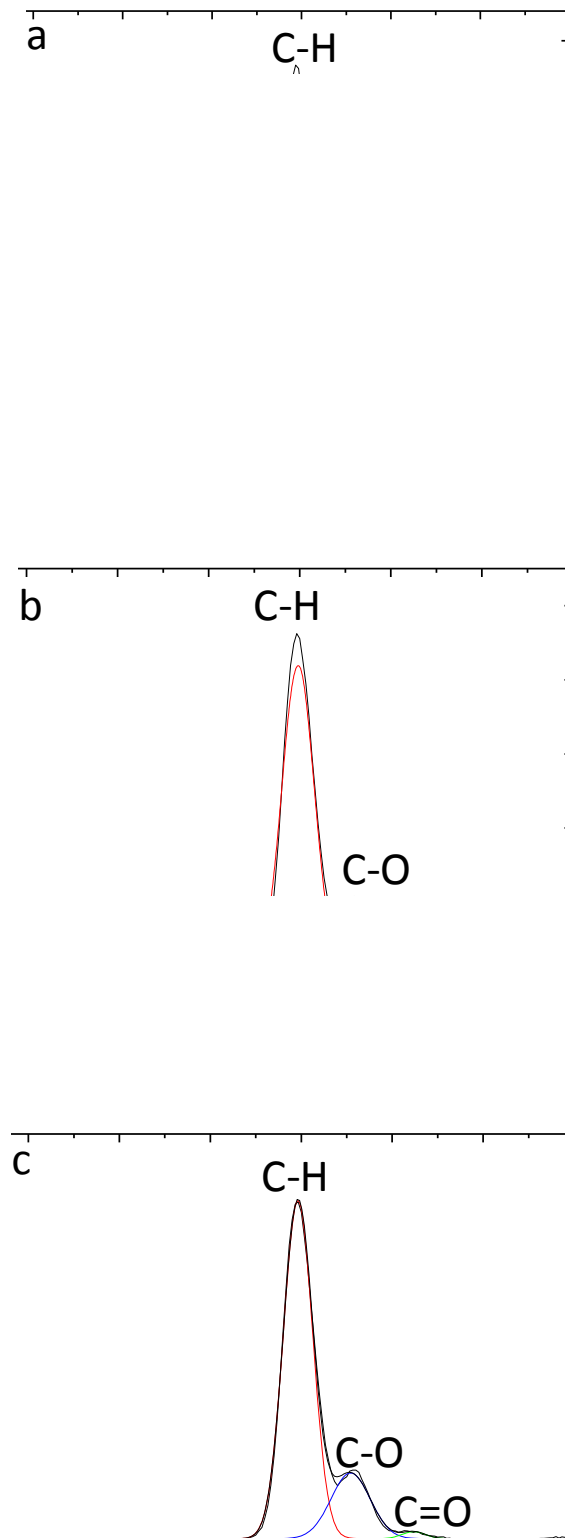


Figure 5.3. High resolution XPS spectra of the C (1s) region corresponding to (a) intact PDMS, (b) after the adsorption of PVA and (c) after the silanization process with TESU (c).

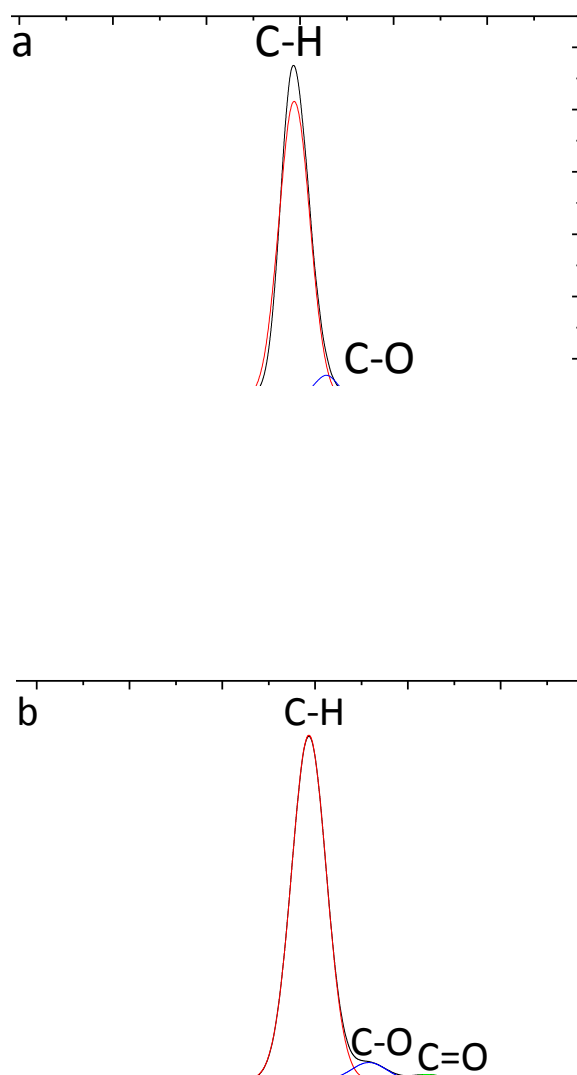


Figure 5.4. High resolution XPS spectra of the C (1s) region corresponding to PEG-modified PDMS (a) before and (b) after the silanization process with TESU.

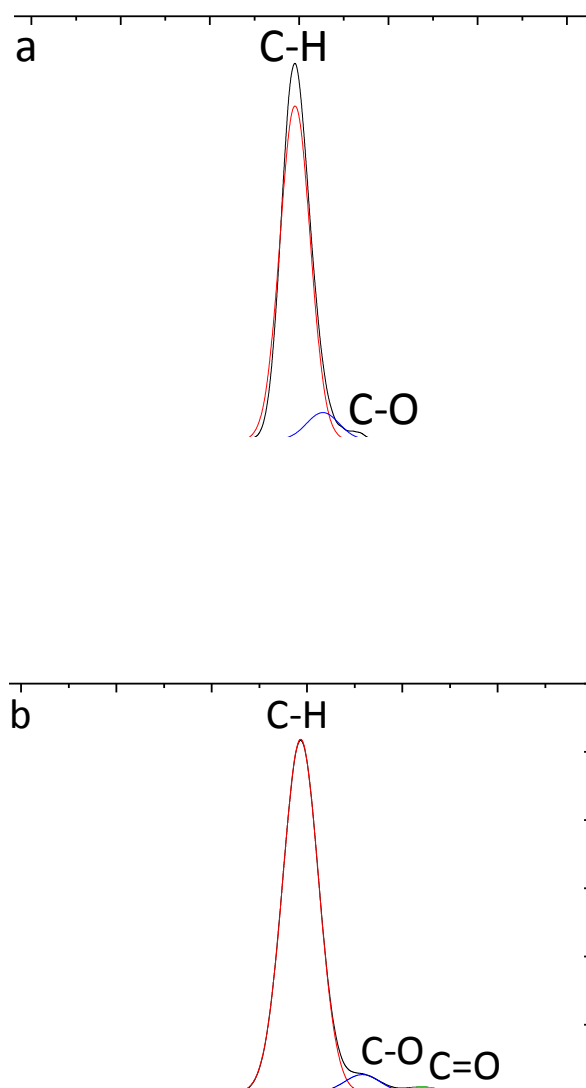


Figure 5.5. High resolution XPS spectra of the C(1s) region corresponding to PDMS (a) after the chemical oxidation and (b) after the silanization process.

Table 5.2. C percentages corresponding to the different chemical groups introduced on the PDMS surface after each modification step.

Sample	Bond	Position (eV)	Atomic percentage
PDMS	C-H	284.90	100
PDMS + PVA	C-H	284.90	77.96
	C-O	286.68	22.06
PDMS + PVA + TESU	C-H	284.90	78.21
	C-O	286.68	19.78
	C=O	288.33	2.01
PDMS + PEG	C-H	284.89	95.40
	C-O	286.50	4.60
PDMS + PEG + TESU	C-H	284.89	89.23
	C-O	286.50	9.70
	C=O	288.80	1.07
Oxidation	C-H	284.93	91.79
	C-O	286.50	8.21
Oxidation + TESU	C-H	284.93	90.98
	C-O	286.50	8.24
	C=O	288.78	0.78

The topographic and phase images obtained by AFM (Figure 5.6) show that the unmodified PDMS surface is topographically flat as well as structurally and chemically homogeneous. In all cases, the modified surfaces upon each modification step exhibit from slight to dramatic variations in topography and composition, depending on the applied procedure. Branch-like structures can be observed on the PVA-modified surfaces (also shown in Figure 5.6), which are likely to be related to the linear structure of the PVA polymer chains randomly adsorbed on to the PDMS. Furthermore, the PDMS surface significantly changed upon the silanization process with TESU and a honeycomb-like polymeric structure was imaged (last two images of Figure 5.6). Here, a polymerization process could have taken place among the TESU molecules starting at those ones attached to the PDMS surface, which could somewhat act as nucleation points for the growing of such a polymer layer eventually covering the entire substrate. The adsorption of PEG did not seem to affect the topography of the PDMS substrates (Figure 5.7). By contrast, the further silanization process with TESU appeared to generate homogeneously dispersed dots, which are likely to be related to TESU-based polymer structures generated at specific positions where an isolated –OH group, coming from the adsorbed PEG molecules, appeared. As pointed out above, such big differences between PVA and PEG-modified surfaces could be explained taking into consideration that PEG contains a much lower density of –OH groups than PVA in their respective structures. These results are in good agreement with those obtained by XPS and contact angle measurements. Regarding the chemical oxidation process, AFM images show a surface roughness increase compared with that one of the native PDMS (Figure 5.8). However, no significant differences were observed upon the silanization process. These results indicate that the chemical oxidation process generated a very low density of –OH

groups on the PDMS surface and so the further silanization with TESU appeared to slightly change the topography of these samples.

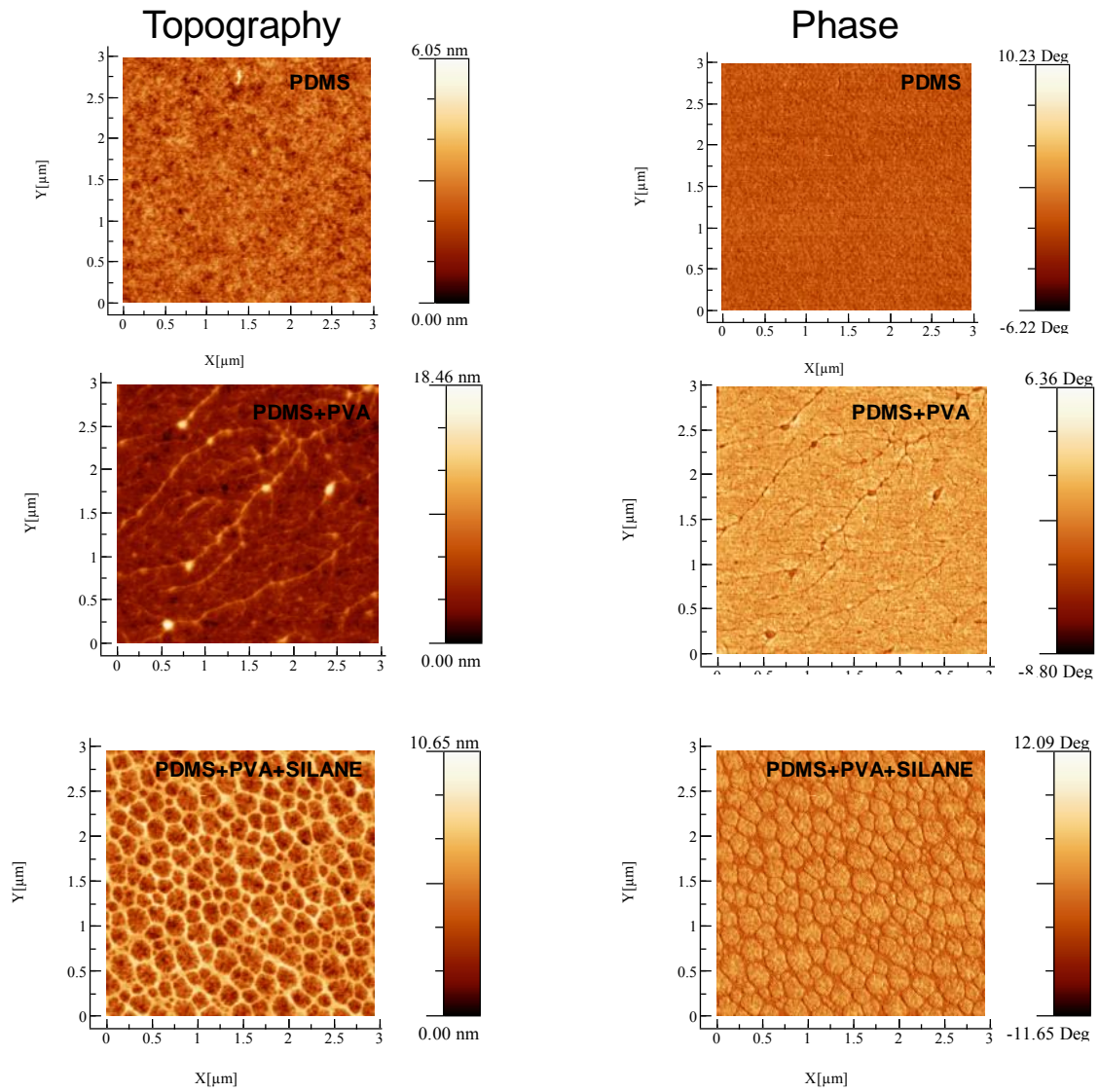


Figure 5.6. Topographic and phase AFM pictures of the PDMS surface before and after the modification with PVA and silane.

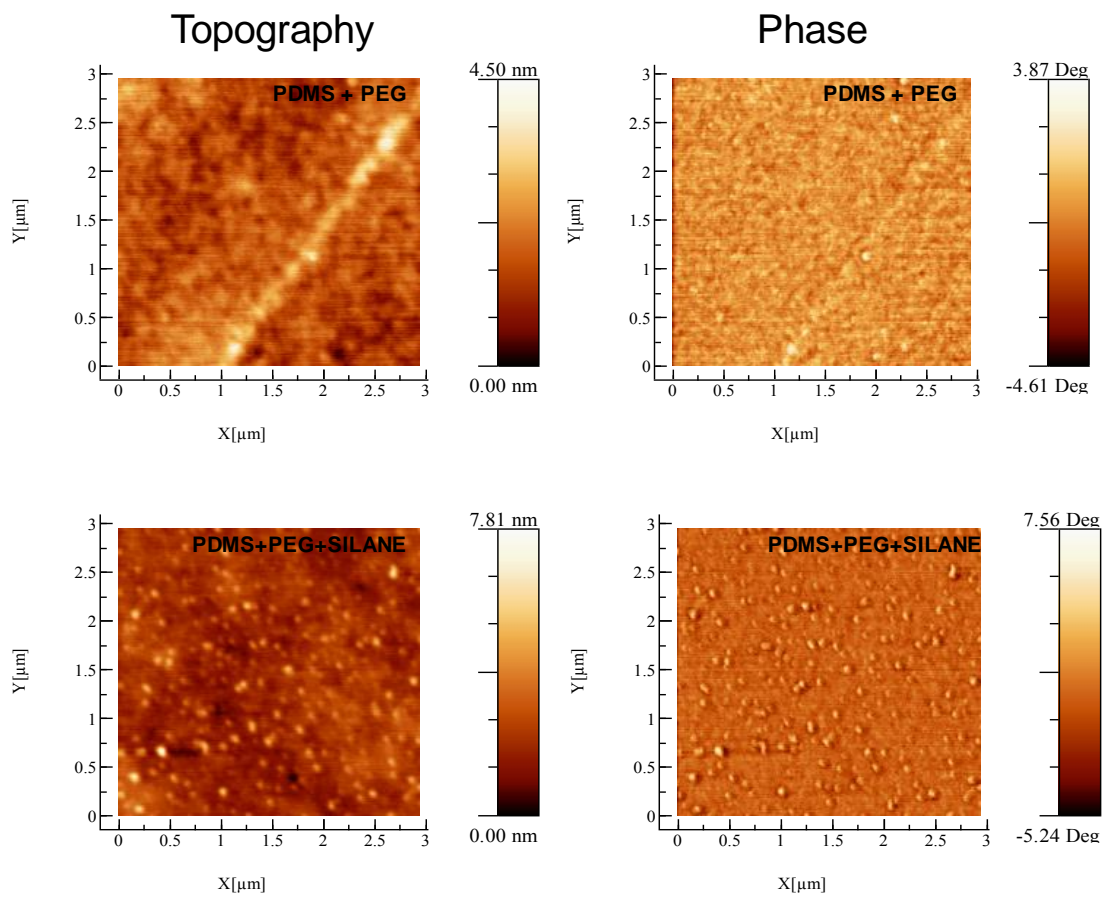


Figure 5.7. Topographic and phase AFM pictures of the PDMS surface after the modification with PEG and further silanization with TESU.

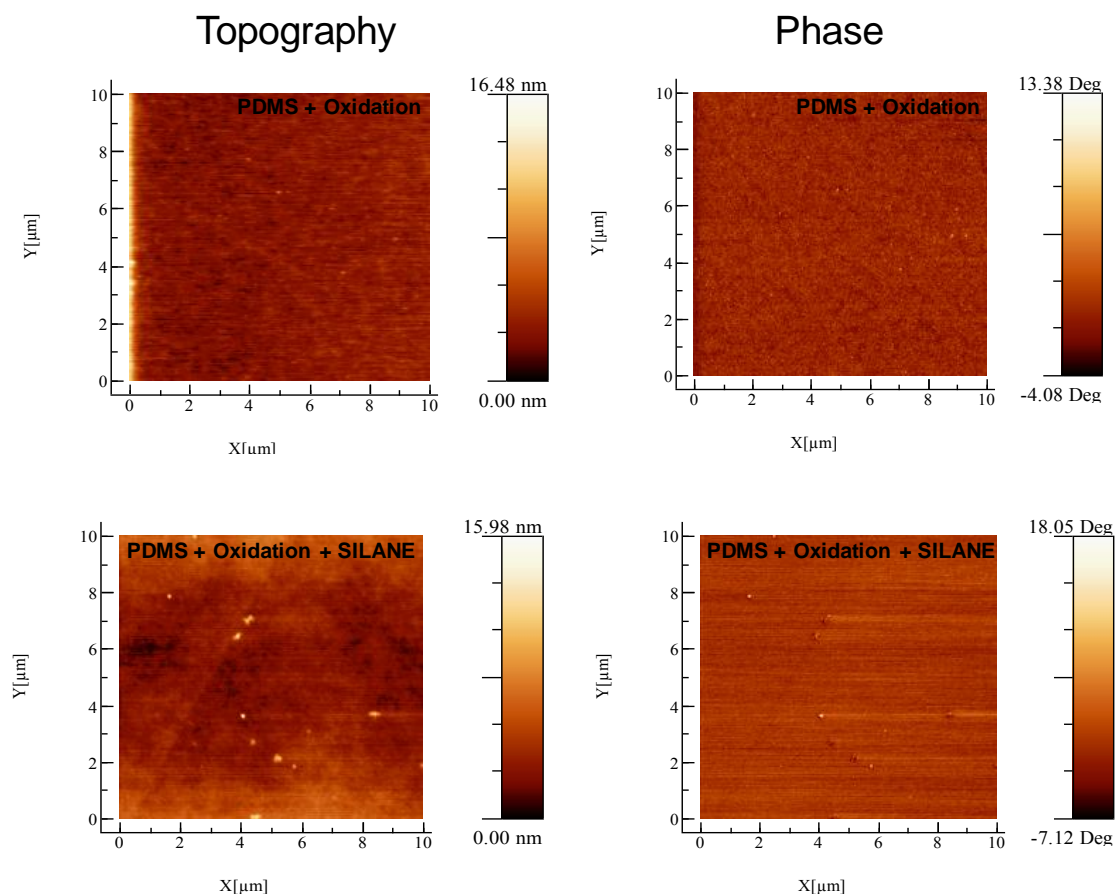


Figure 5.8. Topographic and phase AFM images of the PDMS surface after the chemical oxidation and further silanization with TESU.

5.4.2. Analytical performance of the different biosensor approaches

Once the HRP receptor was immobilized on the different modified-PDMS surfaces, the analytical performance of the resulting biosensor approaches was tested in H_2O_2 solutions in a concentration range from $0.10 \mu M$ to $100 \mu M$. The corresponding calibration plots (Figure 5.9) showed a linear increase in the measured absorbance at 420 nm up to a H_2O_2 concentration of $24.2 \mu M$. Therefore, a linear fitting was carried out in this range and the analytical parameters were calculated (Table 5.3). No significant differences were observed among the different approaches. Nevertheless, the estimated error was higher for the adsorption approach, this being related to the lack of control of the adsorption process itself and the reported instability of the adsorbed molecules when carried out repeated measurements with the same PhLOC. A lowest limit of detection around $0.10 \mu M H_2O_2$ was attained, this being between 10 and 100-fold lower than those values previously reported with similar analytical systems based on the use of a HRP receptor^{5,15}. Additionally, the sensitivity of the modified PhLOC improved 150 times when compared with another reported application using the same system⁸.

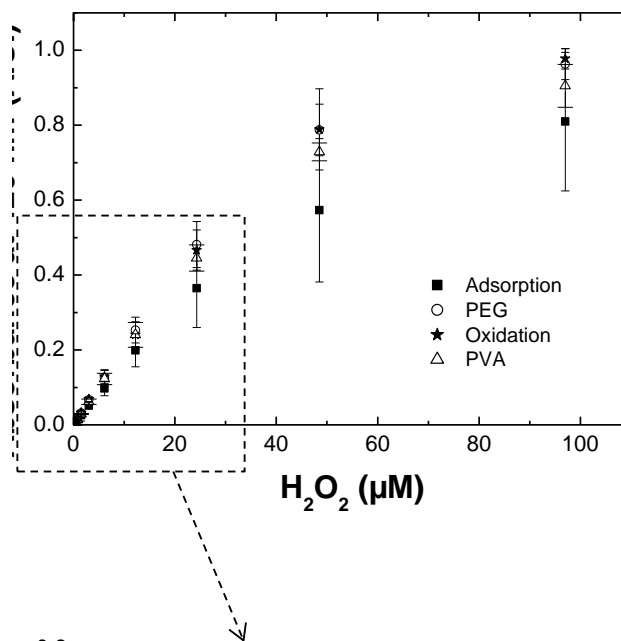


Figure 5.9. Calibration plots recorded with the different biosensor approaches. Each point is the mean value obtained for each hydrogen peroxide concentration in three different experiments, the error bars being the corresponding standard deviation. A linear range from 0 to 24.3 μM H_2O_2 was obtained in all cases.

Table 5.3. Analytical parameters of the four different biosensor approaches.

Modification	Sensitivity ^a (A.U./ μM)	LOD (μM) ^{a,b}	R ²
Adsorption	0.017±0.003	0.12±0.08	0.996
PEG + TESU	0.019±0.001	0.28±0.08	0.990
PVA + TESU	0.019±0.001	0.14±0.08	0.996
Oxid. + TESU	0.021±0.005	0.10±0.01	0.998

^aMean values and corresponding standard deviations of the parameters extracted from three calibration curves recorded with different devices in three consecutive days are represented.

^bLOD calculated following the 3 σ IUPAC criteria using the lowest order of the linear concentration range from 0.1 μM to 1.53 μM .

Finally, the operational stability of the PhLOC was systematically tested for over a month. Figure 5.10 shows the shift in the sensitivity values with time. Two different trends were observed. Those devices based on the adsorption and PEG-modification processes show a rapid decrease in the sensitivity values during the first week of operation while those based on PVA-modification and chemical oxidation processes remained more stable for at least one month. However, a clear shift towards lower sensitivity values was observed for the oxidation approach after one month of operation while it was estimated that the PVA-based one retained 82% of its initial sensitivity after two months of operation.

Figure 5.10. Sensitivity measurements of the microsystems through time after keeping them in PBS pH 7 at 4°C.

Overall, from the results presented above, the PVA and oxidation approaches gave rise to the PhLOC systems with a better analytical performance in terms of reproducibility and stability. Nevertheless, the structural characterization together with the analytical studies clearly indicate that the PVA-based approach is the one to be chosen considering the apparent higher density of chemical functional groups introduced on the PDMS surface and the longer stability of the resulting biosensor device.

5.5. Conclusions

Different chemical modification processes that enabled the introduction of hydroxyl groups on the surface of PDMS and the further attachment of a silane molecule for the selective immobilization of a biomolecule receptor are reported. A thorough structural and analytical characterization clearly indicated that the modification with PVA polymer is the most suitable approach for the biofunctionalization of PDMS PhLOC systems. These processes do not require any specific instrumentation, thus enabling their easy and rapid implementation in chemical and biological laboratories working with PDMS microfluidic systems.

5.6. References

1. J.C. McDonald, G.M. Whitesides. Poly(dimethylsiloxane) as a material for fabricating microfluidic devices. *Accounts of Chemical Research* 35(7), **2002**, 491-499.
2. D. Bodas, C. Khan-Malek. Hydrophilization and hydrophobic recovery of PDMS by oxygen plasma and chemical treatment—An SEM investigation. *Sensors and Actuators B* 123, **2007**, 368-373.
3. Y. Berdichevsky, J. Khandurina, A. Guttman, Y.H. Lo. UV/ozone Modification of Poly(dimethylsiloxane) Microfluidic Channels. *Sensors and Actuators, B* 97, **2004**, 402-408.
4. G. Sui, J. Wang, C.C. Lee, W. Lu, S.P. Lee, J.V. Leyton, A.M. Wu, H.R. Tseng. Solution-phase surface modification in intact poly(dimethylsiloxane) microfluidic channels. *Analytical Chemistry* 78(15), **2006**, 5543-5551.
5. A. Llobera, R. Wilke, S. Büttgenbach. Poly(dimethylsiloxane) hollow Abbe prism with microlenses for detection based on absorption and refractive index shift. *Lab on a Chip* 4, **2004**, 24-27.
6. C.M. Yu, Q. Li, Q. Zhou, J.H.T. Luong. Poly(vinyl alcohol) functionalized poly(dimethylsiloxane) solid surface for immunoassay. *Bioconjugate Chemistry* 18(2), **2007**, 281-284.
7. P.T. Charles, V.R. Stubbs, C.M. Soto, B.D. Martin, B.J. White, C.R. Taitt. Reduction of Non-Specific Protein Adsorption Using Poly(ethylene) Glycol (PEG) Modified Polyacrylate Hydrogels In Immunoassays for Staphylococcal Enterotoxin B Detection. *Sensors* 9, **2009**, 645-655.
8. A. Llobera, R. Wilke, S. Büttgenbach. Enhancement of the response of poly (dimethylsiloxane) hollow prisms through air mirrors for absorbance-based sensing. *Talanta* 75, **2008**, 473-479.
9. M.L. Hair, C.P. Tripp. Alkylchlorosilane reaction at the silica surface. *Colloids and Surfaces A* 105, **1995**, 95-103.
10. L. Ferreira, M.A. Ramos, J.S. Dordick, M.H. Gil. Influence of Different Silica Derivatives in the Immobilization and Stabilization of a *Bacillus licheniformis* Protease (Subtilisin Carlsberg). *Journal of Molecular Catalysis B: Enzymatic* 21, **2003**, 189-199.
11. E.N. Kadnikova, N.M. Kostic. Oxidation of ABTS by hydrogen peroxide catalyzed by horseradish peroxidase encapsulated into sol-gel glass: Effects of glass matrix on reactivity. *Journal of Molecular Catalysis B: Enzymatic* 18, **2002**, 39-48.
12. B. Huang, H. Wu, S. Kim, R.N. Zare. Coating of poly(dimethylsiloxane) with n-dodecyl-beta-D-maltoside to minimize nonspecific protein adsorption. *Lab on a Chip* 5, **2005**, 1005-1007.
13. A. Mata, A.J. Fleischman, S. Roy. Characterization of polydimethylsiloxane (PDMS) properties for biomedical micro/nanosystems. *Biomedical Microdevices* 7(4), **2005**, 281-293.
14. H. Hillborg, J.F. Ankner, U.W. Gedde, G.D. Smith, H.K. Yasuda, K. Wikström. Crosslinked polydimethylsiloxane exposed to oxygen plasma studied by neutron reflectometry and other surface specific techniques. *Polymer* 41, **2000**, 6851-6863.
15. M. Tamasko, L. Nagy, E. Mikolas, G.A. Molnar, I. Wittman, G. Nagy. An approach to in situ detection of hydrogen peroxide: application of a commercial needle-type electrode. *Physiological Measurement* 28, **2009**, 1533-1542.

6. DUAL OPTICAL/ELECTROCHEMICAL READOUT BIOFUNCTIONALIZED LAB-ON-A-CHIP SYSTEMS

6.1.	Summary	100
6.2.	Introduction	100
6.3.	Experimental details	101
6.3.1.	Materials and reagents	101
6.3.2.	Design and fabrication of the DLOCs	102
6.3.4.	Characterization of the mixer	104
6.3.6.	Enzyme immobilization.....	104
6.3.7.	Optimization of the GOx:HRP ratio	105
6.4.	Results and discussion	106
6.4.1.	Characterization of the mixer	106
6.4.2.	Characterization of the electrodes.....	108
6.4.3.	Optimization of the GOx:HRP ratio	109
6.4.4.	Glucose detection and crosstalk test	110
6.5.	Conclusions	115
6.6.	References	115

The work included in this chapter will be reported in a paper entitled “Dual optical electrochemical readout biofunctionalized Lab-on-a-Chip systems” by Bergoi Ibarlucea, Xavier Munoz-Berbel, Pedro Ortiz, Stephanus Büttgenbach, César Fernández-Sánchez and Andreu Llobera, which is in preparation.

6.1. Summary

Two Lab-on-a-Chip (LOC) systems are presented in this chapter, both of them incorporating a dual detection approach (electrochemical and optical). The so-called DLOC approaches monolithically combine in one single chip a Multiple Internal Reflection (MIR) element and additional microfluidic structures. A microreactor is integrated in the DLOC1, whereas a mixer that plays the role of both a mixer and a reactor was added to the DLOC2, herein simplifying the design by avoiding the integration of an extra reservoir containing the bioreceptors and resulting in a significant reduction of the dead volumes. The concepts were validated by functionalizing the reactor and the mixer with horseradish peroxidase (HRP) and glucose oxidase (GOx), being possible in this way to detect glucose both optically and electrochemically under continuous flow conditions. A limit of detection (LOD) of 1.9 ± 0.1 mM glucose for the DLOC1 at 30 $\mu\text{L}/\text{min}$ and 6.3 ± 0.4 mM glucose for the DLOC2 at 100 $\mu\text{L}/\text{min}$, were achieved, the latter showing a response time of only 20s. By decreasing the flow rate of the DLOC2 to 10 $\mu\text{L}/\text{min}$, a LOD of 0.1137 ± 0.0003 mM glucose was obtained, with a response time of 60 s.

6.2. Introduction

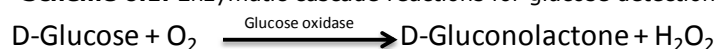
The integration of both optical and electrochemical transduction methods in a single Lab-on-a-Chip (LOC) is anticipated to be advantageous in different scenarios. They can provide with either complementary information or enhanced the system performance: i) if the linear range of each detection method is different, their combination in a single LOC improves the concentration range where such LOC may be used (assuming that there is no cross-talk, as discussed by Ordeig and co-workers¹; ii) this integration can be used to detect analytes with different optical and electrochemical properties (different absorbance bands, fluorescent/non fluorescent analytes, conductivity, etc), and even to induce oxidation to some analytes, resulting in a colored oxidized form which could be measured optically²; iii) when both detection methods have similar sensitivity to a given analyte, their combination ubiquitously provides the LOC with a self-verifying mechanism, which reduces the number of false positives/negatives, resulting in a more robust and reliable LOC.

In addition to the transduction mechanism, there are several strategies towards providing the LOC with biosensing abilities such as the development of immunosensors (by using antibodies as recognition element)³, enzyme-based sensors⁴ or DNA biosensors⁵. Among them, LOCs that make use of enzymatic reactions have shown better performance in terms of reusability and fast kinetics⁶. The inclusion of microreactors in their structure offers several advantages such as high efficiency and repeatability. Generally, larger surface areas can be obtained, achieving a faster mass transfer compared to the traditional batch devices. Also, reaction conditions and time can be controlled by making changes in the design of the microfluidics⁷. These structures can be used as microreactors for various purposes such as synthesis, catalysis or analytical detections. Tudorache *et al.* for example, developed a microreactor by immobilizing horseradish peroxidase (HRP) on gold patterns for the catalytic oxidation of phenol⁸. Luckarift *et al.* used a silica-immobilization of enzymes in microfluidic systems for multi-step synthesis of

2-aminophenoxazin-3-one from nitrobenzene under continuous flow conditions⁹. Baeza *et al.* fabricated a ceramic device that incorporated a microreactor with immobilized β -galactosidase enzyme for the detection of ortho-nitrophenyl β -D-galactopyranoside in continuous flow¹⁰. However, many of these reactor approaches include several fabrication steps such as the fabrication of additional structures like gold patterns⁸ or the mechanization of several layers¹⁰, or make use of very low flow rates⁹ (in the range of 50-300 μ L/hr) that increase the response time. Therefore, the development of new approaches that make both the fabrication and measurement processes easier is required in this context.

In this work, two LOCs are presented, both of them incorporating a dual detection approach (electrochemical and optical), which monolithically combine in one single chip a Multiple Internal Reflection (MIR) and additional biofunctionalized microfluidic structures: a microreactor for the first LOC (DLOC1) and a mixer that plays the role of both a mixer and a reactor for the second LOC (DLOC2). The reason why this second microfluidic element has this two-folded role is because it has been functionalized with horseradish peroxidase (HRP) and glucose oxidase (GOx) in the same way as the reactor. Here, a reaction between the immobilized enzymes of the mixer and the glucose and the redox mediator 2,2'-Azino-bis(3-ethylbenzothiazoline-6-sulfonic acid) (ABTS) present in the sample occurs together with the downstream propagating of the same. The cascade reaction that takes place is described in Scheme 6.1. Glucose oxidase catalyzes the oxidation of D-glucose by oxygen to produce D-gluconolactone and H₂O₂. H₂O₂ is the substrate for HRP, which catalyzes the reduction to H₂O with the concomitant oxidation of ABTS redox mediator to the ABTS^{•+} green colored radical cation. This cation presents various absorbance peaks at 420, 650, 740 and 835 nm, as described by Cho and co-workers¹¹, being possible in this way to detect glucose both optically and electrochemically and in continuous flow. Nevertheless, this approach is also valid for other optically/electrochemically responsive analytes. These easy-to-fabricate approaches avoid the necessity to add an enzyme reservoir in the system, resulting in a significant reduction of the dead volumes and keeping the advantage of the low reagent consumption that is associated to the LOC concept.

Scheme 6.1. Enzymatic cascade reactions for glucose detection.



6.3. Experimental details

6.3.1. Materials and reagents

Polyvinyl alcohol (PVA), ethanol 99%, triethylamine (TEA), sodium cyanoborohydride (NaBH₃CN), tween 20, potassium hexacyanoferrate (II) ([Fe(CN)₆]⁴⁻, ferrocyanide), , potassium

nitrate (KNO_3), glucose oxidase (GOx) and horseradish peroxidase type VI (HRP) and 2,2'-Azino-bis(3-ethylbenzothiazoline-6-sulfonic acid) diammonium salt were from Sigma-Aldrich (Munich, Germany). Potassium hexacyanoferrate (III) ($[\text{Fe}(\text{CN})_6]^{3-}$, ferricyanide) was from Panreac (Castellar del Vallés, Spain). 11-triethoxysilyl undecanal (TESU) was from ABCR GmbH & Co. (Karlsruhe, Germany). EPON SU-8 25 photoresist and propylene glycol methyl ether acetate (PGMEA) were from MicroChem Corporation (Newton, MA, US). The PDMS Sylgard 184 elastomer kit was from Dow Corning (Midland, MI, US).

6.3.2. Design and fabrication of the DLOCs

DLOC1 is shown in Figure 6.1. It is composed of a branched microreactor and a MIR (Figure 6.1). The branches increase significantly the surface area of the microreactor in order to increase the number of enzymes that can be immobilized and the surface-to-volume ratio. There is one input to direct the functionalizing reagents to the microreactor and a passive valve that avoids the leaking of the samples coming from the reactor and directs the flow to the MIR zone, where the measurements are performed.

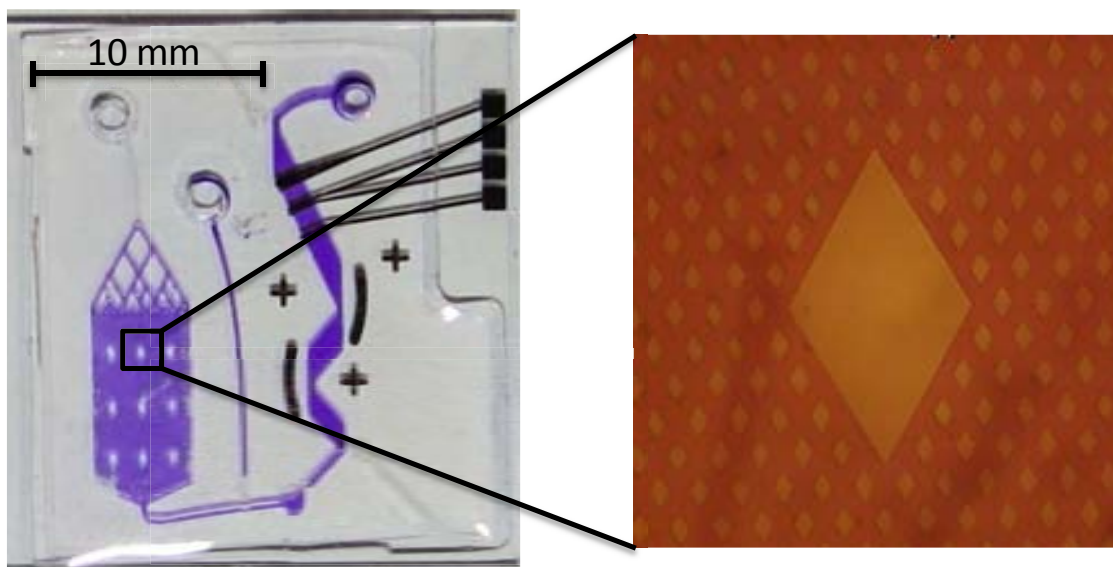


Figure 6.1: photography of DLOC1.

DLOC2 is shown in Figure 6.2. It includes a mixer and a MIR fabricated in PDMS and sealed over a glass substrate. The in-plane passive mixer makes use of the Coanda effect (the tendency of a fluid to be attracted to a nearby surface) in Tesla structures to split and recombine counter propagating liquid flows¹². Up to three fluidic inlets can be simultaneously used with the mixer/reactor. An additional auxiliary inlet has been implemented to directly pump to the MIR the samples that do not need to be mixed or that could negatively affect the immobilized enzymes on the mixer/reactor (as could be washing solutions). Passive unidirectional valves at both downstream the mixer and the auxiliary inlet, and directly connected with the MIR, assure no liquid counter propagation in the DLOC2. The MIR working principle was discussed in chapter 3.

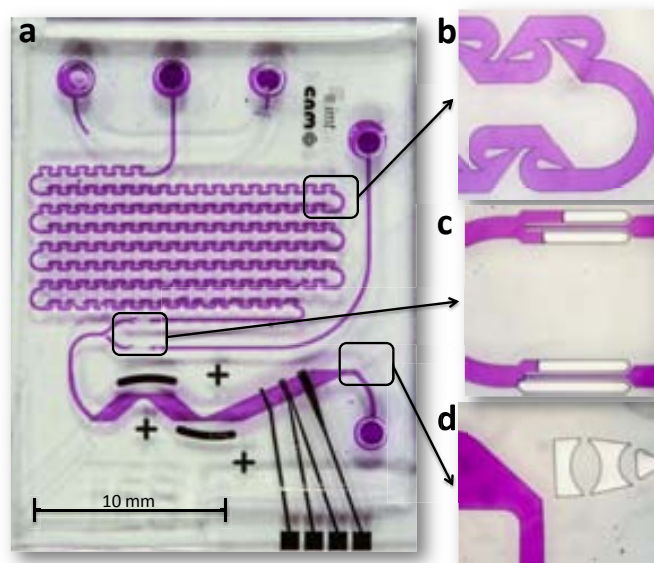


Figure 6.2: (a) Photography of DLOC2. Close view of the (b) mixer structure, (c) passive valves and (d) biconvex lens.

The glass substrate contains alignment patterns as well as the required microband gold electrodes at the MIR zone. They consist of a reference electrode, two working electrodes and a counter electrode with an exposed area of $183.3 \times 1250 \mu\text{m}$, $2 \times (135 \times 1250) \mu\text{m}$ and $475 \times 1250 \mu\text{m}$ respectively. They were fabricated by sputtering two 20 nm-thick adhesion layers of Ti and Ni and a 100 nm Au layer. Then the electrode layout was photolithographically defined and a wet chemical etching was performed. Afterwards, a passivating silicon oxide layer of 600 nm thickness was deposited by plasma-enhanced chemical vapor deposition (PECVD). Then, the electrode areas were opened (leaving $5 \mu\text{m}$ of passivation on the edges of the electrodes, so as to enhance robustness and to avoid early aging) with the help of a second photolithographic step and a further dry etching process. At this point, the substrates were ready to be bonded with the MIR.

All the micro-optical and microfluidic elements of the systems were monolithically fabricated in PDMS by replica molding, following a protocol described in Chapter 3 and using deionized water (DI H_2O) as lubricant for the alignment with the electrodes in the substrate. Finally, after soldering the wires to the electrical contact pads of the electrodes, the DLOC systems were ready to be used.

6.3.3. Experimental set-up

A halogen lamp (HL-2000-FHSA, OceanOptics, Dunedin, FL, US) was used as light source in this work. It was coupled to a $230 \mu\text{m}$ diameter multimode fiber optic (Thorlabs, Dachau/Munich, Germany), previously inserted in the input self-alignment element. Readout comprised an identical fiber optics and connected to a QE65000 miniature spectrophotometer (OceanOptics, Dunedin, FL, US), which was controlled via SpectraSuite software.

Electrochemical measurements were performed with a portable μ STAT2000 bipotentiostat (Dropsens, Spain), which was controlled with Dropview 1.3 software.

Fluid handling was achieved by connecting the DLOCs to a Nemesys syringe pump (Cetoni, Korbussen, Germany) composed of three syringe modules: the first one for activation/cleaning buffers and the other two for the mixing of buffer with and without glucose in order to obtain different glucose concentrations for the calibrations.

6.3.4. Characterization of the mixer

For the bioanalytical application developed with DLOC2, only two inlets were required for pumping the target analyte solution / sample (glucose) and the dilution buffer, while the third one included in the design was only used for washing purposes. Therefore, in order to assess the performance of the mixer / reactor, water and ink solutions were simultaneously injected into the mixer at different proportions, from 20% to 100 % ink. The ink presented an absorbance peak at 430 nm, which was used for obtaining a calibration curve.

6.3.5. Characterization of the electrochemical cell

The amperometric electrochemical cell required the initial pretreatment of the working electrodes by carrying out an electrochemical activation step consisting in applying a repeated cyclic potential scan in 0.5 M KNO_3 , in a potential window from -1 V to 1 V, at least 3 times. Then, 0.5 M KNO_3 solutions containing ferricyanide and ferrocyanide in a concentration range from 0.05 mM to 2 mM were sequentially pumped into the system and the cyclic voltammetric response was recorded under continuous flow at a flow rate of 100 $\mu\text{L}/\text{min}$. The limiting current values at +0.3 V (vs. pseudo-reference Au electrode), corresponding to the oxidation of ferrocyanide, were used as the analytical signal and plotted to assess the correct performance of the electrochemical cell. 100 continuous cyclic voltammetric signals were then performed in the ferri/ferrocyanide solution in order to check the stability of the electrodes.

6.3.6. Enzyme immobilization

For testing the DLOCs, glucose was selected as target analyte. It is worth mentioning that, unlike the work presented by Ordeig et al¹, GOx and HRP enzymes were immobilized in the microreactor and mixer rather than pumping them inside the system together with the sample. The functionalization of these elements was carried out following the protocol described in Chapter 5 and a simplified scheme of it is shown in Figure 6.3.

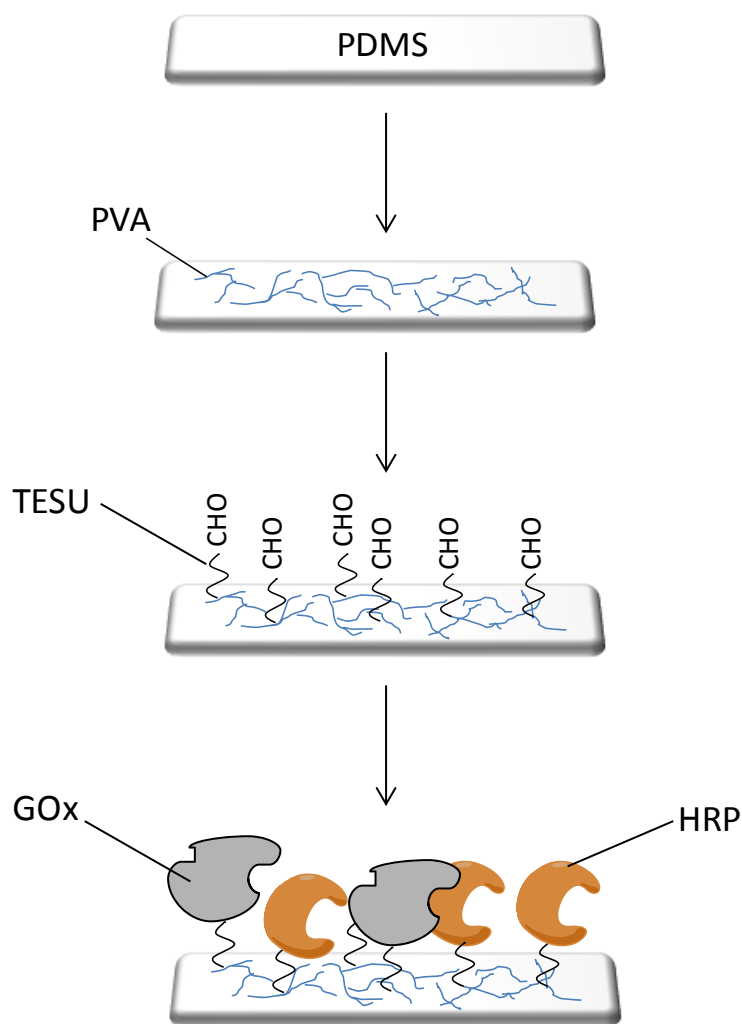


Figure 6.3: Representation of the surface modification protocol.

Aldehyde functional groups were incorporated to the PDMS walls of these fluidic elements by only pumping the modifying solutions through the mixer until its end, avoiding the contamination of the MIR and the electrochemical cell. These groups work as anchoring points for proteins through their amine groups of its lysine residues, by forming a Schiff base. This bond can be stabilized by reducing it to a secondary amine by using sodium cyanoborohydride (NaBH_3CN). Thus, a 0.1 M carbonate buffer solution pH 8.0 containing GOx, HRP and 5 mM NaBH_3CN was pumped inside these elements. After 1h incubation at RT, a 0.1 M phosphate buffer saline solution pH 7.0 containing 0.02% (v/v) Tween 20 (PBST) was pumped to remove the nonspecifically adsorbed proteins. Four different GOx and HRP concentration ratios were used for comparison and optimization of the immobilization protocol, as it is explained later.

6.3.7. Optimization of the GOx:HRP ratio

The kinetics of these two enzymes is different and choosing their correct ratio is important to obtain the optimum performance of the system's response. It is known that excess of H_2O_2 inhibits the enzymatic activity of HRP, due to the oxidative degradation of the compound formed by the reaction of HRP with H_2O_2 ¹³. This reason, together with the instability of the H_2O_2 itself, makes it necessary to have a faster activity of HRP than for glucose oxidase, which

oxidizes glucose, a substrate that is not inhibitory at all¹⁴. Oriented by the literature found in this context¹⁵⁻¹⁷, four different ratios were compared: 2:1, 1:1, 1:2, 1:4 (in terms of enzymatic activity units: 0.0375 KU GOx/mL:0.01875 KU HRP/mL, 0.0375 KU GOx/mL:0.0375 KU HRP/mL, 0.0375 KU GOx/mL:0.075 KU HRP/mL and 0.0375 KU GOx/mL:0.15 KU HRP/mL, respectively). With this purpose, the Abbe prisms used in Chapter 5 were functionalized using these different ratios¹⁸.

2 mM stock D-glucose solution was prepared in phosphate buffered saline (PBS) pH 7.2 24 h prior to the measurements and stored overnight at 4 °C to reach mutarotational equilibrium¹⁹. Then, the enzymatic activity (see Scheme I) was monitored by absorbance measurements at 420 nm, the main absorbance peak of ABTS^{••}. Calibration curves were obtained for each of the enzyme ratios tested by pumping samples of different glucose concentrations (ranging from 7.03 μM to 1.8x10³ μM) in presence of 0.5 mM ABTS (in PBS pH 7.2) and waiting for 10 min for the enzymatic reactions to occur. From the calibration curves, the limit of detection (LOD) and the sensitivity values were obtained in order to choose the optimal enzyme ratio to be immobilized in the presenting microsystems.

6.3.8. Glucose detection and cross-talk test

Once the DLOCs were functionalized and before starting the glucose measurements, the electrodes were activated following the procedure described above.

For the measurements using DLOC1, different concentrations of glucose in presence of ABTS 0.5 M were previously prepared and sequentially pumped at 30 μL/min in a range from 2 mM to 30 mM. For the absorbance measurements, the 420 nm peak of the ABTS^{••} was used, while for the electrochemical measurements, the consumption of ABTS by the HRP reaction was monitored at +0.3 V (vs. Au pseudo-ref. electrode).

For the measurements using DLOC2, glucose and PBS buffer (both in presence of ABTS 0.5 mM) were simultaneously pumped at different flow rates (total flow rate 100 μL/min) in order to obtain different final concentrations from 10 mM to 100 mM. They were mixed in the Tesla mixer and measured in the MIR without stopping the pump (continuous flow).

Simultaneous measurements in a range between 10 mM and 90 mM glucose were performed with DLOC2 to check the absence of cross-talk and identical fast response. Absorbance and amperometric detection was carried out as above. Finally, a calibration experiment was performed at 10 μL/min total flow rate by using the same system in a range from 200 μM to 2 mM glucose to test whether the analytical performance of the system could be enhanced while still keeping the analysis time short.

6.4. Results and discussion

6.4.1. Characterization of the mixer

The absorbance spectra of the ink dilutions and the calibration obtained by measuring the absorbance peak at 430 nm are shown in Figure 6.4. A linear response (fitting: $Y = -0.005 \pm$

$0.003 + 0.00530 \pm 5.538 \times 10^{-5} X$, $R^2 = 0.99946$) was obtained for all the ink dilution range studied. Also, the increasing rate of the absorbance was proportional to the increasing rate of the ink concentration, as it can be seen in Table 6.1. These results show that the mixer was working correctly.

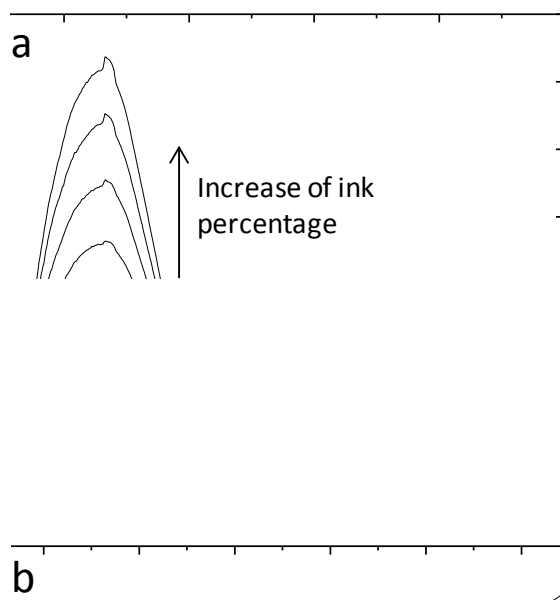


Figure 6.4. (a) Optical spectra of samples containing different ink concentrations and (b) corresponding calibration plot.

Table 6.1. Calculation of the absorbance increase rate depending on the ink increase rate.

Ink percentage range (%)	Ink increase rate	Absorbance increase rate
16,67-33,33	1,999	2,114
33,33-50	1,5	1,575
50-66,67	1,333	1,327
66,67-83,33	1,25	1,266
83,33-100	1,2	1,179

6.4.2. Characterization of the electrodes

The cyclic voltammetric signals of ferri/ferrocyanide recorded with the gold electrochemical cell showed two limiting current plateaus at +0.3 V (corresponding to the ferrocyanide oxidation) and at -0.3 V (due to the ferricyanide reduction) (Figure 6.5a). This is the expected behavior of electrochemical cells working under laminar flow hydrodynamic conditions. The calibration at a set potential of +0.3 V showed a linear response for the whole measured concentration range of ferrocyanide (Figure 6.5b) (fitting: $Y = 0.03 \pm 0.06 + 1.46 \pm 0.06X$, $R^2 = 0.9906$). The electrodes showed a good stability, retaining the whole measuring activity after 100 voltammetries (Figure 6.6).

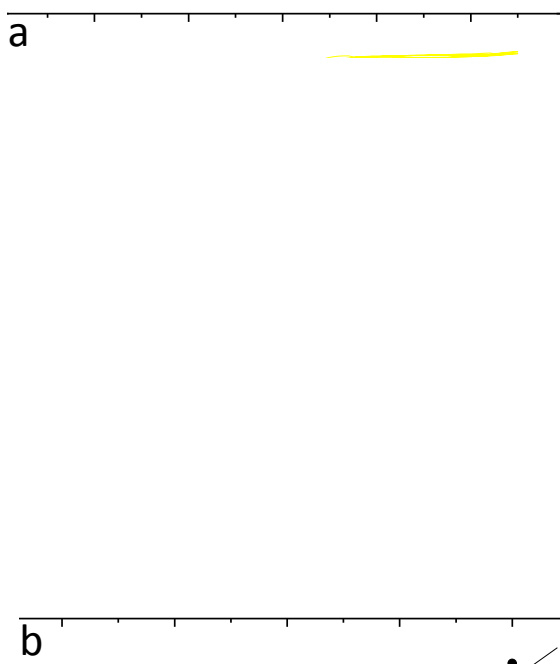


Figure 6.5 (a) Cyclic voltammograms recorded in solutions containing different ferri/ferrocyanide concentrations at 100 $\mu\text{L}/\text{min}$ flow rate. (b) Calibration curve obtained by plotting the current values corresponding to the ferrocyanide oxidation at +0.3 V vs. Au pseudo-reference.

Figure 6.6. Stability test of the electrodes. First and last three out of 100 cyclic voltammograms are shown.

6.4.3. Optimization of the GOx:HRP ratio

This study was carried out by measuring the absorbance of the $\text{ABTS}^{•+}$ cation radical. The absorbance spectrum of this redox species is shown in Figure 6.7, where it can be seen the peaks at 420, 650, 740 and 835 nm.

Figure 6.7. Absorbance spectrum of $\text{ABTS}^{•+}$.

Out of the four different ratios compared, 1:2 was the one which showed the best LOD and sensitivity, $4.83 \pm 0.13 \mu\text{M}$ glucose and $4.70 \times 10^{-4} \pm 1 \times 10^{-5} \text{ A.U./}\mu\text{M}$ glucose respectively, as shown in Figure 6.8. For the ratios 1:4, 1:1 and 2:1, LODs and sensitivities were found to be $8.2 \pm 0.4 \mu\text{M}$ glucose and $2.5 \times 10^{-4} \pm 1 \times 10^{-5} \text{ A.U./}\mu\text{M}$ glucose, $28 \pm 5 \mu\text{M}$ glucose and $3.4 \times 10^{-4} \pm 5 \times 10^{-5} \text{ A.U./}\mu\text{M}$ glucose, $18 \pm 2 \mu\text{M}$ glucose and $1.6 \times 10^{-4} \pm 2 \times 10^{-5} \text{ A.U./}\mu\text{M}$ glucose, respectively.



Figure 6.8. (a) Limit of detection and (b) sensitivity for glucose of the Abbe prism microsystems functionalized with different glucose oxidase and horseradish peroxidase ratios.

6.4.4. Glucose detection and crosstalk test

Prior to the enzymatic measurements, cyclic voltammetric measurements were performed in a PBS buffer solution containing ABTS between -0.2 V and $+0.4 \text{ V}$ (vs. Au pseudo-ref. electrode) in order to detect the potential at which the oxidation limiting current is reached. From the signals shown in Figure 6.9, a potential of $+0.3 \text{ V}$ can be chosen.

Figure 6.9. Cyclic voltammetry of ABTS and PBS buffer. As ABTS concentration decreases, current at 0.3 V also decreases.

For DLOC1, a range from 2.5 to 30 mM glucose was measured at 30 $\mu\text{L}/\text{min}$ (Figure 6.10). A linear range from 2.5 to 10 mM for the optical detection and from 5 mM to 17.5 mM for the electrochemical detection were considered, obtaining LODs and sensitivities of 3.2 ± 0.6 mM glucose and $(0.21 \pm 0.04) \times 10^{-2}$ A.U./mM glucose, and 1.9 ± 0.10 mM glucose and -0.0024 ± 0.0001 $\mu\text{A}/\text{mM}$ glucose respectively.

Figure 6.10. Electrochemical and optical measurements of glucose at 30 $\mu\text{L}/\text{min}$ using DLOC1.

For DLOC2, a range from 10 to 100 mM glucose was measured at 100 $\mu\text{L}/\text{min}$ (Figure 6.11). A linear range from 10 to 90 mM for the optical detection and from 10 mM to 60 mM for the electrochemical detection were considered, obtaining LODs of 8.9 ± 0.5 mM glucose and 6.3 ± 0.4 mM glucose respectively and sensitivities of $(0.037 \pm 0.002) \times 10^{-2}$ A.U./mM glucose and $-(6.6 \pm 0.3) \times 10^{-4}$ $\mu\text{A}/\text{mM}$ glucose respectively.

Figure 6.11. Electrochemical and optical measurements of glucose at 100 $\mu\text{L}/\text{min}$ using DLOC2.

Simultaneous measurements were also performed with DLOC2 showing absence of crosstalk between detection modes. The two of them also showed identical fast response of just 20 seconds, as it can be seen in Figure 6.12.

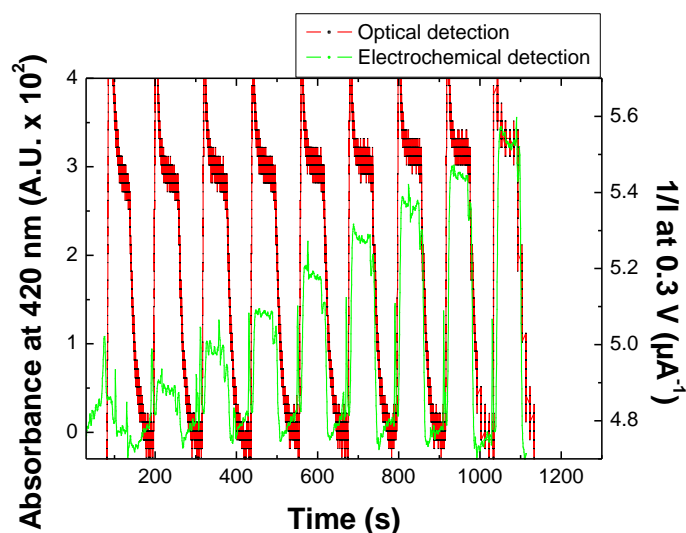


Figure 6.12. Simultaneous measurement of (a) absorbance at 420 nm and current at 0.3 V through time showing signal response after injections of buffer and different glucose concentrations in a range from 10 μM to 90 μM .

Since mixings can be made in DLOC2 itself, providing with a more simple working procedure, this system was selected for the measurements at lower flow rates.

When measurements at a lower flow rate were carried out (10 $\mu\text{L}/\text{min}$), the measurable glucose range decreased to 200 μM – 2 mM (Figure 6.13), being the linear range up to 1.6 mM for the optical detection (for the two measured wavelengths) and up to 2 mM for the electrochemical detection. In this way, the absorbance peak at 750 nm could also be plotted, which would be useful if a sample presents absorbance around 420 nm itself (as may be the case of urine or serum). LOD and sensitivity values for optical measurements at 420 nm and 750 nm were 0.21 ± 0.15 mM glucose and $(4.2 \pm 0.3) \times 10^{-2}$ A.U. /mM glucose, 0.22 ± 0.02 mM glucose and $(2.2 \pm 0.2) \times 10^{-2}$ A.U. /mM glucose, respectively. For the electrochemical measurement LOD and sensitivity values were 0.113 ± 0.003 mM glucose and -0.0101 ± 0.0003 $\mu\text{A}/\text{mM}$ glucose. Since the flow rate was lower, the response time necessary to observe the signal increased to 60 s (Figure 6.14).

Figure 6.13. Optical and electrochemical measurements of glucose at 10 $\mu\text{L}/\text{min}$ using DLOC2.

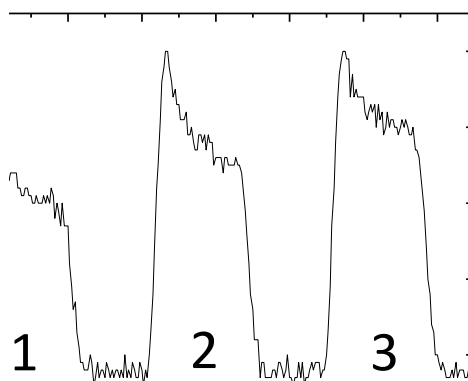


Figure 6.14. Optical detection of glucose samples through time at 10 $\mu\text{L}/\text{min}$ using DLOC2. Peak 1, 2 and 3 represent injections of 600, 1200 and 1800 μM glucose respectively.

Linear fittings, LODs and sensitivities of the glucose detection in continuous flow are shown in Table 6.2 for comparison purposes. DLOC2 shows a better performance in terms of easiness, since mixings can automatically be done, avoiding sample preparation steps. It provides with similar LOD and measurable ranges for glucose compared to other amperometric^{20,21} and optical²²⁻²⁴ microsystems based on enzymatic detection, being in or under the physiological range depending on the flow rate used, and offering additional advantages comparing also to a previously presented DLOC¹, such as reduced response time and sample volumes, and inclusion of the mixer and the MIR in a single substrate, avoiding the tubing for their connection. Finally, the immobilization of the enzymes drastically reduces the reagent consumption.

Table 6.2. Linear fittings, R^2 values, LODs and sensitivity values for the glucose measurements in continuous flow.

Flow rate ($\mu\text{L}/\text{min}$)	Detection method	Results
30 (DLOC1)	Absorbance at 420 nm	Linear fitting: $Y = 0.2 \pm 0.2 + 0.21 \pm 0.04 X$ $R^2: 0.936$ LOD: $3.2 \pm 0.6 \text{ mM}$ Sensitivity: $(0.21 \pm 0.04) \times 10^{-2} \text{ A.U. /mM}$
30 (DLOC1)	Current at +0,3 V	Linear fitting: $Y = 0.3370 \pm 0.0015 - 0.0024 \pm 1 \times 10^{-4} X$ $R^2: 0.988$ LOD: $1.9 \pm 0.10 \text{ mM}$ Sensitivity: $0.0024 \pm 1 \times 10^{-4} \mu\text{A /mM}$
100 (DLOC2)	Absorbance at 420 nm	Linear fitting: $Y = 0.04 \pm 0.11 + 0.037 \pm 0.002 X$ $R^2: 0.976$ LOD: $8.9 \pm 0.5 \text{ mM}$ Sensitivity: $(0.037 \pm 0.002) \times 10^{-2} \text{ A.U. /mM}$
100 (DLOC2)	Current at +0.3 V	Linear fitting: $Y = 0,5930 \pm 0.0014 - 6.6 \times 10^{-4} \pm 3 \times 10^{-5} X$ $R^2: 0.983$ LOD: $6.3 \pm 0.4 \text{ mM}$ Sensitivity: $6.6 \times 10^{-4} \pm 3 \times 10^{-5} \mu\text{A /mM}$
10 (DLOC2)	Absorbance at 420 nm	Linear fitting: $Y = 0.4 \pm 0.3 + 4.2 \pm 0.3 X$ $R^2: 0.971$ LOD: $0.21 \pm 0.15 \text{ mM}$ Sensitivity: $(4.2 \pm 0.3) \times 10^{-2} \text{ A.U. /mM}$
10 (DLOC2)	Absorbance at 750 nm	Linear fitting: $Y = 0.24 \pm 0.16 + 2.15 \pm 0.16 X$ $R^2: 0.967$ LOD: $0.225 \pm 0.017 \text{ mM}$ Sensitivity: $(2.15 \pm 0.16) \times 10^{-2} \text{ A.U. /mM}$
10 (DLOC2)	Current at +0.3 V	Linear fitting: $Y = 0.0013 \pm 3 \times 10^{-4} - 0.0101 \pm 3 \times 10^{-4} X$ $R^2: 0.991$ LOD: $0.113 \pm 3 \times 10^{-3} \text{ mM}$ Sensitivity: $0.0101 \pm 3 \times 10^{-4} \mu\text{A/mM glucose}$

6.5. Conclusions

Two biozymatically biofunctionalized DLOC that combine both optical and electrochemical transduction modes integrated together with a microreactor or a mixer and capable of performing continuous flow measurements have been presented. The DLOCs have been tested for the analysis of glucose. For this purpose, GOx and HRP were immobilized at microreactor and mixer walls. The results show that glucose can be measured at the physiological level using a relatively high flow rate and with fast system response of just 20 seconds for the DLOC2. Simultaneous measurements show absence of crosstalk and identical fast response, enhancing the reliability of the DLOCs by making them self-verifying. By manipulating the flow rate, the LOD could be improved while keeping the response time short, this being of just 60 seconds.

6.6. References

1. O. Ordeig, P. Ortiz, X. Muñoz-Berbel, S. Demming, S. Büttgenbach, C. Fernández-Sánchez, A. Llobera. Dual photonic-electrochemical lab on a chip for online simultaneous absorbance and amperometric measurements. *Analytical Chemistry* 84, **2012**, 3546-3553.
2. K. Nakamura, Y. oda, T. Sekikawa, M. Sugimoto. Electrochromic characteristics of organic materials with a simple molecular structure. *Japanese Journal of Applied Physics* 26, **1987**, 931-935.
3. G. Liu, S.M. Khor, S.G. Iyengar, J.J. Gooding. Development of an electrochemical immunosensor for the detection of HbA1c in serum. *Analyst* 137, **2012**, 829-832.
4. B. Ibarlucea, C. Fernández-Sánchez, S. Demming, S. Büttgenbach, A. Llobera. Selective functionalisation of PDMS-based photonic lab on a chip for biosensing. *Analyst* 136, **2011**, 3496-3502.
5. J.C. Liao, M. Mastali, Y. Li, V. Gau, M.A. Suchard, J. Babbitt, J. Gombein, E.M. Landaw, E.R.B. McCabe, B.M. Curchill, D.A. Haake. Development of an advanced electrochemical DNA biosensor for bacterial pathogen detection. *Journal of Molecular Diagnostics* 9(2), **2007**, 158-168.
6. H.J. Kim, Y. Suma, S.H. Lee, J.A. Kim, H.S. Kim. Immobilization of horseradish peroxidase onto clay minerals using soil organic matter for phenol removal. *Journal of Molecular Catalysis B: Enzymatic* 83, **2012**, 8-15.
7. Y. Asanomi, H. Yamaguchi, M. Miyazaki, H. Maeda. Enzyme-immobilized microfluidic process reactors. *Molecules* 16, **2011**, 6041-6059.
8. M. Tudorache, D. Mahalu, C. Teodorescu, R. Stan, C. Bala, V.I. Parvulescu. Biocatalytic microreactor incorporating HRP anchored on micro-/nano-lithographic patterns for flow oxidation of phenols. *Journal of Molecular Catalysis B: Enzymatic* 69, **2011**, 133-139.
9. H.R. Luckarift, B.S. Ku, J.S. Dordick, J.C. Spain. Silica-immobilized enzymes for multi-step synthesis in microfluidic devices. *Biotechnology and Bioengineering* 98(3), **2007**, 701-705.
10. M. Baeza, C. López, J. Alonso, J. López-Santín, G. Álvaro. Ceramic microsystem incorporating a microreactor with immobilized biocatalyst for enzymatic spectrophotometric assays. *Analytical Chemistry* 82, **2010**, 1006-1011.
11. J.H. Cho, K.M. Kim, D.Y. Noh, H.I. Lee. Synthesis, structure and peroxidase activity of an octahedral Ru(III) complex with a tripodal tetraamine ligand. *Bulletin of the Korean Chemical Society* 32(11), **2011**, 3904-3908.

12. C.C. Hong, J.W. Choi, C.H. Ahn. A novel in-plane passive microfluidic mixer with modified Tesla structures. *Lab on a Chip* 4, **2004**, 109-113.
13. M. Akita, D. Tsutsumi, M. Kobayashi, H. Kise. Structural change and catalytic activity of horseradish peroxidase in oxidative polymerization of phenol. *Bioscience, Biotechnology and Biochemistry*, 65(7), **2001**, 1581-1588.
14. D. Mackey, A.J. Killard, A. Ambrosi, M.R. Smyth. Optimizing the ratio of horseradish peroxidase and glucose oxidase on a bienzyme electrode: Comparison of a theoretical and experimental approach. *Sensors and Actuators B* 122, **2007**, 395-402.
15. Y.L. Yao, K.K. Shiu, A mediator-free bienzyme amperometric biosensor baed on horseradish peroxidase and glucose oxidase immobilized on carbon nanotube modified electrode. *Electroanalysis* 20 (19), **2008**, 2090-2095.
16. D. Choi, E. Jang, J. Park, W.G. Koh. Development of microfluidic devices incorporating non-spherical hydrogel microparticles for protein-based bioassay. *Microfluidics and Nanofluidics* 5, **2008**, 703-710.
17. L. Zhu, R. Yang, J. Zhai, C. Tian. Bienzymatic glucose biosensor based on co-immobilization of peroxidase and glucose oxidase on a carbon nanotubes electrode. *Biosensors and Bioelectronics* 23, **2007**, 528-535.
18. A. Llobera, R. Wilke, S. Büttgenbach. Enhancement of the response of poly(dimethylsiloxane) hollow prisms through air mirrors for absorbance-based sensing. *Talanta* 75, **2008**, 473-479.
19. Q. Shi, Q. Li, D. Shan, Q. Fan, H. Xue. Biopolymer-clay nanoparticles composite system (Chitosan-laponite) for electrochemical sensing based on glucose oxidase. *Materials Science and Engineering C* 28, **2008**, 1372-1375.
20. X. Chu, D. Duan, G. Shen, R. Yu. Amperometric glucose biosensor based on electrodeposition of platinum nanoparticles onto covalently immobilized carbon nanotube electrode. *Talanta* 71, **2007**, 2040-2047.
21. J. Wang, M. Musameh. Carbon-nanotubes doped polypyrrole glucose biosensor. *Analytica Chimica Acta* 539, **2005**, 209-213.
22. G. Chang, Y. Tatsu, T. Goto, H. Imaishi, K. Morigaki. Glucose concentration determination based on silica sol – gel encapsulated glucose oxidase optical biosensor arrays. *Talanta* 83, **2010**, 61-65.
23. H.S.M. Abd-Rabboh, M.E. Meyerhoff. Determination of glucose using a coupled-enzymatic reaction with new fluoride selective optical sensing polymeric film coated in microtiter plate wells. *Talanta* 72, **2007**, 1129–1133.
24. L. Zhu, Y. Li, F. Tian, B. Xu, G. Zhu. Electrochemiluminescent determination of glucose with a sol – gel derived ceramic carbón composite electrode as a renewable optical fiber biosensor. *Sensors and Actuators B* 84, **2002**, 265-270.

7. OTHER FUNCTIONALIZATION APPROACHES EXPLORED

7.1.	Summary	118
7.2.	Introduction	118
7.3.	Experimental details	119
7.3.1.	Materials and reagents	119
7.3.2.	Polymer biofunctionalization.....	120
7.3.3.	Immobilization of bacteria	121
7.3	Results.....	122
7.3.4.	Characterization of the polymer modification steps	122
7.3.5.	Characterization of the analytical performance of the PC surfaces	124
7.3.6.	Characterization of the analytical performance of the biofunctionalized PMMA	127
7.3.7.	Immobilization of bacteria	128
7.4	Conclusions	129
7.5	References	130

7.1. Summary

In this chapter, a simple methodology for the biofunctionalization of PC and PMMA is carried out based on the previous protocol described in Chapter 5 and focused on the biofunctionalization of PDMS. In addition, a PMMA-based photonic LOC (PhLOC) has been functionalized to determine the possibility of transferring the designs of PDMS LOCs to this material. PC flat surfaces were tested by the detection of hydrogen peroxide (H_2O_2) with immobilized horseradish peroxidase (HRP), obtaining a limit of detection (LOD) of $2.5 \pm 0.2 \mu\text{M}$ and a stability of one month. In the case of the PMMA-based PhLOC, GOx and HRP were immobilized and the analysis of glucose was carried out, obtaining a LOD of $24 \pm 1 \mu\text{M}$. *Escherichia coli* (*E. coli*) bacteria was also successfully immobilized, keeping their viability intact. 800 ± 200 viable bacteria/ mm^2 were immobilized on modified PDMS surfaces while 600 ± 300 live bacteria/ mm^2 were immobilized on modified PC surfaces.

7.2. Introduction

Although polydimethylsiloxane (PDMS) offers some advantages for the fabrication of microfluidic chips, there are some drawbacks that hamper its massive implantation in commercially-available systems. For example, its elastic modulus is key to fabricating patterns by soft lithography. Thus, it enables the fabrication of actuated fluidic components such as pneumatic valves to be monolithically integrated with other fluidic components. However, the same property limits the aspect ratios of the structures that can be fabricated with it in order to avoid pairing and sagging negative effects. These can make the geometry of the final microsystem to be altered thus giving rise to a failure in the prediction of flow rates or alteration in the alignment of optical systems and their focusing. Designs that seem to work in PDMS at laboratory level could not work when transferring them to other materials with a different elasticity. Even with an increase in the cross-linker to silicon elastomer ratio above 1:10, rigidity is not significantly increased. Reliable PDMS bonding depends on many variables such as humidity, temperature, applied plasma power and crosslinking agent to polymer ratio. When this bond is made between PDMS and glass, it fails around 30-50 PSI, which makes these microsystems inappropriate for applications where high pressure is required¹. For these reasons different polymers were applied in the fabrication of LOCs, which are also cost-effective and easy to pattern by, for instance, hot embossing or injection molding processes. Therefore, in order to integrate biosensor approaches in LOCs made with other polymers, additional research in the functionalization of these materials is required.

Polycarbonate (PC) is an inexpensive polymer also applied to the fabrication of LOCs. It presents a high impact resistance, low moisture absorption, good machining properties, high glass transition temperature and transparency in the visible region². It has already been applied in the fabrication of a variety of microfluidic chips³⁻⁵. However, its surface chemistry does not enable the covalent stable attachment of biomolecules. In this context, diverse processes have been published for the surface modification of PC. Many of them, however,

modify the properties of the material⁶, make use of solvents such as acetonitrile that could alter the shape of the patterned structures⁷, or involve the use of plasma treatments, which could be difficult to apply in microfluidic channels⁸.

Polymethylmethacrylate (PMMA) has also been widely used for the fabrication of microfluidic chips⁹⁻¹¹. It is a cheap, optically transparent material that can be easily patterned using different methods such as laser ablation, hot embossing, reactive ion etching and deep UV lithography¹². In addition, its surface can be chemically modified and it is biocompatible¹³.

On the other hand, although isolated proteins have only been immobilized in this Thesis, proteins in nature can also be found immersed in more complex systems such as cells. The possibility to immobilize any protein on polymeric surfaces following the protocols described throughout this Thesis can be exploited to immobilize cells through their membrane proteins. In this way, immobilized cells can be used for a variety of purposes, such as biosynthesis of vitamins, amino acids, organic acids, production of monoclonal antibodies, recovery of heavy metals, whole cell enzymatic reactions or ethanol fermentation¹⁴. Different methods have been previously reported for cell immobilization in microfluidic chips, but most of the materials onto which cells were immobilized were not polymers^{15,16}. In most of the already existing works describing bacterial immobilization onto polymers, a non-specific immobilization is used, such as simple adsorption of cells on porous PDMS¹⁷ or by direct immobilization on polycarbonate membranes¹⁸. In addition, the immobilizing protocol must preserve the viability of these cells¹⁹.

In this chapter, a simple methodology for the biofunctionalization of PC and PMMA is carried out based on the previous protocol that is described in Chapter 5 of this Thesis and in the work by Ibarlucea *et al.*²⁰. This methodology avoids the use of specific instrumentation and keeps intact the optical and structural properties of the materials used. In addition, a PMMA-based photonic LOC has been functionalized to determine the possibility of transferring the designs of PDMS LOCs to this material. Finally, *Escherichia coli* (*E. coli*) bacteria have been selectively immobilized through their membrane proteins following the same immobilization protocol on PDMS and PC. The viability of immobilized cells has been determined.

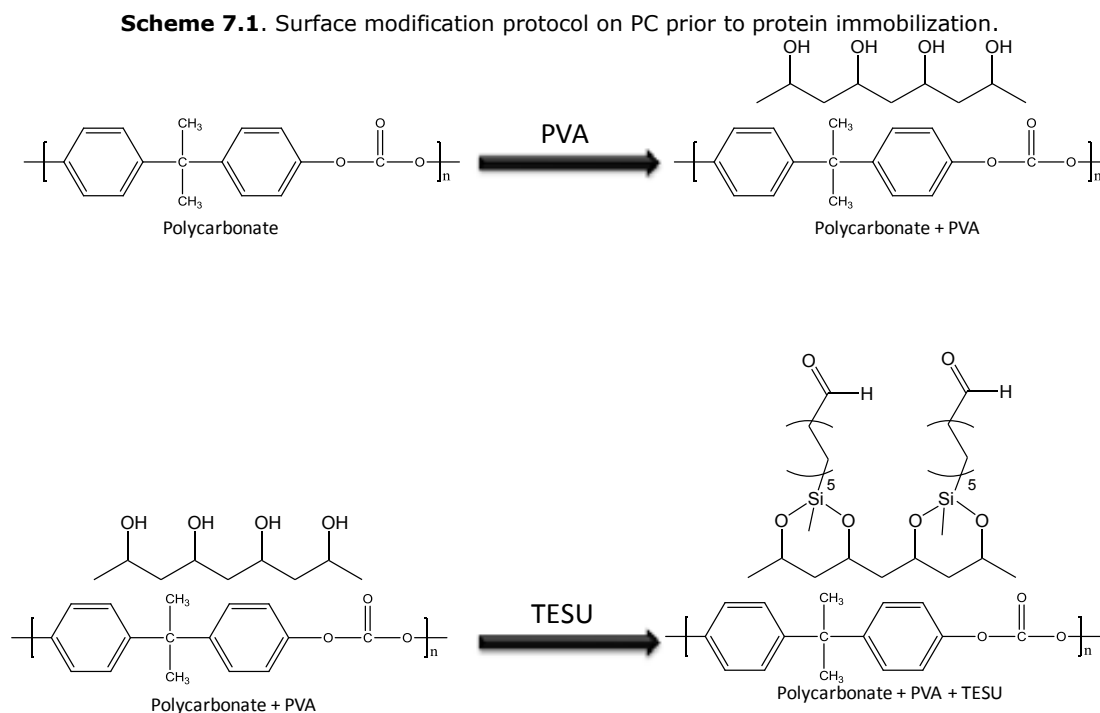
7.3. Experimental details

7.3.1. Materials and reagents

Polyvinyl alcohol (PVA), 99.5% ethanol, 99% triethylamine (TEA), glucose oxidase (GOx), horseradish peroxidase type VI (HRP), sodium cyanoborohydride (NaBH₃CN), tween 20, 99% 2,2'-azino-bis(3-ethylbenzthiazoline-6-sulfonic acid) (ABTS), and 30 % hydrogen peroxide (H₂O₂) were purchased to Sigma-Aldrich Co. (St Louis, MO 63103, USA). 90% 11-triethoxysilyl undecanal (TESU) was from ABCR GmbH & Co. KG (76187 Karlsruhe, Germany). The PDMS Sylgard 184 elastomer kit was bought from Dow Corning (Midland, MI, USA). *Escherichia coli* strain was provided by the Genetics and Microbiology Department (Universitat Autònoma de Barcelona). LIVE/DEAD® *BacLight*™ Bacterial Viability Kit was from Invitrogen (Life Technologies Corporation, Carlsbad, CA 92008, USA).

7.3.2. Polymer biofunctionalization

It has been previously reported that PVA can form coatings on hydrophobic surfaces²¹. Based on this and in our previously described protocol²⁰, PC surfaces were modified as shown in Scheme 7.1.



First, a PC sheet was cut in 4 cm² pieces using a milling machine. They were cleaned in an ultrasonic bath (Thermo Fisher Scientific Inc., Waltham, MA, US) at 37 KHz, first in ethanol for 15 min and then in deionized water (DI H₂O) for 15 min. Then they were immersed in a 1 mg ml⁻¹ solution of PVA in DI H₂O and left to react for 1h. After this step, they were rinsed in water and dried under a N₂ stream. Next, a silanization process was carried out by incubating the modified PC surfaces in a 99.5% ethanol solution containing 2% TESU and 2% TEA for 1h at room temperature (RT). Then the surfaces were rinsed with 99.5% ethanol and dried at 80°C for 2h. Finally, the silanized PC surfaces bound HRP through the amine groups of its lysine residues, by forming a Schiff base that is further reduced to a stable secondary amine with sodium cyanoborohydride. For this, an incubation of 1 hour in a 1 mg ml⁻¹ HRP enzyme solution in 0.05 M carbonate buffer pH 8 at room temperature was done.

Following the same modification procedure, PC wells provided by the Institut für Mikrosystemtechnik (IMTEK, Freiburg, Germany) were biofunctionalized. However, for the enzyme incubation step, a solution containing 0.0375 KU GOx/mL and 0.075 KU HRP/mL was used with the aim of developing glucose sensing systems. The optical detection scheme was the same already applied in Chapter 6.

In the case of PMMA, it has also been previously reported that PVA can form coatings on its surface^{22,23}. A PVA-based modification of PMMA surfaces was carried out following the same

protocol. PMMA wells provided by the Institut für Mikrosystemtechnik (IMTEK, Freiburg, Germany) were modified first for the incubation of a 1:2 ratio of GOx and HRP, using the same concentrations as for PC. Finally, a photonic LOC (PhLOC) fabricated in PMMA provided by the IMTEK was biofunctionalized following the same procedure.

7.3.2.1. Characterization of the polymer modification steps

Contact angle measurements were carried out with the sessile drop method, using a Krüss Easydrop contact angle meter and DS1 analysis software (Krüss GmbH, Hamburg, Germany). A drop of water was deposited on the modified polymer surfaces and the angle formed between the liquid and the solid surfaces was measured. Atomic force microscopy topographic and phase images of the modified surfaces were taken with a Veeco Nanoscope Dimension 3100 (Veeco, Plainview, NY, USA), working in tapping mode.

7.3.2.2. Characterization of the analytical performance of the PC surfaces

The analytical performance of the HRP containing surfaces was tested by measuring their enzymatic activity of this enzyme. The reduction of H₂O₂ in the presence of colorless 2,2'-azino-bis (3-ethylbenzthiazoline-6-sulfonic acid) (ABTS) charge transfer mediator, catalyzed by HRP, was monitored by absorbance measurements at 420 nm, as detailed in Chapter 5. 1 mL acetate buffer pH 5.5 samples containing different H₂O₂ concentrations in presence of 0.5 mM were incubated on the PC surfaces for 4 minutes and the solution was transferred to a standard spectrophotometry cuvette for the absorbance measurement. The calibration curve was plotted and the linear range, LOD and sensitivity for H₂O₂ were calculated. These results were compared to surfaces modified by direct adsorption of the enzyme. Then, the surfaces were stored in PBS at 4 °C for over a month and the stability of the immobilized species was studied by repeating the calibration curve each week.

For the bienzymatic surfaces, a 100 mM glucose and 0.5 mM ABTS containing sample was incubated for 10 minutes and the color formation was observed.

7.3.2.3. Characterization of the analytical performance of the biofunctionalized PMMA

For the PMMA wells, the activity of the immobilized enzymes was checked by the observation of the difference in the green color formation between the biofunctionalized and non-biofunctionalized wells, in the same way as for the PC wells mentioned above.

For the measurement in the PhLOC, a halogen lamp was used as light source and a 1930F-SL power meter (Newport, Irvine, USA) was used as detector. The microsystem consisted of a MIR system similar to that previously published²⁴, being the lenses modified in accordance to the PMMA refractive index and the fabrication constrictions of the milling machine at IMTEK facilities. Samples of PBS buffer pH 7.2 containing glucose in a range from 20 µM to 1 mM in presence of 0.5 mM ABTS were pumped inside the LOC and the increase in the detected power at 420 nm due to the formation of ABTS⁺ after the enzymatic cascade mentioned before was plotted. Finally, the LOD and sensitivity for glucose was calculated.

7.3.3. Immobilization of bacteria

7.3.3.1. Bacteria immobilization protocol

The protocol described in Chapter 5 for PDMS biofunctionalization was followed for the immobilization of bacteria on 4 cm² flat PDMS and PC surfaces through their membrane proteins. The immobilization step was done by immersing overnight the modified surfaces in 2 ml of 1×10^8 *E. coli* ml⁻¹ containing carbonate buffer pH 8 at 4 °C. The surfaces were then thoroughly rinsed in a 0.1M phosphate buffered saline pH 7.0 containing 0.02% (v/v) Tween 20 (PBST) for 1 h in order to remove the nonspecifically adsorbed bacteria. The resulting surfaces were stored at 4°C in PBS until their characterization by epifluorescence microscopy.

7.3.3.2. Viability test and counting of immobilized bacteria

Immobilized bacteria were stained with the LIVE/DEAD® *BacLight*[™] Bacterial Viability Kit to quantify them and to monitor their viability as a function of their membrane integrity. This kit consists of two nucleic-acid-binding stains, SYTO® 9 and propidium iodide. The first one penetrates the cell membranes and labels bacteria with green fluorescence, while the second one is highly charged and does not penetrate the membranes unless they are damaged. In this last case, the bacteria are considered to be non-viable and they are labeled with red fluorescence, while the living ones remain green^{25,26}. These stains were mixed together at a 1:1 ratio and diluted 1:10 in a NaCl solution (0.085%). A volume of 1 ml of the mixture was added to the modified PDMS surfaces with immobilized bacteria and they were incubated in the dark at room temperature for 15 min. After incubation, the surfaces were observed with a Zeiss AXIO Imager A1 epifluorescence microscope and random pictures were captured. Cells were counted on 10 pictures for each material, and the average value was calculated together with the standard deviation. Viable cells were fluorescent green, while non-viable cells were fluorescent red. In this way, viable and total counts were obtained in a single staining step. PDMS surfaces with directly adsorbed bacteria were also observed for comparison purposes.

7.3 Results

7.3.4. Characterization of the polymer modification steps

A rapid estimation of the degree of modification of the PC surfaces after every step carried out in the modification protocol was provided by contact angle measurements (Figure 7.1). The contact angle of a native PC surface was found to be $68 \pm 4^\circ$, which agrees with the value found in the literature²⁷. Following the PVA adsorption step, it decreased to $55 \pm 1^\circ$, as expected due to the hydrophilic nature of its hydroxyl groups. The silanization step gave rise to an increase of the contact angle to $75 \pm 8^\circ$.

Figure 7.1. Contact angle values measured following every step of each modification procedure. Error bars correspond to the standard deviation of three replicates.

The topographic and phase images obtained by AFM (Figure 7.2) show that the unmodified PC surface is topographically flat (25.29 nm) as well as structurally and chemically homogeneous. After the PVA adsorption and silanization process, AFM images show a surface roughness increase (up to 36.23 nm) compared with that one of the native PC and an increase in the surface heterogeneity.

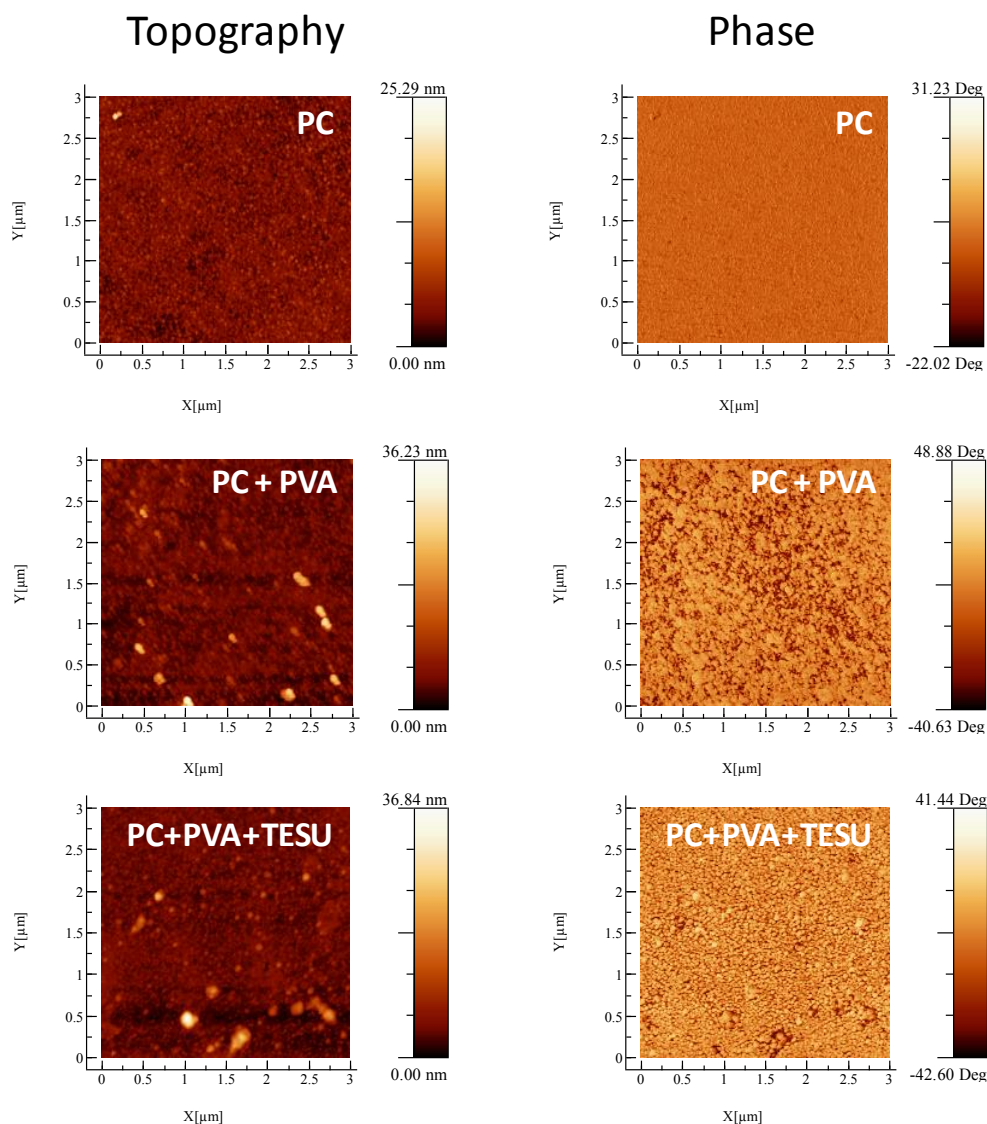


Figure 7.2. Topographic and phase AFM pictures of the PC surface before and after the modification with PVA and silane.

7.3.5. Characterization of the analytical performance of the PC surfaces

After the immobilization of HRP on PC surfaces, the analytical performance of the resulting sensing surfaces was tested in H_2O_2 solutions in a concentration range from 2 μM to 20 μM . For the surfaces with the enzyme directly adsorbed, the measurable range was found to be between 10 μM and 80 μM . The corresponding calibration plots can be seen in Figure 7.3. A LOD of $2.5 \pm 0.2 \mu\text{M}$ H_2O_2 and a sensitivity of $0.0066 \pm 0.0005 \text{ A.U./}\mu\text{M}$ H_2O_2 was obtained with the modified PC surfaces, while for the surfaces with the adsorbed enzyme the LOD and the sensitivity values were $6.3 \pm 0.4 \mu\text{M}$ H_2O_2 and $0.0101 \pm 0.0007 \text{ A.U./}\mu\text{M}$ H_2O_2 respectively. Linear fittings can be seen in Table 7.1.

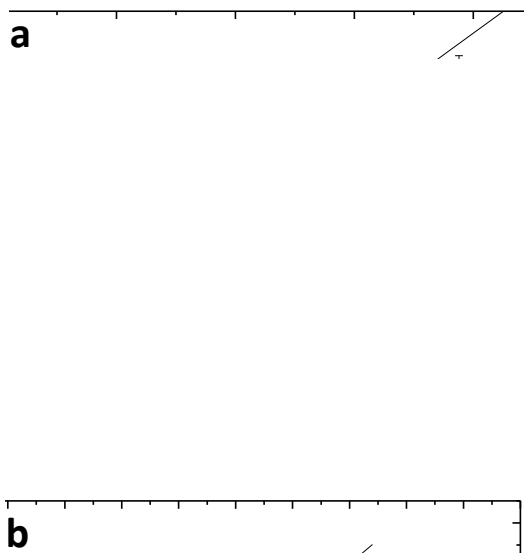


Figure 7.3. Calibration plots for the hydrogen peroxide sensing surfaces on (a) modified PC and (b) directly adsorbed PC.

Table 7.1. Linear fittings, limit of detections and sensitivities of the different polymeric sensing systems obtained.

Material	Results
Modified PC	Linear Fitting:
	$Y = 0.009 \pm 0.006 + 0.0066 \pm 5 \times 10^{-4} X$
	$R^2 = 0.963$
	LOD: $2.5 \pm 0.2 \mu\text{M H}_2\text{O}_2$ Sensitivity: $0.0066 \pm 5 \times 10^{-4} \text{ A.U./}\mu\text{M H}_2\text{O}_2$
Native PC	Linear Fitting:
	$Y = 0.05 \pm 0.02 + 0.0101 \pm 7 \times 10^{-4} X$
	$R^2 = 0.983$
	LOD: $6.3 \pm 0.4 \mu\text{M H}_2\text{O}_2$ Sensitivity: $0.0101 \pm 7 \times 10^{-4} \text{ A.U./}\mu\text{M H}_2\text{O}_2$
PMMA PhLOC	Linear Fitting:
	$Y = 0.025 \pm 0.011 + 0.00139 \pm 8 \times 10^{-5} X$
	$R^2 = 0.977$
	LOD: $24.2 \pm 1.4 \mu\text{M glucose}$ Sensitivity: $0.001 \pm 8 \times 10^{-5} \text{ nW/}\mu\text{M glucose}$

The operational stability of the surfaces was tested for over a month. Figure 7.4 shows the shift in the sensitivity values with time. The surfaces based on the adsorption of HRP show a rapid decrease in the sensitivity values during the first week of operation, while the modified ones remained more stable for one month due to the presence of several bonding points that long PVA chains create over the PC surface, as it occurred when using PDMS surfaces (see Chapter 5). A shift towards lower sensitivity values was observed after this month.

Figure 7.4. Stability study for the hydrogen peroxide sensing surfaces on modified and unmodified PC.

When the analytical performance of the bienzymatic surfaces was observed, a clear color difference was observed between the biofunctionalized wells and the non-biofunctionalized ones (Figure 7.5), showing that the two enzymes can be immobilized at the same time on the modified PC.

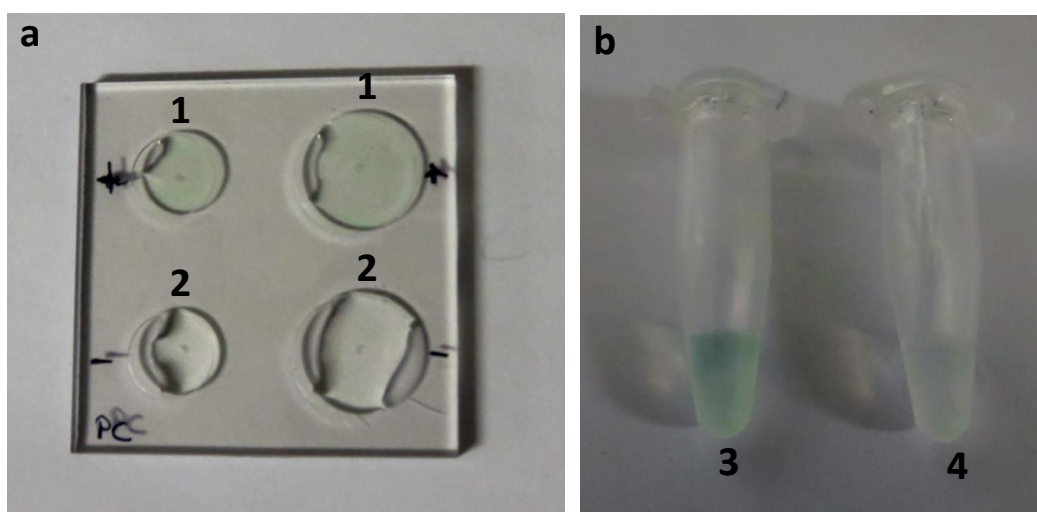


Figure 7.5. (a) PC wells (1) with and (2) without immobilized enzymes. (b) Color comparison between glucose samples after incubation on (3) biofunctionalized and (4) non-biofunctionalized PC wells.

Overall, from the results presented above, it can be seen that the PVA-based modification protocol gives rise to stable sensing surfaces with a good analytical performance.

7.3.6. Characterization of the analytical performance of the biofunctionalized PMMA

The correct activity of the immobilized enzymes was checked on the PMMA wells by the observation of the difference in the green color formation between the biofunctionalized and non-biofunctionalized wells, in the same way as for the PC wells mentioned above. As it can be seen in Figure 7.6, a green color was developed on the solutions incubated on the biofunctionalized wells.

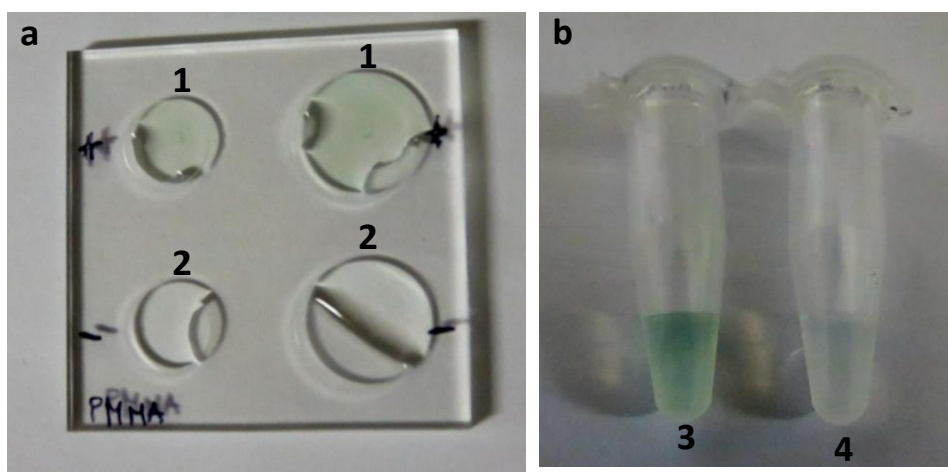


Figure 7.6. (a) PC wells (1) with and (2) without immobilized enzymes. (b) Color comparison between glucose samples after incubation on (3) biofunctionalized and (4) non-biofunctionalized PC wells.

Using the PMMA-based LOC, a linear range between 20 μM and 300 μM was obtained (Figure 7.7). The LOD and sensitivity were found to be $24.2 \pm 1.4 \mu\text{M}$ glucose and $0.001 \pm 8 \times 10^{-5} \text{ nW}/\mu\text{M}$ glucose respectively. Linear fittings can be seen in Table 1.

Figure 7.7. Calibration plots for the glucose biosensor approach in the PMMA PhLOC.

7.3.7. Immobilization of bacteria

On the modified PDMS surfaces, 8000 ± 200 live bacteria/ mm^2 and 300 ± 100 dead bacteria/ mm^2 were found to be immobilized, while on the unmodified PDMS 100 ± 100 live bacteria/ mm^2 and 10 ± 20 dead bacteria/ mm^2 were immobilized, as it can be seen in figure 7.8. Some pictures obtained by microscopy can be seen in Figure 7.9.

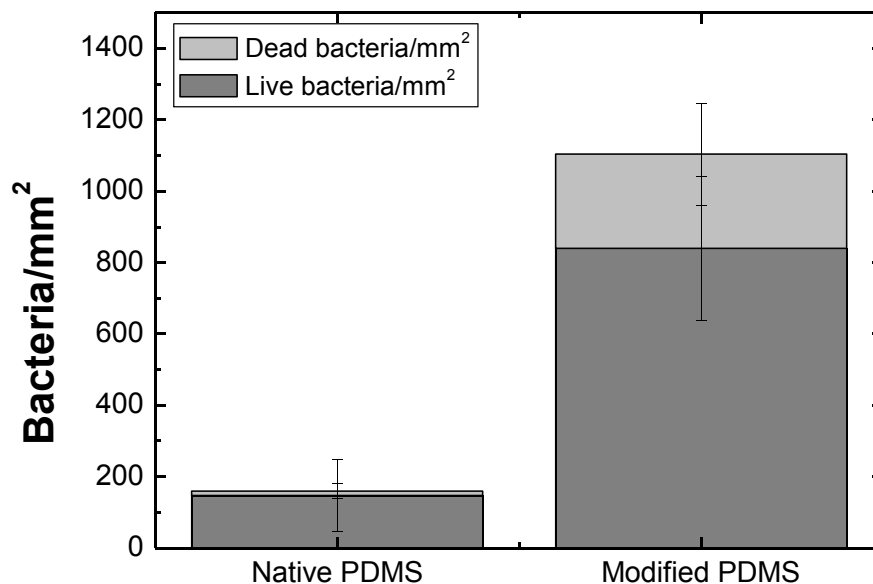


Figure 7.8. Comparative quantification of dead and live immobilized bacteria on unmodified and modified PDMS.

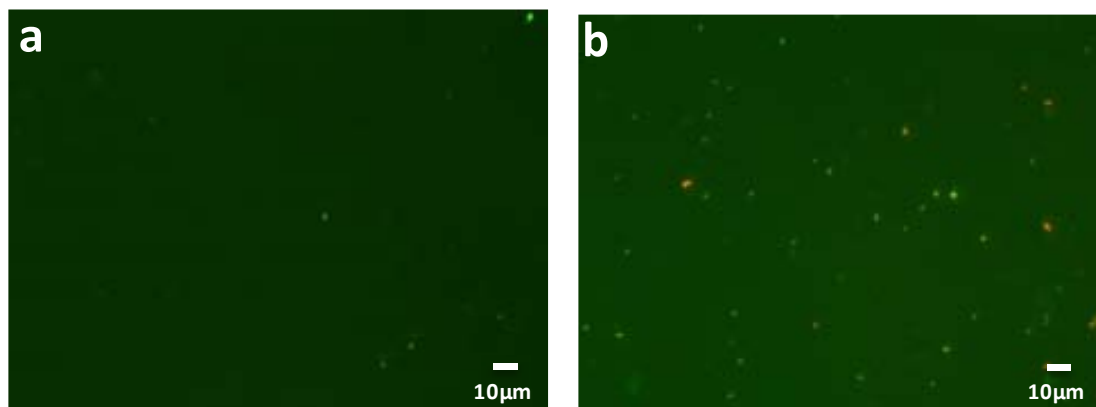


Figure 7.9. Fluorescence microscopy picture of (a) unmodified and (b) modified PDMS after bacteria immobilization protocol.

On the modified PC surfaces, 600 ± 300 live bacteria/ mm^2 and 100 ± 100 dead bacteria/ mm^2 were immobilized, while on the unmodified PC 200 ± 200 live bacteria/ mm^2 and 20 ± 30 dead bacteria/ mm^2 were immobilized, as it can be seen in Figure 7.10. Pictures obtained by microscopy can be seen in Figure 7.11.

Figure 7.10. Comparative quantification of dead and live immobilized bacteria on unmodified and modified PC.

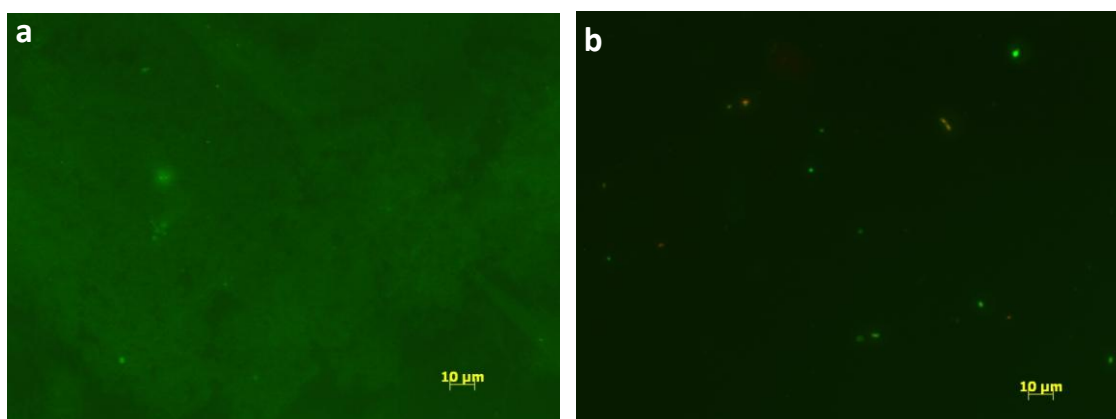


Figure 7.11. Fluorescence microscopy picture of (a) unmodified and (b) modified PC after bacteria immobilization protocol.

From the results, it can be observed that enzymes have been immobilized on PC and PMMA retaining both the enzymatic activity and the optical and structural properties of the polymers intact. The MIR structure has been used in PMMA with minimum changes and glucose has been detected below the physiological level. Cells have also been immobilized through their proteins, retaining their viability.

7.4 Conclusions

Immobilization of enzymes on PC and PMMA has been successfully achieved. The stability has been proved for 1 month for peroxide sensing PC flat substrates. By using a PhLOC fabricated in PMMA, a system for glucose detection was obtained with a LOD below the physiological level. *E. coli* bacteria were also immobilized through their membrane proteins on PDMS and PC

surfaces in a higher number than the ones that can be nonspecifically adsorbed to the same surfaces. Most of the immobilized bacteria were alive, permitting their use for cell-based sensing applications on microfluidic systems.

7.5 References

1. E. Sollier, C. Murray, P. Maoddi, D.D. Carlo. Rapid prototyping polymers for microfluidic devices and high pressure injections. *Lab On a Chip* 11, **2011**, 3752-3765.
2. D. Ogonczyk, J. Wegrzyn, P. Jankowski, B. Dabrowski, P. Garstecki. Bonding of microfluidic devices fabricated in polycarbonate. *Lab on a Chip* 10, **2010**, 1324-1327.
3. Y. Wang, Q. He, Y. Dong, H. Chen. In-channel modification of biosensors electrodes integrated on a polycarbonate microfluidic chip for micro flow-injection amperometric determination of glucose. *Sensors and Actuators B* 145, **2010**, 553-560.
4. Y.X. Wang, Y. Zhou, B.M. Balgley, J.W. Cooper, C.S. Lee, D.L. DeVoe. Electro spray interfacing of polymer microfluidics to MALDI-MS. *Electrophoresis* 26, 2005, 3631-3640.
5. M.Y. Ye, X.F. Yin, Z.L. Fang. DNA separation with low-viscosity sieving matrix on microfabricated polycarbonate microfluidic chips. *Analytical and Bioanalytical Chemistry* 381, **2005**, 820-827.
6. P. Najmabadi, K.S. Ko, J.J. La Clair, M.D. Burkart. A method for fabrication of polycarbonate-based bioactive platforms. *Journal of Laboratory Automation* 13(5), **2008**, 284-288.
7. J.J. La Clair, M.D. Burkart. Molecular screening on a compact disc. *Organic and Biomolecular Chemistry* 1, **2003**, 3244-3249.
8. A. Qureshi, S. Shah, S. Pelagade, N.L. Sing, S. Mukherjee, A. Tripathi, U.P. Deshpande, T. Shripathi. Surface modification of polycarbonate by plasma treatment. *Journal of Physics: Conference Series* 208, **2010**, 012108 1-6.
9. S. Marson, U.M. Attia, G. Lucchetta, A. Wilson, J.R. Alcock, D.M. Allen. Flatness optimization of micro-injection moulded parts: the case of a PMMA microfluidic component. *Journal of Micromechanics and Microengineering* 21, **2011**, 115024-115032.
10. X. Yao, Z. Chen, G. Chen. Fabrication of PMMA microfluidic chips using disposable agar hydrogel templates. *Electrophoresis* 30, **2009**, 4225-4229.
11. J.M. Li, C. Liu, J.S. Liu, Z. Xu, L.D. Wang. Multi-layer PMMA microfluidic chips with channel networks for liquid sample operation. *Journal of Materials Processing Technology* 209, **2009**, 5487-5493.
12. M. Rahbar, S. Chhina, D. Sameoto, M. Parameswaran. Microwave-induced, thermally assisted solvent bonding for low-cost PMMA microfluidic devices. *Journal of Micromechanics and Microengineering* 20, **2010**, 015026-015024.
13. D. Sabourin, J. Petersen, D. Snakenborg, M. Brivio, H. Gudnadson, A. Wolff, M. Dufva. Microfluidic DNA microarrays in PMMA chips: streamlined fabrication via simultaneous DNA immobilization and bonding activation by brief UV exposure. *Biomedical Microdevices* 12, **2010**, 673-681.
14. E. Górecka, M. Jastrzebska. Immobilization techniques and biopolymer carriers. *Biotechnology of Food Science* 75(1), **2011**, 65-86.
15. D.A. Boehm, P.A. Gottlieb, S.Z. Hua. On-chip microfluidic biosensor for bacterial detection and identification. *Sensors and Actuators B* 126, **2007**, 508-514.
16. N.Y. Lee, Y. Yang, Y.S. Kim, S. Park. Microfluidic immunoassay platform using antibody-immobilized glass beads and its application for detection of *Escherichia coli* O157:H7. *Bulletin of the Korean Chemical Society* 24(4), **2006**, 479-483.

17. M.R. Fernández, M.G. Casabona, V.N. Anupama, B. Krishnakumar, G.A. Curutchet, D.L. Bernik. PDMS-based porous particles as support beds for cell immobilization: Bacterial biofilm formation as a function of porosity and polymer composition. *Colloids and Surfaces B: Biointerfaces* 81, **2010**, 289-295.
18. O. Højberg, S.J. Binnerup, J. Sørensen. Growth of silicone-immobilized bacteria on polycarbonate membrane filters, a technique to study microcolony formation under anaerobic conditions. *Applied and Environmental Microbiology* 63(7), **1997**, 2920-2924.
19. K. Nilsson, S. Birnbaum, S. Flygare, L. Linse, U. Schröder, U. Jeppson, P.O. Larsson, K. Mosbach, P. Brodelius. A general method for the immobilization of cells with preserved viability. *European Journal of Applied Microbiology and Biotechnology* 17, **1983**, 319-326.
20. B. Ibarlucea, C. Fernández-Sánchez, S. Demming, S. Büttgenbach, A. Llobera. Selective functionalisation of PDMS-based photonic lab on a chip for biosensing. *Analyst* 136, **2011**, 3496-3502
21. M. Kozlov, T.J. McCarthy. Adsorption of poly(vinyl alcohol) from water to a hydrophobic surface: effects of molecular weight, degree of hydrolysis, salt, and temperature. *Langmuir* 20, **2004**, 9170-9176.
22. V. Bulmus, H. Ayhan, E. Piskin. Modified PMMA monosize microbeads for glucose oxidase immobilization. *The Chemical Engineering Journal* 65, **1997**, 71-76.
23. Y. Zhang, G. Ping, N. Kaji, M. Tokeshi, Y. Baba. Dynamic modification of poly(methyl methacrylate) chips using poly(vinyl alcohol) for glycosaminoglycan disaccharide isomer separation. *Electrophoresis* 28, **2007**, 3308-3314.
24. A. Llobera, S. Demming, R. Wilke, S. Büttgenbach. Multiple internal reflection poly(dimethylsiloxane) systems for optical sensing. *Lab on a Chip* 7, **2007**, 1560-1566.
25. L. Boulous, M. Prévost, B. Barbeau, J. Coallier, R. Desjardins. LIVE/DEAD® BacLight™: application of a new rapid staining method for direct enumeration of viable and total bacteria in drinking water. *Journal of Microbiological Methods* 37, **1999**, 77-86
26. S. Leuko, A. Legat, S. Fendrihan, H. Stan-Lotter. Evaluation of the LIVE/DEAD BacLight Kit for detection of extremophilic archaea and visualization of microorganisms in environmental hypersaline samples. *Applied and Environmental Microbiology*, 70(11), **2004**, 6884-6886
27. K.A. Vijayalakshmi, M. Mekala, C.P. Yoganand, and K. Navaneetha-Pandiyaraj. Studies on modification of surface properties in polycarbonate (PC) film induced by DC glow discharge plasma. *International Journal of Polymer Science*, **2011**, Article ID 426057, 7 pages. doi:10.1155/2011/426057.

8. CONCLUDING REMARKS

The main objective of the PhD Thesis was focused towards the development of low-cost functionalized Lab-on-a-(Bio)Chip (LOC) devices, which could be applied for the analysis of target analytes of interest in the environmental and biomedical field. The results obtained to achieve this objective were quite satisfactory and can be summarized as follows:

1. Analytical procedures for the detection of various analytes (cells and heavy metal ions) using polymeric photonic lab on a chip (PhLOC) systems have been developed. These PhLOCs implemented using a low-cost polymer, polydimethylsiloxane (PDMS), monolithically integrate all the required micro-optical structures. They present air mirrors in order to lengthen the optical path without dramatically enlarging its size, resulting in a sensitivity enhancement, in accordance to the Beer-Lambert law. When analyzing cells, these PhLOCs tackle the drawbacks of the Neubauer cell counters in terms of measuring speed and avoidance of human errors. It has been possible to measure and differentiate live and dead cell populations. Heavy metal ion concentrations have also been determined by combining the use of PhLOCs with selective colorimetric ligands, developing a simple procedure that can be implemented in portable systems for *in situ* measurements. They outperform other previously reported systems just by considering the ease and cost of their fabrication process and the simplicity of the applied absorbance-based detection approach, which avoids the implementation of electrodes, heaters or the incorporation of toxic substances.
2. Protein immobilization protocols in liquid phase for PDMS microchannels have been developed. They retain the optical and structural properties of the material intact, as well as the activity of the enzymes that have been immobilized for the use of PhLOCs as biosensors. These protocols do not require any specific instrumentation, thus enabling their easy and rapid implementation in chemical and biological laboratories. The protocol that involves a surface modification with polyvinyl alcohol (PVA) polymer is the most suitable one and the immobilized enzyme presented a stable activity for more than a month.
3. Additional structures have been added to the PhLOCs, such as a reactor and a microfluidic structure combining properties of a mixer and a reactor (by enzymatically biofunctionalizing a mixer), as well as electrodes which, in combination with the micro-optical structures, make possible to perform simultaneous electrochemical and optical measurements and gave rise to the development of two different dual LOCs (DLOCs). More reliable analytical tools could be developed with these systems, since the optical/electrochemical double response make them to be self-verifying. In addition, it

opens the possibility to perform measurements of the enzymatic activity under continuous flow conditions, reducing response time and sample volumes. Compared to previously published DLOCs, the inclusion of the MIR with the other microfluidic structures in a single substrate avoids the tubing for their connection. Also, the immobilization of the enzymes drastically reduces the reagent consumption.

4. The protein immobilization protocol developed in this work was tested on different polymers and by immobilizing different biological targets. It was demonstrated that enzymes could also be immobilized on polycarbonate (PC) and polymethylmethacrylate (PMMA). The correct performance of the micro-optic elements of the PhLOC when they are transferred to PMMA was verified. *Escherichia coli* bacteria was also immobilized on PC and PDMS substrates, keeping their viability intact and making possible to use this process for its application in cell-based biosensors or for the study of cells in controlled environments that required their attachment to such kind of polymeric substrates.

9. ANNEX: RELATED PUBLICATIONS

Cell Screening Using Disposable Photonic Lab on a Chip Systems

Bergoi Ibarlucea,[†] Elisabet Fernandez-Rosas,^{†,‡} Jordi Vila-Planas,[†] Stefanie Demming,[§] Carme Nogues,[‡] Jose A. Plaza,[†] Stephanus Büttgenbach,[§] and Andreu Llobera^{*,†,§}

Centre Nacional de Microelectrònica (IMB-CNM, CSIC), Barcelona, Spain, Departament de Biologia Cel·lular, Fisiologia i Immunologia, Universitat Autònoma de Barcelona, 08193-Bellaterra, Barcelona, Spain, and Institut für Mikrotechnik, Technische Universität Braunschweig, 38124 Braunschweig, Germany

A low-cost photonic lab on a chip with three different working regimes for cell screening is presented. The proposed system is able to perform scattering, scattering + absorption, and absorption measurements without any modification. Opposite to the standard flow cytometers, in this proposed configuration, a single 30 ms scan allows to obtain information regarding the cell optical properties. An additional novelty is that the whole spectrum is obtained and analyzed, being then possible to determine for each regime which is the optimal working wavelength that would provide the best performance in terms of sensitivity and limit of detection (LOD). Experimental results have provided with an LOD of 54.9 ± 0.7 cells (in the scattering regime using unlabeled cells), 53 ± 1 cells (in the scattering + absorption regime using labeled cells), and 105 ± 4 cells (in the absorption regime using labeled cells). Finally, the system has also been used for measuring the dead/live cell ratio, obtaining LODs between $7.6 \pm 0.4\%$ and $6.7 \pm 0.3\%$, depending on the working regime used.

Nowadays, there is a huge demand of simple, disposable, and low-cost diagnostic tools that could be implemented in any laboratory, even in developing countries with limited resources. Additionally, point-of-care (POC) situations also demand not only such tools but also monitoring systems which provide real-time information about a therapy. When related to cell culture analysis, the main issues that such tools have to address are the isolation of the cells of interest and their fast screening. Cell isolation is generally evaluated with immunofluorescent labeling, which provides high specificity at the expenses of increasing the time and the required steps of sample processing. Additionally, for population measurements, the counting repetition at random points is required in order to avoid errors due to irregular or random patterns of uneven cell distribution.^{1,2} Some interesting

approaches have recently been presented trying to tackle this issue.³ Nevertheless, a microscope is still required, being then necessary for manual counting of the entrapped cells on a single device (with the possibility of having computer-assisted systems). A step forward is the lensless, ultrawide field cell monitoring array platform based on shadow imaging (LUCAS) that records the shadow of each individual cell.^{4,5} Although these results are a significant step toward white light microscopy on a chip, they cannot perform multiwavelength measurements (as could be the case of fluorescent labeling). Hence, the use of the LUCAS configuration is restricted to cell counting.

Generally speaking, manual counting chambers, automated cell counters, and flow cytometry are the standard methods used to determine cell concentration in cultures. Several dyes are also used to evaluate live and dead cells in culture, based on the assumption that only dead cells are stained.⁶ In this approach, human errors caused by operator subjectivity in manual counters and statistical errors due to dilutions or sample concentration in manual and automated counters are common. Flow cytometry solves this issue but at the expense of a high price. Hence, a fast, multiparametric, disposable system for POC applications able to count cells in a constant volume is yet to be presented.

This open issue is currently addressed with the miniaturization and integration of the systems that require a minimal amount of samples and reagent volumes. Manz and co-workers⁷ defined them as micro total analysis systems (μ TAS), also known as lab on a chip. The importance that these configurations have acquired has been favored by the enormous development in two main fields: microfluidics and detection methods. In the first case, the scaling down of the analytical systems does not only mean the reduction in size and price but also a significant improvement of the analytical performance (reagent consumption, response time, and parallelization). Hence, it becomes clear why microfluidics has evolved from the early simple microchannels to a myriad of different systems ranging from drop generators to single-cell cultivation systems.^{8–13}

* To whom correspondence should be addressed. E-mail address: andreu.llobera@imb-cnm.csic.es. Phone: +34935947700. Fax: +34935801496.

[†] Centre Nacional de Microelectrònica (IMB-CNM, CSIC).

[‡] Universitat Autònoma de Barcelona.

[§] Technische Universität Braunschweig.

(1) Chakravarti, G.; Bhattacharya, K. *A Handbook of Clinical Pathology*, 3rd ed.; Academic Publishers: Kolkata, India, 1984; pp 1–8.

(2) Greer, J. P., Ed. *Wintrobe's Clinical Hematology*, Vol. 1, 12th ed.; LWW Medical Book Collection; Lippincott Williams & Wilkins: Philadelphia, PA, 2009; pp 1–19.

(3) Cheng, X.; Irimia, D.; Dixon, M.; Sekine, K.; Demirci, U.; Zamir, L.; Tompkins, R. G.; Rodriguez, W.; Toner, M. *Lab Chip* **2007**, *7*, 170–178.

(4) Cui, X.; Lee, L. M.; Heng, X.; Zhong, W.; Sternberg, P. W.; Psaltis, D.; Yang, C. *Proc. Natl. Acad. Sci. U.S.A.* **2008**, *105* (31), 10670–10675.

(5) Ozcan, A.; Demirci, U. *Lab Chip* **2008**, *8*, 98–106.

(6) Tolnai, S. *A Method for Viable Cell Counting: Tissue Culture Association Manual*, Vol. 1; Evans, V. J., Perry, V. P., Vincent, M. M., Eds.; Tissue Culture Association: Rockville, MD, 1975; pp 37–38.

(7) Manz, A.; Graber, N.; Widmer, H. M. *Sens. Actuators, B* **1990**, *1*, 244–248.

Regarding the detection methods, nowadays the optical readout (defining the so-called photonic lab on a chip) uses light as the interrogation mechanism. Such a configuration has additional advantages as compared to its counterparts, as described in ref 14. Additionally, from an analytical perspective, measurements do not require direct contact with the cell culture or the use of potentials, which could either interfere or modify the cell properties.¹⁵ Two different approaches toward lab on a chip can be found in the literature: performance enhancement, which means the development of high-throughput systems (HTS) for multiparametric detection,¹⁶ or accuracy enhancement, with the most significant example as the use of optical tweezers for single cell analysis and manipulation.¹⁷ In both cases, the low-cost assumption is not fulfilled. The tackling of this issue is generally associated with the use of polymers, especially poly(dimethylsiloxane) (PDMS), using soft lithographic methods.¹⁸ Considering its excellent optical and structural properties, microfluidic and photonic elements can be monolithically defined. Not surprisingly, it has already been used in laser-induced-fluorescence systems¹⁹ and optical cytometers.²⁰ Moreover, multiplexing/filtering can also be included.^{21,22} The integration of photonic elements also allows one to remove the bulky inverted microscope and the external filters from the experimental setup, hence having an in-plane configuration with much higher accessibility. Besides, a final result is given directly, avoiding the possibility of interpretation errors. Finally, its biocompatibility and its low cost make this material the most suitable for meeting the previously mentioned requirements. Hence, polymeric photonic lab on a chip is a promising configuration, especially in the field of cellular biology, where time-dependent multiparametric measurements have to be done without compromising the environmental conditions of either the cells or the media. The low cost also assures having disposable systems, being then possible to use sterile systems for each measurement.

Currently, fluorescence is the most common analytical method.²³ Nevertheless, as it was previously mentioned, the labeling adds another step to the cell preparation. Additionally,

fluorescence is emitted in 4π sr, which makes it challenging to have a reasonable amount of fluorescence reaching the detector. Conversely, absorbance measurements can be done much faster without requiring labeling or with a simpler labeling method. Since the absorbance is directly proportional to the path length, larger interrogation regions reduce the limit of detection (LOD). It has to be noted, however, that the increase of the optical path requires having reflections inside the interrogation volume. Because of the low refractive index contrast between the PDMS and the liquid that fills the interrogation region (as could be phosphate saline buffer, PBS), the reflection coefficients at the PDMS-PBS are 0.029 for TE-polarization and 0.062 for its TM counterpart, requiring hence long integration times for achieving a reasonable signal-to-noise ratio (SNR) and thus inherently preventing the possibility of implementing them in high-throughput screening (HTS).

In an attempt to go beyond this state of the art, the low cost, disposable, polymeric photonic lab on a chip system in multiple internal reflection (MIR) configuration is used. Such MIRs systems have already been used for fluorophore detection,²⁴ but to the best of our knowledge, up to now there has been no contribution regarding using such systems for cell screening. In addition, we show in this manuscript that MIRs can work in the three working regimes: LS (scattering), LS + ABS (scattering + absorption), and ABS (absorption). Opposite to cell cytometers, where the cells are successively counted, in our approach a single measurement of 30 ms is done in the entire interrogation region. If the cells are unlabeled or do not have absorption bands in the wavelength range under study, a scattering band (flat absorption band) is obtained. Conversely, when they are labeled, a superimposed absorbance band is observed. In both working regimes, the population can be determined. Finally, by subtraction of the two previous results, we obtain the spectra related only to the absorption (ABS). To show the viability of the proposed system, it has been used not only for determining the population of labeled and unlabeled cells but also for determining the dead/live ratio. This is the first time, to the best of our knowledge, that a photonic lab on a chip that simultaneously tackles both the human errors of the Neubauer chamber and the cost issue of the cell counters is presented to the scientific community.

MATERIALS AND METHODS

Optofluidic System Design. The working principle of the PDMS-based MIR systems has already been presented.²⁴ Nevertheless, for completeness, it is briefly reproduced here. The interrogation region is tailored so as to reduce the mean flow cell volume. Optically, they form a complex system with a high degree of monolithic integration, since they comprise self-alignment systems for adequate positioning of fiber optics, lenses, and focusing mirrors. Light propagates in the system following a zigzag path with the help of integrated air mirrors.²⁵ In such conditions, the air mirrors meaningfully lengthen the optical path without dramatically increasing the overall size of the reactor.

Cell Culture and Labeling. Human monocytic cell line THP-1 (ECACC No.88081201) was maintained in RPMI 1640 medium (Gibco, 21875-034) with 20% fetal bovine serum (Gibco, 10106-

-
- (8) Applegate, R. W.; Squier, J.; Vestad, T.; Oakey, J.; Marr, D. W. M.; Bado, P.; Dugan, M. A.; Said, A. A. *Lab Chip* **2006**, *6*, 422–426.
- (9) West, J.; Michels, A.; Kittel, S.; Jacob, P.; Franzke, J. *Lab Chip* **2007**, *7*, 981–983.
- (10) Skelley, A. M.; Kirak, O.; Suh, H.; Jaenisch, R.; Voldman, J. *Nat. Methods* **2008**, *6* (2), 147–152.
- (11) Joensson, H. N.; Samuels, M. L.; Brouzes, E. R.; Medkova, M.; Uhlén, M.; Link, D. R.; Andersson-Svahn, H. *Angew. Chem., Int. Ed.* **2009**, *48*, 2518–2521.
- (12) Godin, J.; Chen, C. H.; Cho, S. H.; Qiao, W.; Tsai, F.; Lo, Y. H. *J. Biophoton.* **2008**, *1* (5), 355–376.
- (13) Lindström, S.; Larsson, R.; Andersson-Svahn, H. *Electrophoresis* **2008**, *29*, 1219–1227.
- (14) Flusberg, B. A.; Cocker, E. D.; Piyawattanametha, W.; Jung, J. C.; Cheung, E. L. M.; Schnitzer, M. J. *Nat. Methods* **2005**, *2* (12), 941–950.
- (15) Cheng, X.; Liu, Y. S.; Irimia, D.; Demirci, U.; Yang, L.; Zamir, L.; Rodríguez, W. R.; Toner, M.; Bashir, R. *Lab Chip* **2007**, *7*, 746–755.
- (16) Duffy, D. C.; Gillis, H. L.; Lin, J.; Sheppard, N. F., Jr.; Kellogg, G. J. *Anal. Chem.* **1999**, *71*, 4669–4678.
- (17) Perroud, T. D.; Kaiser, J. N.; Sy, J. C.; Lane, T. W.; Branda, C. S.; Singh, A. K.; Patel, K. D. *Anal. Chem.* **2008**, *80*, 6365–6372.
- (18) Xia, Y.; Whitesides, G. M. *Angew. Chem., Int. Ed.* **1998**, *37*, 550–575.
- (19) Camou, S.; Fujita, H.; Fujii, T. *Lab Chip* **2003**, *3*, 40–45.
- (20) Lin, C. H.; Lee, G. B. *J. Micromech. Microeng.* **2003**, *13*, 447–453.
- (21) Llobera, A.; Wilke, R.; Büttgenbach, S. *Lab Chip* **2004**, *4*, 24–27.
- (22) Hofmann, O.; Wang, X.; Cornwell, A.; Beecher, S.; Raja, A.; Bradley, D. C.; deMello, A. J.; deMello, J. C. *Lab Chip* **2006**, *6*, 981–987.
- (23) Cormack, B. P.; Valdivia, R. H.; Falkow, S. *Gene* **1996**, *173* (1), 33–38.

(24) Llobera, A.; Demming, S.; Wilke, R.; Büttgenbach, S. *Lab Chip* **2007**, *7*, 1560–1566.

(25) Llobera, A.; Wilke, R.; Büttgenbach, S. *Talanta* **2008**, *75*, 473–479.

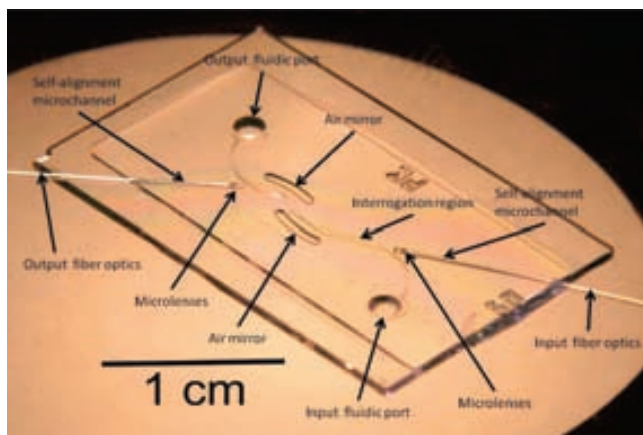


Figure 1. Picture of the PDMS-based MIR system. It comprises self-alignment microchannels for accurate fiber optics positioning, micro-lenses, and air mirrors. All these microoptic elements ensure an adequate zigzag path of the light along the interrogation region, which can be filled through the input fluidic port.

169) at 37 °C in 5% CO₂. Before each experiment, cells were rinsed twice in PBS tempered at 37 °C and kept alive in an incubator under controlled temperature and atmosphere. To obtain the dead cell population, monocytes were fixed with 4% paraformaldehyde in PBS for 10 min. Afterward, cells were stained with trypan blue (Gibco, 15250-061) in PBS (1:1) for 5 min and rinsed twice in PBS to maintain the label only inside the cells and not in the buffer. Trypan blue is one of the most commonly used methods for assessment of viability in a given cell population²⁶ and gives the possibility to differentiate the dead/live cells with an easy staining procedure. The trypan chromophore is negatively charged. Hence, this stain does not enter inside the cells unless the membrane is damaged. When it penetrates into the cytoplasm of dead cells through the membrane, it can be seen as a blue color on the whole area of the cells, while live cells are still transparent.²⁷ Finally, for the dead/live ratio measurement, both populations were diluted to obtain the desired cell proportions. All the measurements have been performed in PBS buffer to ensure that results are due only to the cell signals.

Measurement Setup. The MIR system can be seen in Figure 1. A broadband light source (Ocean Optics HL2000, Dunedin, FL) is coupled into the input multimode fiber optics with a diameter of 230 μm, which in turn is located in the self-alignment microchannels. At the end of this microchannel, a microlens corrects the numerical aperture of the fiber optics, having then parallel beams. Light enters into the interrogation region and interacts with the media that fills this region. As previously discussed, because of the reflection coefficients, most of the light is transferred to the PDMS. When it reaches the air mirror, the conditions of total internal reflection (TIR) hold. Hence, light is reflected toward the interrogation region, reaching the second air mirror, which reflects again the light while focusing it on the vicinity of the collecting fiber optics. Hence, light propagates in the system following a zigzag path. The readout comprises an identical fiber optics, which carries the signal to a spectrometer (Ocean Optics HR4000, Dunedin, FL) with a spectral resolution

of 2 nm. The integration time has been fixed to 30 ms. All measurements have been done at room temperature in a temperature-controlled lab. This setup remains unchanged throughout the experiment, that is, for the three regimes and for labeled/unlabeled cells.

RESULTS AND DISCUSSION

Measurement Protocols. Three different experiments have been carried out with the proposed systems and using the previously mentioned working regimes: counting of living cells by LS, counting of trypan blue dyed cells (both by LS + ABS and ABS) and finally the determination of the dead/live ratio at a constant population (again by LS + ABS and ABS). The main objective is to determine the LOD of the system for each experiment and for each regime. The following experimental procedure has been carried out: first, the system has been filled with buffer solution (PBS) and the readout obtained was considered as the reference for all subsequent experiments. Then, for the LS and the LS + ABS experiments, dilutions with progressively higher concentrations of live or dead cells from 50 to 2000 kcells/mL have been injected in the MIR. In the case of determining the LOD of dead cells, trypan blue is used since it is a direct, nearly instantaneous vital stain able to be used at room temperature with an optimal detection peak located at a wavelength of 580 nm. For each cell concentration, the average of 10 consecutive scans was taken. After measurement of the highest available cell concentration, the buffer solution is injected again to check possible drifts of the reference signal. In all the measured sets, the reference signal had a constant value within the experimental error. Then, the absorbance as a function of the cell concentration has been plotted, obtaining a linear fit for different wavelengths. In accordance to the 3σ IUPAC definition,²⁸ from the values of this linear fit, the LOD are obtained for live and dead cells. It is noteworthy mentioning IUPAC states that the LOD is not the lowest detectable cell concentration but also depends both on the sensitivity and the accuracy of the linear fit. From these data, it is possible to determine at which wavelength the LOD has a minimum and the sensitivity is maximal, being then able to obtain the optimal working parameters according to the cells under study. Once this optimization has been done, a third experiment (live/dead) is pursued. A total of 11 serial tubes were arranged with a 10% of variation in the live/dead cell ratio between them and a constant cell concentration of 2000 kcells/mL. In this case, LS + ABS and ABS working regimes were used to measure the dead cells percentage. The value obtained therein was afterward compared and confirmed using a Neubauer-counting chamber; images of this experiment were recorded with a digital camera under an IX71 inverted microscope (Olympus) with a differential interference contrast and a 20× objective.

To avoid undesired cell death and minimize noncontrolled variations in the optical measurements, all the experimental work was carried out with the minimum required time and keeping the monocytic cell line under culture conditions (37 °C in 5% CO₂) until the measurements were done.

Live Cells: LS Regime. The absorbance spectra as a function of the live cell concentration are shown in Figure 2a. As expected, because of the size of such cells (between 7 and 15 μm in

(26) Uliasz, T. F.; Hewett, S. J. *J. Neurosci. Methods* **2000**, *100*, 157–163.

(27) Cheng, L. L.; Luk, Y. Y.; Murphy, C. J.; Israel, B. A.; Abbott, N. L. *Biomaterials* **2005**, *26*, 7173–7182.

(28) Long, G. L.; Winefordner, J. D. *Anal. Chem.* **1983**, *55* (7), A712–A724.

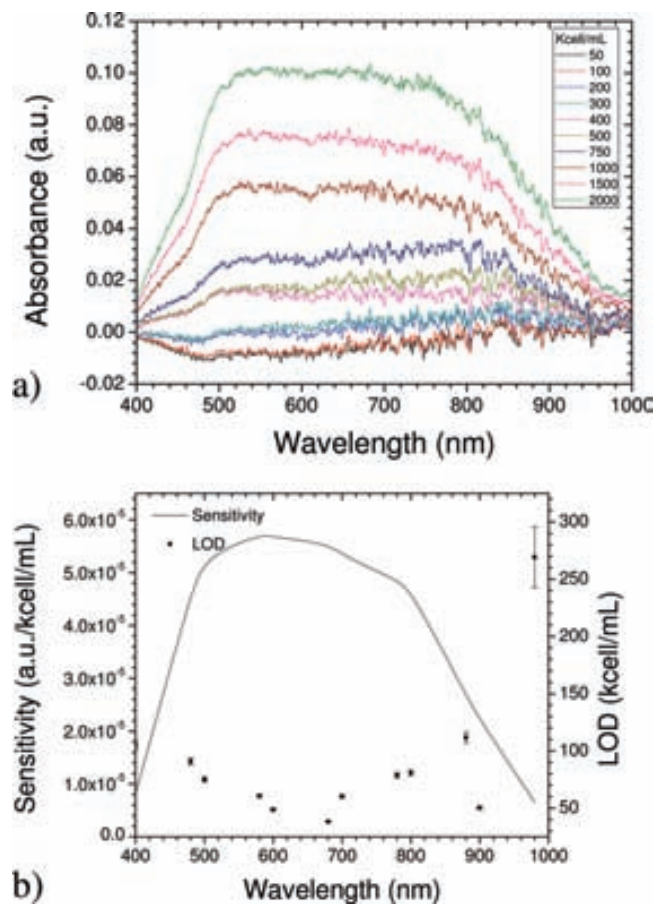


Figure 2. Results obtained for the scattering measurements using unlabeled cells: (a) absorbance as a function of the wavelength for concentrations ranging from 50 to 2000 kcell/mL. The flat absorption band is due to the cell scattering, which have a size between 7 and 15 μm . From these results, the absorbance as a function of the concentration is obtained, which can afterward be linearly fitted (Beer–Lambert regime). From this fit, sensitivity and LOD as a function of the wavelength for the LS regime is obtained, which is shown in part b, which determines the optimal working wavelength.

diameter), a nearly flat absorption band can be observed for all cell concentrations. There are two main differences of the proposed photonic lab on a chip with those previously presented: (i) The cell detection is done in parallel. That is, it does not work cell by cell (serial counting) as most of the cytometers but is able to provide information regarding the cell population in the volume by a single 30 ms measurement. (ii) Instead of measuring the absorption at a concrete wavelength, with the proposed MIR systems, the whole cell spectral response is obtained. This approach allows simultaneous in situ multiparametric detection by choosing the appropriate working wavelengths. Once the LS spectral response is obtained for the different cell concentrations, the absorbance as a function of the cell concentration can also be determined for several wavelengths (see Supplementary table S-1 in the Supporting Information), obtaining the expected linear behavior in all cases, which is in accordance to the Beer–Lambert law. Interestingly, and as an improvement of the state of the art, the linear fits allow one to determine the sensitivity and the LOD for each wavelength. From them, it is possible to determine which wavelength has the highest sensitivity and/or lower LOD, optimizing the response of the photonic lab on a chip.

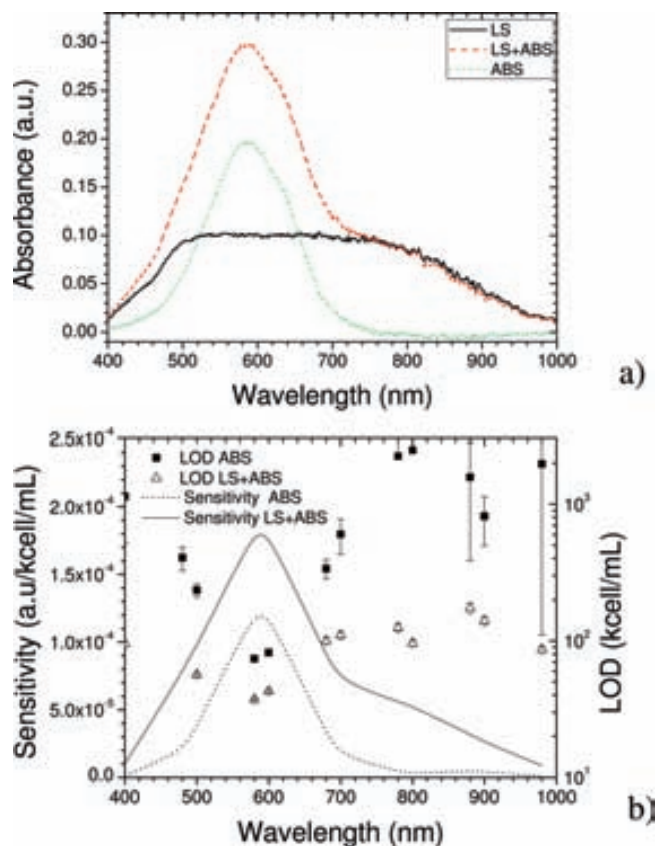


Figure 3. (a) Absorbance as a function of the wavelength for the three regimes studied: LS (flat absorption band), LS + ABS (flat scattering band and a strong trypan peak superimposed), and ABS (only showing the trypan peak) for a cell concentration of 2000 kcell/mL. This latter regime is obtained by subtraction of the first two regimes. Identical to the previous figure, we have use labeled cell concentrations ranging from 50 to 2000 kcell/mL. Absorbance vs concentration is plotted, and from these graphs, the sensitivity and LOD as a function of the wavelength for LS + ABS and ABS regimes are obtained, which are shown in part b.

The results of this optimization for live cells can be seen in Figure 2b, where the sensitivity and the LOD are plotted as a function of the wavelength. It can be seen that a plateau of maximal sensitivity is obtained at wavelengths between 580 and 700 nm, which simultaneously corresponds to an LOD minima, with values between 60 ± 1 and 38.4 ± 0.5 kcell/mL. Considering that the system has a volume of 1.43 μL , these LODs correspond to 86 ± 1 and 54.9 ± 0.7 cells, respectively.

Dead Cells: LS + ABS and ABS Regimes. When a vital stain or a dye are used for cell labeling, two effects simultaneously occur: absorption and scattering. Generally, it is challenging to uncouple them, especially if measurements at a single wavelength are done. This issue is also addressed and solved with the proposed system: as it is shown in Figure 3a, the absorbance as a function of the wavelength for 2000 kcell/mL shows the trypan blue peak at 580 nm and the scattering band in the wavelength range studied. In the previous subsection, the absorption band for such a cell concentration was determined (also shown in Figure 3a for clarification). Hence, simply by subtraction of both spectra, the trypan blue absorption band can be isolated.

Interestingly with labelled cells, the MIR-based photonic lab on a chip system allows working in two distinct regimes: scattering + absorption (LS + ABS) or absorption (ABS). In the first case,

the procedure is identical to that presented in the previous section: The results of these fits are presented in Figure 3b and also in the Supplementary table S-2 in the Supporting Information. As expected, because of the strong trypan absorption band, the maximum sensitivity is obtained at 580–600 nm. At such a range, a minimum LOD between 53 ± 1 and 61 ± 1 cells is obtained. It is also noticeable that the scattering band still can be seen at longer wavelengths, which allows one to have LODs of some hundreds of cells in the NIR range (>700 nm). Such configuration is of interest for measuring samples without preprocessing (such as labeling). Nevertheless, in the most general situation, cell labeling is used. Then, overall spectra is formed both by contributions of biomarkers and scattering. In this situation the scattering can be considered as a background noise, which modifies the overall shape of the spectra. Hence, having the possibility to subtract the scattering effects, and only obtaining the absorption/fluorescence contribution, is highly advantageous. The results obtained in the previous section have been taken as reference and subtracted from the spectra, as previously discussed. Again, several key wavelengths have been taken, and their linear fit is shown in Supplementary table S-3 in the Supporting Information. Since only the trypan blue band is obtained, the mentioned table just shows the linear fits of interest, with a minimum LOD of 105 ± 4 cells. The comparison between both regimes can also be seen in Figure 3b. Although the absorbance has a slightly smaller sensitivity, it provides a much higher specificity, since outside the trypan blue region, LODs higher than 350 cells are obtained.

Up until now, we have shown that the proposed photonic lab on a chip is able to work in three different regimes: scattering (LS), scattering + absorption (LS + ABS), and absorption (ABS), obtaining comparable sensitivities and LODs, although each of them with distinct features. To confirm this last point, we have selected a key application, namely, the detection of dead/live cell ratios. To this effect, different proportions of labeled (dead) and nonlabeled (live) cells (10% variation between conditions) are mixed at a constant concentration (2000 kcells/mL) and afterward injected in the MIR. The results of the conducted experiments are presented in the next subsection.

Dead/Live Ratio Measurement. The absorbance as a function of the wavelength for different dead/live cell ratio is presented in Figure 4a. Since the samples injected range from 0% to 100% labeled cells, the spectra also vary from only the flat absorption band (0% of dead cells) to the conditions where the trypan absorption peak is superimposed (100% of dead cells). An image of labeled and nonlabeled cells inside the MIR can be seen in Figure 4b. Similar to the previous section, these spectra have been analyzed with two of the previously presented regimes: LS + ABS and ABS. In the first case, the absorbance as a function of the % of dead cells is presented in Figure 5a. The highest sensitivity corresponds to the trypan blue region (580–600 nm), decreasing sharply both for longer and shorter wavelengths. The values above the 70% of dead cells do not match the tendency. This effect is understood when the same dead/live cell ratio was placed in a Neubauer counting chamber. While the percentage of dead cells counted corresponds to the dead/live cell ratio analyzed, the total number of cells did not; dilutions above 70% have a significant cell deficit, which explains why these points do not follow the expected linear tendency. This point is also noteworthy, since this

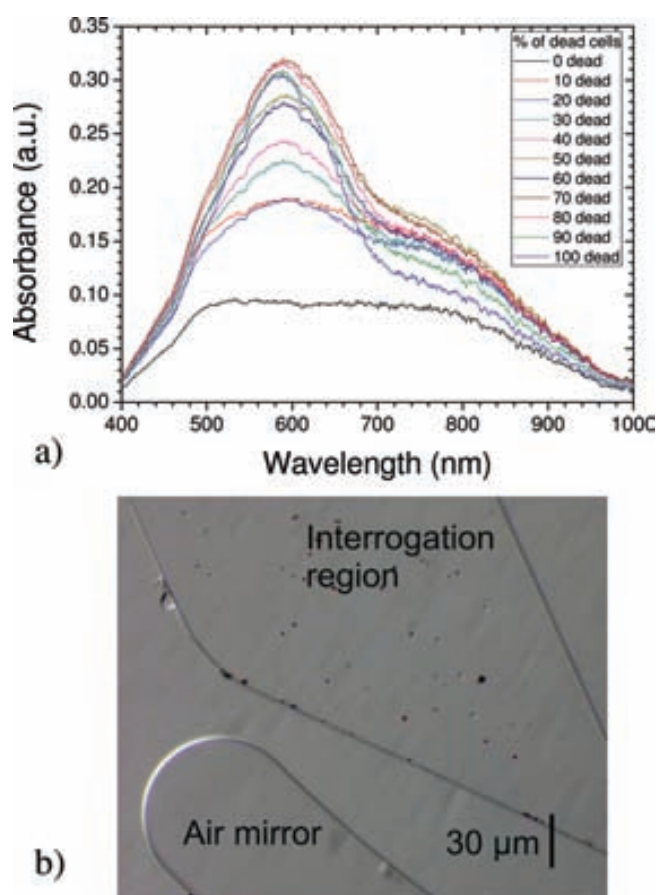


Figure 4. Measurement of the dead/live ratio. A constant cell concentration of 2000 kcell/mL has been selected, varying the live/dead ratio in the 11 samples taken. In the absorbance as a function of the wavelength, the spectra shift from the LS regime (scattering) when all cells are alive to the LS + ABS regime (scattering + trypan peak), when only measuring dead cells. (b) Image of a concrete region of the MIR filled with dead and alive cells in a 50/50 ratio.

behavior can be understood as a self-test system: if the experimental value falls outside the calibration curve, a cell deficit is likely to have happened.

Once the values above 70% had been understood, they have not been used for the determination and the sensitivity and the LOD, which are presented in Figure 5b and Supplementary table S-4 in the Supporting Information. In this case, no scattering effects are observed even though we are using the whole spectra, namely, LS + ABS. Only the wavelengths where the trypan blue absorbs show a high sensitivity peak and an LOD of the percentage of dead cells of $7.6 \pm 0.4\%$. This effect can be understood if we take into account that we are using a constant population of 2000 kcell/mL. Hence, the scattering band is similar in all the samples used, and no difference in both parameters (sensitivity, LOD) should be observed. As it was presented in the previous section, if a variation of any of these parameters were seen, it could only be due to the variation of the population.

Because of the constant population level, the absorption measurements are suitable to provide lower LODs. The procedure has been similar to that previously presented, and the results are shown in Figure 5b and Supplementary table S-5 in the Supporting Information. In this case, the experimental and statistical errors of the LS + ABS make it difficult to compare their specificity, although the thinner full-width half-maximum (FWHM) of the

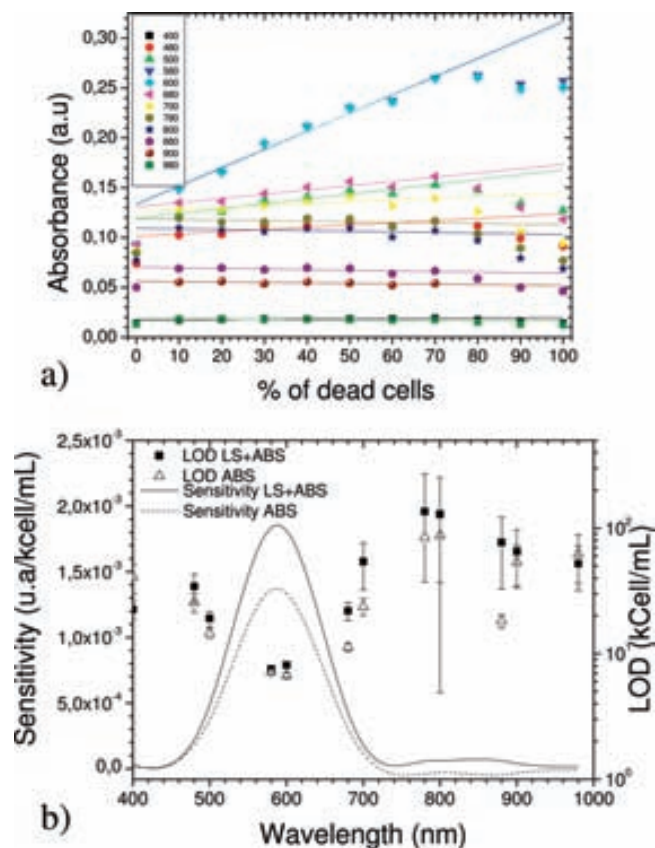


Figure 5. From the results obtained in the previous figure, the absorbance vs % of dead cells for different wavelengths are obtained, which are plotted in part a, together with their respective linear fit (using a constant concentration of 2000 kcell/mL). The wavelengths absorbed by the trypan blue have the highest sensitivity and the lowest LOD (both in the LS + ABS and ABS regimes) as shown in part b.

sensitivity for the ABS may suggest that this latter regime has a slightly higher specificity. Again, a decrease of the sensitivity is obtained, although the LOD for the percentage of dead cells using ABS has been experimentally measured to be $6.7 \pm 0.3\%$.

Regarding the direct applications and as an example, a CD4⁺ T cells count below 200 cells/ μ L is given as a key diagnosis for AIDS.²⁹ Such cells have not been used in our experiments but, due to its size and its common hematopoietic origin, are comparable to these used in our measurements. Therefore, it could be estimated that the performance of the presented photonic lab on a chip would be similar when using CD4⁺ T cells, and the presented LODs of the three detection methods are far below the requested CD4⁺ T cells limit. When comparing the performance of the presented system with the LUCAS configuration,^{4,5} it can be seen that the integration time has been

reduced more than 80 times while having a much lower LOD, reducing the technological complexity and keeping the same error count (less than 10%).

CONCLUSIONS

A low-cost polymeric photonic lab on a chip is presented with the attempt to tackle the inherent drawbacks of the Neubauer cell counters: counting error due to uneven distribution, measuring speed, and cost of the system. The proposed system takes advantage of the definition of air mirrors in the vicinity of the interrogation region which meaningfully lengthen the optical path while keeping the overall dimensions of the system at a reasonable size. Optically, the system has a high degree of integration, since it comprises self-alignment systems, microlenses, and air mirrors. Nonetheless, the whole photonic lab on a chip is defined with a single photolithographic mask using low-cost materials (PDMS and soda-lime glass as substrates). Cell measurement has allowed determining three distinct working regimes: scattering, where no significant absorption band has been observed in the studied UV-NIR spectra, scattering + absorption, where over the scattering band a clear absorption band is superimposed, and absorption, in which the two previously mentioned spectra have been subtracted in order to have a clear view of the bands of interest. For such characterization, and opposite to the standard procedure, a broadband spectrum has been analyzed, being then possible to determine the optimal working wavelengths in terms of sensitivity and LOD. Such regimes have been demonstrated with labeled and nonlabeled cells, obtaining LODs between 53 and 105 cells depending on the working regime. Finally, as a concrete demonstration of the applications of the presented configuration, it has also been used for measuring the dead/live cell ratio of a constant cell concentration. The two studied regimes show LODs between $7.6 \pm 0.4\%$ and $6.7 \pm 0.3\%$, that is, with a performance comparable to the Neubauer cell counters but only requiring 30 ms for its measurements and with the possibility of multiparametric (by detecting different wavelengths) and continuous cell monitoring.

ACKNOWLEDGMENT

The research leading to these results has received funding from the European Research Council under the European Community's Seventh Framework Programme (Grant FP7/2007-2013)/ERC Grant Agreement No. 209243 and also from the IST Programme (P. CEZANNE, Grant IST-2-IP-031867). The authors also thank the research group FOR 856, mikroPART "Mikrosysteme für partikuläre Life-Science-Produkte" for support of this work.

SUPPORTING INFORMATION AVAILABLE

Additional information as noted in text. This material is available free of charge via the Internet at <http://pubs.acs.org>.

Received for review March 4, 2010. Accepted April 14, 2010.

AC100590Z

(29) Centers for Disease Control and Prevention. Revised Classification of HIV Infection and Expanded Surveillance Case Definition for AIDS among Adolescents and Adults. In *MMWR Morbidity and Mortality Weekly Report*, 1992; p p1–19.

Ibarlucea et al. "Cell screening using disposable photonic lab on a chip systems"

Supplementary data

Supplementary table S-1: Linear fits and LODs of LS measurements for different wavelengths.

LS							
Wavelength (nm)	Intercept		Slope		R ²	LOD (kcell/ml)	
	Value	Error	Value	Error		Value	Error
400	-0,0015	2E-4	8,2E-6	3E-7	0,988	105	4
480	-0,013	1E-3	4,6E-5	1E-6	0,991	90	3
500	-0,012	1E-3	5,3E-5	1E-6	0,994	75	2
580	-0,013	1E-3	5,7E-5	1E-6	0,996	60	1
600	-0,0121	9E-4	5,6E-5	1E-6	0,997	48,7	0,9
680	-0,0105	7E-4	5,55E-5	8E-7	0,998	38,4	0,5
700	-0,012	1E-3	5,3E-5	1E-6	0,996	60	1
780	-0,004	1E-3	4,8E-5	1E-6	0,993	79	2
800	-0,007	1E-3	4,7E-5	1E-6	0,993	81	2
880	0,002	1E-3	2,7E-5	1E-6	0,986	112	5
900	0,0012	3E-4	2,23E-5	4E-7	0,997	50,2	0,9
980	0,0018	6E-4	6,5E-6	6E-7	0,926	269	26

Supplementary table S-2: Linear fits and LODs of the LS+ABS measurements for different wavelengths.

LS+ABS							
Wavelength (nm)	Intercept		Slope		R ²	LOD (kcell/ml)	
	Value	Error	Value	Error		Value	Error
400	8E-4	3E-4	1,04E-5	4E-7	0,984	95	4
480	-0,009	2E-3	9,3E-5	2E-6	0,994	57	1
500	-0,016	2E-3	1,85E-4	3E-6	0,997	37,4	0,7
580	-0,016	2E-3	1,80E-4	4E-6	0,997	42,7	0,9
600	-0,011	3E-3	9,0E-5	4E-6	0,982	100	5
680	-0,011	3E-3	7,0E-5	4E-6	0,978	110	6
700	-0,005	2E-3	5,6E-5	3E-6	0,972	125	7
780	-0,006	2E-3	5,2E-5	2E-6	0,983	96	4
800	-0,001	2E-3	3,2E-5	3E-6	0,947	174	14
880	-0,004	1E-3	2,6E-5	2E-6	0,965	141	9
900	3E-4	2E-4	8,8E-6	3E-7	0,986	86	3
980	8E-4	3E-4	1,04E-5	5E-7	0,984	95	4

Supplementary table S-3: Linear fits and LODs of the ABS measurements for the wavelengths of interest.

ABS							
Wavelength (nm)	Intercept		Slope		R ²	LOD (kcell/ml)	
	Value	Error	Value	Error		Value	Error
480	0,008	2E-3	1,9E-5	3E-6	0,761	405	79
500	0,004	3E-3	3,8E-5	4E-6	0,907	234	26
580	0,003	3E-3	1,24E-4	4E-6	0,990	74	3
600	0,003	3E-3	1,21E-4	5E-6	0,988	82	3
680	0,001	4E-3	3,2E-5	5E-6	0,823	338	54

Supplementary table S-4: Linear fits and LODs of the live/dead cell measurements using LS+ABS for different wavelengths with a constant population of 2000 kcell/mL.

LS+ABS							
Wavelength (nm)	Intercept		Slope		R ²	LOD (% of dead cells)	
	Value	Error	Value	Error		Value	Error
400	0,017	2E-4	2,7E-5	4E-6	0,851	22	4
480	0,101	3E-3	2,2E-4	6E-5	0,704	34	9
500	0,119	3E-3	4,9E-4	7E-5	0,889	19	3
580	0,133	5E-3	0,0018	1E-4	0,981	7,6	0,4
600	0,134	5E-3	0,0018	1E-4	0,978	8,1	0,5
680	0,131	3E-3	4,3E-4	7E-5	0,857	22	3
700	0,127	3E-3	1,8E-4	7E-5	0,460	54	22
780	0,119	3E-3	6E-5	6E-5	0,000	135	137
800	0,109	3E-3	6E-5	6E-5	0,013	129	124
880	0,070	2E-3	6E-5	3E-5	0,251	77	44
900	0,0561	8E-4	4E-5	2E-5	0,348	65	32
980	0,0183	3E-4	1,4E-5	6E-6	0,483	52	20

Supplementary table S-5 Linear fits and LODs of the live/dead cell measurements using ABS for the wavelengths of interest with a constant population of 2000 kcell/mL.

ABS							
Wavelength (nm)	Intercept		Slope		R ²	LOD (% of dead cells)	
	Value	Error	Value	Error		Value	Error
480	-0,003	2E-3	1,8E-4	3E-5	0,828	26	4
500	-0,004	2E-3	3,7E-4	4E-5	0,939	14	1
580	7E-4	3E-3	0,00136	6E-5	0,985	7,1	0,3
600	2E-4	3E-3	0,00134	6E-5	0,986	6,7	0,3
680	5E-4	1E-3	3,0E-4	2E-5	0,962	11,3	0,8
700	0,0028	9E-4	1,1E-4	2E-5	0,850	23,7	3

Cell analysis using a multiple internal reflection photonic lab-on-a-chip

Jordi Vila-Planas¹, Elisabet Fernández-Rosas², Bergoi Ibarlucea¹, Stefanie Demming³, Carme Nogués², Jose A Plaza¹, Carlos Domínguez¹, Stephanus Büttgenbach³ & Andreu Llobera^{1,3}

¹Centre Nacional de Microelectrònica (IMB-CNM, CSIC), Barcelona, Spain. ²Departament de Biologia Cel·lular, Fisiologia i Immunologia, Universitat Autònoma de Barcelona, Bellaterra, Barcelona, Spain. ³Institut für Mikrotechnik, Technische Universität Braunschweig, Braunschweig, Germany. Correspondence should be addressed to A.L. (andreu.llobera@imb-cnm.csic.es).

Published online 29 September 2011; doi:10.1038/nprot.2011.383

Here we present a protocol for analyzing cell cultures using a photonic lab-on-a-chip (PhLoC). By using a broadband light source and a spectrometer, the spectrum of a given cell culture with an arbitrary population is acquired. The PhLoC can work in three different regimes: light scattering (using label-free cells), light scattering plus absorption (using stained cells) and, by subtraction of the two former regimes, absorption (without the scattering band). The acquisition time of the PhLoC is ~30 ms. Hence, it can be used for rapid cell counting, dead/live ratio estimation or multiparametric measurements through the use of different dyes. The PhLoC, including microlenses, micromirrors and microfluidics, is simply fabricated in a single-mask process (by soft lithographic methods) using low-cost materials. Because of its low cost it can easily be implemented for point-of-care applications. From raw substrates to final results, this protocol can be completed in 29 h.

INTRODUCTION

Microfluidic research has enabled the huge development of portable point-of-care (POC) medical diagnostic systems. Microfluidics offers a major step forward in analytical systems through the reduction in size, weight and reagent consumption, as well as the enhancement of sensitivity, accuracy and parallelization¹. Thus, microfluidics has been applied to a variety of assays, including drug screening², cell sorting and detection³, *in vivo* imaging of dynamic cellular processes⁴ and biodetection. Microfluidic developments have enabled the integration of analytical steps from initial raw clinical samples to final, purified volumes with a minute concentration of etiological agent, using the so-called lab-on-a-chip (LoC) configuration⁵. In addition to the myriad of applications for LoC systems in developed countries, it is broadly accepted that microfluidic diagnostic technology may be a valuable methodology in the developing world⁵. LoC systems designed for applications in the developing world ideally should be fast, mechanically and chemically robust, low cost, easy to use even for occasional users, autonomous and able to work in a broad temperature range (–10 °C to 40 °C). In addition, they should have self-containing reagents and self-calibration or, ideally, not require calibration at all. Such stringent requirements are the reason why only lateral-flow analysis or microfluidic paper-based devices^{6,7} have shown their capability until now. Although they are effective for immunochromatographic assays, these devices have not been proven suitable for cell counting and screening. This is crucial for many applications; for example, a CD4⁺ T cell count below 200 cells per μl is a key diagnostic indicator for AIDS⁸. In developing countries, access to automated cell counters or cytometers is rare, owing to their cost and maintenance requirements. Cells are most commonly counted manually using Neubauer chambers. However, the measurement errors caused by operator subjectivity, the statistical errors due to sample concentration and the time required make the Neubauer chambers suboptimal for massive POC applications.

Photonics applied to life sciences, such as total internal reflection (TIR), fluorescence, fluorescence resonance energy transfer, scattering, surface-enhanced Raman spectroscopy, localized surface

plasmon resonance or fluorescence correlation spectroscopy, has become popular for cell screening and sorting, mainly because of its speed and noninvasiveness⁹. The fluorescence-based cytometer, or fluorescence-activated cell sorting (FACS), has become most popular¹⁰. Using FACS, cells can be sorted with frequencies up to 10 kHz (10⁴ cells per s). As POC applications in developing countries, however, most of the above-mentioned methods are not ideal, as they require full-sized laboratory benchtop instruments with strict technical requirements and have high cost. The combination of photonics and microfluidics (giving rise to the concept ‘photonic LOC’ (PhLoC)¹¹, sometimes also called optofluidics) is a potential low-cost alternative. As an example, the combination of FACS with microfluidics¹² provides portable flow cytometers with frequencies up to 1 kHz (corresponding to analysis of 10³ cells per s). Clearly, this is progress, although the cost and technical constraints already mentioned still prevail¹³. In addition, the integration of as many optical and photonic components as possible with the microfluidic network can reduce costs. These components can be combined with polymeric materials, particularly poly(dimethylsiloxane) (PDMS)¹⁴, to define the PhLoC.

Fluorescence-based approaches require the implementation of very accurate optical systems and filters. As fluorescence is emitted in 4 π sr, enhancement of the readout signal requires to refocus the emitted light and/or use with highly sensitive detectors (photomultiplier or avalanche photodiodes). To discriminate between excitation and emission wavelengths in fluorescence measurements, it is also required to use filters. With regard to PhLoC for fluorescence detection, the optimal situation in order to retain a low cost is to integrate the filters in the PhLoC using the same technology¹⁵. Although PhLoC with an in-plane configuration and a very high level of accessibility can be obtained, integrated filters are mainly absorbance-based filters and therefore do not have the same filtering effectivity as external interferometric filters; thus, the overall performance of the PhLoC is hampered. This issue can be addressed by using the principle of absorbance rather than fluorescence. The Beer-Lambert law states that absorbance is directly proportional to path length. Therefore,

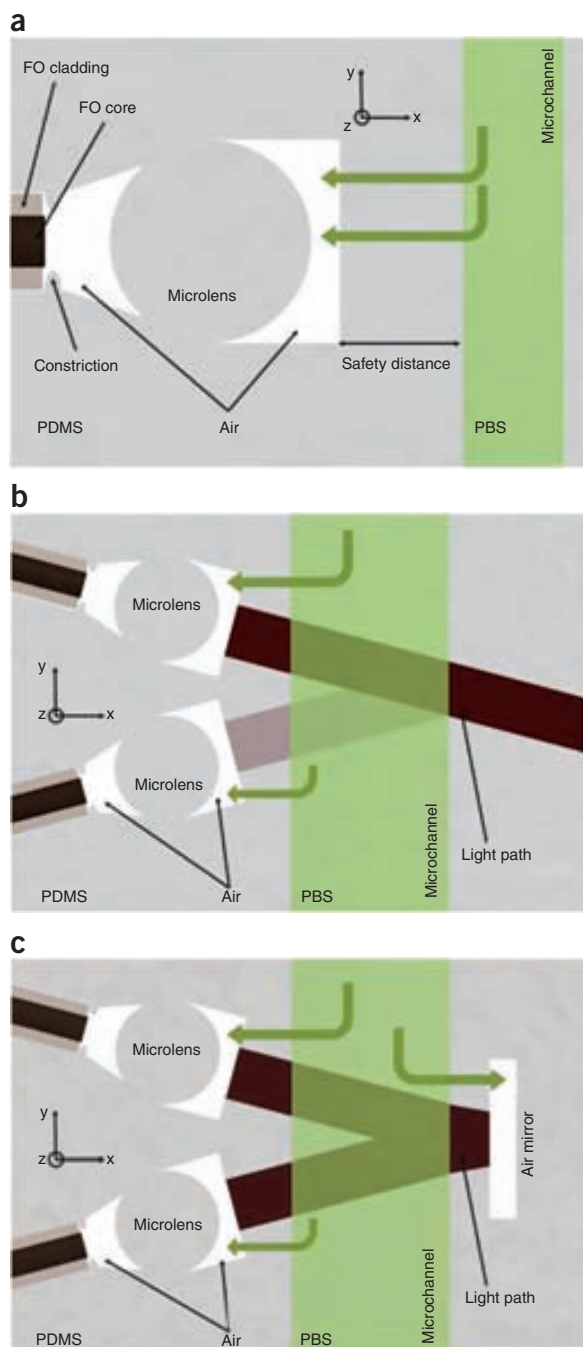


Figure 1 | Schematic representation of the merging of micro-optics and microfluidics. (a) Microlens defined at the vicinity of a microchannel. Constrictions can be defined to clamp the fiber at the position defined by the PDMS-air microlens. Safety distance assures that no leak from the microchannel reaches the air regions (green arrows). (b) Reflection at the PDMS-PBS surface is very weak, requiring long integration times to capture a significant amount of reflected light. This issue can be tackled with the inclusion of air mirrors. (c) If TIR condition holds, light bounces back toward the output fiber optics with a high efficiency. FO, fiber optics.

longer paths provide higher sensitivity and lower limits of detection (LOD). To enable the lengthening of the optical path without increasing the size of the PhLoC, light can follow a zigzag path inside the system by using air mirrors¹⁶. They have already been implemented in multiple internal reflection (MIR) systems for detection of minute quantities of fluorophore¹¹.

In this protocol, we describe the manufacture and use of a PhLoC system with an accuracy similar to that of Neubauer chambers; however, it only requires a sampling time of 30 ms. Rather than consecutively measuring each cell, the signal related to the whole volume sample is acquired. By using only white light to scan, there is a reduction in cost and the ability to work, without any change of its geometry, in three different regimes: light scattering (LS), LS + absorbance (LS + ABS) and ABS. LS occurs when the cells under study are label free or have absorbance bands outside the spectrum screened. If a specific dye is used or the cells have an absorbance band, its effect can be seen on the LS + ABS regime. Finally, by subtracting the two previous regimes, the effect of the absorbance bands can be obtained. In all these regimes, a quantitative measurement of the cell population can be recorded.

Details of the cell culture types and labeling that we have used in our PhLoC system can be found in ref. 17. The following equipment is required: a broadband light source, a microspectrometer and two multimode fiber optics. The PhLoC is defined in a single photolithographic step using SU-8 as master, replicated by soft lithography with PDMS and bonded to a cheap soda-lime substrate. The PhLoC and the working regimes have been used for screening monocytes (label free or stained with trypan blue). This protocol was used in ref. 17 for cell counting as well as for determining the dead/live cell ratio of a constant monocyte concentration. Because of their size (between 7 and 15 μm) and their common hematopoietic origin, monocytes are similar to CD4⁺ T cells; therefore, the protocol presented here could also be used in AIDS diagnosis. This protocol could also be used in a large variety of other applications. For example, it could be used to determine the number of different cone cells in a given volume, which are responsible for human color vision¹⁸; to analyze conformational changes of proteins¹⁹; or to screen tumor cells²⁰.

Experimental design

The protocol comprises three distinct parts: first, the design of the MIR; second, the fabrication; and finally, the benchmarking.

MIR design. The key issue in the development of a PhLoC system is the integration of all micro-optical elements. In addition, to reduce the fabrication complexity and costs to a minimum level, the photolithographic steps have to be reduced, if possible, to a single-mask process. These strict requirements limit the design to in-plane micro-optics to basically three refractive indices: air ($n_{\text{air}} = 1.00$), PDMS ($n_{\text{PDMS}} = 1.41$) and the liquid carrier (in our case, PBS, $n_{\text{PBS}} = 1.334$). Although these refractive indices can seem too close in value to obtain micro-optical elements with high-enough performance, in a previous paper, it was shown how microlenses²¹ or micromirrors¹⁶ can be easily defined. For this integration, two main aspects have to be considered (Fig. 1): (i) the working configuration of the micro-optical elements so as to obtain the required flow of light (light focalization, reflection) and (ii) the bonding process of the system to avoid leakage from the microfluidic to the micro-optics components, which would result in the air regions being filled with the liquid carrier and the malfunction of the micro-optical elements.

Correct implementation of the microlenses requires the adequate positioning of the light source. With respect to fiber optics, its relative positioning and its numerical aperture are the key parameters. Self-alignment channels for positioning and clamping of the fiber

PROTOCOL

optics greatly simplifies these issues. Nevertheless, the positioning in the x axis is of key importance on the light propagation inside the system, and this cannot be accurately provided unless constrictions are defined within the self-alignment systems. These constrictions assure the clamping of the fiber optics when they reach the required position in the x axis. The size of these constrictions has to be defined so that they cover the cladding of the fiber optics, but with minimum blocking of the core, in order not to modify the numerical aperture.

Concerning the light path, several aspects have to be considered. Assuming at this stage that the light beam is properly injected into an optofluidic system, sensitivity enhancement and decrease of the LOD is directly related to the length where light-analyte interaction occurs (Beer-Lambert law). Therefore, this length has to be maximized. A possibility is to use liquid-liquid waveguides²², yet accurate fiber optics alignment is required. If, with a different approach, micro-optical elements are used, other issues should be taken into account. Generally, the larger the system, the longer the propagation length. Nevertheless, this approach clearly goes against integration and minute reagent quantity. A simple way of doubling the propagation length and keeping the same system size is to define light input and output at the same side of the microfluidic channel, and measure the light that reflects at the PBS-PDMS interface. Although effective, basic calculations of the Fresnel coefficient at the PBS-PDMS interface provide with extremely low values (0.029 and 0.062 for transverse electric (TE) and transverse magnetic (TM) polarization, respectively), and hence most of the light simply crosses the microfluidic channel, thus requiring long integration times to collect the small reflected part and hampering its application in high-throughput systems. To maximize the reflection, mirrors should be defined at the opposite size of the microfluidic system. Again, mirrors (coated with metal and noncoated) could be easily defined on the substrate, but this would entail aligning and would increase the system fragility, which is not consistent with low cost and robustness. Conversely, very basic calculations provide with critical angles of $\theta_c^{\text{PDMS-air}} = 45.17^\circ$ and $\theta_c^{\text{PDMS-PBS}} = 70.60^\circ$, which means that any light directed toward a PDMS-air interface will undergo TIR if the respective angle is higher than 45.17° (same situation as the previously mentioned critical angle at the PDMS-PBS interface). The optimal situation, presented in **Figure 1c**, is to have TIR conditions at the PDMS-air interface but not at the PDMS-PBS (to assure that light reaches the output fiber optics). These kinds of structures were labeled as air mirrors in a previous paper¹⁶, which improved the performance of hollow prisms for absorbance detection 80 times²³ without requiring any additional technological steps. The integration of microlenses and an air mirror in a PhLoC is what we defined as single internal reflection systems. Once the lenses and the mirrors for readout enhancement were optimized, LODs for fluorescein and methyl orange (used as calibration samples) below the micromolar range were obtained. LODs could be further decreased by increasing the single internal reflection size, but again at a cost of integration complexity.

A further development is the shift from single to multiple reflections. Air mirrors can be defined at both sides of a given microfluidic system. If TIR conditions are held, light follows a zigzag path, meaningfully lengthening the optical path without a marked increase in the size. In addition, the shape of the air mirrors can be arbitrarily defined, making it possible to focus the light inside the microfluidic system or correct its divergence. Another advantage

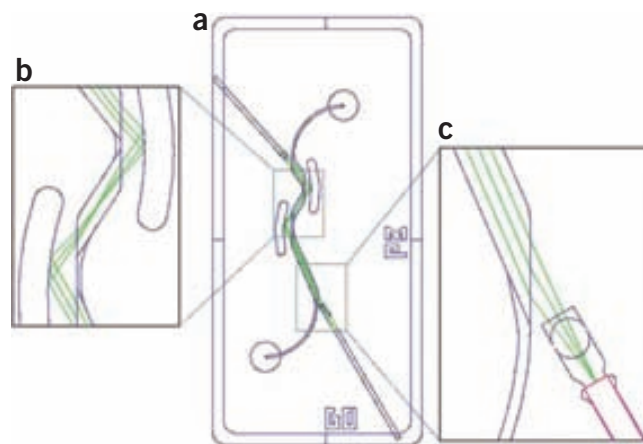


Figure 2 | Layout of the mask used for implementing the PhLoC system. (a) General view showing the self-alignment microchannels, micromirrors, microlenses and the microfluidic parts. The ray tracing simulation (shown with green lines) predicts TIR at the convergent mirrors, assuring a zigzag light path inside the system. (b,c) Expanded views show the region between the air mirrors (b) and the input region (c), with simulated fiber optics (magenta).

is that the shape of the microfluidic system can be tailored so as to match with the optical path, resulting in a reduction of the required volume sample as well as in a reduction of the dead volumes. This approach has been demonstrated in ref. 13, obtaining LODs between 110 and 41 nM using fluorescein.

One of the weak points when implementing in-plane single-mask PhLoC is the distance between photonics and microfluidics. Clearly, the longer the distance the higher the background noise, but also the less possibility that leakages from the microfluidic part reach the micro-optical elements (shown as green arrows in **Fig. 1a-c**). Although the PDMS-to-glass bond with O_2 plasma is broadly known²⁴, when the replicated master has several patterns very close to each other, the irreversible bonding between glass and PDMS can be suboptimal. In the worst cases, it does not bond properly, even when increasing the time and/or the power. In our case, trial and error experience has allowed us to define a rule of thumb that states that this distance (safety distance) has to be at least 0.4 times the thickness of the master.

The layout of our final system, optimized as discussed above, is presented in **Figure 2a**. From a fluidic point of view, it can be seen as a tailored microchannel with one inlet and one outlet. Photonically, it comprises two biconvex microlenses, two self-alignment microchannels (with constrictions) and two air mirrors. Ray tracing inside the system is also presented (in green), where it can be seen that light undergoes TIR at the air mirrors and propagates in the expected zigzag path. At the macroscopic scale, alignment of all these optical elements will be bulky and will require a considerable space in an optics laboratory. Conversely, as this process is done using a single mask, all the structures are inherently self-aligned, markedly simplifying the required setup. **Figure 2** also shows close-up views of the air mirror region (**Fig. 2b**) and the input microchannel with the constrictions (**Fig. 2c**, with the fiber optics in magenta), together with the required microlenses. Notice that all the edges of the structure have been rounded on purpose. This has been done considering that the material used for defining the master is the negative-tone photocurable SU-8 with high internal stresses. Such stresses can be minimized by rounding the edges of the structures defined^{25,26}, assuring a longer half-life of the fabricated masters.

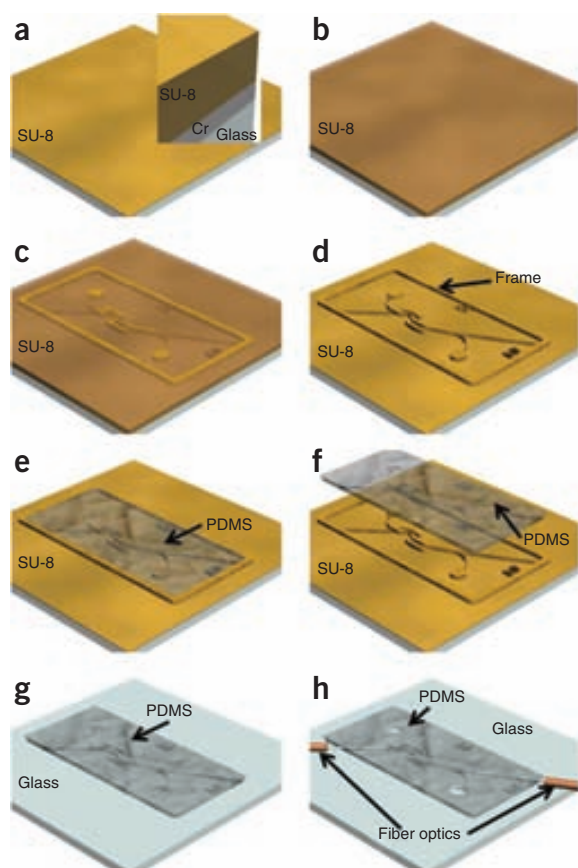


Figure 3 | Fabrication steps. (a–h) Definition of the double adhesion layer (a), spinning of the 250- μm -thick SU-8 layer (b), UV-lithography of the PhLoC (c), development with PGMEA (d), PDMS pouring without having overflow (provided by the frame) (e), PDMS release from the master (f), PDMS-glass bonding by O₂ plasma (g) and fluidic ports opening and fiber optics positioning (h).

Fabrication steps. To produce a robust, low-cost and portable system, we use low-cost substrates and polymers, such as soda-lime glass (as substrate), SU-8 (for implementing the masters) and PDMS (to define the PhLoC). Although the fabrication steps are thoroughly described in the procedure section, some key points of the fabrication process that require further discussion are explained here.

The fabrication starts with the cleaning and dehydration of a low-cost, 700- μm -thick soda-lime glass. The adhesion between glass and SU-8 is known to be suboptimal. Some adhesion promoters can be used, either from organic or inorganic origin. Among them, a thin (10 nm) chromium layer is a good alternative. Even with this adhesion layer, if a thick (>200 μm) SU-8 layer has patterns that are very close to each other, developing becomes challenging, causing loss of adherence and/or cracks during long rinsing times in SU-8 developer. An alternative is to use a double-layer adhesion promoter comprising Cr and a thin (<5 μm) SU-8 layer. The subsequent polymeric layer adheres to this initial SU-8 film, resulting in better mechanical stability for long developing times. This double-layer adhesion promoter (inset in Fig. 3a) is suitable for thin and thick SU-8 layers. Nevertheless, owing to the hydrophobic character of this polymer, uneven thin layers of non-exposed SU-8 are likely to be obtained. This can be solved by applying O₂ plasma just before making the spinning. In our case, we used a 75 W and 85 sccm. O₂ plasma for 5 min, but these conditions are

highly system dependent. Therefore, some tests are required in order to optimize this step.

At this point, a single spin-on process is done using SU-8 50 (Fig. 3b). Two issues are important at this point: (i) use a spinner with lid to assure even polymer distribution, and (ii) allow planarization of the SU-8 just after the spinning step. Thereafter, bake, cool and expose substrates to UV light (Fig. 3c). To minimize the stresses on the master, it is important to avoid sharp edges on the geometries. It is also of key importance to allow SU-8 relaxation after the post-exposure bake (PEB; typically overnight). In this case, substrates are maintained under clean room (CR) conditions for at least 8 h before proceeding to development (Fig. 3d). SU-8 swells owing to humidity, even after this PEB²⁷. To improve the durability of the masters even more, remove all possible remaining solvent, and partially repair possible cracks occurred during the development via a hard-bake step. Special care has to be taken to hard bake under nitrogen atmosphere to minimize oxidation during heating. Masters fabricated using this protocol have a thickness of 250 μm , allowing the hassle-free insertion of the optical fibers (with a diameter of 230 μm).

Instead of making a flat PDMS layer, we define a frame of SU-8 that functions as a hydrophobic barrier that defines the exact dimensions of the system and avoids the manual cutting of the PDMS with a scalpel (Fig. 3e). PDMS-coated masters are cured and then PDMS is peeled off with the aid of tweezers (Fig. 3f). A soda-lime substrate with the suitable dimensions is, together with the PDMS, exposed to oxygen plasma in a barrel etcher. Both surfaces are immediately brought into contact and left to seal the system. This step finishes the fabrication of the PhLoC systems.

Although PDMS is permeable to gases, the fabricated system is sealed and thus it can be presumed to have a very high level of sterility until the fluidic ports are opened. Directly before the use of the PhLoC system (Fig. 3g), the ports have to be mechanically opened. In our case, we use a stainless steel tip, but other systems can also be used. Thereafter, two multimode fiber optics are inserted in the microchannels until they reach the constrictions (Fig. 3h). Although this step can be done without the use of a microscope, during the training phase, the use of the microscope is highly recommended. In addition, filling the self-alignment systems with ethanol assures a smoother fiber optics insertion. When ethanol is used, it requires some time (between 2 and 10 min, depending on the PDMS thickness) until it completely evaporates from the system (Fig. 4).

Benchmarking and measurement protocol. The experimental setup requires low-weight and relatively low-cost parts. We have used components mainly from Ocean Optics and Thorlabs, but equivalent ones can be purchased from other brands. What is desirable is that all the components are connectorized. The first step is the opening of the fluidic ports with the stainless steel tip. Thereafter, the microfluidics is filled with the analyte to be measured. We use a micropipette and manual injection. For a more systematic approach, setups similar to that described⁴ could easily be implemented.

MIR systems can be used with a monochromatic light and a photodiode for the measurement of optical density (OD). An alternative that provides more information about the cell culture injected in the microfluidic system is using a broadband light source and a microspectrometer. Here, instead of having a given OD value, quantitative results as a function of the absorbance peaks can be

PROTOCOL

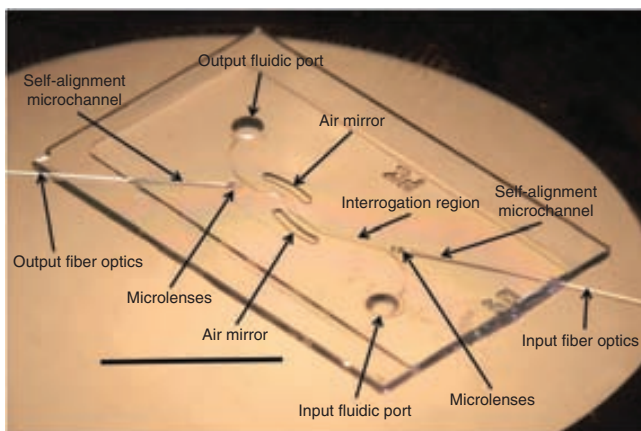


Figure 4 | Picture of the completed PhLoC, having self-alignment microchannels for accurate fiber optics positioning, microlenses and air mirrors. The PhLoC can be filled through the input fluidic port. Scale bar, 1 cm.

provided. This allows, for instance, an estimation of the live/dead cell ratio, as discussed below.

We benchmark using a connectorized broadband light source (Ocean optics HL-2000), which, according to its data sheet, has a wavelength range between 360 and 2,000 nm. It is coupled to the input fiber optics (Thorlabs BFL22-200), which has previously been inserted in the self-alignment microchannel. The readout comprises an identical fiber optic, which is connected to a microspectrometer (Ocean optics HR-4000), with a detection range between 200 and 1,100 nm. Combining both systems provides a window of working wavelengths between 360 and 1,100 nm. We fix integration time to 30 ms throughout the experiment so as to obtain a signal-to-noise ratio higher than 14 dB. Shorter times are possible if the system is shielded against stray light.

LS measurements can be recorded when the cells injected do not have any significant absorbance band in the wavelength range used (label free). Furthermore, from an optical point of view, such cells

can be envisaged as a material with a different refractive index (RI). Light interacting with such cells will be scattered—the amount of this scattering will also depend on the roughness of the cell—and its optical path will be modified. Scattered light will not reach the output fiber optics. As a rule, the higher the cell concentration the higher is the scattering and the lower the signal at the microspectrometer. Typically, the cell size is much bigger than the working wavelengths (in our case, we used monocytes, with mean size between 7 and 15 μm). Therefore, the spectral response consists of a flat band (scattering band) with increasing absorbance values as a function of cell concentration.

To obtain an LS + ABS reading, some cells need to be stained. Several dyes have been reported, which specifically stain a given part of the cell. In our case, to enable live versus dead cells to be distinguished, we have used Trypan blue, as it can only enter a cell if its membrane is damaged. Thus, dead cells present a homogeneous blue color, whereas live cells retain their transparency²⁸. In this context, the readout will consist of an absorbance peak (centered at 584 nm) superimposed over the previously discussed scattering band.

Finally, the ABS regime can be obtained. Working with a broadband light source enables some wavelengths to remain unaffected by the dye absorption band (Trypan blue). Therefore, wavelengths higher than 700 nm should provide an identical absorbance value for stained and nonstained cells. Therefore, by subtracting the LS spectra from the results obtained in the LS + ABS regime, the absorption peaks that are due only to the dyes can be obtained.

Hence, cell screening with broadband light can provide multiparametric analysis²⁹, either by using different dyes or a single dye and determining the cell population with the scattering band. Alternatively, this approach allows determination of the wavelength that provides the highest sensitivity and the lowest LOD for a given cell culture. Only recently, it was demonstrated that local monitoring of yeast *Saccharomyces cerevisiae* was strongly wavelength dependent³⁰. Changing the working wavelength from 425 to 470 nm gave rise to an increase of the sensitivity by a factor of nine.

MATERIALS

REAGENTS

- Appropriate substrates. We used soda-lime glass wafers (Schott) with a diameter of 100 mm and a thickness of 700 μm .
- SU-8 2005 (e.g., MicroChem, Microresist) **! CAUTION** It is highly flammable. Wear chemical goggles, gloves resistant to organic acids and protective clothing when handling SU-8 resists. Avoid contact with eyes, skin or clothing.
- SU-8 50 (e.g., MicroChem, Microresist) **! CAUTION** It is highly flammable. Wear chemical goggles, gloves resistant to organic acids and protective clothing when handling SU-8 resists. Avoid contact with eyes, skin or clothing.
- Propylene glycol methyl ether acetate (e.g., PGMEA, MicroChem or mr-dev 600, Microresist) **! CAUTION** Wear chemical goggles, gloves resistant to organic acids and protective clothing. It may form explosive peroxides and has a vapor explosion hazard.
- Poly(dimethylsiloxane) (PDMS, e.g., Sylgard 184 kit, which includes the Sylgard 184 silicone elastomer base and the Sylgard 184 silicone elastomer curing agent, both from Dow Corning)
- Cell sample to be analyzed (we used human monocytic cell line THP-1 (ECACC, cat. no. 88081201))
- Isopropyl alcohol
- Ethanol
- Deionized (DI) water
- Ultrapurified water (e.g., Milli-Q, Millipore)
- Nitrogen or argon gas supply

- RPMI 1640 medium (Gibco, cat. no. 21875-034)
- FBS (Gibco, cat. no. 10106-169)
- L-Glutamine (200 mM, Gibco, cat. no. 25030)
- PBS (10 \times , Sigma, cat. no. P4417-100TAB)
- Paraformaldehyde (Electron Microscope Sciences, cat. no. 19200) **! CAUTION** It is very hazardous in case of skin or eye contact, as well as in case of ingestion or inhalation.
- Trypan blue (Gibco, 15250-061) **! CAUTION** It is hazardous in case of ingestion. It is slightly hazardous in case of skin and eye contact or inhalation.

EQUIPMENT

- Sterile cell culture flasks
- Spin coater (e.g., D80 controller, SÜSS Microtec)
- UV mask aligner (e.g., MA6/BA6, SÜSS Microtec)
- Hot plate (e.g., Harry Gestigkeit)
- Automatic pipettors with sterile plastic serology pipettes
- Automatic pipettes with sterile disposable tips
- Biosafety hood with vertical laminar flow and equipped with UV light for decontamination
- Water bath with temperature control
- Incubator with both temperature and gas composition controls
- Centrifuge (no temperature control is needed)
- Optical microscope with phase-contrast equipment (optional)
- Neubauer counting chamber

- Vacuum chamber
- Sterile conical tubes, 15 ml
- Sterile microcentrifuge tubes, 1.5 ml
- Connectorized microspectrometer (e.g., Ocean Optics HR4000, QE65000 and so on (Ocean Optics))
- Multimode optical fiber, 230 μm diameter
- Broadband light source (e.g., Ocean Optics HL-2000 (Ocean Optics))

REAGENT SETUP

Complete RPMI 1640 medium (with 20% (vol/vol) FBS) Adjust to 50 ml by adding RPMI 1640 medium to a solution containing 10 ml of

FBS and 2 mM of L-glutamine. Complete culture medium can be stored for 1 week at 4 °C.

PBS 1 \times solution Dissolve one tablet in 200 ml of Milli-Q dH_2O and sterilize. This solution can be stored at room temperature (RT; 25 °C) for months.

Paraformaldehyde solution (4% (wt/vol)) Add 4 ml of the paraformaldehyde stock solution to 96 ml of 1 \times PBS. Mix it until paraformaldehyde is completely diluted. The solution is stable at RT.

Trypan blue solution (1:1) Mix 50 ml of Trypan blue stock with 50 ml of 1 \times PBS and stir it. Freshly prepare each time.

PROCEDURE

Master fabrication ● TIMING 24 h

- 1| Clean the soda-lime wafer with acetone and ethanol. If the cleaning is not complete, proceed with high-pressure DI water before using acetone and ethanol.
- 2| Dehydrate the soda-lime wafer by placing it on a hot plate (or oven) at 150 °C for 60 min. Allow it to cool down to RT (25 °C) before further processing (cooling will take ~60 min).
- 3| Sputter a thin chromium layer (10 nm) with the required process parameters according to in-house equipment. This layer should appear translucent.
? TROUBLESHOOTING
- 4| Dehydrate the substrate by placing it on a hot plate (or oven) at 150 °C for 60 min. Allow it to cool down to RT before further processing (cooling will take ~60 min.).
▲ CRITICAL STEP Proceed to Step 5 immediately so as to avoid substrate rehydration.
- 5| Center the wafer on the spinner chuck and apply vacuum. Dispense 4 ml of SU-8 2005 on a centered position of the wafer. Program a two-step spinning program using a spinner with a lid. Start with 400 r.p.m. \times 15 s to homogenize, followed by 2,500 r.p.m. \times 60 s to obtain a 4- μm thick layer. The thickness of this layer is not critical.
? TROUBLESHOOTING

- 6| Planarize the wafer for 5 min by placing it in a holder with a lid (assuring solvent-saturated atmosphere).

▲ CRITICAL STEP Planarization must be done on a level surface.

? TROUBLESHOOTING

- 7| Dry the substrates for 2 min at 65 °C, followed by 4 min at 95 °C. The same hot plate can be used. Control the temperature ramp so that it is not higher than 5 °C min^{-1} . Allow to cool down to RT before further processing (cooling will take ~30 min).

! CAUTION This step evaporates a substantial part of the organic solvent (cyclopentanone). Perform this step in a fume hood.

- 8| Flood expose to UV light using a mask aligner with a dose of 75 mJ cm^{-2} .

- 9| PEB the substrate, starting at 65 °C with a ramp of 5 °C min^{-1} until it reaches 95 °C. Bake at 95 °C for 5 min. Allow it to cool down to RT before further processing (cooling will take ~30 min).

! CAUTION This step evaporates a substantial part of the organic solvent (cyclopentanone). Perform this step in a fume hood.

■ PAUSE POINT Wafers can be stored at this point for months under CR conditions.

- 10| Plasma activate the SU-8 surface. Conditions strongly depend on the in-house equipment. Our conditions were 5 min at 75 W and with 85 sccm O_2 . Immediately afterward, proceed with Steps 11 and 12. If, after Step 12, uneven SU-8 distribution still occurs, increase plasma time and/or power.

▲ CRITICAL STEP Plasma activation is reversible, with a very short half-life (<30 min). Assure complete access to the spinner before starting the activation.

PROTOCOL

11| Center the wafer on the spinner chuck and apply vacuum. Dispense 4 ml of SU-8 50 on a centered position of the wafer. Program a two-step spinning program using a spinner with lid. Start with 400 r.p.m. × 15 s to homogenize, followed by 400 r.p.m. × 30 s to obtain a 250- μm -thick layer.

? TROUBLESHOOTING

12| Planarize the wafer for 30 min by placing it in a holder with a lid (assuring solvent-saturated atmosphere).

▲ CRITICAL STEP Planarization must be done on a level surface.

13| Dry the substrates for 5 min at 65 °C and then for 3 h at 95 °C. The same hot plate can be used. Control the temperature ramp so that it is not higher than 5 °C min⁻¹. Allow it to cool down to RT before further processing (cooling will take ~30 min). Gently press with the tweezers at the edges of the SU-8 after reaching RT. If it is dry enough, very small or no scratches will occur. If the SU-8 is scratched, it will stick to the mask in the next step. To avoid this situation, bake for an additional 30 min at 95 °C and repeat the test with the tweezers.

▲ CRITICAL STEP Keep the wafer in a leveled position until the exposure is complete. Even the hot plates must be leveled.

! CAUTION This step evaporates a substantial part of the organic solvent (γ -butyrolactone). Proceed only in a fume hood.

? TROUBLESHOOTING

14| Load the mask into the mask aligner strictly according to the requirements of the in-house mask aligner. Position the wafer centered on the chuck and apply vacuum. Expose with a dose of 750 mJ cm⁻². Use hard contact for optimal results.

15| PEB the substrate, starting at 65 °C with a ramp of 5 °C min⁻¹ until it reaches 95 °C. Bake during 20 min. Allow it to cool down to RT before further processing (cooling will take ~30 min).

▲ CRITICAL STEP Keep the wafer under CR conditions for 8 h before further processing to minimize internal stresses.

16| Develop the substrate in PGMEA. It is best if two flasks are used: the first, filled with PGMEA, for removal of the bulky nonexposed SU-8 50 and the second, with fresh PGMEA, for pattern developing. Apply vigorous agitation for faster development. Periodically remove substrate from the flask, and dry with an air gun to check under microscope. Rinse the substrate with isopropyl alcohol and dry again with an air gun. The appearance of a crack indicates that further development cannot be done. Consider the yield to decide when to stop the development step. Be careful, if you aim to develop all the systems in one wafer, you may end up with a broken substrate.

! CAUTION PGMEA is harmful. Proceed only in a fume hood.

? TROUBLESHOOTING

17| Hard-bake the substrate, starting at 65 °C with a ramp of 5 °C min⁻¹ until it reaches 120 °C. Place a lid filled with an inert gas (nitrogen or argon) over the substrate and bake during 60 min. Allow to cool down until RT before further processing (cooling will take about 60 min).

▲ CRITICAL STEP Having the lid filled with inert gas prevents SU-8 oxidation. Keep lid on until substrate reaches RT again.

■ PAUSE POINT Wafers can be stored at this step under CR conditions.

? TROUBLESHOOTING

PDMS replica ● TIMING 50–80 min

18| Prepare PDMS pre-polymer by mixing the curing agent and the elastomer base in a 1:10 ratio (v/v) in a flask. Thorough mixing is obtained when the resulting mixture becomes opaque (due to a high amount of small air bubbles). Degas it in a vacuum chamber. Use an appropriately sized flask. Bear in mind that when applying vacuum, the bubbles increase several orders of magnitude in size, which may result in an overflow from the flask.

? TROUBLESHOOTING

19| Pour the degassed PDMS on the SU-8 master. Insert the PDMS in a syringe and use minute amounts of PDMS prepolymer to fill the systems without having a PDMS overflow over the frame (hydrophobic barrier). Degas once again to remove entrapped air bubbles.

▲ CRITICAL STEP Assure that there is PDMS on the top surface of the SU-8 master.

20| Bake the prepolymer for 20 min at 80 °C, starting at RT and with a ramp of 5 °C min⁻¹.

■ PAUSE POINT Wafers can be stored at this step under CR conditions.

21| Dice a second soda-lime wafer with dimensions slightly larger than the system (this will simplify the fiber optics insertion, minimizing the facet damage). Use a diamond blade or in-house equipment. Microscope glass slides also work.

22| Clean the substrates with acetone and ethanol. If the cleaning is not complete, proceed with high pressure DI water before using acetone and ethanol.

23| Dehydrate the substrates by placing them on a hot plate (or oven) at 150 °C for 60 min. Allow to cool down until RT before further processing (cooling will take about 60 min).

24| Peel off the elastomer from the mold by gently pressing with the tweezers at one PDMS edge. Use the in-house PDMS bonding procedure (thermal, chemical or oxygen plasma). Oxygen plasma requires set-up of suitable conditions for the sealing process for each plasma system. Preliminary tests are required. Use dummy nonpatterned PDMS samples and clean substrates. Start with 30 s at 75 W and with 85 sccm O₂. Increase time and/or power. If PDMS surface turns into a milky color, reduce power. After plasma, immediately bring both surfaces into contact and maintain for 60 min at 60 °C.

■ **PAUSE POINT** Systems are completed and remain stable for months even outside CR conditions.

Culture of THP-1 cells ● **TIMING 50 min**

25| Maintain human monocytic cell line THP-1 in complete RPMI 1640 medium at 37°C in 5% CO₂, in a concentration in the range (0.5–1.0) × 10⁶ cells per ml. Subculture the cell line every 3 days.

Preparing cells for measurement

26| For each experiment, transfer 2.00 × 10⁶ cells per ml to a culture tube and rinse twice in PBS heated to 37 °C. Each rinsing consists of three stages: first centrifuge the samples for 3 min at 60g, then discard the remaining suspension and finally resuspend the pellet in 10 ml 1× PBS. Maintain healthy cells by growing in an incubator under controlled temperature and atmosphere. To avoid cell lysates, centrifuge at a maximum of 60g. To avoid cell death, do not store them in the buffer for more than 30 min.

? TROUBLESHOOTING

Labeling the dead cell population

27| To obtain a dead cell population control, fix monocytes with 4% (wt/vol) paraformaldehyde solution for 10 min. Afterward, rinse cells twice with 1× PBS solution (as explained in Step 26).

▲ **CRITICAL STEP** The cell concentration is critical for a valid measurement. Avoid cell loss during the rinsings, verifying the presence of a pellet each time and removing the supernatant carefully.

28| Stain cells with Trypan blue solution for 5 min and rinse them twice in PBS to ensure that label is retained only inside appropriate cells and not in the buffer.

▲ **CRITICAL STEP** When the stain penetrates into the cytoplasm of dead cells through the membrane, it can be seen as a blue color throughout the cells. Live cells are transparent.

? TROUBLESHOOTING

Experimental setup ● **TIMING 20 min**

29| Punch out the microfluidic ports with an appropriate tool (stainless steel tip, stencil).

30| Cut and peel off the optical fibers. Insert them on the self-alignment system. To facilitate the process, use an ethanol droplet as a lubricant. Wait until the ethanol is completely evaporated (between 2 and 10 min). This time depends on the PDMS thickness and on the length of the self-alignment microchannels.

? TROUBLESHOOTING

31| Connect the input fiber optics to the broadband light source (HL-2000 or similar) and the output fiber optics to the microspectrometer. Allow the light to warm up for 15 min before starting the measurements.

? TROUBLESHOOTING

32| Fill the MIR with DI water using a micropipette. Note the increase in the collected signal, as air mirrors are optimized to work with a refractive index similar to that of water. Select the highest integration time that does not have a saturated signal (an acquisition time of 30 ms should be appropriate). Set the number of scans to ten to reduce the noise level. Close the shutter of the light source and collect the dark noise spectra. When opening the shutter again, there must be a smooth spectral response, with intensity values close to zero below 360 nm and above 1,100 nm.

PROTOCOL

33 Fill a micropipette with 5 ml of PBS and dispense it on the fluidic inlet. Apply a small vacuum on the fluidic outlet to aspirate the PBS. Repeat the injection three times before taking the reference value.

▲ CRITICAL STEP Be careful when aspirating the solution in order to ensure that no bubbles enter into the MIR. If no microscope is available, a bubble entrance can be seen as a strong decrease of the intensity values. This reference will be subtracted from all further measurements. It is of key importance to measure it accurately.

PhLoC working in LS regime (live monocytes) ● TIMING 60 min

34 Considering that the system has a volume of 1.43 μl , prepare the volume of cells required to ensure a minimal error in the dilutions, as well as possible measurement repetition. In our case, the aliquots were obtained by resuspending the cells obtained in step 26 in 1 \times PBS to obtain the desired concentrations: 2.00×10^6 , 1.50×10^6 , 1.00×10^6 , 0.75×10^6 , 0.50×10^6 , 0.40×10^6 , 0.30×10^6 , 0.20×10^6 , 0.10×10^6 and 0.05×10^6 cells per ml. Store the cultures in the incubator until their use.

? TROUBLESHOOTING

35 Before pipetting the prepared concentrations, stir cells gently. Dispense 3 ml on the inlet and gently apply vacuum at the outlet. Fix the time between pipetting and acquisition at a constant value throughout the experiment. Cells settle down, causing a variation in response. Alternatively, wait until a steady state is achieved.

▲ CRITICAL STEP Between each measurement, rinse the system with the necessary amount of 1 \times PBS to remove unspecific cell adsorption at the PDMS surface of the PhLoC.

? TROUBLESHOOTING

36 Convert the intensity spectrum to an absorbance spectrum using the following equation:

$$\text{Abs} = -\frac{I}{I_0}$$

where I is the acquired spectrum of a given cell concentration and I_0 is the reference spectrum of PBS. Plot the absorbance as a function of the wavelength. A graph similar to that presented in **Figure 5a** should be obtained, in which absorbance is plotted as a function of the wavelength for several concentrations. A flat scattering band (no peaks) is due to the monocyte size (between 7 and 15 μm) being much larger than the wavelengths used.

37 To determine the sensitivity and the limit of detection, plot absorbance versus concentration. From the results obtained in Step 36, this can be easily obtained (transpose the data sheet). The plot should look similar to **Figure 5b**. The Beer-Lambert law is only valid at the region in which the absorbance is directly proportional to the concentration, with the formula

$$\text{Abs} = \epsilon LC$$

where ϵ is the molar absorptivity, L is the path length and C is the cell concentration. Check if all concentrations match with this behavior; otherwise, discard the values where saturation has been reached. Perform the lineal regressions for a large number of wavelengths and store them in a different data sheet.

38 Plot the slope (sensitivity) of the linear regression as a function of the wavelength. Include the errors also provided in the linear regression fit. The LOD is, according to IUPAC, not the lowest detectable cell concentration, as it also depends on both the sensitivity and the accuracy of the linear fit³¹. In this case, the LOD can be obtained with the formula

$$\text{LOD}(k\text{cell}/\text{ml}) = \frac{3\sigma_a}{m}$$

where σ_a is the intersection error, m is the slope and $k\text{cell}$ is 'per 10^3 cells'. Basic error propagation allows determining the error of the LOD as $\sigma_{\text{LOD}}(k\text{cell}/\text{ml}) = \text{LOD} \sigma_m/m$ where σ_m is the error of the slope.

Different R^2 values will be obtained, depending on the regime used and the sensitivity of the wavelength. These results allow choosing the optimal working wavelength for each regime.

? TROUBLESHOOTING

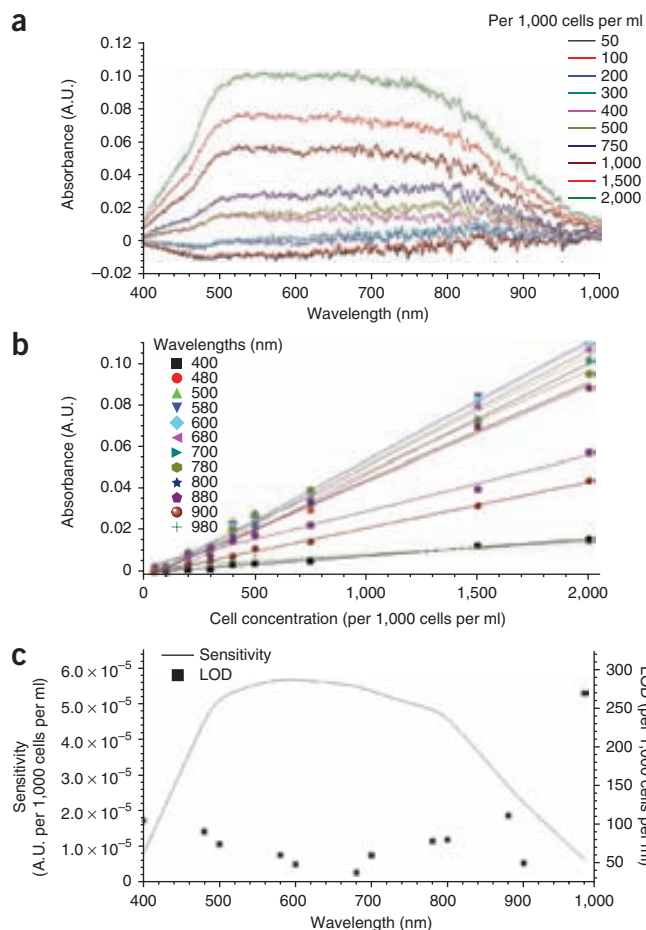


Figure 5 | Characterization in the LS regime. (a) Spectra obtained using unlabeled monocytes for concentrations ranging from 0.05 to 2.00 million cells per ml. (b) Beer-Lambert plots as a function of the wavelength and for concentrations ranging from 0.05 to 2.00 million cells per ml. (c) Sensitivity and LOD as a function of the wavelength, showing a broad range of optimal wavelengths.

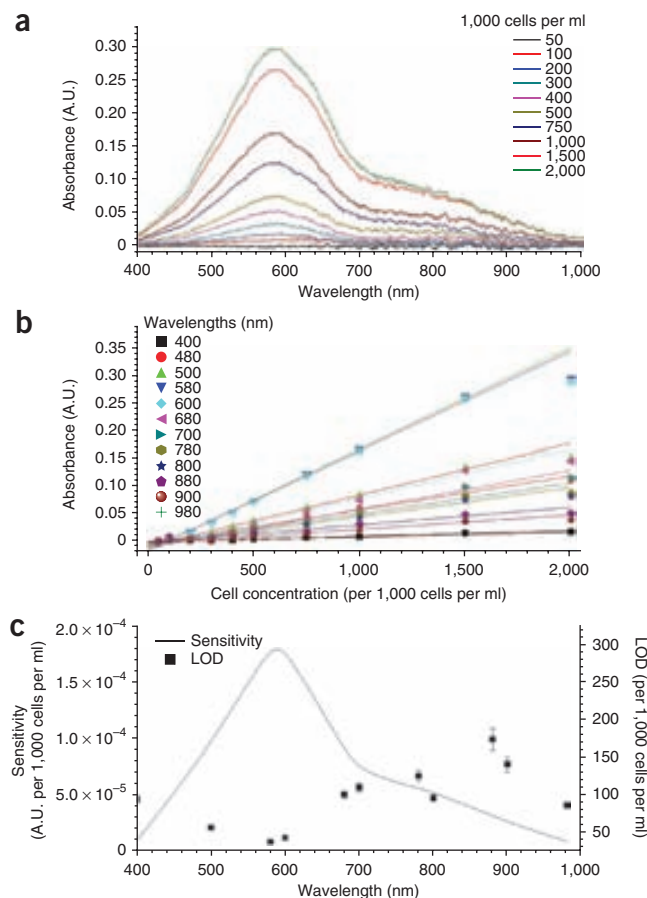


Figure 6 | Characterization in the LS + ABS regime. (a) Spectra obtained using monocytes labeled with Trypan blue for concentrations ranging from 0.05 to 2.00 million cells per ml. Noticeable are the trypan blue absorption band (584 nm) and the scattering band ($\lambda > 700$ nm). (b) Beer-Lambert plots as a function of the wavelength and for concentrations ranging from 0.05 to 2.00 million cells per ml. This last concentration falls outside the linear regime (saturation region), and therefore it is not used for the linear fit. (c) Sensitivity and LOD as a function of the wavelength, with main two working regions: in the Trypan blue band (584 nm) or in the scattering band ($\lambda > 700$ nm). Error is as described previously in the protocol.

© 2011 Nature America, Inc. All rights reserved.



39 | Plot the obtained LOD, with its respective error as a function of the wavelength. A graph similar to that presented in **Figure 5c** should be obtained.

PhLoC working in LS + ABS regime (dead monocytes) ● TIMING 60 min

40 | Resuspend the labeled cells obtained in step 27–28 in $1\times$ PBS to obtain the desired concentrations: 2.00×10^6 , 1.50×10^6 , 1.00×10^6 , 0.75×10^6 , 0.50×10^6 , 0.40×10^6 , 0.30×10^6 , 0.20×10^6 , 0.10×10^6 and 0.05×10^6 cells per ml.

41 | Repeat Steps 35–39. Check if all concentrations match with this behavior; otherwise, discard the values where saturation has been reached (for instance, 2.00×10^6 cells per ml in **Figure 6** has not been used for the regression). Plots similar to **Figure 6a–c** should be obtained.

PhLoC working in ABS regime (dead monocytes without scattering) ● TIMING 30 min

42 | Copy the results obtained in Steps 36–41 into a different data sheet.

43 | Subtract, for each concentration, the absorbance obtained in LS regime from the LS + ABS. A graph similar to **Figure 7a** should be obtained, where no scattering band at longer wavelengths is obtained.

44 | Repeat Steps 36–39. Check if all concentrations match with this behavior; otherwise, discard the values where saturation has been reached (for instance, in **Fig. 7b** the value corresponding to 2.00×10^6 cells per ml has not been used for the regression). Plots similar to **Figure 7b,c** should be obtained.

PROTOCOL

Figure 7 | Characterization in the ABS regime obtained by subtraction of the spectra obtained in LS and LS + ABS regimes. **(a)** Spectra obtained using monocytes labeled with Trypan blue for concentrations ranging from 0.05 to 2.00 million cells per ml. Only the Trypan blue absorption band (584 nm) is observed, without any contribution of the scattering band. **(b)** Beer-Lambert plots as a function of the wavelength and for concentrations ranging from 0.05 to 2.00 million cells per ml. This last concentration falls outside the linear regime (saturation region), and therefore it is not used for the linear fit. **(c)** Sensitivity and LOD as a function of the wavelength, showing a sharp sensitivity peak at the Trypan blue band (584 nm). As expected, no sensitivity and very high LOD is obtained at the scattering band ($\lambda > 700$ nm). Error is as described previously in the protocol. See **Figures 5a** and **6a**.

▲ CRITICAL STEP Notice that in this regime, there is no working wavelength associated with the scattering band. This is logical, as the scattering effects have been removed in Step 43. Therefore, in this regime, simultaneous multiparametric measurements can only be recorded if several dyes are simultaneously used.

Comparison between the different regimes ● TIMING 30 min

45 | Note the difference between the suitable working wavelengths: for the LS regime, a broad region of wavelengths provides with the highest sensitivity, being $(7.9 \pm 0.1) \times 10^{-5}$ A.U. per thousand cells (between 600 and 700 nm). In the LS + ABS, two working wavelength regions are accessible: the one that features with the highest sensitivity ($(26.49 \pm 0.4) \times 10^{-5}$ A.U. per thousand cells) is associated with the Trypan blue band (584 nm). A second wavelength is associated with the scattering band.

As an example, a working wavelength of 750 nm provides a respectable sensitivity and an LOD = 160 ± 4 cells. Therefore, in this regime, simultaneous multiparametric measurements can be taken, by taking advantage of absorption and scattering bands. Finally, in the ABS regime, a single Trypan blue band is obtained, with a maximum sensitivity of $(17.7 \pm 0.1) \times 10^{-5}$ A.U. per thousand cells.

? TROUBLESHOOTING

Troubleshooting advice is presented in **Table 1**.

TABLE 1 | Troubleshooting table.

Step	Problem	Possible reason	Solution
3	Chromium layer is not translucent	Sputtering of the chromium conditions results in a thick layer, with the possibility of cracks forming	Reduce sputtering time and/or applied power
5	SU-8 seed layer too thin/thick	Different spinner produces different thicknesses	As long as the layer is homogeneous, this thickness is not critical. Thick layers, however, cause high mechanical stresses on the wafer
6	Thickness of the SU-8 seed layer is not homogeneous	Planarization and/or bake have not been done on a level surface	Remove SU-8, spin again and use a level surface for planarization and baking
11	SU-8 thick layer is not homogeneously spun on the wafer	The SU-8 seed layer activation is not complete	Increase activation time and/or applied power. It is best to optimize this step with dummy wafers

(continued)

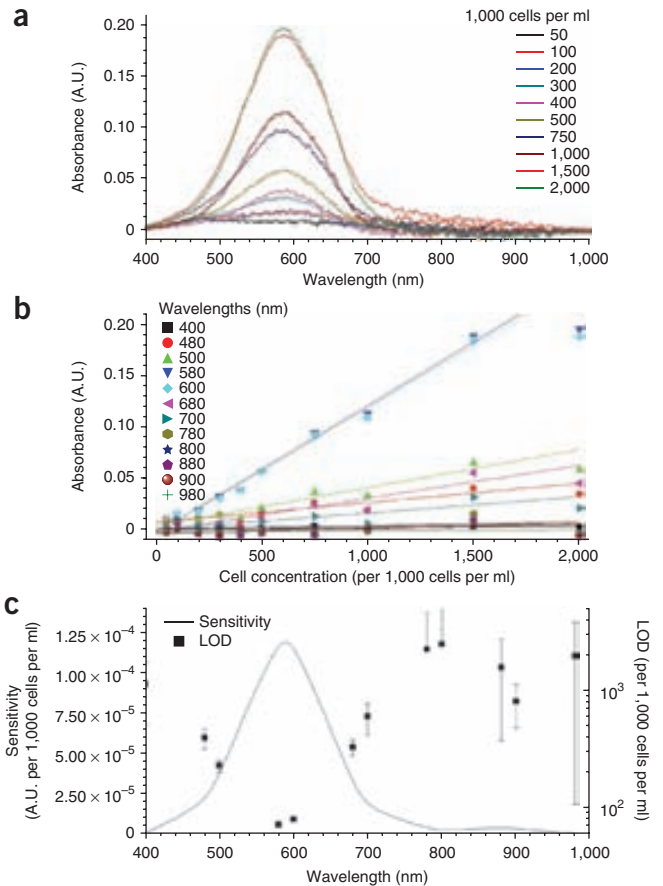


TABLE 1 | Troubleshooting table (continued).

Step	Problem	Possible reason	Solution
13	Wafers stick to the mask	SU-8 thick layer is not dry enough	Press gently with the tweezers on the wafer edge. If a deep scratch is present, bake for at least 30 min more
16	Cracks appear during the development	Development cannot be continued	Stop development and rinse with isopropyl alcohol. If cracks are small, they are healed during the hard bake (Step 17)
17	SU-8 is brown after the hard bake	Oxygen reacted with the SU-8	This master can still be used but is highly stressed (minor half-life). In the next process, assure the lid is filled with N ₂ or Ar
18	PDMS overflows during degassing	Bubbles largely expand during vacuum	Use a more appropriate (taller) flask
26	Cell lysates	Excessive acceleration during centrifugation and/or time in PBS	Centrifuge at a maximum of 60g and do not store them in the buffer for more than 30 min
28	Blue color is not only in the dead cells but also in the PBS	Suboptimal rinsing	Rinse again with PBS
	Total cell population varies between the different aliquots	Incomplete pellet recovery during rinsing	Do not completely remove the supernatant from the aliquots and/or check for any loss of pellet during the PBS removal
30	Fiber optics breaks at the self-alignment microchannels	Self-alignment microchannels with strict dimensions to clamp the fiber	Use ethanol as lubricant. Allow its evaporation before starting the measurements
31	The spectrum of the broadband light varies with time	Lamp is cold	Wait for 15 min before starting the measurements
34	Random cell apoptosis/necrosis in live monocytes	Cells stored in PBS	Once in PBS, cells can be maintained in the incubator for no more than 30 min
35	Cell spectral response varies with time	Cells settle down, causing a variation of its response	Fix the time between pipetting and acquisition at a constant value throughout the experiment. Alternatively, wait until a steady state is achieved
38	Wavelengths with deficient linear fit (low R ²)	Wavelengths not optimal for the measurement	Choose wavelengths with at least R = 0.99 for performing the experiments

● TIMING

Steps 1–17, Master fabrication: 24 h (includes overnight relaxation time)

Steps 18–24, PDMS replica: 50 min (with the cut substrates available; if not, add additional 30 min)

Steps 25–28, Cell culture preparation: 50 min

Steps 29–33, Experimental setup: 20 min

Steps 34–39, Measurement in LS regime: 60 min (markedly shorter if a data sheet template is used)

Steps 40–41, Measurement in LS + ABS regime: 60 min (markedly shorter if a data sheet template is used)

Steps 42–44, Measurement in ABS regime: 30 min (no additional measurements are required)

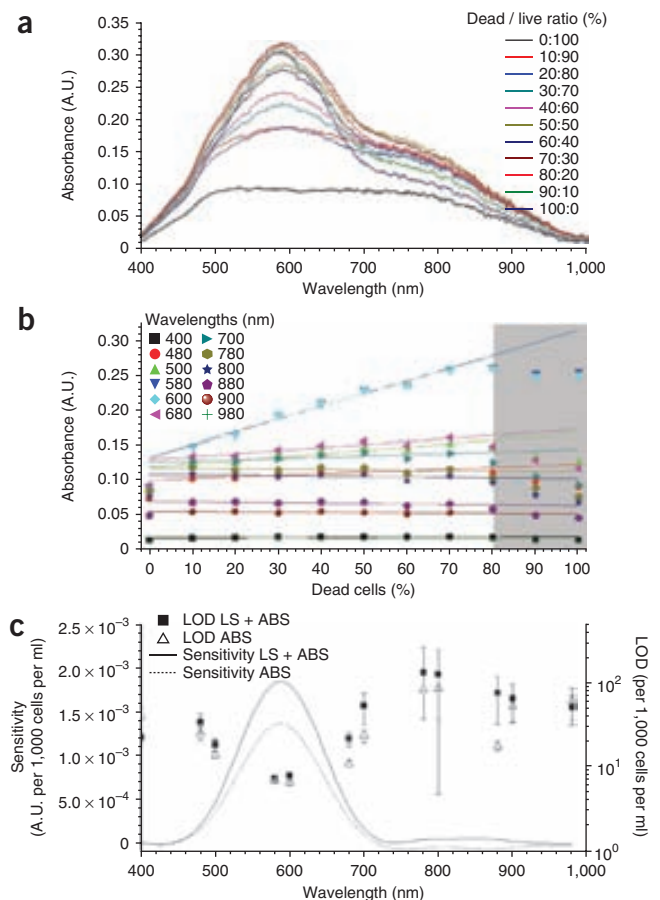
Step 45, Comparison of the different regimes: 30 min (no additional measurements are required)

ANTICIPATED RESULTS

This protocol allows the fabrication and the benchmarking of a PhLoC system capable of screening an arbitrarily large cell concentration in a single measurement. The use of broadband light and a spectrometer provides the spectral response of the cells under study (photonic fingerprint). In our case, we used monocytes because they have the same hematopoietic origin

PROTOCOL

Figure 8 | Measurement of the monocytes dead/live ratio. A constant cell concentration of 2.00 million cells per ml has been selected. Eleven aliquots have been prepared, with a varying dead/live ratio (10% variation on each). (a) Spectra show a clear shift from the ABS regime (100% label-free alive monocytes) to the LS + ABS regime (100% labeled dead monocytes). (b) Absorbance versus percentage of dead cells for different wavelengths, with their respective linear fit. The gray region corresponds to values where the scattering band presented a significant shift, meaning a decrease of the total cell population (confirmed with a Neubauer chamber). These points have not been used for the linear fit. (c) Sensitivity and LOD as a function of the wavelength, showing only the sensitivity peak at the Trypan blue band (584 nm). No scattering band is observed as a constant total cell concentration was used. Further, there is no significant variation of this band among the different aliquots, resulting in the expected small sensitivity at the scattering band ($\lambda > 700$ nm). Error is as described previously in the protocol.



as the CD4⁺ T cells (used for AIDS diagnosis), but their handling is easier. Three different protocols (LS, LS + ABS and ABS) can be used for screening the monocytes. In the first case, the measurements are recorded label free, only considering the scattering band. Conversely, if dyes are used, LS + ABS and ABS result in a higher sensitivity.

To assess the validity of the PhLoC, we measured the dead/live ratio of a cell culture. Eleven aliquots containing different proportions of labeled (dead) and label-free (live) cells diluted in 1× PBS were prepared by keeping the total monocyte concentration at a constant value (2.00×10^6 cells per ml). These volumes were successively injected, and the spectral response was obtained. As it can be seen in

Figure 8a, the acquired spectra show a clear shift from the ABS regime (100% label-free alive monocytes) to the LS + ABS regime (100% labeled dead monocytes). The scattering band remains quite similar in all the spectra. This is consistent with the fact that the total cell concentration has a constant value. The scattering band therefore functions as a self-test method: if a large displacement of this band occurs, then a variation of the population has occurred. Therefore, the scattering band does not exhibit variation as a function of the wavelength. From these spectra, the absorbance as a function of the percentage of dead cells can be obtained, exhibiting a linear response. In our case, we observed that values of dead cells higher than 80:20 did not match this regime (gray region in **Fig. 8b**). These aliquots were measured using a Neubauer chamber, exhibiting a population of $1.322 \pm 10\%$ (80:20), $1.205 \pm 10\%$ (90:10) and $0.915 \pm 10\%$ (100:0) million cells per ml, verifying the self-test protocol. These values were then discarded for the linear regression. A reason for this variation may be incomplete pellet recovery when removing the supernatant during rinsing with PBS. Thereafter, the sensitivity and the LOD were determined (including the errors calculated as before). It can be seen that the LS + ABS and ABS regimes show quite similar results (**Fig. 8c**), with LODs ranging between $7.6 \pm 0.4\%$ (LS + ABS) and $6.7 \pm 0.3\%$ (ABS), that is, more precise than the Neubauer chamber (typically 10%), more than 80 times faster than the lensless, ultra wide-field cell monitoring array platform based on shadow imaging (LUCAS)³² and holding the low cost and the portability issues.

ACKNOWLEDGMENTS The research leading to these results has received funding from the European Research Council under the European Community's Seventh Framework Programme (FP7/2007-2013)/ERC grant agreement no. 209243 and also from the IST Programme (P. CEZANNE, IST-2-IP-031867). We thank the research group FOR 856, mikroPART 'Mikrosysteme für partikuläre Life-Science-Produkte', for support of this work. Discussions with A. Voigt and G. Gruetzner of Microresist (Germany) regarding the fabrication steps are highly appreciated.

AUTHOR CONTRIBUTIONS J.V.-P., E.F.-R. and B.I. conducted the experiments. E.F.-R. and C.N. prepared the cell culture. S.D., S.B. and A.L. designed and fabricated the PhLoC. J.A.P., C.D., S.B. and A.L. defined the broadband screening protocol. A.L. supervised the project at all stages.

COMPETING FINANCIAL INTERESTS The authors declare no competing financial interests.

Published online at <http://www.natureprotocols.com/>.

Reprints and permissions information is available online at <http://www.nature.com/reprints/index.html>.

1. Yeo, L.Y., Chang, H.C., Chan, P.P.Y. & Friend, J.R. Microfluidic devices for bioapplications. *Small* **7**, 12–48 (2011).
2. Dittrich, P.S. & Manz, A. Lab-on-a-chip: microfluidics in drug discovery. *Nat. Rev. Drug. Discov.* **5**, 210–218 (2006).
3. Nagrath, S. *et al.* Isolation of rare circulating tumour cells in cancer patients by microchip technology. *Nature* **450**, 1235–1239 (2007).
4. Gilleland, C.L., Rohde, C.B., Zeng, F. & Yanik, M.F. Microfluidic immobilization of physiologically active *Caenorhabditis elegans*. *Nat. Protoc.* **5**, 1888–1902 (2010).
5. Yager, P. *et al.* Microfluidic diagnostic technologies for global public health. *Nature* **442**, 412–418 (2006).

6. Martinez, A.W., Phillips, S.T. & Whitesides, G.M. Diagnostics for the developing world: microfluidic paper-based analytical devices. *Anal. Chem.* **82**, 3–10 (2010).
7. Zhao, W. & van den Berg, A. Lab on paper. *Lab. Chip* **8**, 1988–1991 (2008).
8. Centers for Disease Control and Prevention. Revised classification system for HIV infection and expanded surveillance case definition for AIDS among adolescents and Adults. *Morbidity and Mortality Weekly Report* 1–19 (18 December 1992).
9. Myers, F.B. & Lee, L.P. Innovations in optical microfluidic technologies for point-of-care diagnostics. *Lab. Chip* **8**, 2015–2031 (2008).
10. Mayer, G. *et al.* Fluorescence-activated cell sorting for aptamer SELEX with cell mixtures. *Nat. Protoc.* **5**, 1993–2004 (2010).
11. Llobera, A., Demming, S., Wilke, R. & Büttgenbach, S. Multiple internal reflection poly(dimethylsiloxane) systems for optical sensing. *Lab. Chip* **7**, 1560–1566 (2007).
12. Godin, J. *et al.* Microfluidics and photonics for Bio-System-on-a-Chip: a review of advancements in technology towards a microfluidic flow cytometry chip. *J. Biophoton.* **1**, 355–376 (2008).
13. Chung, T.D. & Kim, H.C. Recent advances in miniaturized microfluidic flow cytometry for clinical use. *Electrophoresis* **28**, 4511–4520 (2007).
14. Qin, D., Xia, Y. & Whitesides, G.M. Soft lithography for micro- and nanoscale patterning. *Nat. Protoc.* **5**, 491–502 (2010).
15. Llobera, A. *et al.* Monolithic PDMS passband filters for fluorescence detection. *Lab. Chip* **10**, 1987–1992 (2010).
16. Llobera, A., Wilke, R. & Büttgenbach, S. Enhancement of the response of poly(dimethylsiloxane) hollow prisms through air mirrors for absorbance-based sensing. *Talanta* **75**, 473–479 (2008).
17. Ibarlucea, B. *et al.* Cell screening using disposable photonic lab on a chip systems. *Anal. Chem.* **82**, 4246–4251 (2010).
18. Merbs, S.L. & Nathans, J. Absorption-spectra of human cone pigments. *Nature* **356**, 433–435 (1992).
19. Kajihara, D. *et al.* FRET analysis of protein conformational change through position-specific incorporation of fluorescent amino acids. *Nat. Methods* **3**, 923–929 (2006).
20. Gao, X.H., Cui, Y.Y., Levenson, R.M., Chung, L.W.K. & Nie, S.M. *In vivo* cancer targeting and imaging with semiconductor quantum dots. *Nat. Biotechnol.* **22**, 969–976 (2004).
21. Llobera, A., Wilke, R. & Büttgenbach, S. Poly(dimethylsiloxane) hollow Abbe prism with microlenses for detection based on absorption and refractive index shift. *Lab. Chip* **4**, 24–27 (2004).
22. Mayers, B.T., Vezenov, D.V., Vullev, V.I. & Whitesides, G.M. Arrays and cascades of fluorescent liquid-liquid waveguides: broadband light sources for spectroscopy in microchannels. *Anal. Chem.* **77**, 1310–1316 (2005).
23. Llobera, A., Wilke, R. & Büttgenbach, S. Optimization of poly(dimethylsiloxane) hollow prisms for optical sensing. *Lab. Chip* **5**, 506–511 (2005).
24. Bhattacharya, S., Datta, A., Berg, J.M. & Gangopadhyay, S. Studies on surface wettability of poly(dimethyl)siloxane (PDMS) and glass under oxygen-plasma treatment and correlation with bond strength. *J. Microelectromech. Syst.* **14**, 590–597 (2005).
25. Blanchard, D., Ligrani, P., Gale, B. & Harvey, I. Micro-structure mechanical failure characterization using rotating Couette flow in a small gap. *J. Micromech. Microeng.* **15**, 792–801 (2005).
26. Martin, C. *et al.* Stress and aging minimization in photoplastic AFM probes. *Microel. Eng.* **86**, 1226–1229 (2009).
27. Feng, R. & Farris, R.J. Influence of processing conditions on the thermal and mechanical properties of SU-8 negative photoresist coatings. *J. Micromech. Microeng.* **13**, 80–88 (2003).
28. Cheng, L.L., Luk, Y.Y., Murphy, C.J., Israel, B.A. & Abbott, N.L. Compatibility of lyotropic liquid crystals with viruses and mammalian cells that support the replication of viruses. *Biomaterials* **26**, 7173–7182 (2005).
29. Llobera, A. Device for particle analysis and counting. WIPO patent application no. PCT/ES2011/070011 (11 January 2010).
30. Demming, S. *et al.* Poly(dimethylsiloxane) photonic microreactors based on segmented waveguides for local absorbance measurement. *Electrophoresis* **32**, 431–439 (2011).
31. Long, G.L. & Wineforder, J.D. Limit of detection: a closer look at the IUPAC definition. *Anal. Chem.* **55**, A712–A724 (1983).
32. Cui, X. *et al.* Lensless high-resolution on-chip optofluidic microscopes for *Caenorhabditis elegans* and cell imaging. *PNAS* **105**, 10670–10675 (2008).



Cite this: *Analyst*, 2011, **136**, 3496

www.rsc.org/analyst

PAPER

Selective functionalisation of PDMS-based photonic lab on a chip for biosensing†‡

Bergoi Ibarlucea,^a César Fernández-Sánchez,^{*a} Stefanie Demming,^b Stephanus Büttgenbach^b and Andreu Llobera^{*a}

Received 24th November 2010, Accepted 6th January 2011

DOI: 10.1039/c0an00941e

A comparative study of different approaches for the selective immobilisation of biomolecules on the surface of poly(dimethylsiloxane) (PDMS) is reported. The motivation of this work is to set a robust and reliable protocol for the easy implementation of a biosensor device in a PDMS-based photonic lab-on-a-chip (PhLoC). A hollow prism configuration, previously reported for the colorimetric detection of analytes was chosen for this study. Here, the inner walls of the hollow prism were initially modified by direct adsorption of either polyethylene glycol (PEG) or polyvinyl alcohol (PVA) linear polymers as well as by carrying out a light chemical oxidation step. All these processes introduced hydroxyl groups on the PDMS surface to a different extent. The hydroxyl groups were further silanised using a silane containing an aldehyde end-group. The interaction between this group and a primary amine moiety enabled the selective covalent attachment of a biomolecule on the PDMS surface. A thorough structural characterisation of the resulting modified-PDMS substrates was carried out by contact angle measurements, X-ray photoelectron spectroscopic (XPS) analysis and atomic force microscopy (AFM) imaging. Using horseradish peroxidase as a model recognition element, different biosensor approaches based on each modification process were developed for the detection of hydrogen peroxide target analyte in a concentration range from 0.1 μM to 100 μM . The analytical performance was similar in all cases, a linear concentration range between 0.1 μM and 24.2 μM , a sensitivity of 0.02 a.u. μM^{-1} and a limit of detection around 0.1 μM were achieved. However, important differences were observed in the reproducibility of the devices as well as in their operational stability, which was studied over a period of up to two months. Considering all these studies, the PVA-modified approach appeared to be the most suitable one for the simple fabrication of a biosensor device integrated in a PDMS PhLoC.

Introduction

Microfluidics is the science devoted to the study of fluids in channels with a size that varies from the units to the hundreds of micrometres. Making use of microfluidics it is possible to fabricate Lab-on-chip (LoC) systems, miniaturising diverse functionalities that typically require a whole (bio)chemical laboratory. These systems provide several advantages compared to the standard ones, such as high sensitivity, faster analysis, decrease in sample, reagent and waste volume, automatization and standardisation of processes.^{1,2}

The huge impact of the LoC concept cannot be understood without the development of polymeric materials. Indeed, polycarbonate (PC), poly(methyl methacrylate) (PMMA) and poly(dimethylsiloxane) (PDMS) have been widely applied for the fabrication of LoC, thereby providing high versatility and reduction of both time and cost of the fabrication process. By using PDMS, microsystems can rapidly be fabricated by cast moulding with resolutions down to 0.1 μm (ref. 3) and in turn easily sealed to a variety of different substrates.⁴ It is a cheap material that polymerises at low temperatures,⁵ it is optically transparent in a very wide wavelength range (from UV to NIR) and as such is compatible with many optical detection methods. Its non-permeability to water, non-toxicity and permeability to gases makes it fully compatible with biological studies. It is flexible and elastic, with a Young's modulus of 2.5 MPa when it is fabricated with a 10 : 1 ratio of base : curing agent.⁶ This elasticity enables its easy releasing from the master during the fabrication process and it also facilitates the mechanical pumping of fluids inside the microchannels.^{5,7} Among the different transduction modes applied in LoC technology, those systems that use

^aInstituto de Microelectrónica de Barcelona, IMB-CNM (CSIC), Campus UAB, 08193 Bellaterra, Spain. E-mail: andreu.llobera@imb-cnm.csic.es; cesar.fernandez@imb-cnm.csic.es; Fax: +34 935801496; Tel: +34 935947700

^bInstitut für Mikrotechnik, Technische Universität Braunschweig, 38124 Braunschweig, Germany; Fax: +49 (0)531 391 8101; Tel: +49 (0)531 391 3320

† This article is part of a themed issue on Emerging Investigators.

‡ Electronic supplementary information (ESI) available. See DOI: 10.1039/c0an00941e

light as interrogation mechanism (usually called photonic LoCs or, PhLoC) exhibit some advantages. These include immunity to electromagnetic interferences and/or multiplexed detection in a single system.⁸ PhLoCs have already successfully been applied to the detection and quantification of different targets such as cells,⁹ DNA¹⁰ or glucose.¹¹ In addition, PhLoCs can also take advantage of the optical properties of PDMS, thus enabling the fabrication of low-cost systems with the potential of being highly sensitive, and easy-to-integrate with other microoptic and microfluidic elements.

One important drawback of PDMS lies in its ability to non-specifically adsorb biomolecules and other macromolecules, which hampers its application for chemical sensing. In this context, its surface can be easily tailored in order to avoid such undesirable process or, by contrast, to selectively immobilise different molecules.¹² The application of PDMS-based microsystems to (bio)chemical analysis and other disciplines requires carrying out surface modification processes, both chemical and physical, aiming at, for instance, decreasing biomolecular adsorption, as pointed out above, or increasing the hydrophilic/hydrophobic character of the surface. Moreover, other processes are directed to attach a biologically active molecule that alters the lubricity of the polymer surface¹³ or provides the material with the capacity to give a selective answer to a specific target analyte.¹⁴ Surface modification techniques can be divided into two groups: physical adsorption and covalent modification. The first one has been widely used due to its great simplicity but the resulting surfaces present thermal, mechanical and solvolytic instability because the interactions between the adsorbed material and the surface are weak. Covalent modification can overcome these drawbacks and give rise to a more robust modification of the surface.¹⁵ In this context, PDMS surfaces have been treated with oxygen plasma¹⁶ or UV/ozon,¹⁷ in order to make the surface hydrophilic by replacing the surface methyl groups, bound to the Si on the PDMS structure, by silanol groups (Si–OH). These new groups are prone to chemically interact with different functional groups, thus enabling the selective modification of the PDMS surface. However, it should be taken into account that the properties of these silanol groups are dynamic in the sense that the surface progressively recovers its hydrophobicity. Keeping in mind this drawback, the fact that these processes required special instrumentation and cannot be applied in microfluidic channels that were embedded in PDMS matrices,¹⁸ alternative processes for the selective modification of PDMS surfaces, which were easy to implement, are required.

In this work, a study of different liquid-based surface chemical biofunctionalisation methods was carried out using a PDMS PhLoC consisting of a hollow Abbe prism transducer configuration (Fig. 1).¹⁹ On one hand, physical adsorption of two different polymers containing hydroxyl groups, such as polyethylene glycol (PEG) or polyvinyl alcohol (PVA) enabled the further silanisation of the surface for the introduction of chemical functional groups and the eventual covalent immobilisation of the protein receptor. Both polymers were previously applied to the modification of PDMS in order to avoid the non-specific binding of proteins.^{20,21} On the other hand, a covalent modification approach was tested based on the chemical oxidation of the PDMS surface, thus generating silanol groups onto which a silanisation process and further immobilisation of the protein

receptor were carried out, as above. A thorough structural and analytical characterisation of the resulting modified PDMS surfaces was carried out. These methods could be performed in chemical and biological laboratories and applied to PDMS microfluidic systems without the need for special instrumentation.

Materials and methods

Chemicals and materials

The EPON SU-825 photoresist and the propylene glycol methyl ether acetate (PGMEA) were purchased from MicroChem Corporation (Newton, MA, USA). The PDMS Sylgard 184 elastomer kit was bought from Dow Corning (Midland, MI, USA) and used according to the datasheet.

99% PVA, PEG (molecular weight: 12 000 g), 30% (v/v) H₂O₂, 99% triethylamine (TEA), HRP type VI, 99% 2,2'-azino-bis(3-ethylbenzthiazoline-6-sulfonic acid) (ABTS), sodium cyanoborohydride (NaBH₃CN) and Tween 20 were from Sigma-Aldrich Co. (St Louis, MO 63103, USA). 90% 11-triethoxysilyl undecanal (TESU) was from ABCR GmbH & Co. KG (76187 Karlsruhe, Germany). All other chemicals were of analytical grade.

Fabrication of the microsystem

The PhLoC was fabricated by cast moulding, following a previously reported protocol.²² First, a master was fabricated with EPON SU-8 25 negative photoresist. A spin coating process of this photoresist was twice carried out with the aim of reaching a height of 250 μm. The resist was dried at 95 °C for 3 hours and then a standard UV-photolithographic process was carried out, followed by a baking step for 20 min at 95 °C and a consecutive developing step in PGMEA. The final step was a hard bake (HB) at 120 °C for 2 hours in an inert atmosphere so as to harden the master. Then, PDMS was used for the replication of the master. Pre-polymer was prepared by mixing the curing agent and the base elastomer in a 1 : 10 (v/v) proportion and degasifying it in a vacuum chamber. After pouring the pre-polymer on the master, the PDMS was cured on a hot plate at 80 °C for 20 min. The PDMS was then peeled off from the mould and sealed over

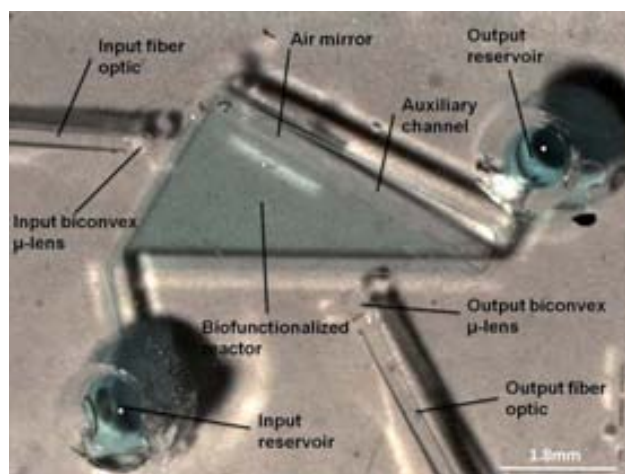


Fig. 1 Picture of the PDMS PhLoC microfluidic system.

a flat soda-lime glass substrate. For the sealing, both PDMS and glass surfaces received a plasma treatment.²³ That is, they were placed in a barrel etcher (Surface Technology Systems, Newport, UK) and exposed to oxygen plasma (75 sccm O₂, 85 W, 30 seconds). Immediately after the treatment they were put in contact and kept at 70 °C for 30 min, thus irreversibly sealing the fluidic system. Finally, the fluidic ports were opened the final volume of the PhLoC is 1.6 μL.

Modification and characterization of the PDMS surfaces

The three selected approaches for the PDMS surface modification are based on the introduction of hydroxyl (–OH) groups. Fig. 2 shows a scheme of the different steps required for each functionalization process. First, the PDMS surfaces were cleaned with ethanol and deionised water (DI H₂O). For the modification shown in Fig. 2A, a 1 mg ml^{–1} PEG solution in DI H₂O was pumped inside the system and left to react for 1 hour at room temperature (RT). For the modification in Fig. 2B, the system was filled with a 1 mg ml^{–1} PVA solution in DI H₂O and left to react for 1 hour at room temperature (RT). Fig. 2C shows the direct introduction of –OH groups on the PDMS surface, using an acidic solution containing DI H₂O, 37% HCl and 30% H₂O₂ in a 5 : 1 : 1 (v/v/v) ratio.¹⁸ After each of these steps, the surfaces were rinsed with DI H₂O and dried under a N₂ stream. Next, a silanisation process was carried out by incubating the modified PDMS systems in a 99.5% ethanol solution containing 2% TESU (2%) and 2% TEA for 1 hour at RT. Then the surfaces were thoroughly rinsed with 99.5% ethanol and dried at 80 °C for 2 hours. The TEA induces a highly nucleophilic oxygen in the –OH group that readily interacts with a silane²⁴ having its ethoxy groups previously hydrolysed. In this way, the silane covalently bound to the surface. All these modifications were also applied to flat PDMS surfaces having an area of 1 cm² to facilitate the structural characterisation of the resulting modified material by the different techniques described below.

Contact angle measurements were carried out with the sessile drop method, using a Krüss Easydrop contact angle meter and DS1 analysis software (Krüss GmbH, Hamburg, Germany). A drop of water was deposited on the modified PDMS surface and the angle formed between the liquid and the solid surface was measured. XPS analysis was carried out at the facilities of the Instituto de Nanociencia de Aragon (Spain) on an Axis Ultra-DLD spectrometer (Kratos Analytical Ltd, Manchester, England), using a monochromatised Al K α source (1486.6 eV). Signals were deconvoluted with the software provided by the manufacturer, using a weighted sum of Lorentzian and Gaussian component curves after background subtraction. The binding energies were referenced to the internal standard C1s (284.9 eV). Atomic force microscopy topographic and phase images of the modified surfaces were taken with a Veeco Nanoscope Dimension 3100 (Veeco, Plainview, NY, USA), working in tapping mode.

Fabrication of the biosensor approach

The analytical performance of the different modification protocols was tested by developing a biosensor for the detection of H₂O₂ based on the use of HRP as a model recognition element.

The resulting aldehyde-modified PDMS surfaces bound HRP through the amine groups of its lysine residues, by forming a Schiff base that is further reduced to a stable secondary amine with sodium cyanoborohydride.²⁵ HRP catalyzes the reduction of H₂O₂ in the presence of colourless 2,2'-azino-bis (3-ethylbenzthiazoline-6-sulfonic acid) (ABTS) charge transfer mediator, which is concomitantly oxidized to the green-coloured ABTS⁺ radical cation (Fig. S1, ESI†).²⁶ This redox species shows an absorption peak at 420 nm and two secondary peaks at 650 nm and 720 nm, the first one being chosen for the absorbance detection of this enzymatic reaction.

The overall procedure is described in detail below. PhLoC was filled with a solution containing 1 mg ml^{–1} HRP type VI and 5 mM sodium cyanoborohydride in 0.05 M carbonate buffer pH 8, and incubated for 1 hour at RT. Then, a 0.1 M phosphate buffer saline solution pH 7.0 containing 0.02% (v/v) Tween 20 (PBST) was pumped inside the system in order to remove the non-specifically adsorbed HRP molecules. The resulting biosensor systems were filled with PBS and stored at 4 °C until use.

A fourth biosensor approach was developed by direct adsorption of the HRP enzyme on the intact PDMS surface of the microsystem. It has been previously reported that proteins easily physisorbed on the surface of PDMS due to its high hydrophobicity.¹³ In this work, the PDMS system was incubated in a 1 mg ml^{–1} HRP solution in 0.05 M carbonate buffer pH 8 for 1 hour at RT. Then, the system was rinsed in PBST and stored at 4 °C, in the same fashion as above.

Finally, solutions of 0.1 M acetate buffer pH 5.5 containing 0.5 mM ABTS and increasing concentrations of H₂O₂, from 0.1 μM to 100 μM were sequentially pumped inside each PhLoC. The resulting response was detected by using a LED working at a wavelength of 430 nm (spectrally very close to the previously mentioned first absorption band of ABTS⁺), and measuring the spectral response using a microspectrometer (OceanOptics HR4000).

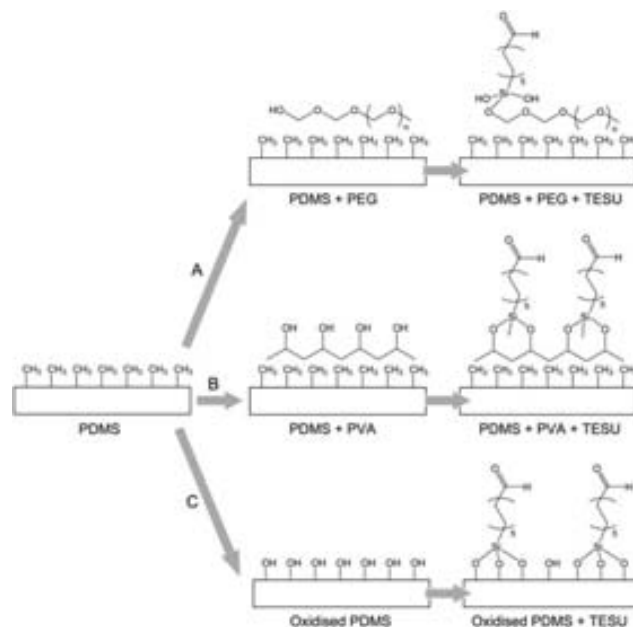


Fig. 2 Scheme of the different modification approaches tested for the biofunctionalisation of PDMS.

Stability of the microsystems

The microsystems were stored in PBS at 4 °C for over two months. The stability of the immobilized enzyme was studied by repeating the calibration curve in a H₂O₂ concentration range from 0.1 μM to 1.53 μM. The slope (sensitivity) of the calibration curve was plotted over time for comparative purposes.

Results and discussion

Each one of the three different approaches for the modification of PDMS was chosen with the aim of providing the surface with a different density of hydroxyl groups. The PVA adsorption process could give rise to a higher proportion of these groups comparing with the PEG adsorption one, taking into account the chemical structures of both polymers. As for the chemical oxidation process of the PDMS surface, the conditions were set following an optimisation study, which showed that higher concentrations of H₂O₂ and HCl in the solution or longer incubation times gave rise to the PDMS surface degradation. As for the selection of the TESU aldehyde-terminated silane, this molecule enabled the straightforward covalent immobilisation of the biomolecule receptor without the need of using cross-linking molecules.

Structural characterisation of the modified PDMS surfaces

A rough but rapid estimation of the degree of modification of the PDMS surface following every step of each modification protocol was firstly provided by contact angle measurements. Given the hydrophobic nature of the intact PDMS surface, it was apparent that the introduction of chemical functional groups would give rise to a decrease of the contact angle value. The PVA-based approach was the one that appeared to induce the most significant changes on the PDMS surface. The contact angle of a native PDMS surface was found to be 114.57°, which is a similar value to that reported in previous studies.²⁷ Following the PVA modification step, it decreased to 102.47°. However, the contact angle did not change when PEG was adsorbed. This may be related to the higher density of hydroxyl groups that PVA contains in its linear structure compared with PEG, which only presents two hydroxyl groups at both ends of its chain. This facilitates the incorporation of a higher number of silane molecules during the silanisation step, which indeed gave rise to a further decrease of the contact angle on the PVA-modified surface to 96.9°, whereas no difference in this value was measured with the PEG-modified samples. The chemical oxidation approach induced a change in the contact angle value to 110.75°, which appeared to be not significant since such a value was not altered following the silanisation process. The light chemical oxidation of the PDMS surface that took place using the HCl/H₂O₂/H₂O solution may account for such small differences in the measured contact angles. All these values were plotted in a bar graph, which can be found in the ESI† (Fig. S2†).

XPS analysis was carried out to make a fine estimation of the density of hydroxyl and aldehyde groups introduced on the PDMS surface during the different modification steps. Table 1 shows the atom content in percentage values extracted from the XPS survey scan. An increase in the carbon content occurred following the PVA modification step, from 43.38% to 51.74%,

while the Si percentage decreased from 36.90% to 27.05%. This is a clear indication of the adsorption of PVA molecules on to the PDMS surface. These changes were smaller in the samples prepared by the other treatments. High resolution spectra of the C1s region were also recorded. After the deconvolution of the C1 signal (Fig. S3–S5, ESI†), new peaks could be detected that were related to each step of the PDMS modification processes. The native PDMS presents a unique peak that corresponds to the carbon atom of the methyl group, with a binding energy of 284.90 eV. After the first modification steps carried out to introduce –OH groups on the PDMS surface, a new peak was observed in all cases with energy of 286.50 eV, which is ascribed to C–O bonds (Table S1, ESI†). Both PVA and PEG molecules contain this bond, but PEG has it in lower quantities, thus giving a smaller signal in the XPS spectra. In the case of the modification by chemical oxidation, Si–OH groups must have been introduced on the PDMS surface, instead of C–O bonds. However, it is reported that the oxidation of PDMS could give rise to –OH groups bound to the carbon atom of its methyl groups (–CH₃).²⁸ This may be responsible for the appearance of such a peak in the XPS analysis of the chemically oxidized samples. Nevertheless, its signal is significantly lower than that of the PVA-modified surface. Additionally, a new peak was observed in all samples further silanised with TESU. This peak is ascribed to the C=O bonds being part of the aldehyde end group of the silane molecules. Again, the highest density of this group appeared in the PVA-modified PDMS. From these results, it can be assumed that the PVA-based modification process seems to be more effective for the introduction of chemical functional groups on the surface of PDMS, which enabled the attachment of biomolecule receptors and thus the fabrication of biosensors.

The topographic and phase images obtained by AFM (Fig. 3) show that the unmodified PDMS surface is topographically flat as well as structurally and chemically homogeneous. In all cases, the modified surfaces upon each modification step exhibit from slight to dramatic variations in topography and composition, depending on the applied procedure. Branch-like structures can be observed on the PVA-modified surfaces (also shown in Fig. 3), which are likely to be related to the linear structure of the PVA polymer chains randomly adsorbed on to the PDMS. Furthermore, the PDMS surface significantly changed upon the silanisation process with TESU and a honeycomb-like polymeric structure was imaged (last two images of Fig. 3). Here, a polymerisation process could have taken place among the TESU molecules starting at those ones attached to the PDMS surface, which could somewhat act as nucleation points for the growing of such a polymer layer eventually covering the entire substrate. The adsorption of PEG did not seem to affect the topography of the PDMS substrates (Fig. S6, ESI†). By contrast, the further silanisation process with TESU appeared to generate homogeneously dispersed dots, which are likely to be related to TESU-based polymer structures generated at specific positions where an isolated –OH group, coming from the adsorbed PEG molecules, appeared. As pointed out above, such big differences between PVA and PEG-modified surfaces could be explained taking into consideration that PEG contains a much lower density of –OH groups than PVA in their respective structures. These results are in good agreement with those obtained by XPS and contact angle

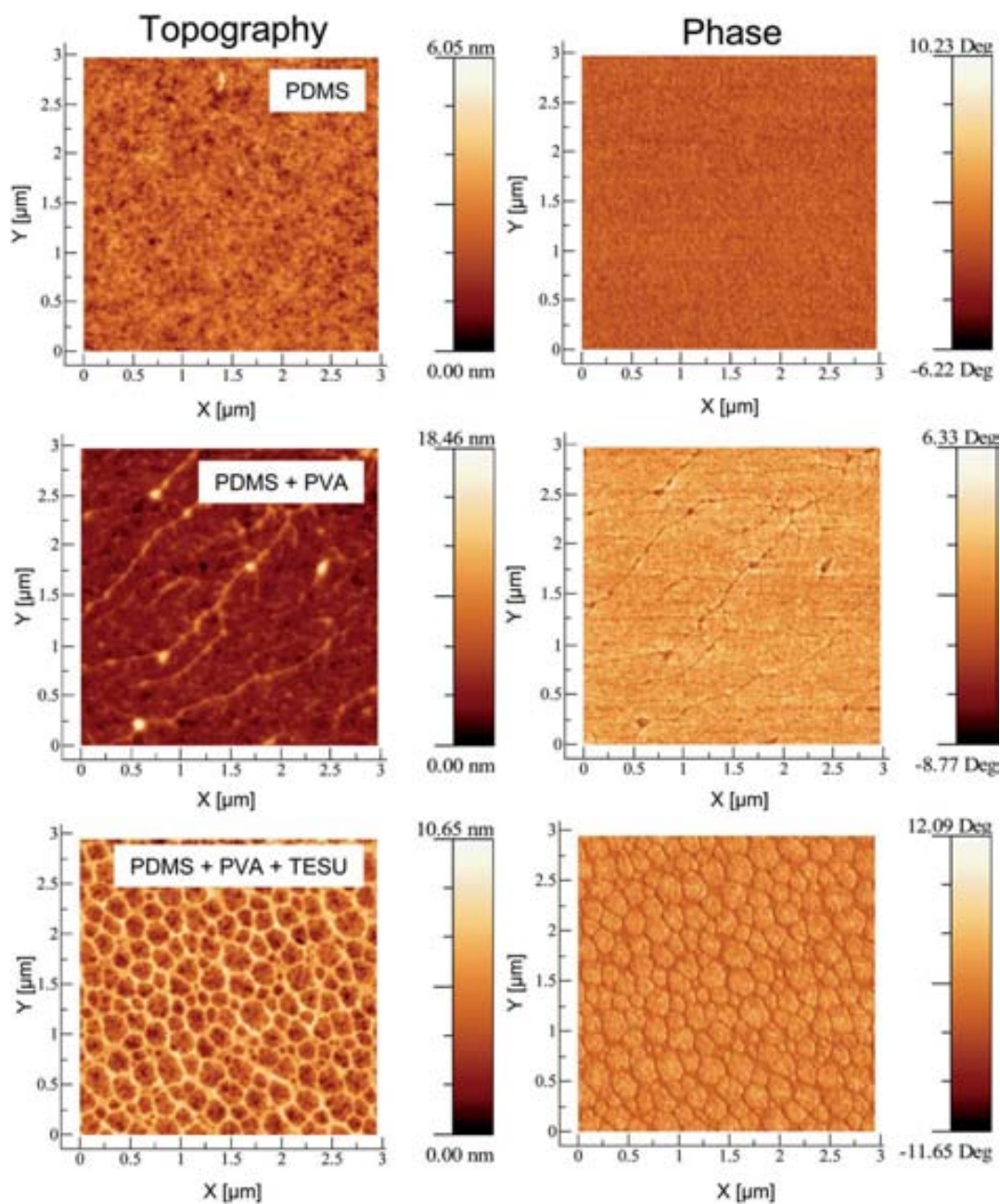


Fig. 3 Topographic and phase AFM pictures of the intact PDMS surface, after modification with PVA and after the silanization process.

measurements. Regarding the chemical oxidation process, AFM images show a surface roughness increase compared with that of the native PDMS (Fig. S7, ESI†). However, no significant differences were observed upon the silanisation process. These results indicate that the chemical oxidation process generated a very low density of $-OH$ groups on the PDMS surface and so the further silanisation with TESU appeared to slightly change the topography of these samples.

Analytical performance of the different biosensor approaches

Once the HRP receptor was immobilised on the different modified-PDMS surfaces, the analytical performance of the resulting biosensor approaches was tested in H_2O_2 solutions in

a concentration range from $0.10 \mu M$ to $100 \mu M$. The corresponding calibration plots (Fig. S8, ESI†) showed a linear increase in the measured absorbance at 420 nm up to a H_2O_2 concentration of $24.2 \mu M$. Therefore, a linear fitting was carried out in this range and the analytical parameters were calculated (Table 2). No significant differences were observed among the different approaches. Nevertheless, the estimated error was higher for the adsorption approach, this being related to the lack of control of the adsorption process itself and the reported instability of the adsorbed molecules when carried out repeated measurements with the same PhLoC. A lowest limit of detection around $0.10 \mu M H_2O_2$ was attained, this being between 10 and 100-fold lower than those values previously reported with similar analytical systems based on the use of a HRP receptor.^{19,29}

Table 1 Atomic percentages of the different surfaces extracted from the XPS survey scans

Sample	Atomic concentration (%)	
PDMS	O1s	19.71
	C1s	43.38
	Si2p	36.90
PVA	O1s	21.21
	C1s	51.74
	Si2p	27.05
PEG	O1s	19.05
	C1s	43.85
	Si2p	37.11
Oxidation	O1s	20.09
	C1s	44.92
	Si2p	34.99
PVA + TESU	O1s	21.29
	C1s	50.69
	Si2p	28.02
PEG + TESU	O1s	19.13
	C1s	45.36
	Si2p	35.51
Oxidation + TESU	O1s	20.26
	C1s	44.25
	Si2p	35.48

Table 2 Analytical parameters of the four different biosensor approaches

Modification	Sensitivity ^a /a.u. μM^{-1}	LOD ^{ab} / μM	<i>r</i>
Adsorption	0.017 \pm 0.003	0.12 \pm 0.08	0.996
PEG + TESU	0.019 \pm 0.001	0.28 \pm 0.08	0.990
PVA + TESU	0.019 \pm 0.001	0.14 \pm 0.08	0.996
Oxid. + TESU	0.021 \pm 0.005	0.10 \pm 0.01	0.998

^a Mean values and corresponding standard deviations of the parameters extracted from three calibration curves recorded with different devices in three consecutive days are represented. ^b LOD calculated following the 3σ IUPAC criteria using the lowest order of the linear concentration range from 0.1 μM to 1.53 μM .

stability. Nevertheless, the structural characterisation together with the analytical studies clearly indicate that the PVA-based approach is the one to be chosen considering the apparent higher density of chemical functional groups introduced on the PDMS surface and the longer stability of the resulting biosensor device.

Conclusions

Different chemical modification processes that enabled the introduction of hydroxyl groups on the surface of PDMS and the further attachment of a silane molecule for the selective immobilisation of a biomolecule receptor are reported. A thorough structural and analytical characterisation clearly indicated that the modification with PVA polymer is the most suitable approach for the biofunctionalisation of PDMS PhLoC systems. These processes do not require any specific instrumentation, thus enabling their easy and rapid implementation in chemical and biological laboratories working with PDMS microfluidic systems.

Acknowledgements

This work has received funding from the European Research Council under the European Community's Seventh Framework Programme (FP7/2007-2013) / ERC grant agreement no. 209243. The authors thank Dr Manuel Gutierrez for his kind help with the AFM study.

References

- 1 A. Llobera, R. Wilke and S. Büttgenbach, *Lab Chip*, 2005, **5**, 506–511.
- 2 O. Ordeig, N. Godino, J. del Campo, F. X. Muñoz, F. Nikolajeff and L. Nyholm, *Anal. Chem.*, 2008, **80**, 3622–3632.
- 3 Y. Xia and G. M. Whitesides, *Annu. Rev. Mater. Sci.*, 1998, **28**, 153–184.
- 4 S. K. Sia and G. M. Whitesides, *Electrophoresis*, 2003, **24**, 3563–3576.
- 5 H. Makamba, J. H. Kim, K. Lim, N. Park and J. H. Hahn, *Electrophoresis*, 2003, **24**, 3607–3619.
- 6 D. S. Gray, J. Tien and C. S. Chen, *J. Biomed. Mater. Res., Part A*, 2003, **66**(3), 605–614.
- 7 D. W. Lee and Y. S. Choi, *Microelectron. Eng.*, 2008, **85**, 1054–1058.
- 8 A. Crespi, Y. Gu, B. Ngamson, H. J. W. M. Hoekstra, C. Dongre, M. Pollnau, R. Ramponi, H. H. van den Vlekkert, P. Watts, G. Cerullo and R. Osellame, *Lab Chip*, 2010, **10**, 1167–1173.
- 9 B. Ibarlucea, E. Fernández-Rosas, J. Vila-Planas, S. Demming, C. Nogues, J. A. Plaza, S. Büttgenbach and A. Llobera, *Anal. Chem.*, 2010, **80**, 4246–4251.
- 10 X. Fang, Y. Liu, J. Kong and X. Jiang, *Anal. Chem.*, 2010, **82**, 3002–3006.

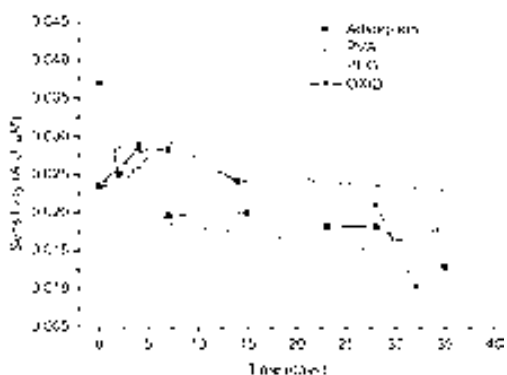


Fig. 4 Operational stability of the different PhLoC approaches measured as the sensitivity of the calibration plots sequentially recorded over a 35 day period.

Additionally, the sensitivity of the modified PhLoC improved 150 times when compared with another reported application using the same system.²²

Finally, the operational stability of the PhLoC was systematically tested for over a month. Fig. 4 shows the shift in the sensitivity values with time. Two different trends were observed. Those devices based on the adsorption and PEG-modification processes show a rapid decrease in the sensitivity values during the first week of operation while those based on PVA-modification and chemical oxidation processes remained more stable for at least one month. However, a clear shift towards lower sensitivity values was observed for the oxidation approach after one month of operation while it was estimated that the PVA-based one retained 82% of its initial sensitivity after two months of operation.

Overall, from the results presented above, the PVA and oxidation approaches gave rise to the PhLoC systems with a better analytical performance in terms of reproducibility and

- 11 V. Srinivasan, V. K. Pamula and R. B. Fair, *Anal. Chim. Acta*, 2004, **507**, 145–150.
- 12 J. C. McDonald and G. M. Whitesides, *Acc. Chem. Res.*, 2002, **35**(7), 491–499.
- 13 B. Huang, H. Wu, S. Kim and R. N. Zare, *Lab Chip*, 2005, **5**, 1005–1007.
- 14 Y. Bai, C. G. Koh, M. Boreman, Y. J. Juang, I. C. Tang, L. J. Lee and S. T. Yang, *Langmuir*, 2006, **22**, 9458–9467.
- 15 I. Wong and C. M. Ho, *Microfluid. Nanofluid.*, 2009, **7**, 291–306.
- 16 D. Bodas and C. Khan-Malek, *Sens. Actuators, B*, 2007, **123**, 368–373.
- 17 Y. Berdichevsky, J. Khandurina, A. Guttman and Y. H. Lo, *Sens. Actuators, B*, 2004, **97**, 402–408.
- 18 G. Sui, J. Wang, C. C. Lee, W. Lu, S. P. Lee, J. V. Leyton, A. M. Wu and H. R. Tseng, *Anal. Chem.*, 2006, **78**(15), 5543–5551.
- 19 A. Llobera, R. Wilke and S. Büttgenbach, *Lab Chip*, 2004, **4**, 24–27.
- 20 L. Yu, C. M. Li, Q. Zhou and J. H. T. Luong, *Bioconjug. Chem.*, 2007, **18**(2), 281–284.
- 21 P. T. Charles, V. R. Stubbs, C. M. Soto, B. D. Martin, B. J. White and C. R. Taitt, *Sensors*, 2009, **9**, 645–655.
- 22 A. Llobera, R. Wilke and S. Büttgenbach, *Talanta*, 2008, **75**, 473–479.
- 23 B. H. Jo, L. M. Van Lerberghe, K. M. Motsegood and D. J. Beebe, *J. Microelectromech. Syst.*, 2000, **9**(1), 76–81.
- 24 M. L. Hair and C. P. Tripp, *Colloids Surf., A*, 1995, **105**, 95–103.
- 25 L. Ferreira, M. A. Ramos, J. S. Dordick and M. H. Gil, *J. Mol. Catal. B: Enzym.*, 2003, **21**, 189–199.
- 26 E. N. Kadnikova and N. M. Kostic, *J. Mol. Catal. B: Enzym.*, 2002, **18**, 39–48.
- 27 A. Mata, A. J. Fleischman and S. Roy, *Biomed. Microdevices*, 2005, **7**(4), 281–293.
- 28 H. Hillborg, J. F. Ankner, U. W. Gedde, G. D. Smith, H. K. Yasuda and K. Wikström, *Polymer*, 2000, **41**, 6851–6863.
- 29 M. Tamasko, L. Nagy, E. Mikolas, G. A. Molnar, I. Wittman and G. Nagy, *Physiol. Meas.*, 2009, **28**, 1533–1542.

Supplementary Information for

Selective functionalization of PDMS-based photonic lab on a chip for biosensing

Bergoi Ibarlucea^a, César Fernández-Sánchez^{a,*}, Stefanie Demming^b, Stephanus Büttgenbach^b and Andreu Llobera^{a,*}

^a Instituto de Microelectrónica de Barcelona, IMB-CNM (CSIC), Campus UAB, 08193, Bellaterra, Spain

^b Institut für Mikrotechnik, Technische Universität Braunschweig, 38124-Braunschweig, Germany.

* To whom correspondence should be addressed: andreu.llobera@imb-cnm.csic.es, cesar.fernandez@imb-cnm.csic.es

Contents:

Figures S1-S8

Table S1

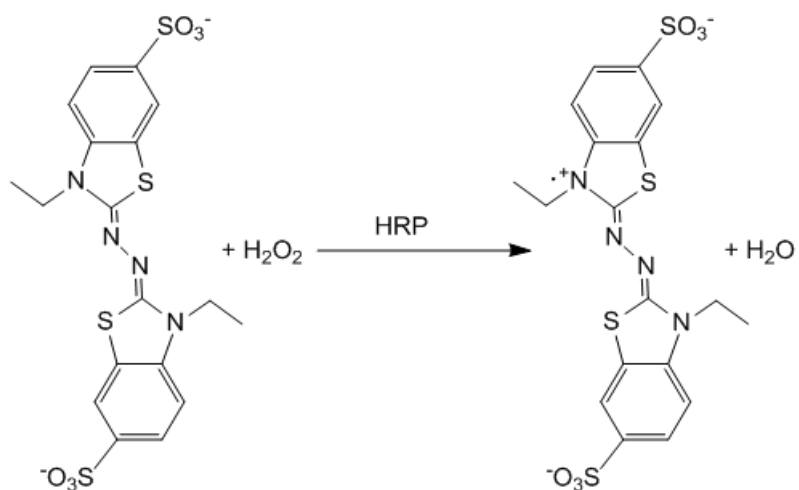


Figure S1. HRP-catalyzed reduction of hydrogen peroxide mediated by colourless ABTS, which generates water and green-colour ABTS radical cation counterpart.

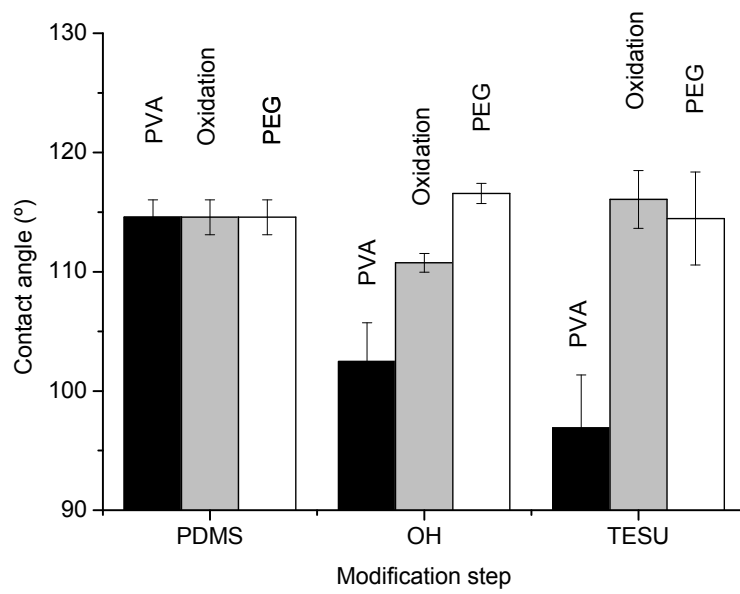


Figure S2. Contact angle values measured following every step of each modification procedure. Error bars correspond to the standard deviation of three replicates.

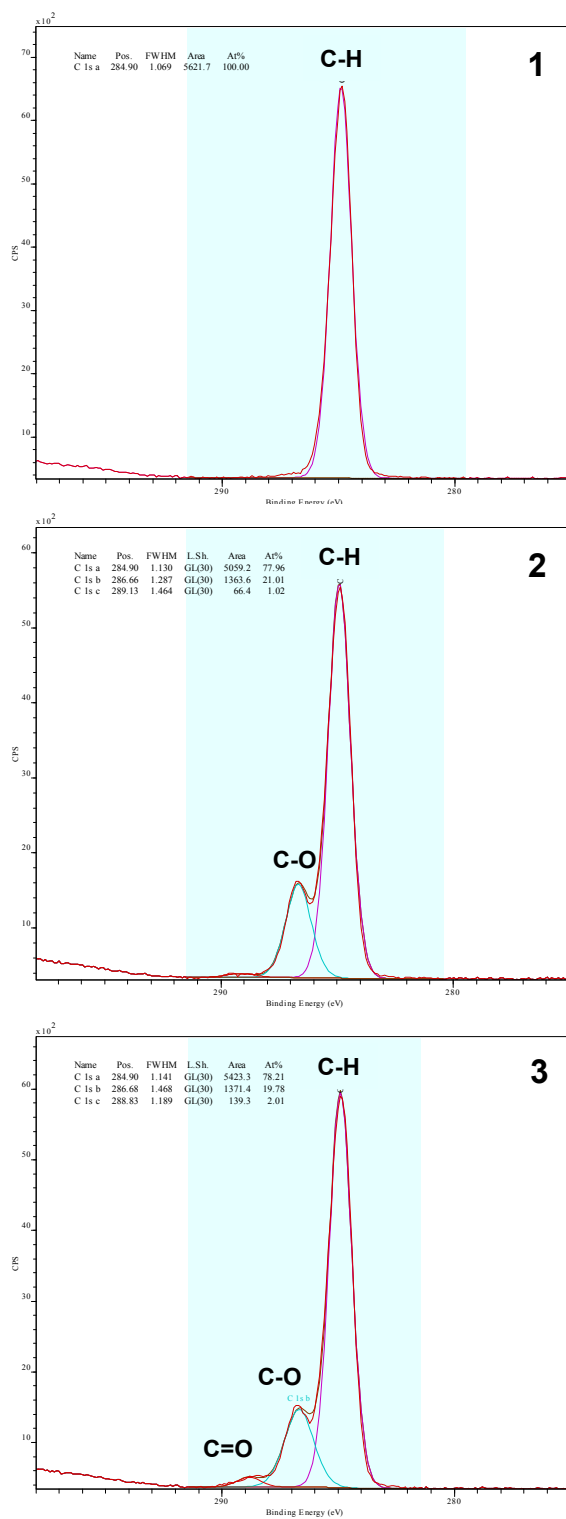


Figure S3. High resolution XPS spectra of the C (1s) region corresponding to intact PDMS (1), after the adsorption of PVA (2) and after the silanisation process with TESU (3).

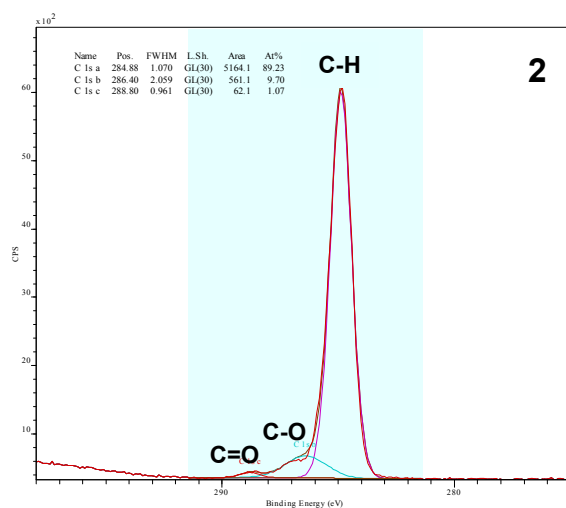
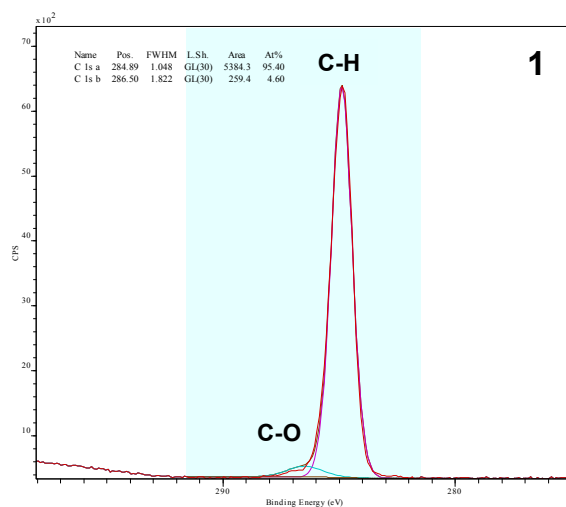


Figure S4. High resolution XPS spectra of the C (1s) region corresponding to PEG-modified PDMS before (1) and after (2) the silanization process with TESU.

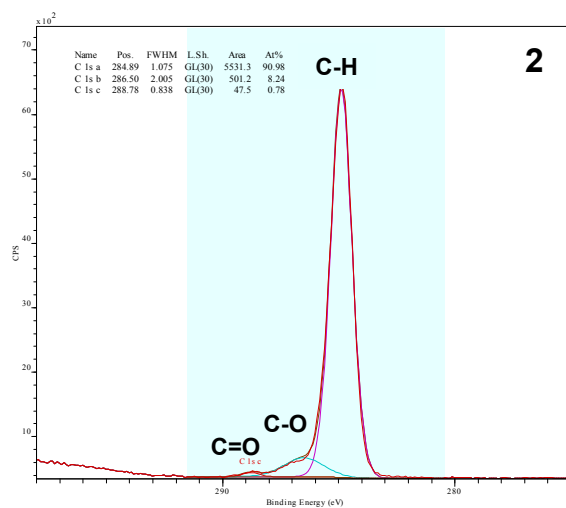
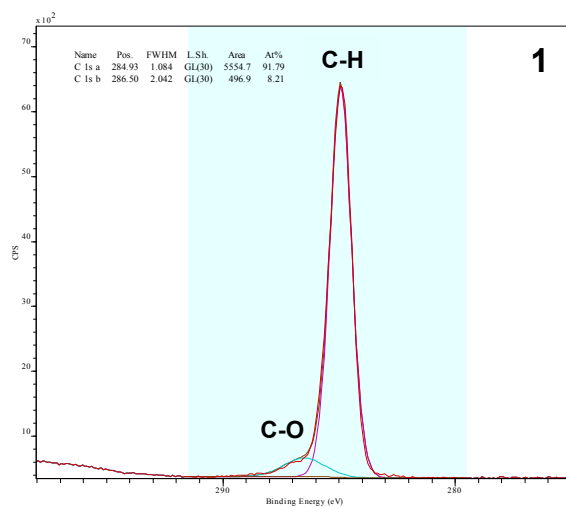


Figure S5. High resolution XPS spectra of the C(1s) region corresponding to PDMS after the chemical oxidation (1) and after the silanisation process (2).

Sample	Bond	Position / eV	Atomic percentage
PDMS	C-H	284.90	100
PDMS+ PVA	C-H	284.90	77.96
	C-O	286.68	22.06
PDMS +PVA+ TESU	C-H	284.90	78.21
	C-O	286.68	19.78
	C=O	288.83	2.01
PDMS+ PEG	C-H	284.89	95.40
	C-O	286.50	4.60
PDMS + PEG + TESU	C-H	284.89	89.23
	C-O	286.50	9.70
	C=O	288.80	1.07
Oxidation	C-H	284.93	91.79
	C-O	286.50	8.21
Oxidation + TESU	C-H	284.93	90.98
	C-O	286.50	8.24
	C=O	288.78	0.78

Table S1. C percentages corresponding to the different chemical groups introduced on the PDMS surface alter each modification step.

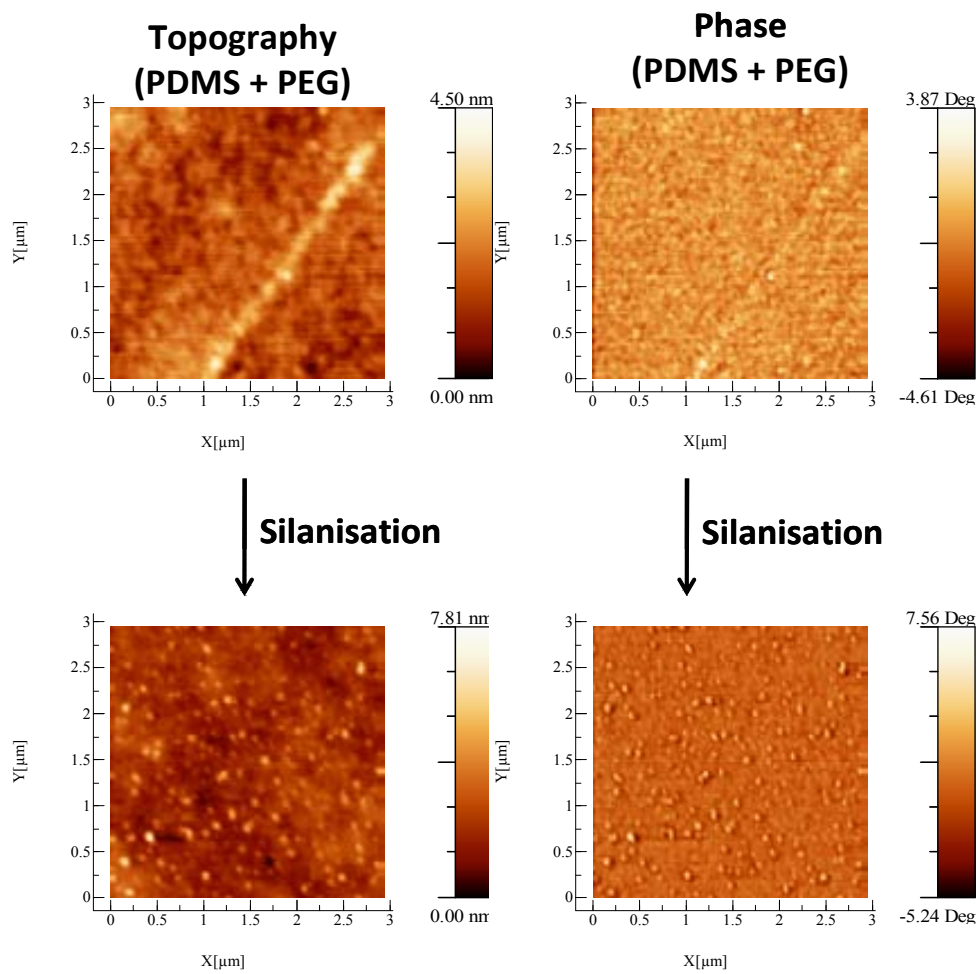


Figure S6. Topographic and phase AFM pictures of the PDMS surface after the modification with PEG and further silanisation with TESU.

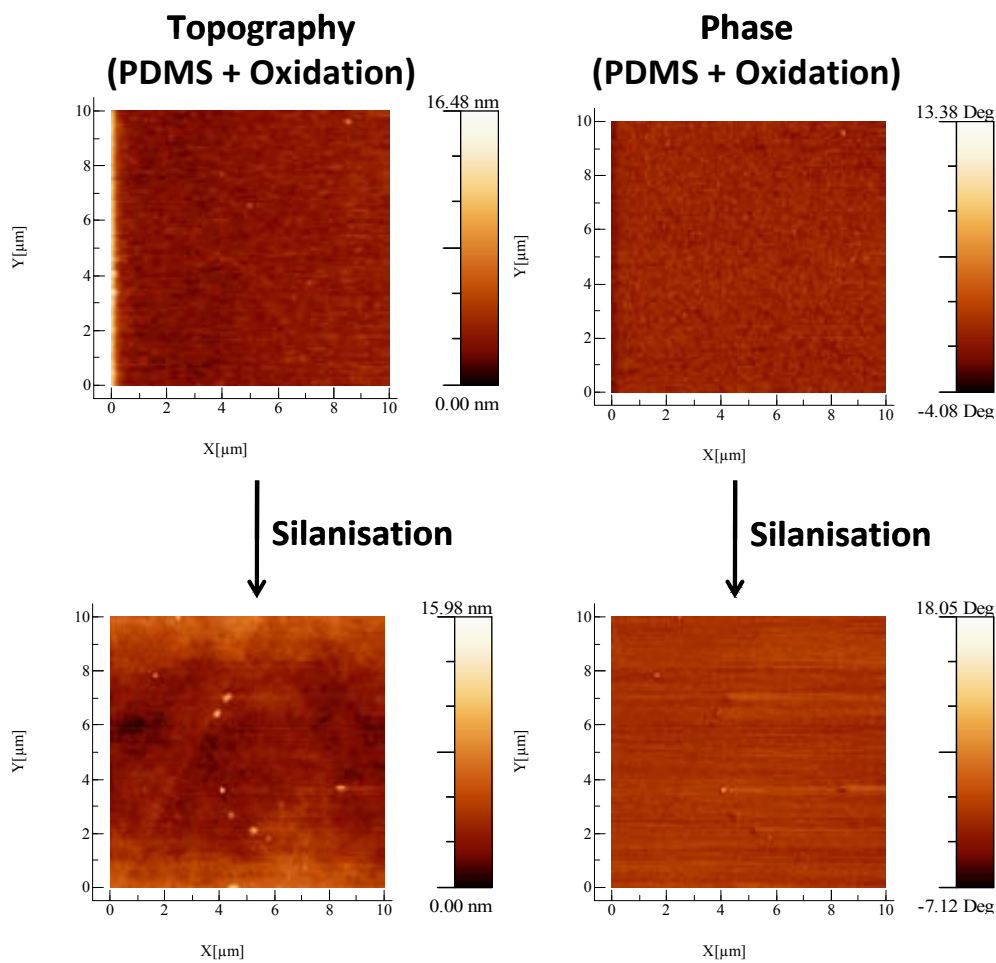


Figure S7. Topographic and phase AFM images of the PDMS surface after the chemical oxidation and further silanisation with TESU.

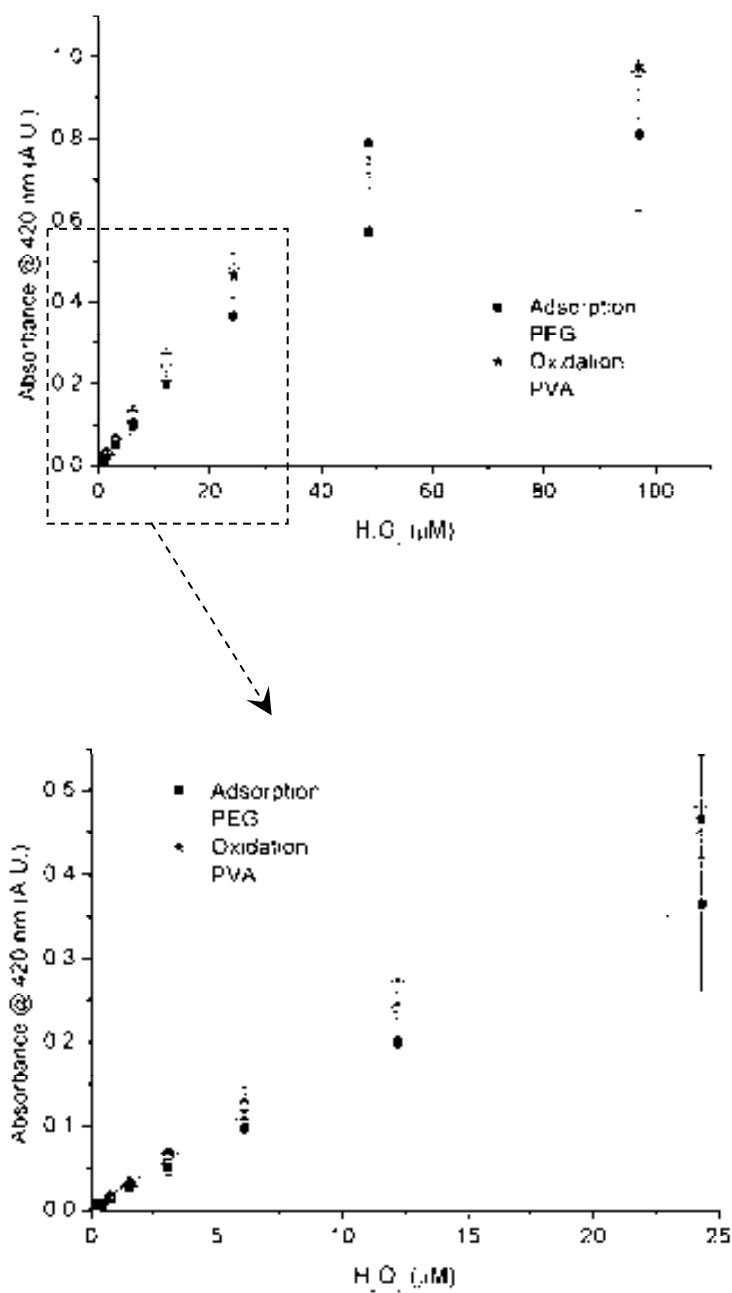


Figure S8. Calibration plots recorded with the different biosensor approaches. Each point is the mean value obtained for each hydrogen peroxide concentration in three different experiments, the error bars being the corresponding standard deviation. A linear range from 0 to 24.3 μM H₂O₂ was obtained in all cases.

Biofunctionalization of PDMS-based microfluidic systems

Bergoi Ibarlucea¹, César Fernández-Sánchez¹, Stefanie Demming², Stephanus Büttgenbach² and Andreu Llobera^{1,2}

¹Instituto de Microelectrónica de Barcelona, IMB-CNM (CSIC), Campus UAB, 08193 Bellaterra (Barcelona), Spain. ²Institut für Mikrotechnik, Technische Universität Braunschweig, 38124 Braunschweig, Germany.

Correspondence should be addressed to A.L. (andreu.llobera@imb-cnm.csic.es) and C.F.-S. (cesar.fernandez@imb-cnm.csic.es)

Laboratory Group: Chemical Transducers Group

Subject Term: Chemical Modification

Keywords: PDMS, biofunctionalization, microfluidics, lab-on-a-chip

Abstract

Three simple approaches for the selective immobilization of biomolecules on the surface of poly(dimethylsiloxane) (PDMS) microfluidic systems that do not require any specific instrumentation, are described and compared. They are based in the introduction of hydroxyl groups on the PDMS surface by direct adsorption of either polyethylene glycol (PEG) or polyvinyl alcohol (PVA) as well as by a liquid-based oxidation step. The hydroxyl groups are then silanized using a silane containing an aldehyde end-group that allows the surface to interact with a primary amine moiety of the biomolecule structure to be immobilized. The entire process takes 4.5h. The required steps can be characterized in less than 15 hours by contact angle measurements, X-ray photoelectron spectroscopy (XPS) and atomic force microscopy (AFM). The performance of the biofunctionalization process can be assessed by using peroxidase enzyme as a model biomolecule. Its correct immobilization and stability is easily tested by developing an analytical approach for hydrogen peroxide (H₂O₂) detection in the biofunctionalized microfluidic system and carrying out analytical measurements for a period of up to two months.

Introduction

Microfluidic systems have been highly evolving with the simultaneous development of polymer materials. Polymer technology has been key in the realization and definition of the so-called Lab-on-a-Chip (LoC) concept. The current high impact of LoC systems is partly due to the application of polymers such as polycarbonate (PC), poly (methyl methacrylate) (PMMA), SU-8 and poly(dimethylsiloxane) (PDMS), which have made them more versatile while in turn have enabled reducing their fabrication cost and time. PDMS (Figure 1a) is a cheap material that polymerizes at low temperatures¹. It is optically transparent in a very wide wavelength range, from ultra-violet (UV) to the Near-Infrared (NIR)². This last property makes the material compatible with many optical detection methods. It is also compatible with biological studies, since it is non-permeable to water, non toxic and permeable to gases. PDMS is an elastomer with a 2.5 MPa Young modulus when prepared with a 10:1 ratio of a base:curing agent³. Cast molding of the as-prepared PDMS provides a rapid fabrication of microsystems with resolution down to 0.1 μm ⁴. The resulting systems can easily be sealed to many different substrates³. When LoCs are fabricated with PDMS, low-cost systems can be obtained with the potential of being highly sensitive. However, this polymer has a disadvantage: biomolecules and other macromolecules easily adsorb non-specifically to it, thus hindering its application for chemical sensing. This disadvantage can easily be turned into an advantage as it can easily be modified in order to avoid that process or, by contrast, to selectively immobilize different molecules². These surface modification processes are usually needed for the application of PDMS-based microsystems to (bio)chemical analysis. The aims of the modification are diverse and include from the minimization of the biomolecular adsorption, to the increase of the hydrophilic/hydrophobic character of the surface. Some processes are directed to bind a biologically active molecule that changes the lubricity of the surface⁵ or provides the material with the capacity to give a selective answer to a specific target analyte by binding antibodies⁶ or enzymes⁷.

Biofunctionalization of PDMS surfaces can be carried out following two different strategies: physical adsorption and covalent modification. The first one is very simple but, due to the weak interactions between the adsorbed molecules and the surface, the modifications are instable both thermally and mechanically. Also, solvolytic processes can also occur. Covalent modification can overcome these problems and provide more stable modifications⁸. It is carried out by the initial introduction of hydroxyl groups ($-\text{OH}$) on the PDMS surface, which can further be modified by a silanization process. These hydroxyl groups react with silane molecules to form covalent Si-O-Si (siloxane) bonds. Different functional groups, to which the biomolecules can be covalently attached, are introduced on the surface depending on the chosen silane⁹. In this context, PDMS surfaces have been treated with oxygen plasma¹⁰ or UV/ozone¹¹, in order to make the surface hydrophilic by replacing the surface methyl groups, bound to the Si atom within the PDMS structure, by silanol groups (Si-OH). These new groups tend to chemically interact with other functional groups, allowing to selectively modify the surface. Silanol groups can be useful as an initial step in the PDMS surface modification for covalently binding enzymes, as Yasukawa *et al.* did⁷. They immobilized glucose oxidase on a PDMS layer after a hydrophilization step using a plasma process and further silanization, with the aim of fabricating a glucose sensor. Sandison *et al.* made also use of a plasma and silanization process to immobilize antibodies on a PDMS column for protein purification applications¹². But this process also has some drawbacks: the modification is temporal because the plasma oxidized surface progressively recovers its hydrophobicity. It also requires special instrumentation and cannot be applied in the microfluidic channels of LoCs¹³. This means that alternative processes

must be found to selectively modify PDMS surfaces, which were easy to implement and could be applied in channels embedded in PDMS matrices.

The previously mentioned UV/ozone treatment could be an alternative process. The modification consists in firstly generating ozone from molecular oxygen by 185 nm wavelength light exposition and then photodissociating it to atomic oxygen under 254 nm wavelength light exposure. This oxygen abstracts hydrogen from the backbone of PDMS and silanol (Si–OH) structures are formed on it, becoming a hydrophilic surface¹⁴. This treatment is slower than a plasma activation process¹⁵ but it facilitates a much deeper modification without cracking or mechanical weakening side-effects¹¹. This fact enables its application to the microchannels. But, as pointed out before, the process is reversible, and PDMS surface eventually recovers its hydrophobicity after exposure to air for a few hours.

Chemical Vapour Deposition (CVD) can also be used to create polymer coatings on PDMS microchannels, as Chen and Lahann did for the eventual deposition of poly(4-benzoyl-p-xylylene-co-p-xylylene) films. A light reactive coating film of carbonyl groups was obtained, which was exposed to UV light in order to generate the free radicals that could react with poly(ethylene oxide) (PEO) and create PEO-functionalized regions that avoided the adsorption of fibrinogen¹⁶.

Silanol groups can also be obtained on PDMS surfaces by using sol–gel methods. Silica nanoparticles can be created in a PDMS piece by mixing it in a tetraethyl orthosilicate (TEOS) sol–gel precursor and then incubating it in an ethylamine catalyzing solution and heating it¹⁷. Glasslike layers can also be formed on a PDMS surface by applying the same sol–gel technique with transition metal sol-gel precursors¹⁸. However, these sol-gel methods are time consuming and therefore the production costs increase.

An acidic solution containing hydrogen peroxide (H₂O₂) can also be pumped inside the microchannels, which oxidizes the PDMS surface and creates silanol groups¹³. The process should be carefully controlled since an excess of acidity could lead to a loss of optical transparency of the PDMS.

Physical adsorption methods can also be applied for PDMS microchannel modification. These methods are applied to suppress electroosmotic flow in capillary electrophoresis and to avoid nonspecific binding of proteins. The hydrophobic parts of molecules can be physisorbed onto the PDMS surface while the hydrophilic parts keep exposed to the buffer, thus changing the surface properties of the PDMS. A coating process of polymers that contain hydrophobic and hydrophilic parts can be achieved by simply incubating the surface with the aqueous coating solution¹⁹. The so-called Layer by Layer (LBL) technique can also be carried out by electrostatic adsorption of positively and negatively charged alternating layers²⁰.

Here, the details of the protocol used in a previous work²¹ for different liquid-based surface chemical biofunctionalization methods are provided. The developed methods can easily be performed in standard chemical and biological laboratories avoiding the need of special instrumentation. Both physical adsorption and covalent modification methods are analyzed. On one hand, physical adsorption of two different polymers containing hydroxyl groups, such as polyethylene glycol (PEG) or polyvinyl alcohol (PVA) (figure 1b) enable the further silanization of the surface for the introduction of chemical functional groups and the eventual covalent immobilization of the bioreceptor. In some applications, as Yu *et al* did²², the aim of the PVA immobilization was to avoid the non-specific binding of proteins. Other groups used

PEG instead of PVA, since it offers the same advantage^{23,24}. In the present application, the objective is totally different. These polymers are used as anchoring points for further silanization and final protein receptor immobilization. On the other hand, a covalent modification approach was tested based on the chemical oxidation of the PDMS surface that generates silanol groups (figure 1c) onto which a silanization process and further immobilization of the protein receptor are carried out, as above. This chemical oxidation protocol was already described by Sui *et al.* for creating hydroxyl groups that could be used as anchoring points for the immobilization of other molecules¹³. A deep structural characterization of the resulting modified surfaces is carried out. The analytical performance and the stability of the modified surfaces following the different methods are also tested using a PDMS-based photonic LoC (PhLoC) microsystem consisting of a hollow Abbe prism transducer configuration²⁵.

Experimental design

Modification of the PDMS surfaces

As it can be seen in Figure 2, the proposed three approaches for PDMS surface modification are based on the introduction of hydroxyl (-OH) groups and further silanization. PDMS surfaces were cleaned with ethanol and deionized water (DI H₂O). For the modification shown in Figure 2A, the PDMS surfaces were incubated in a PEG solution and left to adsorb. For the modification in Figure 2B, they were incubated in a PVA solution and left to adsorb. The backbone of these two polymers is able to physisorb from aqueous solutions to hydrophobic surfaces²⁶. The third approach was carried out by a chemical oxidation process with an acidic solution containing DI H₂O, HCl and H₂O₂¹³ (Figure 2C). After each of these steps, the surfaces were rinsed with DI H₂O and dried.

For the previously mentioned silanization process, the modified PDMS systems were incubated in 11-triethoxysilyl undecanal (TESU) and triethylamine (TEA) containing ethanol solutions. Then the surfaces were thoroughly rinsed with ethanol and dried. The TEA induces a highly nucleophilic oxygen in the -OH group that readily interacts with the chosen silane²⁷ having its ethoxy groups previously hydrolyzed. In this way, the silane molecules covalently bound to the surface (Figure 3).

Characterization of the PDMS surfaces

For the characterization process, flat PDMS surfaces were modified. The techniques used for this characterization were contact angle measurements, XPS and AFM.

Contact angle measurements were carried out with the sessile drop method. Images with a high contrast should be obtained with the camera of the angle meter, with as less light reflections as possible in the drop. If these conditions are hold, the software is able to automatically detect the shape of the drop and measure the contact angle.

XPS analysis was carried out on an Axis Ultra-DLD spectrometer, using a monochromatized Al K α source (1486.6 eV). Signals were deconvoluted with the software provided by the manufacturer, using a weighted sum of Lorentzian and Gaussian component curves after background subtraction. The binding energies were referenced to the internal standard C 1s (284.9 eV).

Atomic force microscopy topographic and phase images of the modified surfaces were taken with a Veeco Nanoscope Dimension 3100, working in tapping mode and using phosphorous doped n-type silicon tips (Micromasch, San Jose, CA, USA).

MATERIALS

REAGENTS

- Poly(dimethylsiloxane) (PDMS) Sylgard 184 elastomer kit (Dow Corning)
- Polyvinyl alcohol 99% (PVA, molecular weight: 89,000-98,000g) (Sigma-Aldrich Co., cat. no. 341584)
- Polyethylene glycol (PEG, molecular weight: 12,000g) (Sigma-Aldrich Co., cat. no. 81285)
- Triethylamine 99% (TEA) (Sigma-Aldrich Co., cat. no. T0886) **! CAUTION** Corrosive, Highly flammable
- 11-triethoxysilyl undecanal 90% (TESU) (ABCR GmbH & Co. KG, cat. no. AB152514) **! CAUTION** Irritant

EQUIPMENT

- Automatic pipettes with disposable tips
- Krüss Easydrop contact angle meter and DS1 analysis software (Krüss GmbH)
- Axis Ultra-DLD spectrometer (Kratos Analytical Ltd)
- Atomic Force Microscope: Veeco Nanoscope Dimension 3100 (Veeco)
- AFM tips (Micromasch): n-type silicon tip (phosphorous doped) (NSC15/AIBS)

REAGENT SETUP

PVA solution: dissolve 25 mg in 25 mL DI H₂O. **? TROUBLESHOOTING** High temperature (60 °C) and stirring is needed to dissolve it.

PEG solution: dissolve 25 mg in 25 mL DI H₂O.

TESU solution: dilute 50 µL TESU and 50 µL TEA in 2.5 mL ethanol 99.5%. **! CAUTION** Avoid the vapors coming from TEA by preparing the solution mix in a fume hood.

PROCEDURE

Modification of the PDMS surfaces

- 1 | Clean flat PDMS surfaces: first with ethanol 96% and then with DI H₂O. **? TROUBLESHOOTING.** Flat PDMS surfaces are used for an easier characterization of the resulting modifications.
- 2 | Create hydroxyl groups on the PDMS surface. Select the appropriate chemistry protocol:
 - A. Modification with PEG: immerse the PDMS in a 1 mg/ml PEG solution in DI H₂O. Leave to react for 1 hour. Then rinse with DI H₂O and dry with N₂.
 - B. Modification with PVA: immerse the PDMS in a 1 mg/ml PVA solution in DI H₂O. Leave to react for 1 hour. Then rinse with DI H₂O and dry with N₂.
 - C. Chemical oxidation: immerse the PDMS in an acidic solution containing DI H₂O, 37% HCl and 30% H₂O₂ in a 5:1:1 (v/v/v) ratio¹⁸. Then rinse with DI H₂O and dry with N₂. **? TROUBLESHOOTING.** This step can generate bubbles on the PDMS surface. Try to avoid them as far as possible by stirring the media. **! CAUTION** Avoid the HCl vapors by carrying out this step in a fume hood. Use gloves, since apart from the acidic conditions of the liquid mixture, a direct contact with H₂O₂ could lead to a whitish irritating skin color.

3 | Create aldehyde groups on the PDMS surface by incubating them in a 99.5% ethanol solution containing 2% TESU and 2% TEA for 1 hour. Then rinse with 99.5% ethanol and dry them at 80°C for 2 hours. **! CAUTION** Avoid the vapors coming from TEA by preparing the solution mix in a fume hood. **? TROUBLESHOOTING**. This step should be done in a closed container and using enough solvent to avoid the total evaporation of the liquid. It should be carried out in an inert atmosphere like nitrogen or argon without humidity presence.

■ PAUSE POINT After this step, systems can be stored overnight at 4°C in carbonate buffer pH 8.

Characterization of the modified PDMS surfaces

4 | Measure the contact angle with a contact angle meter: deposit a drop of water on the modified PDMS surfaces and compare the angle formed between the drop and the surface to the angle formed using a non-modified PDMS surface. Make several drops and calculate the mean value of the angle and its standard deviation. **? TROUBLESHOOTING**. Try to always use the same drop size. Try to obtain pictures with a high contrast to facilitate the automatic detection of the drop shape by the software of the contact angle meter. There should only appear one drop in each picture acquired by the camera. If there are more drops, the software could understand that the other drops form part of the drop that should be detected.

5 | Make an XPS analysis of the modified and non-modified PDMS surfaces. Use a monochromatized Al K α source or similar (1486.6 eV). Deconvolute the signals using a weighted sum of Lorentzian and Gaussian component curves after background subtraction.

6 | Obtain topographic and phase images by using an atomic force microscopy in tapping mode. In this mode, the cantilever oscillates up and down at its resonance frequency. The interaction between the tip and the surface when they come close causes a decrease of the oscillation amplitude, and the control system changes the height of the cantilever to maintain this amplitude constant. In phase images, changes in phase oscillations give information about the different type of materials that can be found on the surface. Topographic images give information about the surface roughness. **? TROUBLESHOOTING** Try to avoid an excess of contact between the tip and the surface because PDMS is a soft material and its deformation caused by the tip could appear in the pictures as noise. By contrast, if the distance between the surface and the tip is too large, a flat surface could be recorded.

? TROUBLESHOOTING

Troubleshooting advices are presented in Table 1

Table 1| Troubleshooting table.

Step	Problem	Possible reason	Solution
2 B	PVA does not dissolve correctly	The needed time, temperature or stirring has not been applied	The solution should be left for 30 min at 60 °C with enough stirring using a magnetic stirrer (the revolutions per minute should be experimentally considered by the performer)
2 C	PDMS becomes white during the chemical oxidation	HCl concentration is too high or oxidation time is too long	Decrease the HCl concentration or oxidation time
3	The surface appears totally dry after the required incubation time	The solvent evaporates	Use more solvent and a closed container.
4	The shape of the drop is not correctly detected by the software of the contact angle meter	There may be too many light reflections or more drops on the surroundings	Try to use the correct light conditions to avoid reflections in the drop. There should only appear one drop in each acquired

			picture
5	Unexpected bonds or elements are found on the XPS analysis	The sample is contaminated	Preserve the samples in inert atmosphere (N ₂ or Ar) until the XPS analysis
6	There is too much noise in the AFM picture	The PDMS deforms when the tip of the AFM touches it	Increase the distance between the surface and the tip
6	The surface in the AFM picture is completely flat	The distance between the tip and the surface is too large	Decrease the distance between the surface and the tip

• TIMING

Steps 1-3 Modification of the PDMS surfaces: 4h 30 minutes

Steps 4-6: Characterization of the modified PDMS surfaces: 30 minutes for the contact angle measurements, 7 hours for the XPS analysis, 7 hours for the AFM.

ANTICIPATED RESULTS

This protocol allows the selective and stable modification of PDMS substrates with biomolecules containing primary amine groups.

The processes described do not require any specific instrumentation, thus enabling the easy and rapid implementation in chemical and biological laboratories that work with PDMS-based microfluidic systems.

Structural characterization of the modified PDMS surfaces

Three different approaches were chosen for the modification of PDMS with the aim of providing different densities of hydroxyl groups on the surface and studying the influence on the immobilization of proteins and their eventual analytical performance. A higher density was expected for the PVA adsorption comparing to the PEG adsorption, due to the nature of their chemical structure. The conditions for the chemical oxidation process were set by an optimization study. It could be seen that a higher concentration of hydrogen peroxide and HCl or longer incubation times degraded the PDMS surface too much. The step for the introduction of aldehyde groups was the same for all the procedures. This molecule enables the one-step covalent immobilization of the enzyme.

Contact angle measurements provided a rapid estimation of the degree of modification after each step by simply measuring the hydrophobic/hydrophilic character of the modified surface. Given the hydrophobic nature of the PDMS but the hydrophilic nature of groups sequentially introduced on its surface, a steady decrease in the water contact angle was expected. Once hydroxyl groups were introduced by PVA adsorption, a clear change from the 114.57° contact angle of the native PDMS to 102.47° of the PVA-modified surface was measured. The value found in the native PDMS was similar to that reported in previous studies²⁸. This decrease was not observed after the PEG adsorption. This is likely to be related to the lower density of hydroxyl groups that PEG provides. PEG only presents two hydroxyl groups at both ends of its chain, while PVA contains these groups all along its whole linear structure. The higher amount of introduced hydroxyl groups should facilitate the incorporation of a higher number of silane

molecules during the silanization step. This step also gave rise to another change in the contact angle value when working with the PVA-modified surfaces, which decreased to 96.9°. However no difference was observed in the PEG-modified surfaces, which also suggests a low density of silane molecules on the PDMS surface and in turn corroborates the above-mentioned assumption that the number of silanol groups introduced by this modification approach is rather low. Also, no changes in the contact angle values were obtained following each step of the chemical oxidation approach. Again, this light chemical oxidation process may give rise to a low density of silanol groups and of silane molecules on the PDMS surface. The values were plotted in a bar graph, which can be found in Figure 4.

A more in depth study of the surface modification processes was carried out by XPS analysis. With this technique an identification and rough estimation of the density of the introduced groups during the modification steps can be done. The percentage values of the different atoms present on the PDMS surface were extracted from the XPS survey scan. They are shown in Table 2. The carbon percentage increased after the PVA adsorption, from 43.38% to 51.74%, while the Si content decreased from 36.90% to 27.05%. This was a consequence of the adsorption of PVA molecules on the PDMS surface. The changes were not so clear in the surfaces prepared by the other procedures. High resolution spectra of the C1s region were recorded for the detection of the new peaks formed by the introduced groups. The deconvolution of the C1s region showed that new peaks appeared after each PDMS modification step (Figures 5, 6 and 7). The non-modified PDMS presented one peak with a binding energy of 284.90 eV. This peak corresponded to the carbon atom of the methyl group. After the different steps that introduce hydroxyl groups on the surface, a new peak appeared with an energy of 286.50 eV, which corresponded to the C–O bond. Both PVA and PEG molecules contain this bond, but PEG has it in lower quantities, so it gave a smaller signal in the spectra, as expected. C–O bonds are not expected in the PDMS surface modified by the chemical oxidation procedure and just Si–OH groups should be detected. However, it is reported that oxidation of PDMS could give rise to hydroxyl groups that are bound to the carbon atom of the methyl groups²⁹. This could be the reason of the presence of the C–O peak after the chemical oxidation step. Additionally, another peak was observed in all the surfaces after the silanization step. This peak corresponded to the C=O bond that is part of the aldehyde group of the applied functional silane. The highest signal was again found in the surfaces corresponding to the PVA adsorption procedure. These results reflect that the PVA modification process is more effective for the introduction of chemical functional groups on the surface of PDMS, in accordance with the contact angle measurement.

AFM studies were also carried out to the resulting surfaces after each modification steps. The recorded topographic and phase images (Figure 8) showed that the native PDMS surface was flat and structurally and chemically homogeneous. After each modification step, the modified surfaces exhibited slight or dramatic variations depending on the applied procedure. After PVA adsorption, branch-like structures could be observed (also shown in Figure 8). These branches might be related to the linear structure of the PVA polymer chains that were adsorbed to the PDMS. After the silanization process with TESU, a honeycomb-like structure was observed (last two images of Figure 8). In this case, a polymerization process could have taken place among the TESU molecules, forming a layer that covered the entire surface.

The adsorption of PEG did not seem to affect the PDMS substrates (Figure 9). By contrast, after the silanization process, homogeneously dispersed dots appeared on the surface. These might be TESU-based structures generated at the specific positions where isolated hydroxyl groups

belonging to the adsorbed PEG molecules were located. The reason for the differences between the TESU layer in the PVA modified surface and the PEG modified one may be that PEG contains only hydroxyl groups at the ends of its chain, as mentioned above.

In the case of the surfaces modified by chemical oxidation, AFM images (Figure 10) showed an increase in the roughness compared to the non-modified PDMS surface, but no changes were observed after the silanization process. This indicates that the chemical oxidation generated a very low density of hydroxyl groups, thereby making the silanization less effective.

Fabrication and stability of a biosensor approach

The described PDMS biofunctionalization approaches were applied to the modification of a photonic Abbe prism based LoC system. Horseradish peroxidase was selected as a model biomolecule. The analytical performance of the resulting modified systems was then tested by carrying out the analysis of H₂O₂. HRP was chosen because it is a widely used enzyme that exhibits a high turnover number and can be applied with a high number of different mediators. Also, as H₂O₂ is the product of many other enzymatic reactions, HRP catalysis can be coupled in more complex enzymatic systems in order to get a cascade reaction to be applied for signal amplification.

For this aim, photonic LoCs were fabricated by a cast molding process, following a previously reported protocol³⁰. The aldehyde-modified PDMS microchannels obtained after the different modification methods were incubated for 1 hour with 1 mg/mL HRP solution in carbonate buffer pH 8, getting it bound through the amine groups of its lysine residues by forming a Schiff base that is then reduced to a stable secondary amine with sodium cyanoborohydride (NaBH₃CN)³¹. The time of incubation and concentration of biomolecule could change depending on the biomolecule to be immobilized, while the used buffer has the adequate composition for the reaction to take place. The weakly and non-specifically adsorbed enzymes were removed by rinsing the surfaces with a Phosphate Buffered Saline (PBS) solution pH 8 containing Tween 20, a rinsing step commonly applied for this purpose^{32,33}. HRP catalyzes the reduction of H₂O₂ in the presence of 0.5 mM of colorless 2,2'-azino-bis (3-ethylbenzthiazoline-6-sulfonic acid) (ABTS) mediator in acetate buffer pH 5.5, which is in turn oxidized to the green-colored ABTS^{•+} radical cation³⁴ (Figure 11). This cation presents an absorption peak at 420 nm and two secondary peaks at 650 and 720 nm wavelengths. The first one was chosen for the absorbance detection of this enzymatic reaction. Since proteins can easily adsorb on the surface of native PDMS due to their high hydrophobicity⁷, a fourth LoC was modified by direct adsorption of the enzyme under the same experimental conditions applied in the other approaches and tested for comparative purposes.

The modified LoCs were stored for over two months and the operational stability of the immobilized enzyme was studied by calculating the sensitivity along with time. A better stability was expected for those systems selectively modified with the enzyme compared with that one where HRP directly adsorbed. This behavior could be anticipated considering the lack of control of the adsorption process and the fact that adsorbed proteins tend to expose the highest area possible to the surface in order to maximize this interaction, which produced irreversible changes in their structure and conformation and resulted in their extensive unfolding and inactivation³⁵.

As it can be seen in Figure 12, the absorbance at 420 nm increased together with the H₂O₂ concentration for all the tested systems. This increase was lineal in the range 0-24.3 μM H₂O₂ and then saturation occurred. A linear fitting was carried out in this range and the analytical parameters were calculated (Table 3). There were no significant differences among the different approaches, but the estimated error was higher for the adsorption approach. The lowest LOD was 0.10 μM H₂O₂. This result was between 10 and 100 times lower than the previously reported values in similar analytical systems based on the use of HRP as a receptor^{25,36}. In addition, the sensitivity of the modified PhLoC was 150 times better than in other applications using the same system³⁰.

The storage stability of the modified PhLoC systems was studied by calculating their changes in sensitivity with time, as mentioned above (Figure 13). Two different behaviors could be observed. The systems based on the modification with PEG showed a rapid decrease in the sensitivity during the first week, while those based on the PVA modification and chemical oxidation remained more stable for at least one month. However, the latter showed a decrease in the sensitivity after the first month, while the PVA-based system retained 82% of the initial sensitivity after two months.

The present results indicate that the PVA and chemical approaches provide the PhLoC systems with a better analytical performance in terms of both reproducibility and stability. The structural characterization together with the analytical studies also verify that the PVA-based procedure should be the one chosen for the modification of PDMS with enzymes considering the higher density of functional groups introduced during the modification steps and the longer stability of the resulting analytical PhLoC system.

REFERENCES

1. Makamba H., Kim J.H., Lim K., Park N., Hahn J.H. Surface modification of poly(dimethylsiloxane) microchannels. *Electrophoresis* **24**, 3607-3619 (2003).
2. McDonald J.C., Whitesides G.M. Poly(dimethylsiloxane) as a material for fabrication of microfluidic devices. *Acc. Chem. Res.* **35**(7), 491-499 (2002).
3. Gray D.S., Tien J., Chen C.S. Repositioning of cells by mechanotaxis on surfaces with micropatterned Young's modulus. *J. Biomed. Mater. Res., Part A* **66**(3), 605-614 (2003).
4. Xia Y., Whitesides G.M. Soft lithography. *Annu. Rev. Mater. Sci.* **28**, 153-184 (1998).
5. Huang B., Wu H., Kim S., Zare R.N. Coating of poly(dimethylsiloxane) with n-dodecyl-beta-D-maltoside to minimize nonspecific protein adsorption. *Lab Chip* **5**, 1005-1007 (2005).
6. Bai Y. et al. Surface modification for enhancing antibody binding on polymer-based microfluidic device for Enzyme-Linked Immunosorbent Assay. *Langmuir* **22**, 9458-9467 (2006).
7. Yasukawa, T., Maekawa, E. Mizutani, F. Immobilization of glucose oxidase on a poly(dimethylsiloxane) layer by using poly(L-lysine) as a polymer backbone. *Anal. Sci.* **25**, 1159-1162 (2009).
8. Wong I., Ho C.M. Surface molecular property modifications for poly(dimethylsiloxane) (PDMS) based microfluidic devices. *Microfluid. Nanofluid.* **7**, 291-306 (2009). Slentz, B.E., Penner, N.A., Lugowska, E., Regnier, F. Nanoliter capillary electrochromatography columns based on collocated monolithic support structures molded in poly(dimethyl siloxane). *Electrophoresis* **22**, 3736-3743 (2001).
9. Slentz, B.E., Penner, N.A., Lugowska, E., Regnier, F. Nanoliter capillary electrochromatography columns based on collocated monolithic support structures molded in poly(dimethyl siloxane). *Electrophoresis* **22**, 3736-3743 (2001).

10. Bodas D., Khan-Malek C. Hydrophilization and hydrophobic recovery of PDMS by oxygen plasma and chemical treatment – An SEM investigation. *Sens. Actuators B* **123**, 368-373 (2007).
11. Berdichevsky Y., Khandurina J., Guttman A., Lo Y.H. UV/Ozone modification of Poly(dimethylsiloxane) microfluidics channels. *Sens. Actuators B* **97**, 402-408 (2004).
12. Sandison, M.E., Cumming, S.A., Kolch, W., Pitt, A.R. On-chip immunoprecipitation for protein purification. *Lab Chip* **10**, 2805-2813 (2010).
13. Sui G. et al. Solution-phase surface modification in intact poly(dimethylsiloxane) microfluidic channels. *Anal. Chem.* **78(15)**, 5543-5551 (2006).
14. Phely-Bobin, T.S., Muisener, R.J., Koberstein, J.T., Papadimitrakopoulos, F. Site-specific self-assembly of Si/SiO_x nanoparticles on micropatterned poly(dimethylsiloxane) thin films. *Synthetic Met.* **116**, 439-443 (2001).
15. Efimenko, K., Wallace, W.E., Genzer, J. Surface modification of Sylgard-184 poly(dimethylsiloxane) networks by ultraviolet and ultraviolet/ozone treatment. *J. Colloid Interface Sci.* **254**, 306-315 (2002).
16. Chen, H.Y., Lahann, J. Fabrication of discontinuous surface patterns within microfluidic channels using photodefinable vapour-based polymer coatings. *Anal. Chem.* **77**, 6909-6914 (2005).
17. Roman, G.T., Hlaus, T. Bass, K.J., Seelhammer, T.G., Culbertson, C.T. Sol-gel modified poly(dimethylsiloxane) microfluidic devices with high electroosmotic mobilities and hydrophilic channel wall characteristics. *Anal. Chem.* **77**, 1414-1422 (2005).
18. Roman, G.T., Culbertson, C.T. Surface engineering of poly(dimethylsiloxane) microfluidic devices using transition metal sol-gel chemistry. *Langmuir* **22**, 4445-4451 (2006).
19. Towns, J.K., Regnier, F.E. Capillary electrophoretic separations of proteins using nonionic surfactant coatings. *Anal. Chem.* **63**, 1126-1132 (1991).
20. Makamba, H., Hsieh, Y.Y., Sung, W.C., Chen, S.H. Stable permanently hydrophilic protein-resistant thin-film coatings on poly(dimethylsiloxane) substrates by electrostatic self-assembly and chemical cross-linking. *Anal. Chem.* **77**, 3971-3978 (2005).
21. Ibarlucea B., Fernández-Sánchez F., Demming S., Büttgenbach S., Llobera A. Selective functionalisation of PDMS-based photonic lab on a chip for biosensing. *Analyst* (2011) DOI: 10.1039/c0an00941e
22. Yu L., Li C.M., Zhou Q., Luong J.H.T. Poly(vinyl alcohol) functionalized poly(dimethylsiloxane) solid surface for immunoassay. *Bioconjug. Chem.* **18(2)**, 281-284 (2007).
23. Charles P. T. et al. Reduction of non-specific protein adsorption using poly(ethylene) glycol (PEG) modified polyacrylate hydrogels in immunoassays for staphylococcal enterotoxin B detection. *Sensors* **9**, 645-655 (2009).
24. Zimmermann J.L., Nicolaus T., Neuert G., Blank K. Thiol-based, site-specific and covalent immobilization of biomolecules for single-molecule experiments. *Nature Protocols* **5(6)**, 975-985 (2010).
25. Llobera A., Wilke R., Büttgenbach S. Poly(dimethylsiloxane) hollow Abbe prism with microlenses for detection based on absorption and refractive index shift. *Lab Chip* **4**, 24-27 (2004).
26. Kozlov, M. Quarmyne, M., Chen, W., McCarthy, T.J. Adsorption of poly(vinyl alcohol) onto hydrophobic substrates. A general approach for hydrophilizing and chemically activating surfaces. *Macromolecules* **36**, 6054-6059 (2003).
27. Hair M.L., Tripp C.P. Alkylchlorosilane reactions at the silica surface. *Colloids Surf. A* **105**, 95-103 (1995).
28. Mata A., Fleischman A.J., Roy S. Characterization of polydimethylsiloxane (PDMS) properties for biomedical micro/nanosystems. *Biomed. Microdevices* **7(4)**, 281-293 (2005).
29. Hillborg H. et al. Crosslinked polydimethylsiloxane exposed to oxygen plasma studied by neutron reflectometry and other surface specific techniques. *Polymer* **41**, 6851-6863 (2000).
30. Llobera A., Wilke R., Büttgenbach S. Enhancement of the response of poly(dimethylsiloxane) hollow prisms through air mirrors for absorbance-based sensing. *Talanta* **75**, 473-479 (2008).

31. Ferreira L., Ramos M.A., Dordick J.S., Gil M.H. Influence of different silica derivatives in the immobilization and stabilization of a *Bacillus licheniformis* protease (Subtilisin Carlsberg). *J. Mol. Catal. B: Enzym.* **21**, 189-199 (2003).
32. Zhang, K., Diehl, M.R., Tirrell, D.A. Artificial polypeptide scaffold for protein immobilization. *J. Am. Chem. Soc.* **127**, 10136-10137 (2005).
33. Shriver-Lake, L.C. et al. Antibody immobilization using heterobifunctional crosslinkers. *Biosens. Bioel.* **12(11)**, 1101-1106 (1997).
34. Kadnikova E.N., Kostic N.M. Oxidation of ABTS by hydrogen peroxide catalyzed by horseradish peroxidase encapsulated into sol-gel glass. Effects of glass matrix on reactivity. *J. Mol. Catal. B: Enzym.* **18**, 39-48 (2002).
35. Di Risio, S., Yan, N. Adsorption and inactivation behavior of horseradish peroxidase on various substrates. *Colloid Surface B* **79**, 397-402 (2010).
36. Tamasko M. et al. An approach to in situ detection of hydrogen peroxide: application of a commercial needle-type electrode. *Physiol. Meas.* **28**, 1533-1542 (2009).

ACKNOWLEDGEMENTS

This work has received funding from the European Research Council under the European Community's Seventh Framework Programme (FP7/2007-2013)/ERC grant agreement no. 209243. The authors thank Dr. Manuel Gutierrez for his kind help with the AFM study.

ASSOCIATED PUBLICATIONS

This protocol was developed and described in Ibarlucea *et al.* 2011 (DOI: 10.1039/c0an00941e).

FIGURE CAPTIONS

Figure 1: Chemical structure of, **a**) poly(dimethylsiloxane); **b**) (1) polyethylene glycol and (2) polyvinyl alcohol; **c**) oxidized PDMS presenting silanol groups.

Figure 2: Scheme of the different modification approaches tested for the biofunctionalization of PDMS.

Figure 3: Scheme of the silanization process of the hydroxyl- containing PDMS surfaces.

Figure 4: Contact angle values measured following every step of each modification procedure. Error bars correspond to the standard deviation of three replicates.

Figure 5: High resolution XPS spectra of the C (1s) region corresponding to intact PDMS (1), after the adsorption of PVA (2) and after the silanization process with TESU (3).

Figure 6: High resolution XPS spectra of the C (1s) region corresponding to PDMS after the chemical oxidation (1) and after the silanization process (2).

Figure 7: High resolution XPS spectra of the C (1s) region corresponding to PEG-modified PDMS before (1) and after (2) the silanization process with TESU.

Figure 8: Topographic and phase AFM pictures of the intact PDMS surface, after modification with PVA and after the silanization process.

Figure 9: Topographic and phase AFM pictures of the PDMS surface after the modification with PEG and further silanization with TESU.

Figure 10: Topographic and phase AFM images of the PDMS surface after the chemical oxidation and further silanization with TESU.

Figure 11: HRP- catalyzed reduction of hydrogen peroxide mediated by colorless ABTS, which generates water and green-color ABTS radical cation counterpart.

Figure 12: Calibration plots recorded with the different biosensor approaches. Each point is the mean value obtained for each hydrogen peroxide concentration in three different experiments carried out with three modified LoCs, the error bars being the corresponding standard deviation.

Figure 13: Operational stability of the different PhLoC approaches measured as the sensitivity of the calibration plots sequentially recorded over a 35-day period.

Figure 1

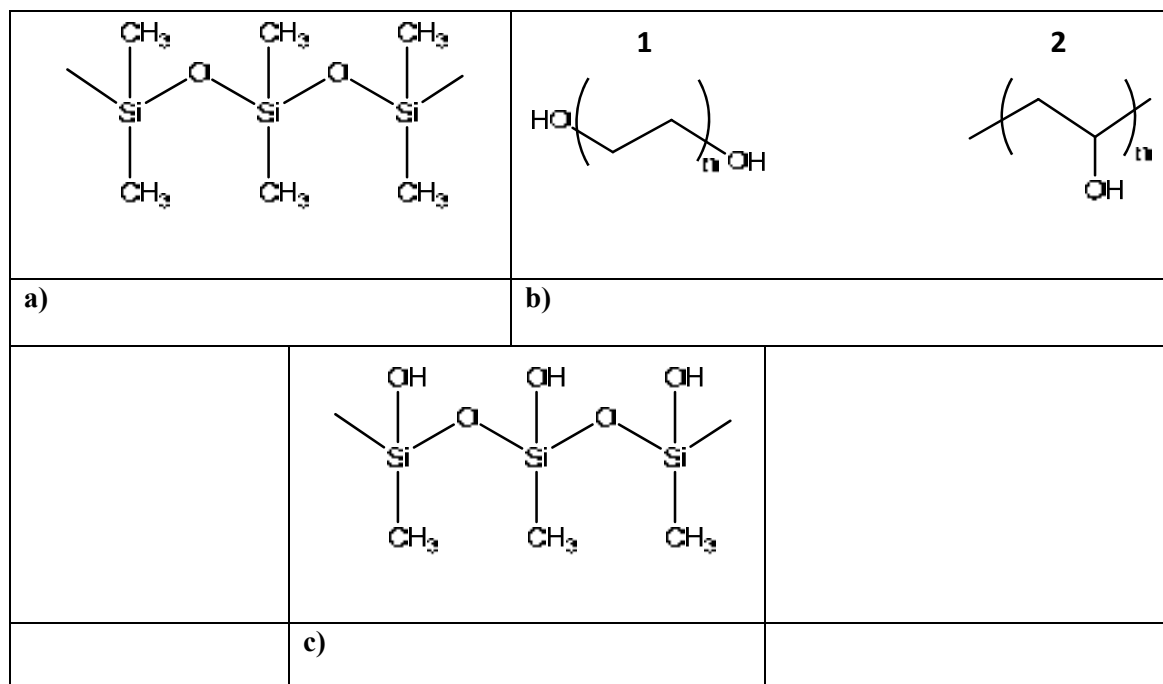


Figure 2

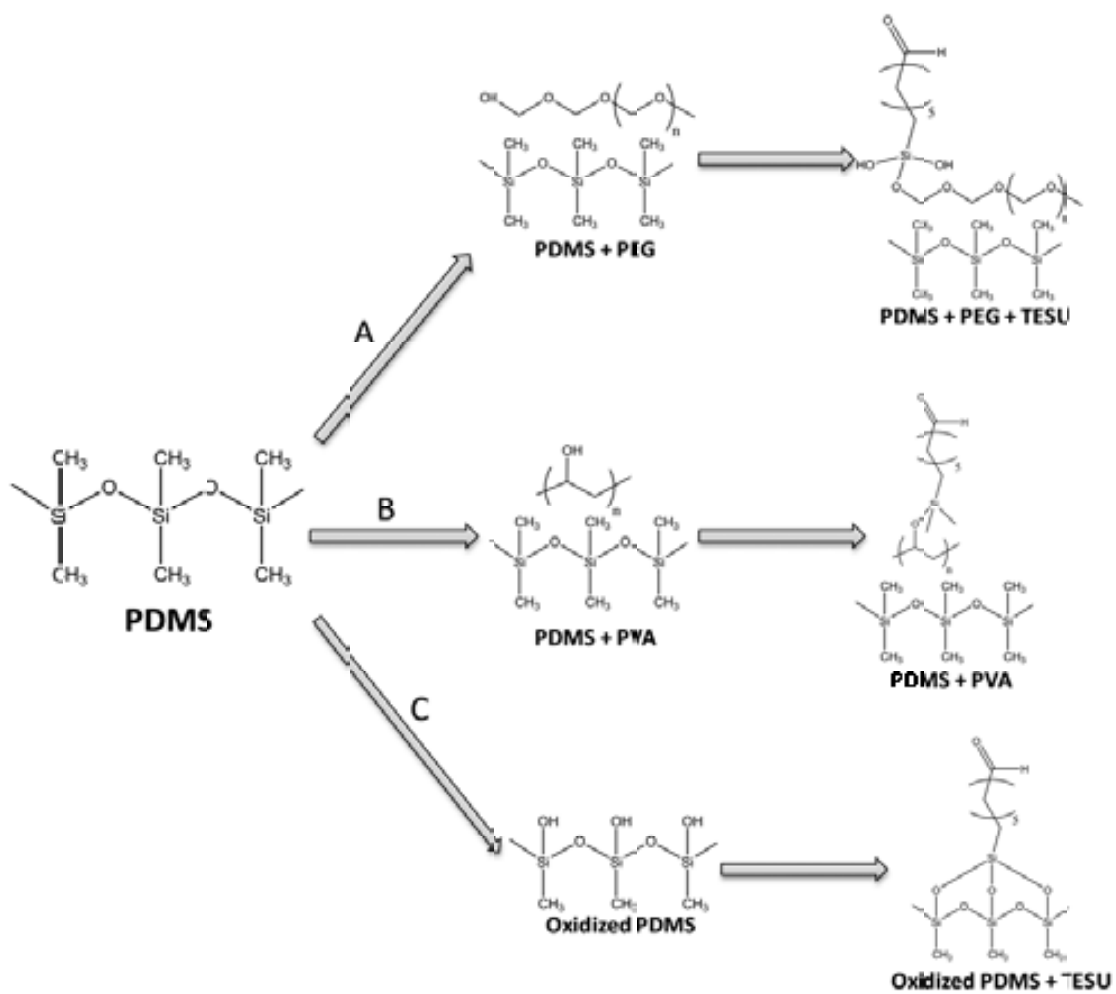


Figure 3

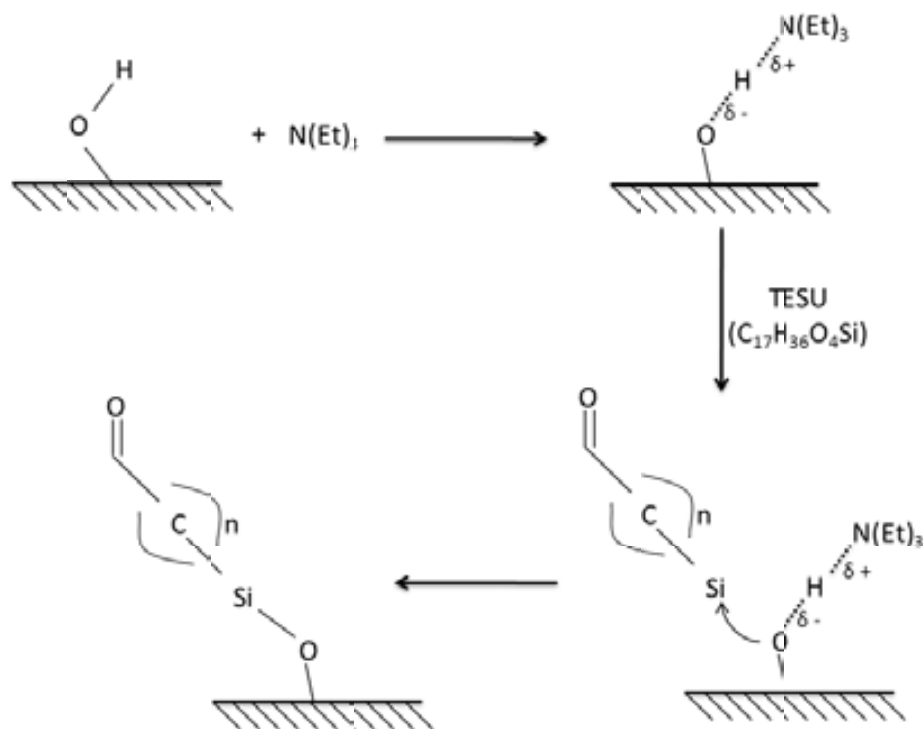


Figure 4

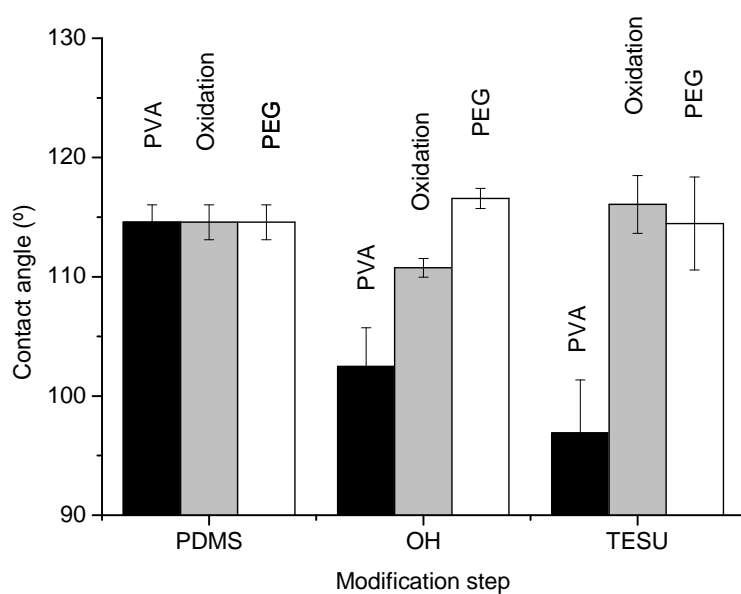


Figure 5

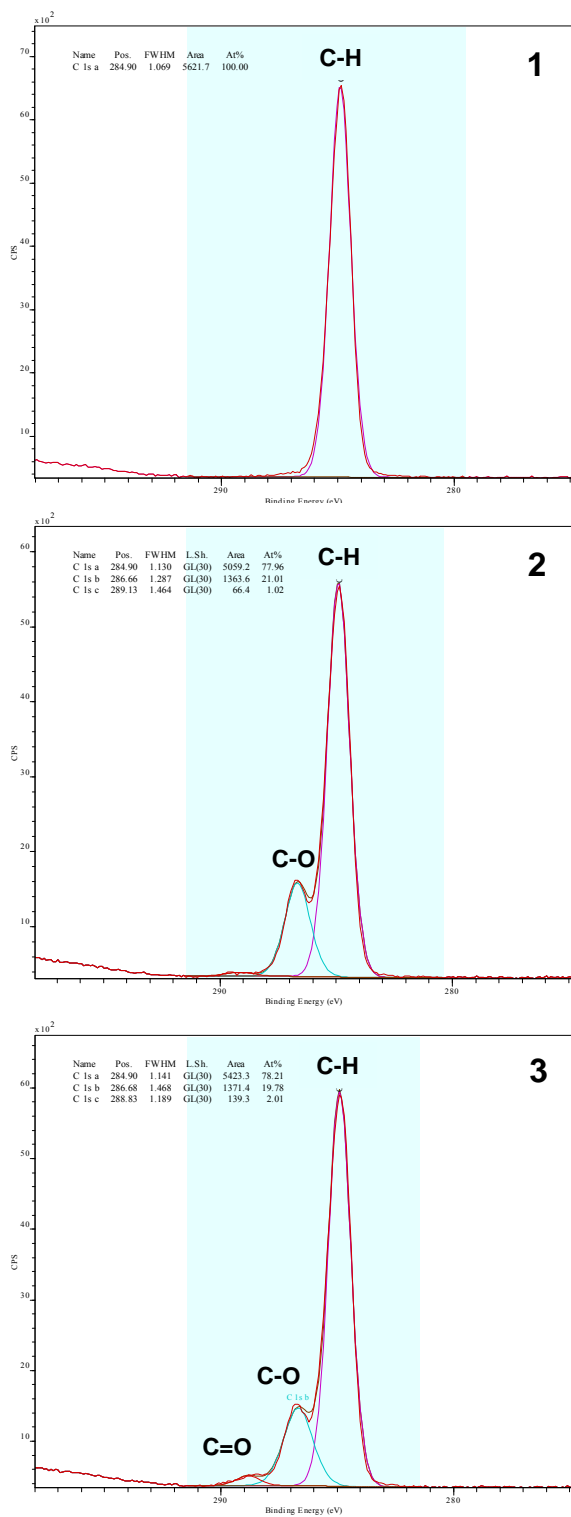


Figure 6

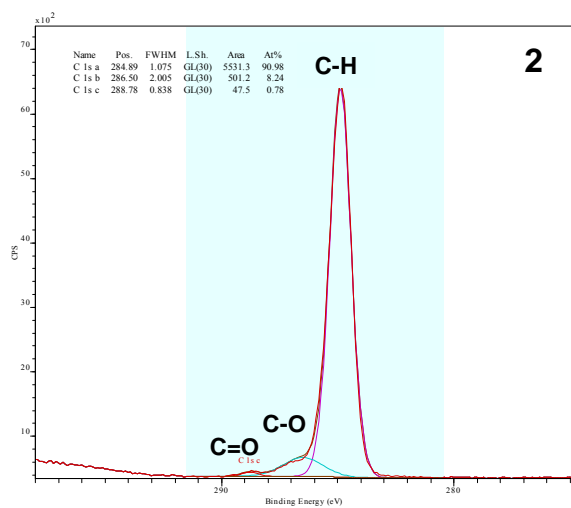
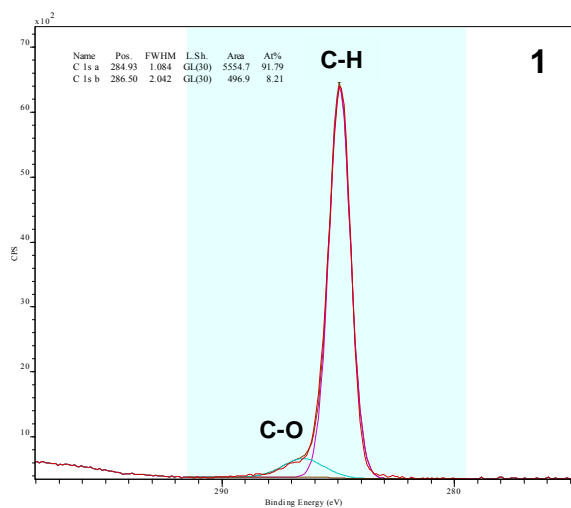


Figure 7

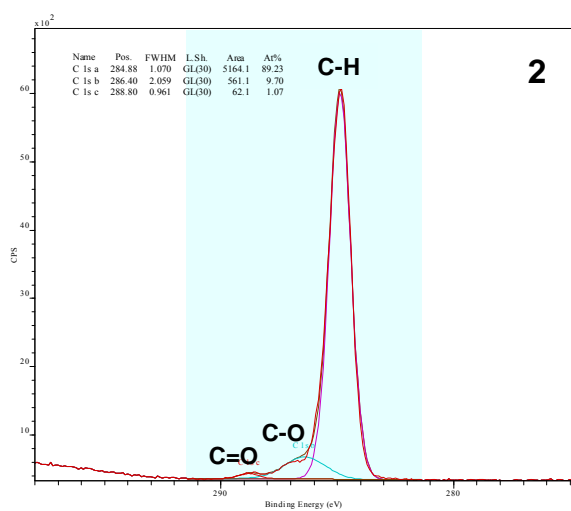
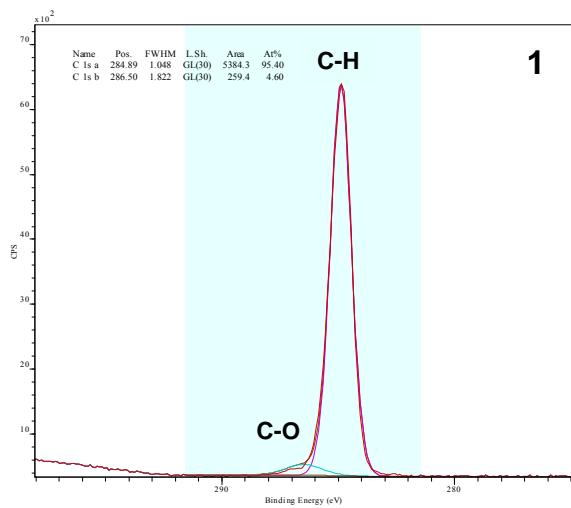


Figure 8

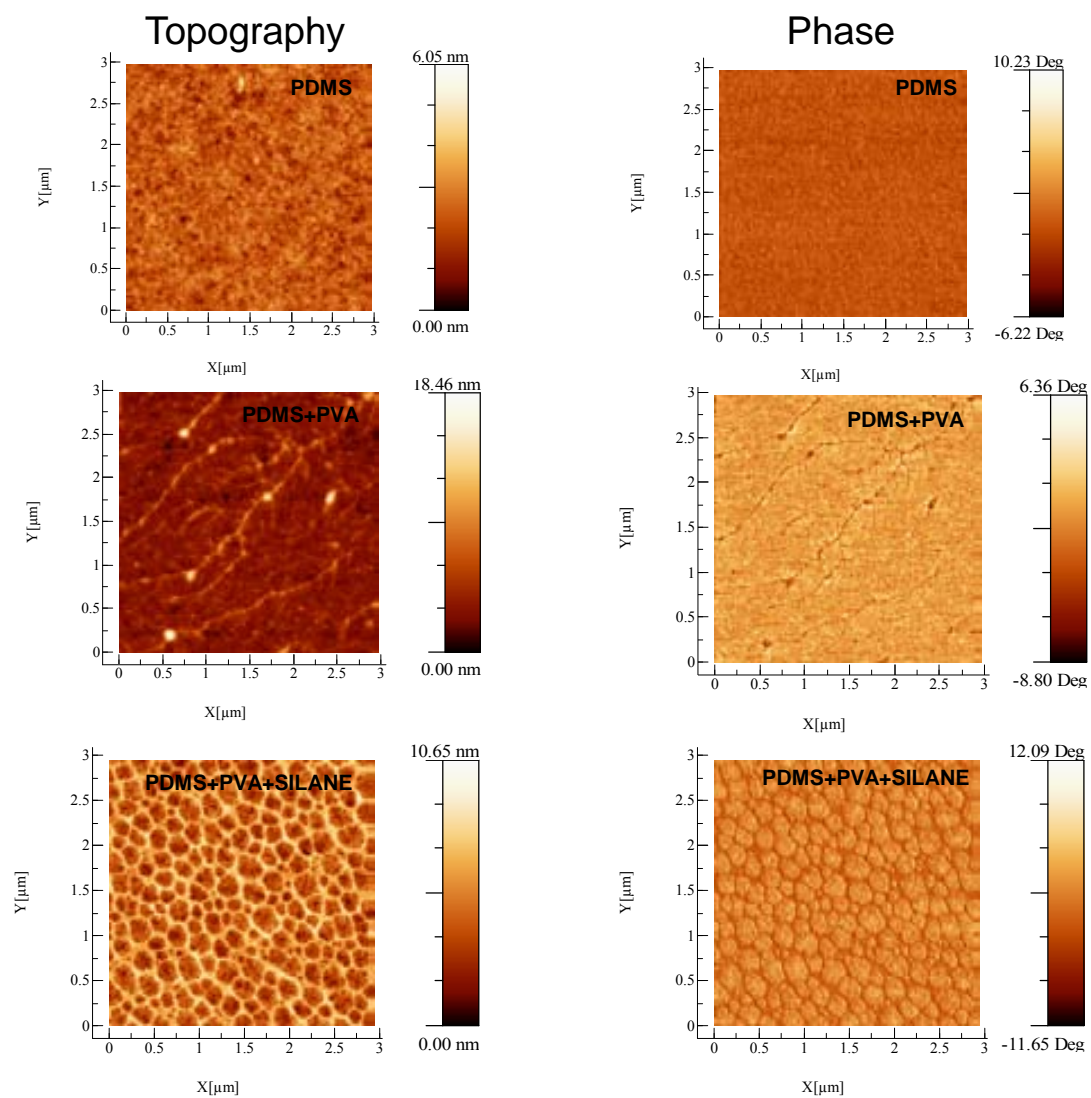


Figure 9

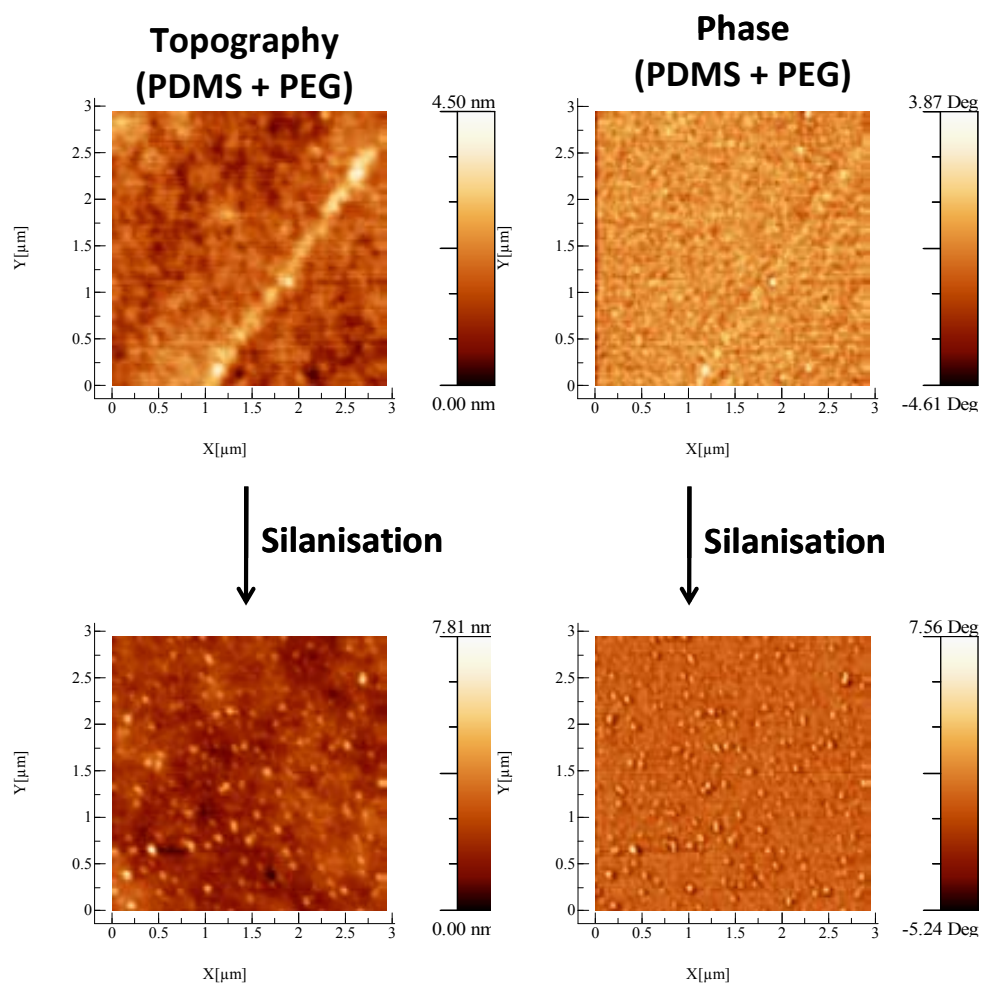


Figure 10

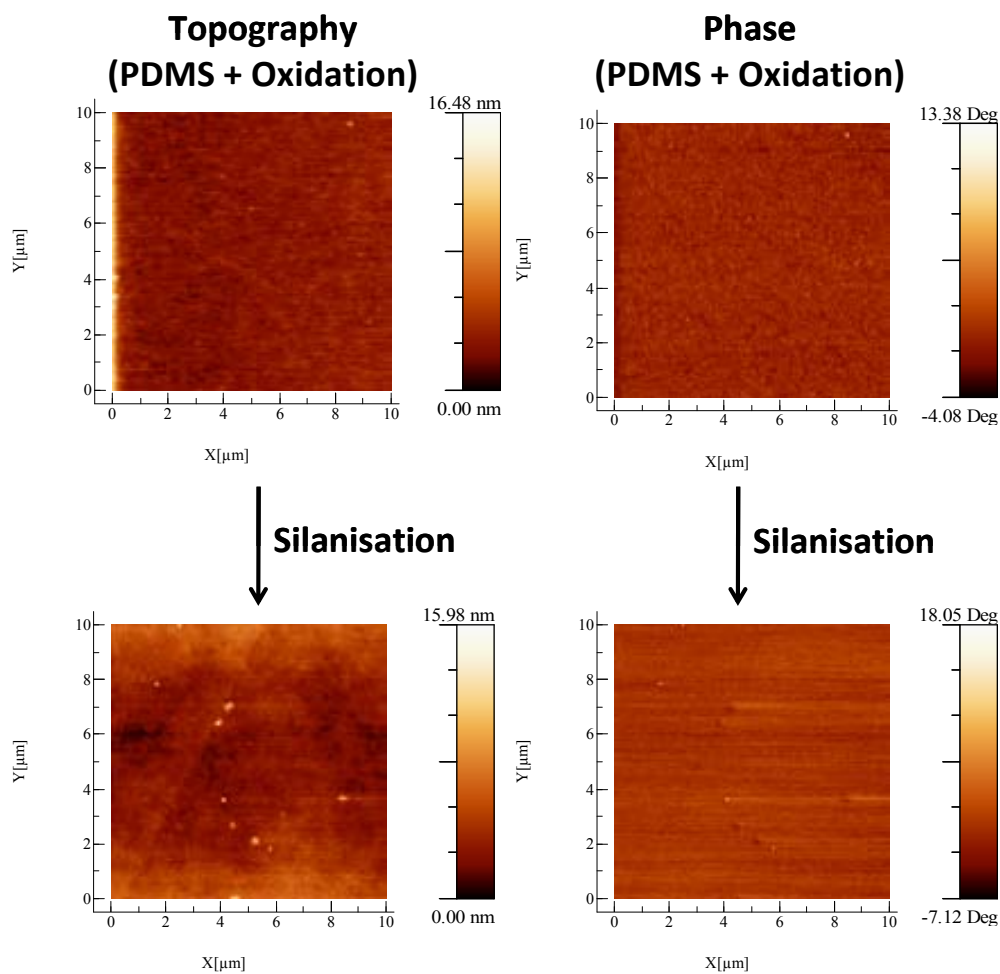


Figure 11

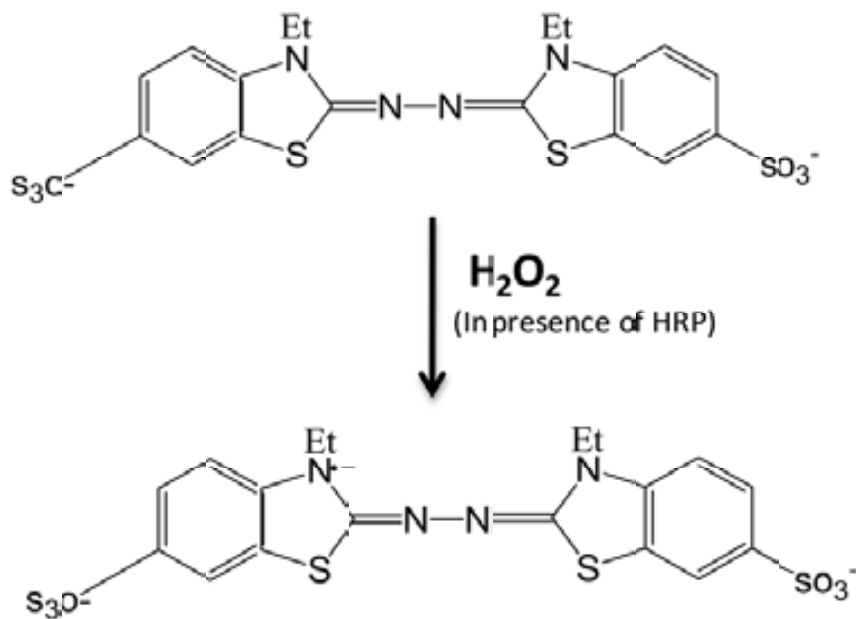


Figure 12

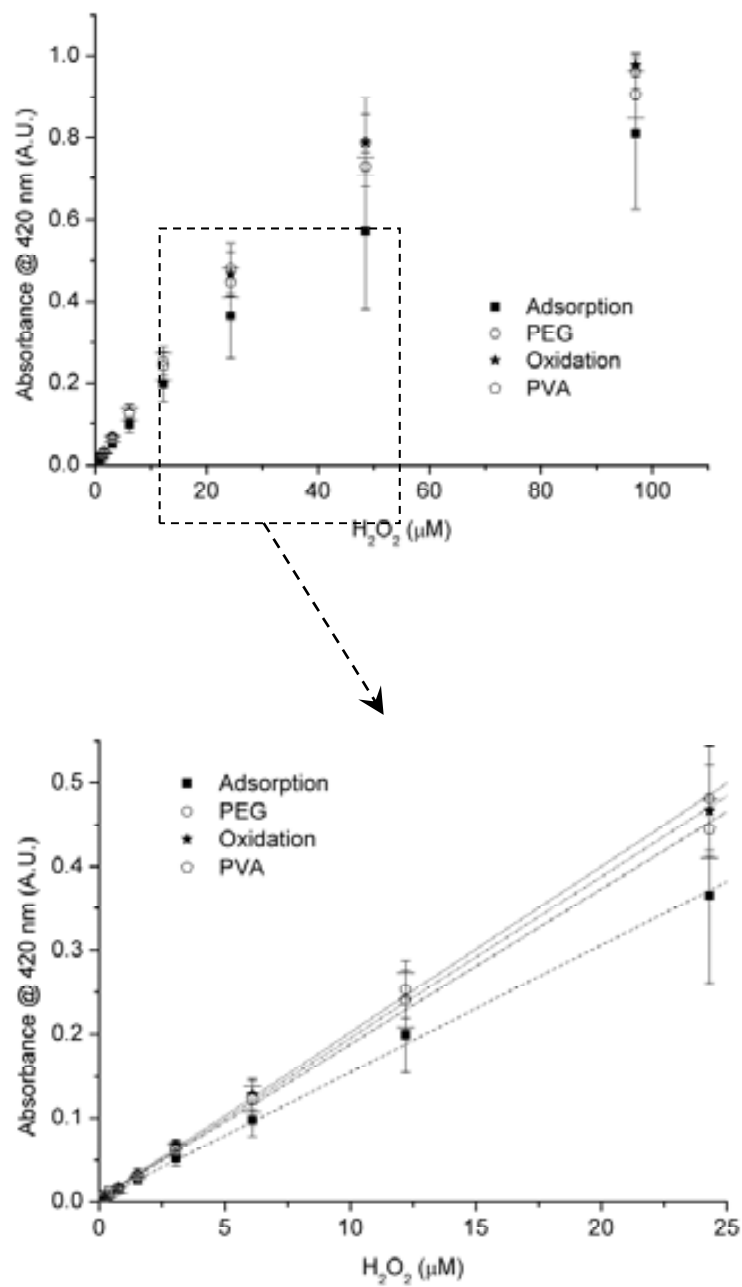
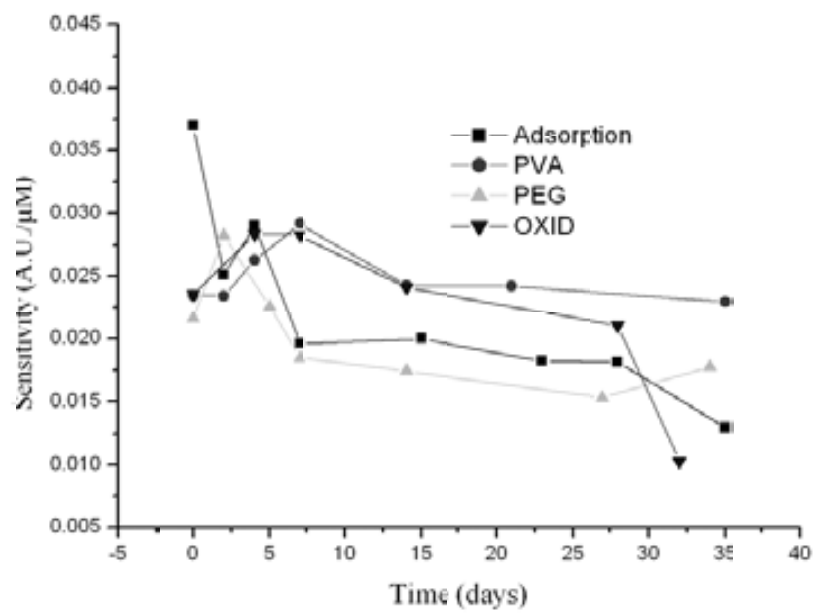


Figure 13



Tables

Table 2: Atomic percentages of the different surfaces extracted from the XPS survey scans.

Sample	Atomic Concentration (%)	
PDMS	O1s	19.71
	C1s	43.38
	Si 2p	36.90
PVA	O1s	21.21
	C1s	51.74
	Si 2p	27.05
PEG	O1s	19.05
	C1s	43.85
	Si 2p	37.11
OXIDATION	O1s	20.09
	C1s	44.92
	Si 2p	34.99
PVA + TESU	O1s	21.29
	C1s	50.69
	Si 2p	28.02
PEG + TESU	O1s	19.13
	C1s	45.36
	Si 2p	35.51
OXIDATION + TESU	O1s	20.26
	C1s	44.25
	Si 2p	35.48

Table 3: Analytical parameters of the four different biosensor approaches

Modification	Sensitivity (A.U./ μM) ¹	LOD (μM) ^{1,2}	r
Adsorption	0.017 \pm 0.003	0.12 \pm 0.08	0.996
PEG + TESU	0.019 \pm 0.001	0.28 \pm 0.08	0.990
PVA + TESU	0.019 \pm 0.001	0.14 \pm 0.08	0.996
Oxid. + TESU	0.021 \pm 0.005	0.10 \pm 0.01	0.998

¹Mean values and corresponding standard deviations of the parameters extracted from three calibration curves recorded with different devices in three consecutive days are represented.

²LOD calculated following the 3σ IUPAC criteria using the lowest order of the linear concentration range from 0.1 μM to 1.53 μM .

PDMS based photonic lab-on-a-chip for the selective optical detection of heavy metal ions

Cite this: *Analyst*, 2013, **138**, 839

Bergoi Ibarlucea,^a César Díez-Gil,^b Inma Ratera,^b Jaume Veciana,^b Antonio Caballero,^c Fabiola Zapata,^c Alberto Tárraga,^c Pedro Molina,^c Stephanie Demming,^d Stephanus Büttgenbach,^d César Fernández-Sánchez^a and Andreu Llobera^{*ad}

The selective absorbance detection of mercury(II) (Hg²⁺) and lead(II) (Pb²⁺) ions using ferrocene-based colorimetric ligands and miniaturized multiple internal reflection (MIR) systems implemented in a low-cost photonic lab on a chip (PhLoC) is reported. The detection principle is based on the formation of selective stable complexes between the heavy metal ion and the corresponding ligand. This interaction modulates the ligand spectrum by giving rise to new absorbance bands or wavelength shifting of the existing ones. A comparative study for the detection of Hg²⁺ was carried out with two MIR-based PhLoC systems showing optical path lengths (OPLs) of 0.64 cm and 1.42 cm as well as a standard cuvette (1.00 cm OPL). Acetonitrile solutions containing the corresponding ligand and increasing concentrations of the heavy metal ion were pumped inside the systems and the absorbance in the visible region of the spectra was recorded. The optical behaviour of all the tested systems followed the expected Beer-Lambert law. Thus, the best results were achieved with the one with the longest OPL, which showed a linear behaviour in a concentration range of 1 μM –90 μM Hg²⁺, a sensitivity of 5.6×10^{-3} A.U. μM^{-1} and a LOD of 2.59 μM (0.49 ppm), this being 1.7 times lower than that recorded with a standard cuvette, and using a sample/reagent volume around 190 times smaller. This microsystem was also applied for the detection of Pb²⁺ and a linear behaviour in a concentration range of 3–100 μM was obtained, and a sensitivity of 9.59×10^{-4} A.U. μM^{-1} and a LOD of 4.19 μM (0.868 ppm) were achieved. Such a simple analytical tool could be implemented in portable instruments for automatic in-field measurements and, considering the minute sample and reagent volume required, would enable the deployment of high throughput environmental analysis of these pollutants and other related hazardous species.

Received 2nd July 2012
Accepted 27th November 2012

DOI: 10.1039/c2an36402f

www.rsc.org/analyst

Introduction

Heavy metal ions can injure human health and pollute the environment. It is well known that these metals are able to enter organisms and interfere with metabolic processes,¹ producing physiological problems including neurological, neuromuscular, or nephritic disorders. Among the different metals, mercury and lead are considered to be the most toxic nonradioactive chemical elements. They are highly water-soluble, being bioavailable for animals by ingestion of water.² The divalent cation of mercury (Hg²⁺) is non-biodegradable, accumulative and toxic even at very low concentrations. It can damage heart,

kidney, stomach and intestines, also causing sensory and neurological damage.³ In the case of the divalent cation of lead (Pb²⁺), exposure to very low levels can cause neurological, reproductive, cardiovascular and developmental disorders.⁴

There are several analytical techniques that enable the sensitive detection of heavy metal ions, such as inductively coupled plasma mass spectrometry (ICP-MS),⁵ cold vapour atomic absorption spectrometry (CV-AAS),⁶ X-ray fluorescence (XRF) spectroscopy⁷ and high performance liquid chromatography (HPLC).⁸ However, the corresponding analyses have to be carried out in centralised laboratories, making them expensive and not suitable for the rapid detection of these target analytes.^{2,3} In this context, the high toxicity of heavy metal ions has given rise to a necessity of new systems for their detection and quantification that were simple, portable and inexpensive. Miniaturization of analytical systems is nowadays a trendy topic in environmental monitoring and biomedical diagnostics. Size reduction does not only mean a decrease in production costs, analysis time, reagent and sample volume consumption as well as waste production,⁹ but also an enhancement of the analytical performance in terms of faster response time and potential for

^aInstituto de Microelectrónica de Barcelona, IMB-CNM (CSIC), Campus Universitat Autònoma de Barcelona, 08193, Bellaterra, Spain. E-mail: andreu.llobera@imb-cnm.csic.es; Fax: +34 93 580 1496; Tel: +34 93 594 7700

^bInstitut de Ciència dels Materials de Barcelona (CSIC)/CIBER-BBN, Campus Universitat Autònoma de Barcelona, 08193, Bellaterra, Spain

^cDepartamento de Química Orgánica, Universidad de Murcia, Campus de Espinardo, 30100, Murcia, Spain

^dInstitut für Mikrotechnik, Technische Universität Braunschweig, Alte Salzdhahmler Straße 203, 38124, Braunschweig, Germany

multiplexed analysis.^{1,10} Thus, there is a current demand for simple, disposable and low cost analytical tools to perform *in situ* and continuous monitoring of pollutants, which could be used as alarm systems to target potential contamination outbreaks and thus give rise to a faster response to tackle the problem.

Analytical microsystems being fabricated by micro-fabrication technologies, comprising diverse functionalities of a laboratory in a single system, are known as lab-on-a-chip (LoC). Among the myriad of different applications, LoCs have also been applied for the detection and quantification of heavy metal ions. Most of them rely on electrochemical or optical detection approaches. Among the former, Zhu *et al.*¹¹ developed a chip including a mercury droplet based microelectrode to detect lead and cadmium ions. Zou *et al.*¹² further incorporated the possibility to carry out *in situ* and online measurements to their electrochemical detection based chip. However, these approaches are based on the cumbersome implementation of different materials and the application of highly toxic electrodes. Optical detection approaches are gaining a preeminent position mainly because they are highly sensitive non-contact techniques that show immunity to electromagnetic interferences and provide with the capability of multiplexed detection in a single analytical system.¹³ In this context, the LoC concept has been extended to include the so-called photonic lab-on-a-chip (PhLoC) approach,¹⁴ which comprises the integration of microoptical and/or integrated optical elements together with microfluidic systems. The impact that PhLoCs have caused on the scientific community is directly related to the significant improvement in the technology applied in their fabrication. To this effect, the change from silicon bulk micromachining to polymeric materials (mainly SU-8 and polydimethylsiloxane, PDMS) as well as the use of soft lithographic fabrication processes has resulted in a dramatic decrease of the LoC cost and fabrication time. Regarding PhLoC, the excellent optical properties of the PDMS, which is optically transparent in the UV-NIR range, allow defining absorbance-based microsystems with a high level of integration with the potential of being highly sensitive. Moreover, these systems require very short integration times and are compatible with many optical detection methods.^{15,16} Since the absorbance is directly proportional to the optical path length (OPL), it can be anticipated that the larger the interrogation regions, the lower the limit of detection (LOD) that can be attained. Here, the integration of micro-optical and/or photonic elements like air mirrors also allows the increase of the optical path of the PhLoC even further, which is important for the device miniaturization but also to get a better performance and sensitivity.¹⁷ Such kinds of PhLoC approaches have already successfully been applied for the detection of different targets such as cells¹⁵ or lactate.¹⁸

In environmental applications, optical approaches have also been reported for the measurement of heavy metal ions. There is a wealth of molecular metal ion receptors that provide with the possibility of performing optical detection, many of them included in a recent review by Kim *et al.*,¹⁹ such as 1-pyrenecarboxaldehyde thiosemicarbazone (a fluorescent ligand that binds Hg^{2+}),²⁰ or an hybridized DNzyme with an intercalated Picogreen (PG) fluorescent molecule (which is cleaved in

the presence of Pb^{2+} resulting in a release of PG and a decrease of the fluorescent signal).²¹

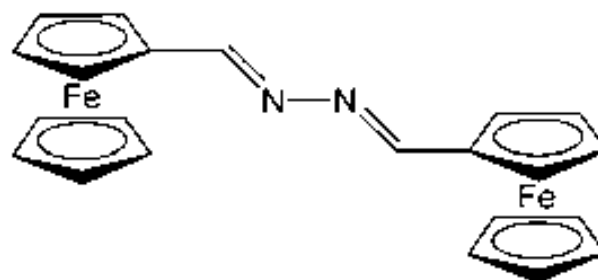
In this context, this work aims to show the benefits of simply combining two colorimetric ferrocene-based ligands,^{22,23} which selectively interacted in solution with Hg^{2+} and Pb^{2+} ions, with low-cost miniaturized PhLoCs for the rapid detection of these pollutants. Two different PhLoCs based on MIR approaches,¹⁴ showing different OPLs, are applied for the detection and quantification of highly toxic metal ions (Hg^{2+} and Pb^{2+}) by using colorimetric ligands that form selective stable complexes with the corresponding ion and, upon complex formation, new absorbance bands or wavelength shift of the existing ones appear. The successful performance of these PhLoCs make them potential candidates to carry out rapid decentralised studies directed towards monitoring these pollutants in the environment.

Materials and methods

Ligands

Analytical measurements in the PhLoCs were carried out by previously mixing the heavy metal ions with the corresponding selective ligands. Previously published works have already demonstrated that certain derivatives of 2,3-diaza-1,3-butadiene can act as sensitive and very selective molecular probes for the detection and preconcentration of Hg^{2+} in standard solutions^{22,24,25} and real water samples.²⁶ Here, an azine derivative bearing two ferrocene groups was used (Scheme 1, ligand 1). This molecule was prepared using previously reported procedures.²⁷ A solution of ligand 1 in acetonitrile shows an absorbance band at 476 nm. The addition of increasing amounts of an aqueous solution of $\text{Hg}(\text{ClO}_4)_2$ (Sigma Aldrich, St. Louis, MO, US) to this solution causes the appearance of a new band at 551 nm, a secondary peak at 405 nm and the disappearance of the initial band at 476 nm. The three well-defined isosbestic points indicate that a neat interconversion between the uncomplexed and complexed species occurs. The new band is red-shifted by 45 nm and is responsible for the change in colour from yellow (neutral ligand 1) to deep purple (complexed ligand 1). The absorption spectral data indicate a 1:1 binding model and an association constant of $4.35 \times 10^5 \text{ M}^{-1}$ in acetonitrile.²²

The detection of Pb^{2+} was carried out using an imidazophenazine-ferrocene ligand (Scheme 2, ligand 2) whose absorbance spectra also change upon complexation with Pb^{2+} cations. This ligand was prepared using a previously published



Scheme 1 Chemical structure of ligand 1 (1,4-disubstituted 2,3-diaza-1,3-butadiene bearing two ferrocene groups) for the detection of Hg^{2+} .

method.²⁷ A solution of ligand **2** in acetonitrile shows an absorbance band at 503 nm. The addition of increasing amounts of $\text{Pb}(\text{ClO}_4)_2$ (Sigma Aldrich, St. Louis, MO, US) to this solution gives rise to a new absorbance band at 404 nm and the shift of the initial band from 503 nm to 515 nm. Binding assays previously performed²³ using the method of continuous variations (Job's plot) suggest a 1:1 binding model with an association constant of $1.4 \times 10^5 \text{ M}^{-1}$.

Design and fabrication of the PhLoC

The PhLoC design has already been reported in a previous work.¹⁴ It consists of a microfluidic system with a defined geometry embedded in a PDMS chip and sealed on a soda-lime glass. The analyzed volume/region is constructed so as to reduce the mean flow cell volume. Thus, in the vicinity of the micro channels, microoptical elements are defined in the PDMS in the same fabrication step. These microoptical elements include alignment channels for positioning the input/output optical fibres as well as bioconvex microlenses for the correction of the fibres numerical aperture. In addition, air mirrors have been included to meaningfully lengthen the optical path without dramatically increasing the overall size of the analytical system. Taking into account the low cost issue, all these elements have been defined considering the refractive indices of air ($n_{\text{air}} = 1.00$), PDMS ($n_{\text{PDMS}} = 1.41$) and acetonitrile ($n_{\text{ace}} = 1.34$),²⁸ the latter being used as the solvent for the preparation of the heavy metal ion samples. It has been reported that this solvent does not swell the PDMS or induce other negative effects that could affect the performance of the analytical system.²⁹

Images of the two PhLoC systems presented in this work can be seen in Fig. 1. Both are based on a MIR detection approach. The first one is the Propagating Multiple Internal Reflection (PMIR) system (Fig. 1a), in which two air mirrors are included, causing the light to follow a zigzag path along the detection region with a total OPL of $6357 \mu\text{m}$. The second system is the Ring Multiple Internal Reflection (RMIR) approach (Fig. 1b), in which three air mirrors have been included in order to increase the light path without significantly increasing the chip size. The total OPL in the RMIR is $14\,264 \mu\text{m}$.

The systems were fabricated by casting of PDMS (Sylgard 184 elastomer kit, Dow Corning, Midland, MI, USA) against a master made of the EPON SU-8 negative tone polymer (SU8-25, MicroChem Corporation, Newton, MA, USA), which in turn was fabricated by standard photolithographic processes.

The fabrication process is briefly described below and further details can be found in the paper by Llobera *et al.*¹⁴ First, a two-step

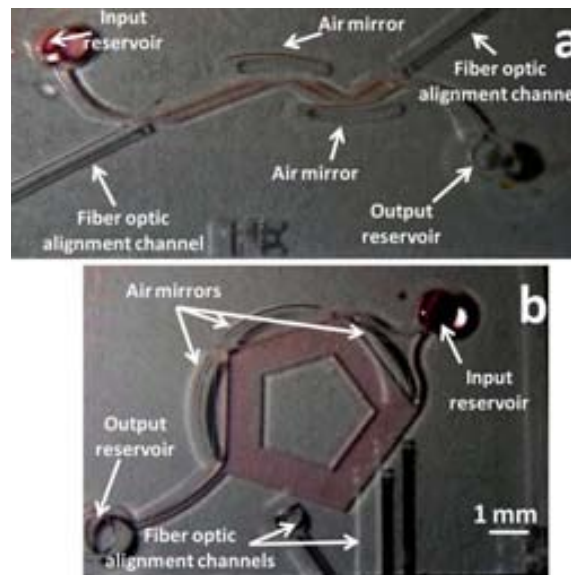


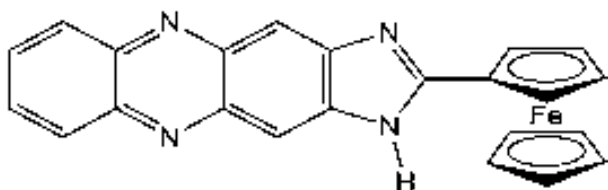
Fig. 1 (a) PMIR and (b) RMIR systems used for the detection of heavy metals. The detection region was filled with a red-colour solution for better contrast.

spin-coating process was carried out with SU-8 on 4-inch silicon wafers. The reason for this two-step process is that a sufficient height is needed in order to fabricate structures that enabled the hassle-free insertion of $230 \mu\text{m}$ diameter input and output optical fibres in the alignment channels. Following a drying process, the coated wafer was exposed to ultraviolet (UV) light through a mask. A post-exposure bake step was followed by the development of SU-8 in propylene glycol methyl ether acetate (PGMEA, MicroChem Corporation, Newton, MA, USA). After a final bake in an inert atmosphere, a $250 \mu\text{m}$ high master was obtained.

The casting of PDMS was carried out as follows. First, a PDMS pre-polymer solution was prepared by mixing the curing agent and the elastomer base in a 1 : 10 ratio (v/v) and then degassing the resulting mixture in a vacuum chamber. Then, it was poured over the master and cured on a hotplate at $80 \text{ }^\circ\text{C}$ for 20 min. Once cured, the PDMS was peeled off the master and sealed on a soda-lime glass substrate. The sealing process required an oxygen plasma based surface treatment³⁰ of both the PDMS and the substrate, which was carried out in a barrel etcher (Surface Technology Systems, Newport, UK) using 75 sccm O_2 at 85 W for 30 s. Immediately after the plasma oxidation, the two surfaces were brought in contact and a thermal treatment was performed at $70 \text{ }^\circ\text{C}$ for 30 min, which irreversibly sealed the microsystem. Holes were punched out with the tip of a syringe luer-lock to have access to the fluidic channels during the analytical procedures. The total volumes of the as-fabricated PMIR and RMIR PhLoCs were $1.43 \mu\text{L}$ and $5.34 \mu\text{L}$, respectively.¹⁴

Experimental setup and measurement protocol

A comparative analytical study of the performance of the two fabricated systems as well as a standard cuvette, which is commonly used in spectrophotometric methods ($10\,000 \mu\text{m}$ OPL, 1 mL, minimum working volume; CVD-UV1S plastic cuvettes, Ocean Optics, Dunedin, FL), was carried out. To this



Scheme 2 Chemical structure of ligand **2** (2-ferrocenylimidazo[4,5-*b*]phenazine) for the detection of Pb^{2+} .

effect, multimode optical fibres with a diameter of 230 μm were inserted in the alignment channels. The input fibre optic was connected to the light source (Ocean Optics HL-2000, Dunedin, FL), whereas the output fibre optic was connected to a microspectrophotometer (Ocean Optics HR4000, Dunedin, FL). The spectral response was recorded using the SpectraSuite software (Ocean Optics, Dunedin, FL).

Samples containing increasing Hg^{2+} concentrations from 1 μM to 1 mM and a 0.1 mM constant concentration of ligand **1** in acetonitrile were pumped into the PhLoC systems by using a vacuum pump and the resulting absorbance spectra were recorded in the visible wavelength range (from 300 nm to 800 nm) under quiescent conditions. For each concentration, the average of 10 spectra recorded consecutively was taken. Measurements were carried out starting with the lowest Hg^{2+} concentration. Acetonitrile was pumped in between measurements to clean the microsystem. The results obtained with the two PhLoC systems were compared to the ones obtained with the standard cuvette.

Once the PhLoC systems for Hg^{2+} detection were characterized, the system that presented the best performance was selected to carry out the analysis of Pb^{2+} using ligand **2** under the same conditions in terms of concentration and experimental setup as for Hg^{2+} .

Results and discussion

Fig. 2 shows the change of the absorbance spectra with increasing concentrations of Hg^{2+} , measured with the RMIR system. A similar behaviour was observed with the PMIR. The signal recorded in an acetonitrile solution just containing ligand **1** was taken as a reference. Two new peaks were observed at 405 nm and 551 nm when solutions with increasing amounts of Hg^{2+} were flowed through the system. Due to the fact that the ligand shows several wavelengths at which a significant change in absorbance takes place upon increasing amounts of Hg^{2+} in the sample, the sensitivity and LOD estimated from the

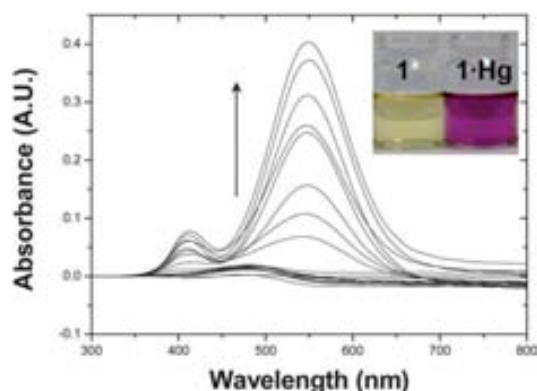


Fig. 2 Absorbance spectra recorded in acetonitrile solutions containing 0.1 mM ligand **1** and increasing concentrations of Hg^{2+} in a range from 1 μM to 90 μM with the RMIR system. The spectrum of the ligand **1** solution was taken as the reference value and two new peaks were observed at 405 nm and 551 nm when Hg^{2+} was present in solution. The inset shows a picture of acetonitrile solutions containing 0.1 mM ligand **1** and the change in colour of this solution upon addition of 1 equivalent of Hg^{2+} .

calibration curves recorded for each wavelength of the spectra were plotted against the wavelength, as in Vila-Planas *et al.*³¹ (Fig. 3a and b, respectively). The LOD was calculated as the lowest analyte concentration for which the signal exceeds the relative standard deviation of the background signal divided by the slope of the calibration curve by a factor of 3. The calibration curves showed in all cases the expected linear behaviour (Beer–Lambert law) in a Hg^{2+} concentration range between 20 μM and 100 μM for the PMIR and between 1 μM and 90 μM for the RMIR system.

Fig. 3 clearly provides with the working wavelength that shows the highest sensitivity (Fig. 3a) and lowest LOD (Fig. 3b) for Hg^{2+} ions. These values were $5.6 \times 10^{-3} \pm 1 \times 10^{-4}$ A.U. μM^{-1} and 2.59 ± 0.04 μM (0.49 ppm), respectively, at a wavelength of 551 nm for the RMIR system. The LOD and sensitivity parameters attained with the cuvette were 4.38 ± 0.14 μM and $4.2 \times 10^{-3} \pm 1 \times 10^{-4}$ A.U. μM^{-1} , whereas for the PMIR these values were 7.0 ± 0.2 μM and $1.67 \times 10^{-3} \pm 6 \times 10^{-5}$ A.U. μM^{-1} , respectively. These variations are consistent with the different optical paths of the RMIR, the cuvette and the PMIR system. Similar analytical values were previously reported using this ligand either in solution or deposited on a nitrocellulose membrane by measuring the absorbance or fluorescence behaviour of this molecular probe.^{22,24} It is worth mentioning that the sample/reagent volume was 190 times lower when

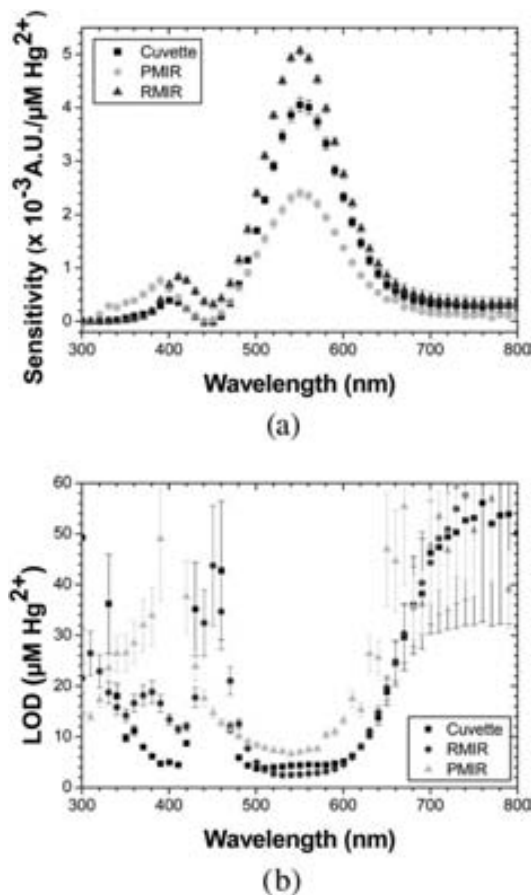


Fig. 3 (a) Sensitivity and (b) LOD values for the detection of Hg^{2+} in a solution of ligand **1** using a cuvette, PMIR and RMIR system in a spectral range that varies from 300 to 800 nm.

applying the RMIR system (5.34 μL) compared with the volume required when the standard cuvette (1 mL minimum working volume) was used.

The versatility of the presented analytical approach, which combines the use of molecular ligands that selectively interact with heavy metal ions with easy-to-use low-cost PhLoC devices, is demonstrated by carrying out the detection of Pb^{2+} . The RMIR system was chosen because of its best performance in the detection of Hg^{2+} . Thus, an identical RMIR device to the one used for the detection of Hg^{2+} was used. The analytical measurement was based on the use of ligand **2** described in the Experimental section. Here, the sensitivity and LOD were also calculated as a function of the detection wavelength and results are shown in Fig. 4. A linear behaviour in a concentration range of 3 μM –100 μM Pb^{2+} was obtained, with $9.6 \pm 0.2 \times 10^{-4}$ A.U. μM^{-1} and 4.2 ± 0.1 μM (0.868 ppm) being the highest sensitivity and lowest LOD values respectively. These results were recorded at 515 nm, at which the spectra of ligand **2** show a peak when interacts with Pb^{2+} , as described above. These results are similar to the ones previously reported using the same ligand and fluorescence detection²³ but with the added advantage of requiring minute sample volumes.

Although the results do not allow detection of mercury³² or lead³³ ion levels below the threshold for drinking water defined by the US Environmental Protection Agency (EPA), the LOD could be decreased by simply lengthening the optical path even more without significantly affecting the overall size of the chip. Nevertheless, it should be highlighted that the LOD is also

limited in this work by the ligands themselves, which have been previously shown to provide similar sensitivities and LOD to those achieved in this work, even when applying a fluorescence detection approach in the case of Hg^{2+} analysis.^{22–25} The increase in the length of the optical path is relatively simple to carry out compared with the application of other more complicated approaches such as surface plasmon resonance,³⁴ or electrochemistry.³⁵ Nevertheless, it is worth mentioning that in some countries the tolerance limits are higher. For example, in India, the allowed levels prescribed by the Bureau of Indian Standards (BIS) for Hg^{2+} are 10 ppm for inland surface water and 1 ppm for drinking water,³⁶ which make the system presented here with the potential to be directly applied in these scenarios.

Conclusions

Two low-cost polymeric PhLoC systems were presented and their potential showed when combined with highly selective ligands for the quick *in situ* testing of heavy metal ions using very small sample volumes. The described systems included air mirrors to lengthen the optical path without increasing their inherent dimensions and presented high absorbance signals, making them useful in miniaturized optical detection approaches.

Overall, the here presented PhLoCs could be implemented as miniaturized analytical systems for detecting Hg^{2+} and Pb^{2+} in an easy and cheap way. They outperform other previously reported systems just by considering the ease and cost of their fabrication process as well as the simplicity of the applied absorbance-based detection approach, which avoids the implementation of electrodes,^{12,37} heaters or the incorporation of toxic substances such as mercury droplets that make the device non-disposable.¹¹ Finally, these PhLoCs offer the possibility of carrying out rapid analysis of such kind of pollutants if a continuous flow operation mode is used. In addition, they can be included in more complex PhLoCs, incorporating mixers for mixing the sample with the ligand or filters to eliminate particles in suspension that would induce light scattering, as it is usually done with real samples following the guidelines from the United States (US)³⁸ and from the European Union.³⁹

Acknowledgements

This work has received funding from the European Research Council under the European Community's Seventh Framework Programme (FP7/2007–2013)/ERC grant agreement no. 209243. It has also been supported by the DGI grants (EMOCIONa (CTQ2006-06333), POMAs (CTQ2010-19501), the Networking Research Center on Bioengineering, Biomaterials and Nanomedicine (CIBER-BBN), and the Generalitat de Catalunya (grants 2009SGR00516 and 2009SGR00277). C.D. is grateful to Ministerio de Educación y Ciencia (MEC) for a predoctoral grant. S.B. gratefully acknowledges the financial support of the Volkswagen Foundation. This work has been made in the framework of the PhD Programme in Chemistry of the Universitat Autònoma de Barcelona.

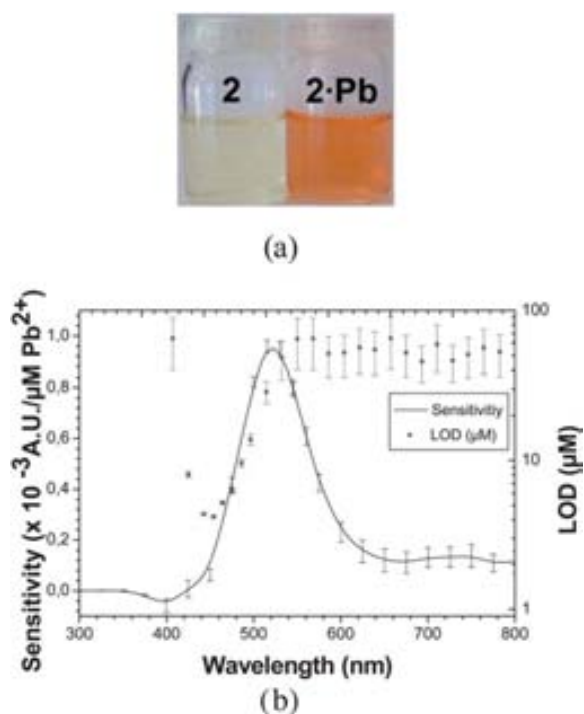


Fig. 4 (a) Picture showing acetonitrile solutions containing 0.1 mM ligand **2** and the change in colour of this solution upon addition of 1 equivalent of Pb^{2+} . (b) Sensitivity and limit of detection (LOD) values for the detection of Pb^{2+} in a solution of ligand **2** using the RMIR system in a spectral range ranging from 300 to 800 nm.

Notes and references

- 1 O. Krystofova, L. Trnkova, V. Adam, J. Zehnalek, J. Hubalek, P. Babula and R. Kizek, *Sensors*, 2010, **10**, 5308.
- 2 F. Loe-Mie, G. Marchand, J. Berthier, N. Sarrut, M. Pucheault, M. Blanchard-Desce, F. Vinet and M. Vaultier, *Angew. Chem., Int. Ed.*, 2010, **49**, 424.
- 3 D. Arunbabu, A. Sannigrahi and T. Jana, *Soft Matter*, 2011, **7**, 2592.
- 4 Y. L. Hung, T. M. Hsiung, Y. Y. Chen and C. C. Huang, *Talanta*, 2010, **82**, 516.
- 5 E. M. Krupp, B. F. Milne, A. Mestrot, A. A. Meharg and J. Feldmann, *Anal. Bioanal. Chem.*, 2008, **390**, 1753.
- 6 F. A. Duarte, C. A. Bizzi, F. Goldschmidt-Antes, V. L. Dressler and E. M. de Moraes-Flores, *Spectrochim. Acta, Part B*, 2009, **64**, 513.
- 7 S. Arzhantsev, X. Li and J. F. Kauffman, *Anal. Chem.*, 2011, **83**, 1061.
- 8 Q. Hu, G. Yang, Y. Zhao and J. Ying, *Anal. Bioanal. Chem.*, 2003, **375**, 831.
- 9 I. H. Chang, J. J. Tulock, J. Liu, W. S. Kim, D. M. Cannon Jr, Y. Lu, P. W. Bohn, J. V. Sweedler and D. M. Cropek, *Environ. Sci. Technol.*, 2005, **39**, 3756.
- 10 A. Manz, N. Graber and H. M. Widmer, *Sens. Actuators, B*, 1990, **1**, 244.
- 11 X. S. Zhu, C. Gao, J. W. Choi, P. L. Bishop and C. H. Ahn, *Lab Chip*, 2005, **5**, 212.
- 12 Z. Zou, A. Jang, E. MacKnight, P. M. Wu, J. Do, P. L. Bishop and C. H. Ahn, *Sens. Actuators, B*, 2008, **134**, 18.
- 13 B. A. Flusberg, E. D. Cocker, W. Piyawattanametha, J. C. Jung, E. L. M. Cheung and M. J. Schnitzer, *Nat. Methods*, 2005, **2**(12), 941.
- 14 A. Llobera, S. Demming, R. Wilke and S. Büttgenbach, *Lab Chip*, 2007, **7**, 1560.
- 15 B. Ibarlucea, E. Fernández-Rosas, J. Vila-Planas, S. Demming, C. Nogués, J. A. Plaza, S. Büttgenbach and A. Llobera, *Anal. Chem.*, 2010, **82**, 4246.
- 16 B. Ibarlucea, C. Fernández-Sánchez, S. Demming, S. Büttgenbach and A. Llobera, *Analyst*, 2011, **136**, 3496.
- 17 A. Llobera, R. Wilke and S. Büttgenbach, *Talanta*, 2008, **75**, 473.
- 18 O. Ordeig, P. Ortiz, X. Muñoz-Berbel, S. Demming, S. Büttgenbach, C. Fernández-Sánchez and A. Llobera, *Anal. Chem.*, 2012, **84**, 3546.
- 19 H. N. Kim, W. X. Ren, J. S. Kim and J. Yoon, *Chem. Soc. Rev.*, 2012, **41**, 3210.
- 20 X. M. Wang, H. Yan, X. L. Feng and Y. Chen, *Chin. Chem. Lett.*, 2010, **21**, 1124.
- 21 L. Zhang, B. Han, T. Li and E. Wang, *Chem. Commun.*, 2011, **47**, 3099.
- 22 A. Caballero, R. Martínez, V. Lloveras, I. Ratera, J. Vidal-Gancedo, K. Wurst, A. Tárraga, P. Molina and J. Veciana, *J. Am. Chem. Soc.*, 2005, **127**, 15666.
- 23 F. Zapata, A. Caballero, A. Espinosa, A. Tárraga and P. Molina, *J. Org. Chem.*, 2009, **74**, 4787.
- 24 C. Díez-Gil, A. Caballero, I. Ratera, A. Tárraga, P. Molina and J. Veciana, *Sensors*, 2007, **7**, 3481.
- 25 C. Díez-Gil, R. Martínez, I. Ratera, A. Tárraga, P. Molina and J. Veciana, *J. Mater. Chem.*, 2008, **18**, 1997.
- 26 M. Soleimani, M. S. Mahmodi, A. Morsali, A. Khani and M. G. Afshar, *J. Hazard. Mater.*, 2011, **189**, 371.
- 27 R. M. T. Casey, P. Guinan, A. Canavan, M. McCann, C. Cardin and N. B. Kelly, *Polyhedron*, 1991, **10**, 483.
- 28 G. Openheim and E. Grushka, *J. Chromatogr., A*, 2002, **942**, 63–71.
- 29 J. N. Lee, C. Park and G. M. Whitesides, *Anal. Chem.*, 2003, **75**, 6544–6554.
- 30 B. H. Jo, L. M. Van Lerberghe, K. M. Motsegood and D. J. Beebe, *J. Microelectromech. Syst.*, 2000, **9**(1), 76.
- 31 J. Vila-Planas, E. Fernández-Rosas, B. Ibarlucea, S. Demming, C. Nogués, J. A. Plaza, C. Domínguez, S. Büttgenbach and A. Llobera, *Nat. Protoc.*, 2011, **6**(10), 1642.
- 32 S. Ando and K. Koide, *J. Am. Chem. Soc.*, 2011, **133**, 2556.
- 33 W. Wang, Y. Jin, Y. Zhao, X. Yue and C. Zhang, *Biosens. Bioelectron.*, 2012, DOI: 10.1016/j.bios.2012.08.006.
- 34 C. Díez-Gil, R. Martínez, I. Ratera, T. Hirsh, A. Espinosa, A. Tárraga, P. Molina, O. S. Wolfbeis and J. Veciana, *Chem. Commun.*, 2011, **47**, 1842.
- 35 W. Jung, A. Jang, P. L. Bishop and C. H. Ahn, *Sens. Actuators, B*, 2011, **155**, 145.
- 36 N. Kannan and S. J. S. Malar, *Indian J. Chem. Technol.*, 2005, **12**, 522.
- 37 J. Tanyanyiwa, E. M. Abad-Villar, M. T. Fernández-Abedul, A. Costa-García, W. Hoffman, A. E. Guber, D. Herrmann, A. Gerlach, N. Gottschlich and P. C. Hauser, *Analyst*, 2003, **128**, 1019.
- 38 R. Wagner, R. W. Boulger, Jr, C. J. Oblinger and B. A. Smith, *U.S. Geological Survey: Guidelines and standard procedures for continuous water-quality monitors: station operation, record computation, and data reporting*, 2006.
- 39 Official Journal of the European Union, *Directive 2008/105/EC of the European parliament and of the Council*, 2008.